

Dissertation zur Erlangung des Doktorgrades
der Fakultät Chemie und Pharmazie der
Ludwig-Maximilians-Universität München



**The evaluation of immunogenicity of therapeutic
antibody drug aggregates using
2D and 3D *in vitro* models**

Teresa Franziska Kraus

aus Weingarten

2019

Erklärung

Diese Dissertation wurde im Sinne von § 7 der Promotionsordnung vom 28. November 2011 von Frau PD Dr. habil. Julia Engert betreut.

Eidesstattliche Versicherung

Diese Dissertation wurde eigenständig und ohne unerlaubte Hilfe erarbeitet.

München, den 01.05.2019

Teresa Kraus

Dissertation eingereicht am: 16.05.2019

1. Gutachter: PD Dr. habil. Julia Engert
2. Gutachter: Prof. Dr. Gerhard Winter

Mündliche Prüfung am: 02.07.2019

Für Opa

SALUS AEGROTI SUPREMA LEX

Hippokrates

Acknowledgements

This thesis was prepared between March 2015 and December 2018 at the Department of Pharmacy, Pharmaceutical Technology and Biopharmaceutics at the Ludwig-Maximilians-Universität München under the supervision of PD Dr. habil. Julia Engert.

First and foremost, I would like to express my deepest gratitude to PD Dr. habil. Julia Engert for her excellent supervision and scientific guidance during my PhD time. I'm deeply thankful for her support and help in all research issues, the lively scientific discussions and for always having an open ear. In addition, I highly appreciated her help in preparing publications.

I'm deeply grateful to Prof. Dr. Gerhard Winter for giving me the chance to work on an innovative and challenging project. I highly appreciated his outstanding scientific advice and support on a professional but also personal level. Besides the professional aims, he also attached importance to a good team spirit and always supported group activities which created an excellent working atmosphere. I would also like to thank Prof. Winter for giving me the opportunity to present my research at numerous national and international conferences.

Moreover, I would like to thank Prof. Dr. Wolfgang Frieß for all the scientific discussions, his help and support in teaching matters and with organizing the ski trip as well as for the fun we had during our group activities. Together with Prof. Winter, Prof. Frieß created an outstanding working environment!

This thesis would not have been possible without our collaboration partner ProBioGen AG in Berlin. Annika Lubitz, Dr. Ulrike Schließer, Dr. Christoph Giese, Jana Reuschel and Dr. Rene Brecht are deeply thanked for their support, immunological input and contribution to this thesis. I always enjoyed the lively discussions and meetings we had! Special thanks to Annika Lubitz for her help with preparing the manuscript for our publication.

Moreover, I would like to thank Prof. Dr. Olivia Merkel and her group for giving me the chance to work in their cell culture lab. Dr. Aditi Mehta and Natascha Hartl are thanked for all their help and support with cell experiments. In addition, I would like to thank Andreas Stelzl for all the TRPS measurements in our joint project.

My deepest gratitude is expressed to my colleagues from the research groups of Prof. Winter, Prof. Frieß and Prof. Merkel for the great time! Special thanks go to my former lab mates, Dr. Laura Engelke-Mücksch, Andreas Stelzl, Ute Rockinger and Bernard Manuel Haryadi for the great time in B.1.076! I always enjoyed the atmosphere in the big lab. Thank you "Team Solida" for being a great teaching team and for all your help and support in organizing the practical course!

Not only did I meet fantastic colleagues but also friends for a lifetime! Thank you Hristo Svilenov, Andreas Tosstorff, Julian Gitter, Tobias Keil, Dr. Katharina Geh, Dr. Leticia Rodrigues Neibecker, Dr. Jacqueline Horn, Dr. Ellen Köpf, Ute Rockinger and Natascha Hartl for the fun times we had in the kitchen, at conferences, the Oktoberfest, during social activities, parties, sport events, skiing and hiking trips and travelling. It made my PhD time unforgettable and thinking of all these events makes me smile all over again!

I cannot express my gratitude in words when it comes to my family. I'm deeply grateful to my parents Barbara and Josef for their unconditional love and support throughout all the years. They taught me to be self-confident and self-reliant, encouraged me to approach new challenges and supported several stays abroad which contributed substantially to my personal and professional development. I'm deeply grateful to have parents like you!

I would like to thank my brother Max for his support and help and especially for his patience when pharmacy was once again the dominating topic at the family table. Moreover, I would also like to express my gratitude to my grandparents Irmgard and Hans Kremer for their love and support throughout all my life.

Last, I would like to say thank you to the best partner I can imagine. Thank you Matze, for your endless and unconditional support, understanding, patience and love. You are my everything.

This thesis is for my grandad Hans Kremer who passed away several years ago. He was a passionate pharmacist himself and one of the most important persons in my life. I wish he could still be with us.

Table of Content

1	General introduction	- 6 -
1.1	Immunogenicity of biopharmaceuticals.....	- 7 -
1.2	Induction factors of immunogenicity	- 7 -
1.3	Clinical consequences.....	- 8 -
1.4	Immunogenicity and protein aggregates	- 10 -
1.5	Test models for the evaluation of immunogenicity of protein aggregates	- 12 -
1.5.1	2D <i>In vitro</i> models	- 12 -
1.5.2	<i>In vivo</i> models.....	- 14 -
1.6	Conclusion and future aspects	- 17 -
1.7	The human artificial lymph node model	- 21 -
1.7.1	Lymph nodes	- 21 -
1.7.2	The human artificial lymph node model	- 21 -
1.7.3	Read-out parameters, advantages and applications of the human artificial lymph node model	- 22 -
1.8	References.....	- 24 -
2	Objectives of this thesis.....	- 33 -
2.1	Objectives of this thesis.....	- 34 -
2.2	References.....	- 36 -
3	Materials and Methods	- 37 -
3.1	Materials.....	- 38 -
3.1.1	Monoclonal antibodies Adalimumab and Bevacizumab	- 38 -
3.2	Methods used for the generation of protein aggregates.....	- 38 -
3.2.1	Light stress.....	- 38 -
3.2.2	Stir stress	- 38 -
3.2.3	Heat stress.....	- 39 -
3.2.4	Chemical oxidation stress using tert-butyl hydroperoxide (tBHP)	- 39 -
3.3	Methods used for the analysis of protein aggregates.....	- 39 -

3.3.1	Turbidity	- 39 -
3.3.2	Light Obscuration	- 39 -
3.3.3	Flow imaging microscopy	- 40 -
3.3.4	Dynamic light scattering (DLS).....	- 40 -
3.3.5	Size exclusion chromatography (SEC).....	- 40 -
3.3.6	Protein A chromatography	- 41 -
3.3.7	Ion exchange chromatography (IEX)	- 41 -
3.3.8	Fourier transform infrared spectroscopy (FT-IR)	- 42 -
3.3.9	Extrinsic fluorescence spectroscopy	- 42 -
3.3.10	Intrinsic fluorescence spectroscopy	- 42 -
3.4	Endotoxins.....	- 43 -
3.4.1	Endochrome - K® Test	- 43 -
3.4.2	Endosafe® - PTS Device	- 43 -
3.5	Methods used for the evaluation of immunogenicity of protein aggregates in a 3D human artificial lymph node model (Chapter 5)	- 44 -
3.5.1	Generation of protein aggregates.....	- 44 -
3.5.2	Extrinsic fluorescence spectroscopy	- 44 -
3.5.3	Fourier transform infrared spectroscopy (FT-IR)	- 45 -
3.5.4	Size exclusion chromatography.....	- 45 -
3.5.5	Cell preparation.....	- 45 -
3.5.6	2D cell culture experiments	- 46 -
3.5.7	Human artificial lymph node (HuALN) bioreactor experiments.....	- 46 -
3.5.8	In-process controls and end point analyses	- 47 -
3.5.9	Analysis of HuALN culture experiments	- 47 -
3.5.10	Analysis of anti-drug antibodies (ADAs)	- 48 -
3.5.11	Investigations on the diffusion behavior of fluorescent particles through a 3D Life dextran-CD hydrogel using a Franz Cell model	- 49 -
3.6	Methods used for investigating the effect of in-line filtration on immunogenicity (Chapter 6)	- 51 -

3.6.1	In-line filtration process used for the evaluation of immunogenicity in a 3D human artificial lymph node model	- 51 -
3.6.2	In-line filtration process used for the evaluation of immunogenicity in a 2D dendritic cell assay	- 52 -
3.6.3	Hold-up volume PharmAssure® filter	- 52 -
3.6.4	Hold-up volume Acrodisc® filter	- 52 -
3.6.5	Filter quality PharmAssure® filter	- 52 -
3.6.6	Methods used for the evaluation of immunogenicity using a 2D dendritic cell assay	- 53 -
3.7	Methods used to investigate the particle burden in biologics (Chapter 7)	- 55 -
3.7.1	Materials.....	- 55 -
3.7.2	Methods to determine the number of subvisible and submicron particles in biologics	- 57 -
3.8	References	- 59 -
4	Aggregation studies on the human monoclonal antibodies Adalimumab and Bevacizumab ..	- 60 -
4.1	Introduction.....	- 61 -
4.2	Results	- 63 -
4.2.1	Turbidity	- 63 -
4.2.2	Light obscuration.....	- 64 -
4.2.3	Dynamic light scattering (DLS).....	- 66 -
4.2.4	Size exclusion chromatography (SEC).....	- 68 -
4.2.5	Extrinsic fluorescence.....	- 70 -
4.2.6	Intrinsic fluorescence	- 72 -
4.2.7	Fourier transform infrared spectroscopy (FT-IR)	- 73 -
4.2.8	Stability of aggregated samples of Adalimumab and Bevacizumab after storage at 2 - 8°C over a period of 6 weeks	- 75 -
4.2.9	Stability of aggregated samples of Adalimumab and Bevacizumab after storage at - 80°C for 6 months and further storage at 2-8°C for 6 weeks after thawing	- 75 -
4.3	Discussion	- 79 -

4.4	References.....	- 85 -
5	The evaluation of immunogenicity of protein aggregates in a 3D human artificial lymph node model.....	- 88 -
5.1	Introduction.....	- 89 -
5.2	Evaluation of a 3D human artificial lymph node model as test model for the assessment of immunogenicity of protein aggregates	- 90 -
5.2.1	Results and Discussion	- 90 -
5.3	Additional Data.....	- 103 -
5.3.1	The analysis of anti-drug antibodies (ADAs)	- 103 -
5.3.2	The analysis of submicron particles in stressed Bevacizumab samples using Tunable Resistive Pulse Sensing (TRPS).....	- 108 -
5.4	Investigations on the diffusion behavior of fluorescent particles through a 3D life dextran-CD hydrogel using a Franz Cell model.....	- 110 -
5.4.1	Abstract	- 110 -
5.4.2	Results	- 111 -
5.4.3	Discussion	- 114 -
5.5	Conclusion	- 115 -
5.6	References.....	- 116 -
6	In-line filtration as a possibility to reduce the immunogenicity of protein aggregates	- 121 -
6.1	Introduction.....	- 122 -
6.2	Evaluation of the effect of in-line filtration using a 3D <i>in vitro</i> human artificial lymph node model	- 123 -
6.2.1	Results of protein analysis.....	- 123 -
6.2.2	Results of 3D <i>in vitro</i> human artificial lymph node experiments	- 135 -
6.3	Evaluation of the effect of in-line filtration using a 2D <i>in vitro</i> dendritic cell assay	- 139 -
6.3.1	Results of protein analysis.....	- 139 -
6.3.2	Results of 2D <i>in vitro</i> dendritic cell assay experiments	- 144 -
6.4	Discussion	- 154 -
6.5	Conclusion	- 157 -

6.6	References	- 159 -
7	Particle numbers in biologics: Can in-line filtration reduce the particle burden?	- 162 -
7.1	Introduction.....	- 163 -
7.2	Results	- 164 -
7.2.1	Turbidity	- 164 -
7.2.2	Analysis of subvisible particles by light obscuration and flow imaging	- 168 -
7.2.3	Analysis of submicron particles by tunable resistive pulse sensing (TRPS).....	- 176 -
7.3	Discussion	- 180 -
7.4	References.....	- 185 -
8	Final summary	- 188 -
8.1	Summary	- 189 -
8.2	Conclusion and Outlook	- 192 -
8.3	References.....	- 194 -
9	Appendix.....	- 195 -
9.1	List of abbreviations	- 196 -
9.2	List of publications and presentations associated with this thesis	- 198 -
9.3	Curriculum Vitae.....	- 199 -

Chapter 1

General introduction

Parts of this chapter were published as review article in International Journal of Pharmaceutics:

Teresa Kraus, Gerhard Winter, Julia Engert

Test Models for the Evaluation of Immunogenicity of Protein Aggregates

International Journal of Pharmaceutics 559 (2019) 192-200.

1.1 Immunogenicity of biopharmaceuticals

The development of therapeutic protein drugs has revolutionized the treatment of many severe diseases such as cancer, rheumatoid arthritis, and Crohn's disease¹. Besides their benefits including less side effects and highly specific treatment, a major drawback of biopharmaceuticals is their ability to induce immune responses in patients². In many cases this bears without any clinical consequences for the patient, but in some cases with severe immune reactions such as pure red cell aplasia (PRCA)³ or anaphylactic responses^{4,5}. One suspects, that the immune response is caused by the development of antibodies to the administered drugs, so called anti-drug antibodies (ADAs)⁶. Generation of anti-drug antibodies has been previously reported after treatment of patients for a considerable number of biologicals such as EPO^{3,7}, Insulin⁸, human GM-CSF⁹, Factor VIII^{4,10}, Interferon alpha¹¹ and several monoclonal antibodies¹². Immunogenicity can have an impact on the safety and efficacy of the drug and is therefore unwanted. The Food and Drug Administration (FDA) has edited a Guideline for Industry "Immunogenicity Assessment for Therapeutic Proteins Products" describing the background of immunogenicity and giving recommendations for risk mitigation of immunogenicity during the development of biopharmaceutical products¹³. In fact, the FDA published recommendations concerning immunogenicity and, of course, the occurrence of clinical consequences related to immunogenicity after administration of a drug to patients emphasizes the significance of this topic. Due to the risk to the patients, there is an essential need for further investigations of the potential of therapeutic protein drugs to elicit undesired immunogenicity. The further sections in this chapter focus on induction factors and clinical consequences of immunogenicity, illustrate the relation between immunogenicity and protein aggregates, and summarize currently used test models for the prediction of immunogenicity. Finally, the human artificial lymph node model, which was mainly used as test model for testing the immunogenicity of protein aggregates during this thesis, is presented in detail.

1.2 Induction factors of immunogenicity

Factors influencing immunogenicity can be distinguished between patient-, production- or drug-related factors¹⁴. The origin of the drug, meaning if the protein is foreign or human, plays a major role¹⁵. Moreover, protein folding or changes in the primary structure of the protein may influence the potential of the drug to induce immunogenicity^{13,14}. Glycosylation or pegylation¹⁶ of a drug may alter the tendency of inducing immunogenicity by reducing protein aggregation and by shielding the protein from the immune system^{17,18}. Among the production related factors, protein aggregates have been discussed for a long time to elicit immunogenic reactions^{19,20}. Besides, the presence of leachables or extractables^{21,22}, production related impurities²³ or additives²⁴ may contribute to immunogenicity. Finally, the packaging process and the interaction between the container and the protein may also

have an impact on immunogenicity²⁵. Fradkin *et al.* found that glass microparticles with adsorbed protein can induce immunogenicity²⁶. Moreover, glass and air interfaces might trigger protein aggregation and denaturation²⁷ and finally, glass can delaminate which might also increase the risk of immunogenic reactions²⁸.

Besides all these product related factors, there are also factors related to the patient affecting immunogenicity. First, the history of allergy, the immunologic status and competence of the patient play a major role¹³. Patients receiving immunosuppressive substances during a treatment might show lower immune response compared to patients having an active immune system as exemplarily shown by Baert *et al.*²⁹ for the treatment of Crohn's disease using Infliximab. Also, the age of the patient may influence the development of an immune response, which is in particular true for infants, small children, and elderly people^{13,30,31}. The route and frequency of administration, as well as the dosing are also factors affecting immunogenicity^{32,33}. One suspects that the subcutaneous route of administration poses a greater risk for immunogenic reactions than intravenous applications³⁴. A review of Hamuro *et al.*³⁵ points out that this was true for four out of six marketed products where clinical data regarding the route of administration was available. However, a review comparing intravenous versus subcutaneous monoclonal antibodies for the treatment of asthma revealed that the described antibodies have a relatively low immunogenicity and, if observed, immunogenic reactions were found for i.v. and s.c. administrations³⁶. Furthermore, genetic factors, especially some human leukocyte (HLA) haplotypes, increase the risk for some patients to develop immunogenic reactions³⁷. In summary, immunogenic reactions occur not only due to one risk factor but can be influenced by several factors at the same time.

1.3 Clinical consequences

Describing clinical consequences of immunogenicity, one can differentiate between consequences regarding the efficacy or the safety of a drug. As regards the efficacy of therapeutic proteins, the generation of anti-drug antibodies (ADAs) is a key issue. There are two types of anti-drug antibodies described in literature: a) Neutralizing and b) non-neutralizing anti-drug antibodies^{38,39} (see Figure 1-1A and B). Neutralizing ADAs, as their name already suggests, bind to the active site of therapeutic proteins and therefore block the efficacy of the drug. In contrast, non-neutralizing ADAs do not target the active site of the drug but bind to a different site, so that the therapeutic protein can still bind to its target³⁸. However, the pharmacokinetic parameters such as the clearance of the drug can be induced. If anti-drug antibodies show cross-reactivity to endogenous protein the clinical consequences might be severe^{7,13,25}.

Immunogenicity does not necessarily result in severe clinical complications, but if so, the safety of the drug is affected. According to the Guidance for Industry about “Immunogenicity Assessment for Therapeutic Protein Products” there is a range of acute effects that may be induced by immunogenicity varying from indisposition to severe acute reactions such as anaphylaxis or cytokine release syndrome^{13,40,41}. These acute reactions are often categorized as “infusion reactions”¹³. Clinical consequences can also occur temporarily delayed, meaning not chronologically linked to the administration of the drug. Non-acute reactions can be delayed hypersensitivity reactions accompanied by symptoms such as delayed outbreak of fever, rash or arthralgia^{42,43}, e.g., as described in the FDA Guideline¹³. The presence of ADAs in patients after administration has been reported for several therapeutic proteins^{12,44}. For example, Adalimumab, a human anti-TNF α monoclonal antibody, leads to the formation of anti-drug antibodies in many patients. Bender *et al.* showed in a trial in regular clinical settings, that 87% of the patients with rheumatoid arthritis participating in this study developed anti-drug antibodies against Adalimumab⁴⁵. Although this study included a rather small number of 15 patients, it shows the clinical relevance of anti-drug antibody formation. Even if immunogenic reactions do not consequently lead to obvious clinical symptoms, it is necessary to diminish the risk for patients and ensure a safe and efficient therapy. A permanent loss in therapy efficacy would also result in an increased therapy cost. Therefore, the risk assessment of immunogenicity of therapeutic proteins is an essential obstacle which must be faced during development to ensure a safe and efficient drug therapy.

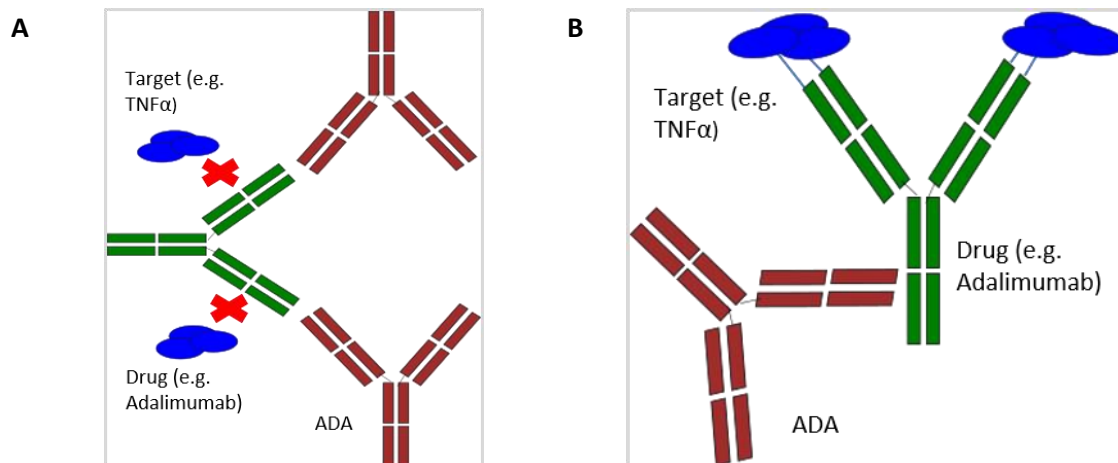


Figure 1-1: Schematic drawing of neutralizing (A) and non-neutralizing anti-drug antibodies (ADAs): Neutralizing ADAs bind to the active site of the drug and therefore block the efficacy of the drug. Non-neutralizing ADAs bind to a different site of the drug, so that the drug can still bind to its target, but the pharmacokinetics of the drug can be influenced; adopted from Carrascosa *et al.*³⁸.

1.4 Immunogenicity and protein aggregates

It has been known for a long time, that protein aggregates contribute to the immunogenicity of biopharmaceuticals^{19,20}. Protein aggregation is one of the instabilities of proteins possibly occurring throughout the entire development and production of a protein drug⁴⁶. In particular during the manufacturing process, biopharmaceutical proteins are exposed to various conditions such as fermentation, purification, pumping, filling, shipment, and storage, which may trigger aggregation processes⁴⁷. Not all types of aggregates are equally immunogenic. Meanwhile one suspects that submicron particles as well as protein aggregates with strong chemical modifications show the strongest immunogenic effects^{48,49}. Until now, only little is known about the exact mechanism of protein aggregates to elicit immune responses. In general, there are two mechanisms for the formation of anti-drug antibodies discussed in literature: T-cell dependent (TD) and T-cell independent (TI) activation of immunogenic reactions. The first describes the “classical” immune response (Figure 1-2): The antigen is recognized, internalized and processed by antigen presenting cells (APCs) such as dendritic cells (DCs)²⁰. Stimulated DCs migrate to the lymph nodes where they present the antigen via MHC class II molecules to T-cells⁵⁰. Finally, an interaction between the antigen primed T-cells and B-cells via T-cell receptor (TCR), MHC II and CD40 ligand and CD40 receptor leads to the activation of B-cells, thus to the formation of ADAs^{20,51,52}. Another hypothesis specifies that protein aggregates can directly activate B-cells to produce anti-drug antibodies (Figure 1-3). Protein aggregates can either lead to polyclonal B-cell activation via binding to Toll-like receptors (TI mechanism type I) or by cross-linking BCRs due to repetitive structures of protein aggregates (TI mechanism type II)⁵³. To date, the relevant mechanism is still not exactly known. The isotypes of secreted anti-drug antibodies as well as the type of secreted cytokines can partially indicate the type of immune response. IgG anti-drug antibodies usually indicate T-cell help, whereas B-cells produce IgM anti-drug antibodies without memory. However, isotype switching from IgM to IgG antibodies can occur, thereby making it difficult to draw conclusions about the underlying mechanisms^{51,52,54}. Thus, further investigations of protein aggregates need to be carried out to gain a deeper understanding of the underlying mechanisms of immunogenicity.

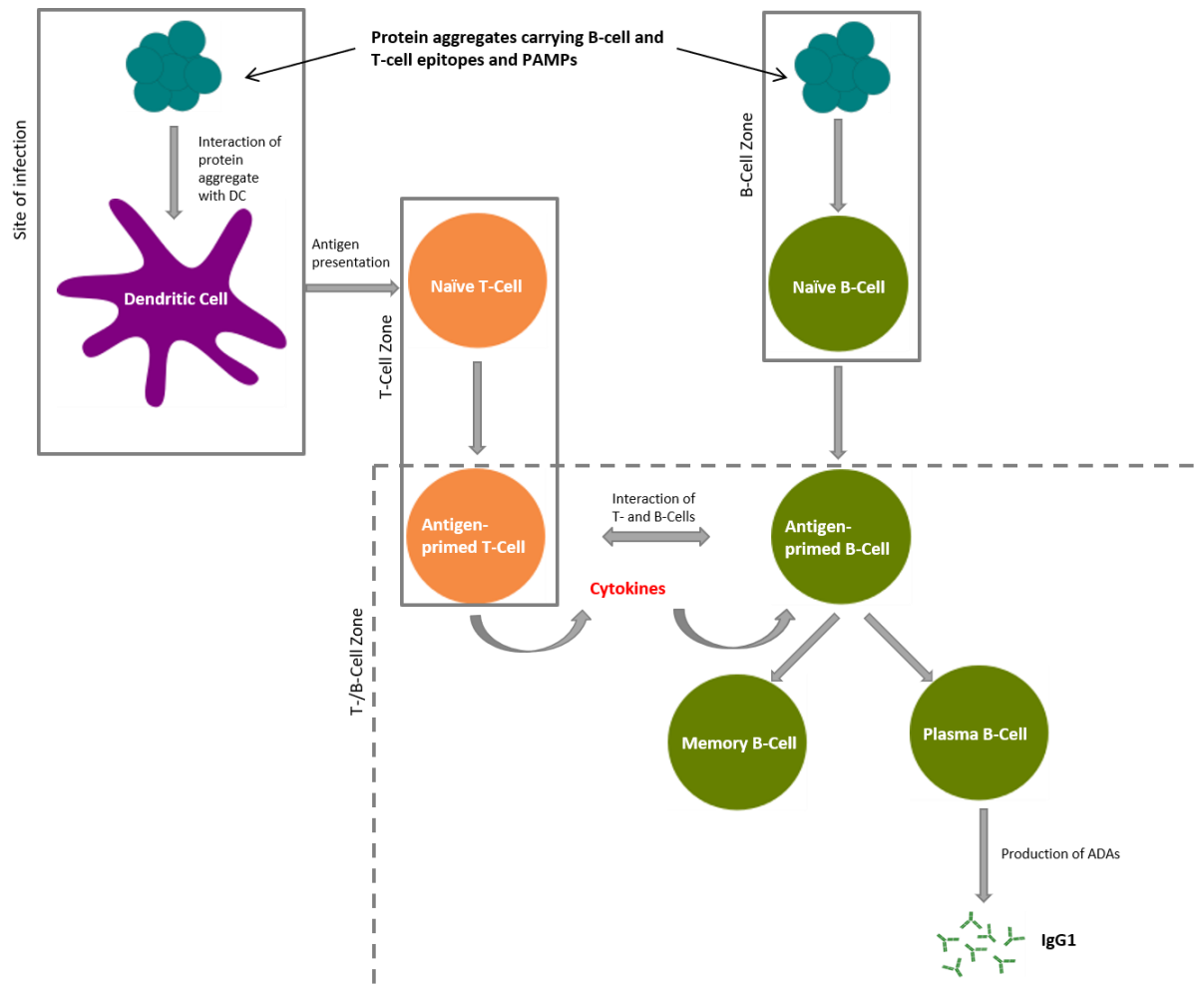


Figure 1-2: Schematic overview of the T-cell dependent mechanism of anti-drug antibody formation.

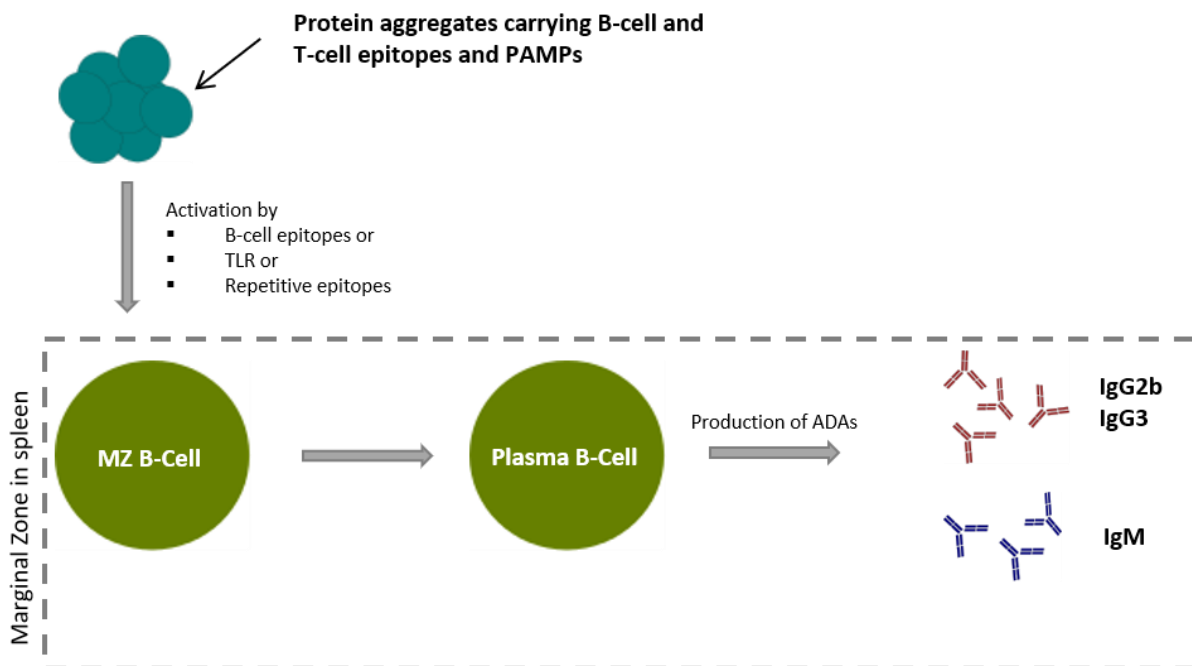


Figure 1-3: Schematic overview of the T-cell independent mechanism of anti-drug antibody formation.

1.5 Test models for the evaluation of immunogenicity of protein aggregates

Over the last years, the capacity of protein aggregates to elicit immunogenicity has been investigated in a variety of studies using different *in vitro* and *in vivo* models (see Table 1-1 and Table 1-2). The most common models used for the assessment of immunogenicity of protein aggregates are mouse models (see Table 1-2). Besides animal models, *in vitro* models have been used to evaluate the immunogenicity of protein aggregates (see Table 1-1). In the following section, the focus is on test models that have been used for the evaluation of immunogenicity of protein aggregates. Their value regarding the prediction of immunogenicity in humans and the mechanisms of immunogenicity are discussed. Furthermore, we summarize advantages and drawbacks of the test models in use and discuss gaps and challenges for the future.

1.5.1 2D *In vitro* models

Most of the *in vitro* assays used for the evaluation of immunogenicity of protein aggregates are based on the use of peripheral blood mononuclear cells (PBMCs) from humans (Table 1-1). Using such system, the aim is to investigate the ability of protein aggregates to induce the maturation of immature monocyte-derived DCs to mature DCs. Therefore, PBMCs are isolated from human blood or buffy coats. Sometimes they are further differentiated into CD14⁺ and CD14⁻ cells using magnetic beads to optimize the purity of the isolated monocytes⁵⁵. Subsequently, monocytes are incubated with different protein aggregate formulations for a few hours until several days, and finally, upregulation of DC maturation markers such as CD83, CD80 and CD86 or the release of different cytokines are investigated⁵⁵⁻⁵⁹. Incubation times of protein aggregates with PBMCs range from several hours until several days to monitor the early and late phase of the cytokine release^{59,60}. Besides PBMC assays, T-cell proliferation assays are also a well-used tool to investigate the ability of protein aggregates to trigger an immune response. Therefore, PBMCs including T-cells are challenged with the desired formulations, and after 5-8 days, the proliferation of CD4⁺ T-cells can be measured using a thymidine incorporation assay^{58,59} or CFSE staining, which is easier to use⁶¹. To date, only few groups investigated the potential of different kind of protein aggregates using PBMC based *in vitro* assays (see Table 1-1). Results showed differences between the potential of certain protein aggregates to induce T-cell proliferation, DC activation and cytokine signals. Ahmadi *et al.*⁵⁸ stimulated dendritic cells and CD4⁺ cells with small amounts of sub-visible aggregates of Rituximab and Trastuzumab. Besides cytokine secretion and T-cell proliferation, they also investigated the uptake of fluorescent-labelled particles of Rituximab into dendritic cells using confocal microscopy. The group could show that Rituximab particles were taken up efficiently by MoDCs, and that low amounts of aggregates (< 3% of total protein) were able to trigger the innate immune system. According to this study, the level of activation

of the immune system also depends on the intrinsic clinical immunogenicity of the investigated proteins. There were only small differences in DC activation and T-cell proliferation of aggregated and unstressed Rituximab (high clinical immunogenicity), whereas aggregated Trastuzumab (low clinical immunogenicity) led to T-cell proliferation. Moussa *et al.*⁵⁶ evaluated the immunogenicity of aggregated intravenous immunoglobulin using PBMCs and primary monocytes in comparison to human monocyte cell lines (THP-1 and MM6 cells). Aggregates generated by mechanical stress (stirring and shaking) led to an increase in cytokine release when tested in PBMCs and primary monocytes. Cytokine secretion in both cell lines, THP-1 and MM6 cells, was comparable to the response in primary monocytes, even though secreted cytokine concentrations were lower. Besides, they also tested the dose-response to aggregates generated by mechanical stress and observed that the relative dose-responsiveness to increasing aggregate doses was similar between THP-1 cells and primary cells. MM6 cells were previously used by Zaitseva *et al.* to develop *in vitro* assays to predict toxicity of adjuvants *in vivo*⁶². Moussa *et al.*⁵⁶ did not report any correlation data of MM6 cells and primary monocytes due to inconsistency and variability of the results of dose responses of MM6 cells with primary monocytes responses. The THP-1 cell line as an *in vitro* cell model is well described by Chanput *et al.*⁶³. Accordingly, advantages of this cell line compared to PBMC derived cells are a faster growing rate, an easy and safe use, the possibility of stock building in liquid nitrogen, culture times up to three months without changes of cell activity or sensitivity and low batch to batch variability. The latter is a disadvantage of cell lines at the same time, since a high donor to donor variability reflects genotype effects which may play an important role regarding immunogenicity^{2,64,65}. A further drawback of cell lines is that the cultivation conditions can influence cell sensitivity and therefore lead to different results than primary cells.

In general, PBMC based *in vitro* assays have many advantages. First of all, large numbers of samples can be investigated at the same time, including a high variety of donors and HLA diversity⁵⁹. They include the essential immune cells to simulate a potential immune response upon administration of a drug without intervention of other blood components. Additionally, the assays can be run for several days to investigate not only an early stage immune response but also a late stage immune response or T-cell proliferation^{57,59,60}. Finally, the range of readout parameters regarding an innate immune response is broad. Multiplex assays allow the analysis of several cytokines at the same time, DC maturation marker and T-cell proliferation can be analyzed (see Table 1-1). However, a major drawback is that 2D *in vitro* assays only represent a small part of the human immune system⁶⁶. Enclosing tissue or lymph nodes are not present, and the influence of biodistribution and circulation cannot be investigated either²⁰. A further disadvantage of *in vitro* assays is that the long-term formation of ADAs cannot be measured, and, with a few exceptions mentioned above, incubation

times of PBMCs and aggregated protein samples are often short. Therefore the focus of such assays is on an early stage immune response^{56,58}. 2D *in vitro* assays present a useful method to investigate the capacity of protein aggregates to elicit immunogenicity on the level of an innate response, but it is questionable, if 2D *in vitro* assays can predict immunogenicity of protein aggregates in humans.

1.5.2 *In vivo* models

In contrast to *in vitro* models, animal models possess a fully trained immune system making them a popular test model used for the assessment of immunogenicity⁶⁷. The most widely spread animal models for the evaluation of immunogenicity of protein aggregates are mice. Non-human primates have been used to test the immunogenicity of different biopharmaceuticals, but to the best of our knowledge no study exists in which higher order animals have been used to test the immunogenicity of protein aggregates^{68–72}. The FDA guidance for Industry “Immunogenicity assessment of therapeutic protein products” also mentions murine models only¹³. Table 1-2 displays an overview of the murine models recently used for the evaluation of immunogenicity of protein aggregates. Among many different models wild-type strains and transgenic mice are the most common mouse models. The further sections will evaluate these different models regarding their utility for the assessment of immunogenicity of protein aggregates.

1.5.2.1 Wild-type mouse models

Even though wild-type mice respond to human recombinant proteins as foreign substances, they are still used in many studies as a model to investigate the immunogenicity of protein aggregates^{32,73–78}. Wild-type strains are commercially available and their breeding is considered simple⁶⁷. However, it is questionable, if wild-type mice are a suitable model to predict immunogenicity in humans. First, the underlying mechanism of immunogenic reactions in humans differs from the classical immune response against foreign species or proteins, since human recombinant proteins are not foreign to humans. However, wild-type mice strains can be used for testing murine proteins and may be a valuable test system to evaluate the relative immunogenicity between different products or protein aggregates^{67,79}. Freitag *et al.*⁷³ investigated the immunogenicity of different types of aggregates of a murine monoclonal antibody, which is closely related to a human drug antibody, in two wild-type mouse strains: BALB/c and C57BL/6 mice. The latter was chosen because the murine monoclonal antibody they used was produced in this strain, thus the protein was not considered as foreign. Additionally, BALB/c mice were also included due to their known sensitivity and strong Th2 response. The study revealed that the results differ strongly between the two mouse strains. While the murine mAb1 was not immunogenic in C57BL/6 J mice, a strong immune response against mAb1 was detected in BALB/c mice. A high anti-drug antibody response towards the buffer control in C57BL/6 J mice made

it difficult to evaluate data and distinguish between the immunogenicity of the different types of aggregates. In contrast in BALB/c mice, all aggregated formulations showed a higher immune response than the native mAb1 and especially insoluble aggregates generated by light resulted in a high IgG1 response. Differences between the two mouse strains are known and described in literature^{80,81}. C57BL/6 J mice belong to Th1 responder while BALB/c mice are preferred Th2 responders. Conversely, Ratanji *et al.* used BALB/c mice to show that sub-visible scFV and OVA aggregates induce a Th1 response⁷⁵. The differences between the strains highlight the difficulty to select an appropriate mouse model for the assessment and prediction of immunogenicity in humans on the one hand but may also reflect the genetic variety among patients on the other hand. However, using a particularly sensitive mouse strain such as BALB/c mice bears the risk of overestimating immunogenicity. Shomali *et al.* used BALB/c and C57BL/6J mice to evaluate the immunogenicity of different dose levels of protein particulates generated by the adsorption of a murine monoclonal antibody (mAb1) onto glass or aluminum hydroxide microparticles and silicon oil droplets³². Also, in this study, the immune responses were different depending on the type of the mouse strains: In general, the immune response to the mAb1 formulations was stronger in BALB/c mice than in C57BL/6 J mice and BALB/c mice produced mainly IgG1 anti-mAb1 antibodies, whereas C57BL/6 J mice produced anti-mAb1 antibodies of IgG3 and IgG2b isotypes. The authors hypothesized that the target of the anti-mAb1 response might be different in the two mouse strains. In BALB/c mice the immune response may be directed against the allogenic Fc region, whereas in C57BL/6 J mice the immune response could be directed against neoepitopes generated by aggregation or adsorption. The authors also performed a PK analysis and found that the concentration of mAb1 in all formulations declined faster in BALB/c mice than in C57BL/6 J mice. These results were in line with the increased ADA levels in BALB/c mice. The mentioned studies show, that results are partially contradictory and that it is challenging not to overestimate immunogenicity using only wild-type mouse strains. In many studies the formulations of interest were therefore tested in wild-type and transgenic mice^{48,74,76–78,82–85}. Moreover, wild-type strains might also be interesting for testing the immunogenicity of aggregates of proteins that are part of a replacement therapy for patients who cannot produce certain proteins such as Factor VIII, for example. In this case, the human recombinant protein might also be discerned as foreign⁶⁷. A further possibility to investigate the immunogenicity of Factor VIII protein aggregates is to use Hemophilia A and von Willebrand Factor knockout (vWF^{-/-}) mice⁸⁶. Accordingly, these mouse models are often used to investigate the relative immunogenicity of Factor VIII formulations. Primarily because of their intolerance towards Factor VIII but also because these mice produce a qualitatively similar immune response to Factor VIII like humans⁸⁷.

1.5.2.2 Transgenic mouse models

Transgenic mice are bred to be immune tolerant to the human recombinant protein supposed to be evaluated for its immunogenicity. The development and generation of such transgenic mouse models is complex and time-consuming^{88,89} and the models can only be used for one type of protein⁶⁷. Van Beers *et al.*⁹⁰ used a transgenic C57Bl/6 x FVB/N hybrid mice and their wild-type littermates⁸⁹ to investigate the immunogenicity of recombinant human IFN β and the induction of an immunological memory. While wild-type mice showed high IgG titer upon the re-challenge with rhIFN β on day 63, transgenic mice did not show any increase of IgG titers. Thus, they did not develop an immunological memory. Fradkin *et al.*⁸⁴ investigated the immunogenicity of aggregates of recombinant human growth hormone using naïve adult, neonatally primed and transgenic mice resulting in different anti-hGH IgG levels of the same formulations in each model. Whereas ADA levels in naïve adult and neonatally primed mice mainly differed in the concentration levels, no ADAs were detected in the transgenic mouse model. On the contrary, the study of Hermeling *et al.* showed that oxidized recombinant human IFN α 2b was able to break the immune tolerance of transgenic mice⁷⁶. According to the publication of Fradkin *et al.*⁸⁴ not only the investigated proteins were different but also the used transgenic mice resulted from cross-breeding different mouse strains. However, differences in the immune response might also depend on the type of protein aggregates. Several studies have shown that not all types of protein aggregates are equally immunogenic^{73,76,82}. In a recent study⁷⁸, only metal-catalyzed oxidized recombinant human IFN2b was able to break the immune tolerance in transgenic mice while protein aggregates generated by oxidation using hydrogen peroxide, by cross-linking with glutaraldehyde or by incubation at elevated temperatures did not trigger the formation of anti-drug antibodies in a transgenic mouse model. Boll and colleagues used a transgenic mouse model to evaluate the immunogenicity of differently produced sub-visible particles⁴⁸ and could show that only sub-visible particles with strong chemical modifications triggered an immune response. These studies indicate that transgenic mouse models can be useful to evaluate the relative immunogenicity between different types of protein aggregates as well as the breaking of immune tolerance. Besides, transgenic mice are also useful to predict neo-epitopes. Bessa and colleagues developed a novel transgenic mouse model to evaluate the immunogenicity of various antibody aggregates. They found that only protein aggregates bearing neo-epitopes, thus chemical modifications, created by exposure to light could break the immune tolerance⁸³. Despite all the diverse studies using transgenic mice as a test model, there are still many drawbacks to overcome. First, transgenic mice still own a murine immune system making the predictability regarding immune reactions in humans questionable. Second, it is also uncertain if the presence of the target protein is sufficient to mimic the situation in humans, since the human recombinant protein is usually not biologically active after administration in mice⁷⁷ and/or

biological effects of the proteins in mice are unforeseeable⁶⁷. Moreover, expression levels of the target proteins might not correspond to those of humans⁶⁷.

1.6 Conclusion and future aspects

The currently used test models for the assessment of immunogenicity of protein aggregates have advantages and disadvantages. One of the essential questions is which test model simulates the human immune system best? At the moment, *in vivo* models are still seen as most suitable model since they have a fully trained immune system and therefore they are valued as “closest” to humans⁶⁷. However, evaluating the immunogenicity of protein aggregates in wild-type and transgenic mouse has not yet provided clearness neither about types of protein aggregates that elicit immunogenicity most nor about the mechanisms of immunogenicity of protein aggregates. Meanwhile one suspects, that especially protein aggregates with chemical modifications as well as protein aggregates in the submicron range are most prone to elicit immunogenicity^{48,49}. Bi and colleagues tried to overcome the drawbacks of transgenic and wild-type mice developing a “Xeno-het mouse”, a crossbreed between the XenoMouse[®] and the wild-type strain C57BL/6 J, to assess the immunogenicity of different aggregated protein formulations⁹¹. This mouse model combined the tolerance to human IgG₂ of the XenoMouse[®] with the robust immune response of the C57BL/6 J strain. However, the model still utilizes mouse MHC, mouse T-cells and APCs to elicit an immune response and therefore the predictability of immunogenicity in humans is again arguable. Compared to *in vitro* cell assays, *in vivo* models enable a long-term exposition of the drug with the possibility of multiple re-stimulations and ADAs can be analyzed. In contrast, the readout parameters of *in vitro* cell assays often base on the analysis of activation marker or cytokines, but the formation of ADAs cannot be monitored. Moreover, exposure times of the investigated drug are rather short. Neither of the used models represents the ideal one to investigate and predict the immunogenicity of protein aggregates in humans. An interesting approach to combine *in vitro* and *in vivo* testing might be to use the secretion of cytokines such as TNF alpha as *in vitro* markers for an increased risk of immunogenicity *in vivo* as shown by Fathallah and co-authors⁹². Nevertheless, to learn more about the underlying mechanisms of immunogenicity, a shift to models based on human cells with a human immune system is indispensable. Recently, a lot of effort has been put in the development of so-called micro-organoid systems such as a 3D *in vitro* skin model or human artificial lymph node models^{66,93}. The latter is especially interesting, since lymph nodes belong to the secondary lymphatic organs and represent the interaction between the adaptive and innate immune response⁶⁶. A human artificial lymph node model was developed by Giese *et al.*⁹⁴ and represents a disposable, matrix-assisted 3D model of a human lymph node. It is operated with cells from human donors which are implanted in a 3D gel matrix where

follicles and micro-organoid structures are formed. The model offers a wide range of read-out parameters on the B- and T-cell level and enables a long-term exposure of the drug including multiple re-stimulations. The human artificial lymph node model has already been used successfully for testing the immunogenicity of vaccines⁹⁵ and might be a promising development to overcome the drawbacks of the currently used models. 3D *in vitro* models such as the human artificial lymph node model might improve the predictability of immunogenicity of protein aggregates and make it possible to gain more insight into the underlying mechanisms of immunogenicity triggered by protein aggregates. Beside the development of 3D *in vitro* models the prediction of immunogenicity *in silico* gained interest of some research groups^{96–98}. Successful correlations between *in silico* prediction of immunogenicity and corresponding experimental data has been published already^{98,99}. However, *in silico* prediction of immunogenicity of therapeutic proteins is mainly based on the prediction and identification of T-cell epitopes binding to MHC molecules⁹⁷. The focus is especially set on the primary structure of the proteins and factors such as aggregation e.g. are not considered¹⁰⁰. Until now there are no publications available on *in silico* prediction of immunogenicity of protein aggregates. However, *in silico* methods for the prediction of immunogenicity will certainly be further developed in the upcoming years and could also be a complementary method to evaluate the immunogenicity of protein therapeutics and maybe also of protein aggregates. In summary, some studies were able to identify certain types of protein aggregates that triggered immunogenicity most in their study^{48,78}, other studies using similar stress conditions of the proteins but different test models led to contradictory results^{76,84}. For future experiments, a harmonized test model would help to evaluate and compare the immunogenicity of various types of protein aggregates.

Finally, it is noteworthy to mention in-line filtration as a strategy to minimize particles in biopharmaceuticals prior to administration. It is without doubt that product manufacturers put a lot of effort in formulation development to release high quality products fulfilling the limitations set for particles in the Pharmacopoeia and USP^{101,102}. However, particles and aggregates that form due to mishandling by the clinic staff or the patients or during transportation are not monitored and such particles can be administered to patients, e.g. during infusion therapy¹⁰³. Ueda *et al.*¹⁰⁴ recently published a study showing that mishandling of a Factor VIII product during reconstitution led to higher particle counts possibly being delivered to patients during administration of the drug. In the context of the immunogenicity risk of protein aggregates, in-line filtration represents a possibility to reduce particle numbers in products that were generated during post production mishandling and thus, to protect patients from particles potentially leading to immunogenic reactions. It has been shown already that filtration is an effective tool to remove larger particles^{104,105}. Moreover, a very detailed report about in-line filtration revealed that almost 16% of all approved protein drugs listed in the Rote

Liste® require a filtration before administration¹⁰⁶. Therefore in-line filtration could be a helpful tool to reduce the particle burden in infusion therapy, e.g., provided that the used filters are compatible with the protein and problems like filter shedding and protein adsorption are investigated. In parallel, test models used for the evaluation of immunogenicity must be further developed regarding their predictability of immunogenicity in humans.

Table 1-1: Summary of studies evaluating the immunogenicity of protein aggregates using *in vitro* models.

<u>Protein</u>	<u>Sample preparation</u>	<u>Model</u>	<u>Investigation of</u>	<u>Reference</u>
Human recombinant mAbs	Freeze/Thaw Shear Heat /Shaking	PBMC Isolation of monocytes and differentiation to immature dendritic cells	DC maturation	Rombach-Riegraf <i>et al.</i> ⁵⁵
Intravenous immunoglobulin	Heat Metal oxidation Mechanical stress (stirring/shaking)	PBMC Primary monocytes Immortalized human monocyte-like cell lines: THP-1 and MM6 cells	Innate immune response Cytokine release Complement activation Innate immune response	E.M. Moussa <i>et al.</i> ⁵⁶
mAb	Stirring Heat (control sample) Fractionation of samples by centrifugation/sedimentation/FACS	PBMC	Early phase Late phase of immune response Cytokine profile	Srivalli Telikepalli <i>et al.</i> ⁶⁰
Human mAbs	Stirring Shear stress Heat	PBMC HLA-DR haplotyping	Innate immune response Cytokine release profile T-cell proliferation	Marisa K. Joubert <i>et al.</i> ⁵⁷
Rituximab Trastuzumab	Mechanical stress Heat Freeze/Thaw	PBMC	Cytokine release profile T-cell proliferation Uptake of aggregated antibodies by MoDCs	Maryam Ahmadi <i>et al.</i> ⁵⁸
mAbs	Stirring	PBMC HLA-DR haplotyping	Cytokine release profile T-cell proliferation	Marisa K. Joubert <i>et al.</i> ⁵⁹

Table 1-2: Summary of studies evaluating the immunogenicity of protein aggregates using *in vivo* models.

<u>Protein</u>	<u>Stress condition</u>	<u>Model</u>	<u>Type of immune response</u>	<u>Reference</u>
mAbs	Heat/ Mechanical UV-Vis light Chemical stress (AAPH or H ₂ O ₂) (in combination with heat and mechanical stress) Fractionation of samples by FACS	hlgG1 transgenic mouse model wild-type mice (C57BL) as control	ADAs	Boll <i>et al.</i> ⁴⁸
mAb	Freeze/Thaw pH shift stress Heat stress Shake stress Metal-catalyzed oxidation	Transgenic and non-transgenic mice	ADAs	V. Filipe <i>et al.</i> ⁸²
mAb and bispecific antibody-based construct	Heat stress	Swiss Webster mice, outbred	ADAs	Fathallah <i>et al.</i> ⁹²
Murine mAb	UV light stress Stirring stress Shaking stress Heat stress Fractionation of samples by AF4/centrifugation	Female C57BL/6 J Female BALB/c	ADAs	Freitag <i>et al.</i> ⁷³
Murine mAb	Adsorption onto silicone oil microdroplets, glass microparticles or Alhydrogel®	Female C57BL/6 J Female BALB/c	ADAs	Shomali <i>et al.</i> ³²
rhIFNβ-1a	Adjuvant solution	Transgenic and non-transgenic mice	ADAs	Kijanka <i>et al.</i> ¹⁰⁷
mAbs	Stirring stress Oxidation using H ₂ O ₂ Coating onto microspheres	Xeno-het-mouse	ADAs	Bi <i>et al.</i> ⁹¹
rhIFNβ-1a rhIFNβ-1b	Bulk Incubation at low pH and in presence of sodium chloride Isolation of soluble aggregates via a Superose 12 SEC column	Transgenic and non-transgenic mice (C57BL/6 x FVB/N hybrid mice)	ADAs	Van Beers <i>et al.</i> ⁷⁴
Humanized scFv	Heat stress Stir stress	Female BALB/c strain mice	ADAs	Rantanji <i>et al.</i> ⁷⁵
rhIFNβ-1a	Metal-catalyzed Oxidation Oxidation using H ₂ O ₂ Guanidine mediated unfolding/refolding	Wild-type mice Transgenic mice	ADAs	Van Beers <i>et al.</i> ⁹⁰
mAb	Low pH value Light stress Fractionation of samples by preparative exclusion chromatography	Transgenic mice	ADAs	Bessa <i>et al.</i> ⁸³
rhIFNα2b	Metal-catalyzed oxidation Heat stress at various pH values	Wild-type mice Transgenic mice	ADAs	Hermeling <i>et al.</i> ⁷⁶
IFNα2a	Cross-linking with glutaraldehyde	Wild-type mice Transgenic mice	ADAs	Braun <i>et al.</i> ⁷⁷
rhGH	Agitation (Shaking) Freeze-thaw stress Disaggregation using high-hydrostatic pressure	Naïve adult mice Neonatally primed mice Transgenic mice	ADAs	Fradkin <i>et al.</i> ⁸⁴
rhIFNα2b	Metal-catalyzed oxidation Cross-linking with glutaraldehyde Oxidation with hydrogen peroxide Heat stress	Wild-type mice Transgenic mice	ADAs	Hermeling <i>et al.</i> ⁷⁸

Factor VIII	Incubation at 37°C and 80°C	Von Willebrandt Factor deficient and Hemophilia A mice	ADAs T-cell proliferation Cytokine analysis	Pisal <i>et al.</i> ⁸⁶
Adalimumab (mAb)	Shaking stress with siliconized and nonsiliconized syringes	BALB/c mice	ADAs	Uchino <i>et al.</i> ¹⁰⁸
Human recombinant IFNα2b	Agitation stress at 37°C Incubation at low pH Metal catalyzed oxidation	Transgenic FVB/N mice Wild type FVB/n mice	ADAs	Human <i>et al.</i> ⁸⁵
Murine monoclonal antibody	Low pH + stirring Elevated temperature + stirring Fractionation of samples by centrifugation/SEC	BALB/c mice	ADAs Follicular T-helper cell detection	Kijanka <i>et al.</i> ⁴⁹
Murine growth hormone	UV radiation	BALB/c mice Nude BALB/c mice	ADAs (IgG ₁ , IgG ₃ , IgM)	Fradkin <i>et al.</i> ¹⁰⁹

1.7 The human artificial lymph node model

1.7.1 Lymph nodes

Beside the spleen and mucosa associated lymphatic tissue, lymph nodes belong to the secondary lymphatic organs. Their function is to develop an adaptive immune response to antigens. The lymph node tissue can be divided into three areas: paracortex, cortex and medulla^{66,110}. Within this area there are fissures and channels draining the lymph fluid and stromal cells such as MRCs (marginal reticular cells), FRCs (fibroblastic reticular cells) and FDCs (follicular dendritic cells) provide the lymphatic compartments with their structure^{66,111}. The cortex is dominated by B-cells which are arranged as follicles and germinal centers, whereas the paracortex is dominated by T-cells⁶⁶. The medulla contains transient plasma cells, macrophages and B-cells⁶⁶. When an antigen presenting cell caught an antigen in the periphery, it will process the antigen, migrate to the lymph node and present it to T-cells in the paracortical zone via MHC class II molecules. Antigen-specific activated T-cells will then proliferate and migrate toward the boarder of the cortical zone, where they get in contact with B-cells⁶⁶. After T/B-cell interaction, B cells will differentiate and start to produce antigen specific antibodies in the germinal centers⁶⁶. Thus, lymph nodes are the site of action regarding the adaptive immune response. The application of a human artificial lymph node for the evaluation of immunogenicity of protein aggregates could therefore be a step into the future to improve the predictiveness of the currently used test models.

1.7.2 The human artificial lymph node model

The human artificial lymph node model (HuALN) (Figure 1-4) is a micro-organoid culture system developed by Giese *et al.*⁹⁴. It is operated with peripheral blood mononuclear cells (PBMCs) and dendritic cells (DCs) from human donors in combination with allogeneic MSC-derived stromal cells which are embedded in hydrogel matrix sheets^{94,112}. The housing is made of polysulfone and consists

of two compartments which are divided by a set of hollow fibres providing a continuous gas supply. The bioreactor can be challenged with the antigen via the injection port which is located at the media inlet port. Beside the continuous perfusion of the bioreactor with gas, the device is also perfused with media and cell suspension to ensure long-term cultivation under steady-state conditions. Moreover the cycling B-cell solutions simulates the lymph flow and ensures B-cell contact with the antigen primed DCs and T-cells⁹⁵. The bioreactor system can be challenged multiple times during a culture time of 15-30 days. Sampling via a needle-free sampling port can be performed daily and a broad selection of read-out parameters can be analyzed⁹⁵ (see 1.7.3).

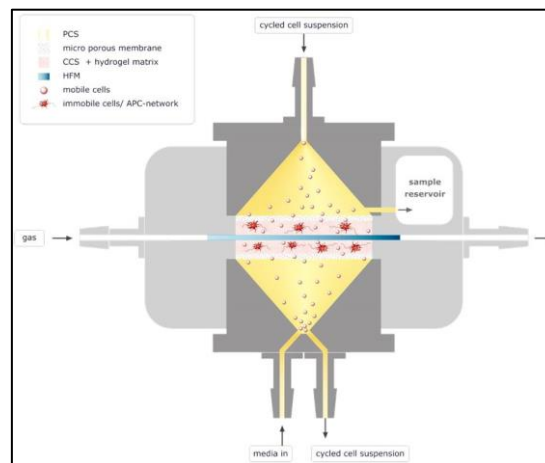


Figure 1-4: Schematic drawing of the HuALN bioreactor device (HIRIS™ III): Oxygenating membranes are surrounded by an immobilized matrix-assisted cell suspension. The gas supply perfuses horizontally and cell culture media and cell suspension flow vertically⁹⁵.

1.7.3 Read-out parameters, advantages and applications of the human artificial lymph node model

The human artificial lymph node system offers various read-out parameters on the level of cellular and humoral immunity. First, the secretion of cytokines as well as of antigen specific antibodies (IgG/IgM) can be analyzed⁹⁵. Moreover, the histology of the cells after finishing the experiment can be investigated by flow cytometry and microscopy to gain further insight to the generation of follicle structures as shown by Giese *et al.*⁹⁵ or to the kind of immune response which was induced (T-cell dependent or T-cell independent). This broad selection of read-out parameters represents one of several advantages that come along with the 3D human artificial lymph node system. The HuALN represents an *in vitro* model based on cells isolated from human donors with a fully developed immune system. Continuous and moderate perfusion enables the formation of antigen-dependent immune competent micro-organoid structures⁹⁵. Besides, a long-term culture of more than four weeks is possible, and sampling can be performed daily. During the HuALN run, multiple re-stimulations by APCs and the drug can be performed simulating the real situations in patients when they get in contact with

an antigen. A further advantage of the HuALN system is its applicability in several fields. So far it has especially been used for testing immune modulators and small molecules, to proof the immunogenicity of vaccines and to exclude toxicity^{94,95}. Due to the complexity of tissue engineering⁶⁶, the development of a human artificial lymph node system has been a progress regarding the need for improved test models. However, the HuALN has not been used to evaluate the immunogenicity of protein aggregates yet and the following studies will show if the HuALN represents a future model for the pre-clinical assessment of immunogenicity.

1.8 References

1. Berger, M., Shankar, V. & Vafai, A. Therapeutic Applications of Monoclonal Antibodies. *Am. J. Med. Sci.* **324**, 14–30 (2002).
2. Kessler, M., Goldsmith, D. & Schellekens, H. Immunogenicity of biopharmaceuticals. *Nephrol. Dial. Transplant.* **21**, 9–12 (2006).
3. Casadevall, N. *et al.* Pure Red-Cell Aplasia and Antierythropoietin Antibodies in Patients Treated with Recombinant Erythropoietin. *N. Engl. J. Med.* **346**, 469–475 (2002).
4. Lusher, J. M., Lee, C. A., Kessler, C. M. & Bedrosian, C. L. The safety and efficacy of B-domain deleted recombinant factor VIII concentrate in patients with severe haemophilia A. *Haemophilia* **9**, 38–49 (2003).
5. Vultaggio, A. *et al.* Anti-infliximab IgE and non-IgE antibodies and induction of infusion-related severe anaphylactic reactions. *Allergy* **65**, 657–661 (2010).
6. Schellekens, H. & Casadevall, N. Immunogenicity of recombinant human proteins: causes and consequences. *J. Neurol.* **251**, II/4-9 (2004).
7. Macdougall, I. C. *et al.* Antibody-mediated pure red cell aplasia in chronic kidney disease patients receiving erythropoiesis-stimulating agents: new insights. *Kidney Int.* **81**, 727–732 (2012).
8. Fineberg, S. E., Galloway, J. A. & Fineberg, N. S. Immunogenicity of Recombinant DNA Human Insulin. *Diabetologia* **25**, 465–469 (1983).
9. Wadhwa, M. *et al.* Production of neutralizing granulocyte-macrophage colony-stimulating factor (GM-CSF) antibodies in carcinoma patients following GM-CSF combination therapy. *Clin Exp Immunol* **104**, 351–358 (1996).
10. Bray, G. L. *et al.* A Multicenter Study of Recombinant Factor VI11 (Recombine): Safety, Efficacy, and Inhibitor Risk in Previously Untreated Patients With Hemophilia A. *Blood* **83**, 2428–2435 (1994).
11. Quesada, B. J. R., Rios, A., Swanson, D., Trown, P. & Gutterman, J. U. Antitumor Activity of Recombinant-Derived Interferon Alpha in Metastatic Renal Cell Carcinoma. *J. Clin. Oncol.* **3**, 1522–1528 (1985).
12. Getts, D. R., Getts, M. T., McCarthy, D. P., Chastain, E. M. L. & Miller, S. D. Have we

- overestimated the benefit of human(ized) antibodies? *MAbs* **2**, 682–694 (2010).
13. U.S. Department of Health and Human Services, FDA, CDER, C. Guidance for Industry Immunogenicity Assessment for Therapeutic Protein Products. (2014).
 14. Deehan, M. *et al.* Managing unwanted immunogenicity of biologicals. *Autoimmun. Rev.* **14**, 569–574 (2015).
 15. Harding, F. A., Stickler, M. M., Razo, J. & DuBridge, R. The immunogenicity of humanized and fully human antibodies. *MAbs* **2**, 256–265 (2010).
 16. Harris, J. M., Martin, N. E. & Modi, M. Pegylation: a novel process for modifying pharmacokinetics. *Clin. Pharmacokinet.* **40**, 539–551 (2001).
 17. Inada, Y. *et al.* Biomedical and biotechnological applications of PEG- and PM-modified proteins. *Trends Biotechnol.* **13**, 86–91 (1995).
 18. Cole, K. S., Steckbeck, J. D., Rowles, J. L., Desrosiers, R. C. & Montelaro, R. C. Removal of N-linked glycosylation sites in the V1 region of simian immunodeficiency virus gp120 results in redirection of B-cell responses to V3. *J. Virol.* **78**, 1525–1539 (2004).
 19. Rosenberg, A. S. Effects of protein aggregates: an immunologic perspective. *AAPS J.* **8**, E501–E507 (2006).
 20. Moussa, E. M. *et al.* Immunogenicity of Therapeutic Protein Aggregates. *J. Pharm. Sci.* **105**, 417–430 (2016).
 21. Markovic, I. Evaluation of safety and quality impact of extractable and leachable substances in therapeutic biologic protein products: a risk-based perspective. *Expert Opin. Drug Saf.* **6**, 487–491 (2007).
 22. Schellekens, H. & Jiskoot, W. Eprex-associated pure red cell aplasia and leachates. *Nat. Biotechnol.* **24**, 613–614 (2006).
 23. Verthelyi, D. & Wang, V. Trace levels of innate immune response modulating impurities (IIRMI)s synergize to break tolerance to therapeutic proteins. *PLoS One* **5**, 1–9 (2010).
 24. Mueller, R. *et al.* Evaluation of the Immuno-Stimulatory Potential of Stopper Extractables and Leachables by Using Dendritic Cells as Readout. *J. Pharm. Sci.* **98**, 3548–3561 (2009).
 25. Seidl, A. *et al.* Tungsten-induced denaturation and aggregation of epoetin alfa during primary

- packaging as a cause of immunogenicity. *Pharm. Res.* **29**, 1454–1467 (2012).
26. Fradkin, A. H., Carpenter, J. F. & Randolph, T. W. Glass Particles as an Adjuvant: A Model for Adverse Immunogenicity of Therapeutic Proteins. *J. Pharm. Sci.* **100**, 4953–4964 (2011).
 27. Gerhardt, A. *et al.* Protein aggregation and particle formation in prefilled glass syringes. *J. Pharm. Sci.* **103**, 1601–1612 (2014).
 28. Ditter, D. *et al.* Evaluation of Glass Delamination Risk in Pharmaceutical 10 mL/10R Vials. *J. Pharm. Sci.* **107**, 624–637 (2017).
 29. Baert, F. *et al.* Influence of Immunogenicity on the Long-Term Efficacy of Infliximab in Crohn's Disease. *N. Engl. J. Med.* **348**, 601–608 (2003).
 30. PrabhuDas, M. *et al.* Challenges in infant immunity: implications for responses to infection and vaccines. *Nat. Immunol.* **12**, 189–194 (2011).
 31. Goronzy, J. J. & Weyand, C. M. Understanding immunosenescence to improve responses to vaccines. *Nat. Immunol.* **14**, 428–436 (2013).
 32. Shomali, M. *et al.* Dose levels in particulate-containing formulations impact anti-drug antibody responses to murine monoclonal antibody in mice. *J. Pharm. Sci.* **104**, 1610–1621 (2015).
 33. Ross, C. *et al.* Immunogenicity of interferon- β in multiple sclerosis patients: Influence of preparation, dosage, dose frequency, and route of administration. *Ann. Neurol.* **48**, 706–712 (2000).
 34. Filipe, V., Que, I., Carpenter, J. F., Löwik, C. & Jiskoot, W. In vivo fluorescence imaging of IgG1 aggregates after subcutaneous and intravenous injection in mice. *Pharm. Res.* **31**, 216–227 (2014).
 35. Hamuro, L. *et al.* Perspectives on Subcutaneous Route of Administration as an Immunogenicity Risk Factor for Therapeutic Proteins. *J. Pharm. Sci.* **106**, 2946–2954 (2017).
 36. Matucci, A., Vultaggio, A. & Danesi, R. The use of intravenous versus subcutaneous monoclonal antibodies in the treatment of severe asthma: A review. *Respir. Res.* **19**, 1–10 (2018).
 37. Lucas, D. P., Leffell, M. S. & Zachary, A. A. Differences in immunogenicity of HLA antigens and the impact of cross-reactivity on the humoral response. *Transplantation* **99**, 77–85 (2015).
 38. Carrascosa, J. M. Immunogenicity in Biologic Therapy: Implications for Dermatology. *Actas*

- Dermosifiliogr* **104**, 471–479 (2013).
39. Sethu, S. *et al.* Immunogenicity to biologics: Mechanisms, prediction and reduction. *Arch. Immunol. Ther. Exp. (Warsz)*. **60**, 331–344 (2012).
 40. Rodrigo, G. J., Neffen, H. & Castro-Rodriguez, J. Efficacy and Safety of Subcutaneous Omalizumab vs Placebo as Add-on Therapy to Corticosteroids for Children and Adults with Asthma. *Chest* **139**, 28–35 (2011).
 41. Lubner, S. J. *et al.* Report of a multicenter phase II trial testing a combination of biweekly bevacizumab and daily erlotinib in patients with unresectable biliary cancer: A phase II consortium study. *J. Clin. Oncol.* **28**, 3491–3497 (2010).
 42. Ellis, G. K. *et al.* Randomized trial of denosumab in patients receiving adjuvant aromatase inhibitors for nonmetastatic breast cancer. *J. Clin. Oncol.* **26**, 4875–4882 (2008).
 43. Herold, K. C. *et al.* Anti-CD3 Monoclonal Antibody in New-Onset Type 1 Diabetes Mellitus. *N. Engl. J. Med.* **346**, 1692–1698 (2002).
 44. Baker, M. P., Reynolds, H. M., Lemicisi, B. & Bryson, C. J. Immunogenicity of protein therapeutics: The key causes, consequences and challenges. *Self. Nonself.* **1**, 314–322 (2010).
 45. Bender, N. K. *et al.* Immunogenicity, efficacy and adverse events of adalimumab in RA patients. *Rheumatol. Int.* **27**, 269–274 (2007).
 46. Wang, W. Protein aggregation and its inhibition in biopharmaceutics. *Int. J. Pharm.* **289**, 1–30 (2005).
 47. Mahler, H.-C., Friess, W., Grauschopf, U. & Kiese, S. Protein aggregation: Pathways, induction factors and analysis. *J. Pharm. Sci.* **98**, 2909–2934 (2009).
 48. Boll, B. *et al.* Extensive chemical modifications in the primary protein structure of IgG1 subvisible particles are necessary for breaking immune tolerance. *Mol. Pharm.* **14**, 1292–1299 (2017).
 49. Kijanka, G. *et al.* Submicron Size Particles of a Murine Monoclonal Antibody Are More Immunogenic Than Soluble Oligomers or Micron Size Particles Upon Subcutaneous Administration in Mice. *J. Pharm. Sci.* **107**, 2847–2859 (2018).
 50. Martín-Fontecha, A., Lanzavecchia, A. & Sallusto, F. in *Handb Exp Pharmacol* (eds. Lombardi, G. & Rizzo-Vasquez, Y.) 31–49 (Springer Berlin Heidelberg, 2009).

51. Ratanji, K. D., Derrick, J. P., Dearman, R. J. & Kimber, I. Immunogenicity of therapeutic proteins: Influence of aggregation. *J. Immunotoxicol.* **11**, 99–109 (2014).
52. Sauerborn, M., Brinks, V., Jiskoot, W. & Schellekens, H. Immunological mechanism underlying the immune response to recombinant human protein therapeutics. *Trends Pharmacol. Sci.* **31**, 53–59 (2010).
53. Bachmann, M. F. & Zinkernagel, R. M. Neutralizing Antiviral B Cell Responses. *Annu. Rev. Immunol* **15**, 235–70 (1997).
54. Avery, D. T. *et al.* Naive B Cells Is Differentially Regulated by IL-4. *J. Immunol.* **181**, 1767–1779 (2008).
55. Rombach-Riegraf, V. *et al.* Aggregation of human recombinant monoclonal antibodies influences the capacity of dendritic cells to stimulate adaptive T-cell responses in vitro. *PLoS One* **9**, e86322 (2014).
56. Moussa, E. M., Kotarek, J., Blum, J. S., Marszal, E. & Topp, E. M. Physical Characterization and Innate Immunogenicity of Aggregated Intravenous Immunoglobulin (IGIV) in an In Vitro Cell-Based Model. *Pharm. Res.* **33**, 1736–1751 (2016).
57. Joubert, M. K. *et al.* Highly aggregated antibody therapeutics can enhance the in vitro innate and late-stage T-cell immune responses. *Journal of Biological Chemistry* **287**, 25266–25279 (2012).
58. Ahmadi, M. *et al.* Small amounts of sub-visible aggregates enhance the immunogenic potential of monoclonal antibody therapeutics. *Pharm. Res.* **32**, 1383–1394 (2015).
59. Joubert, M. K. *et al.* Use of in vitro assays to assess immunogenicity risk of antibody-based biotherapeutics. *PLoS One* **11**, 1–22 (2016).
60. Telikepalli, S. *et al.* Physical characterization and in vitro biological impact of highly aggregated antibodies separated into size-enriched populations by fluorescence-activated cell sorting. *J. Pharm. Sci.* **104**, 1575–1591 (2015).
61. Jawa, V. *et al.* T-cell dependent immunogenicity of protein therapeutics: Preclinical assessment and mitigation. *Clin. Immunol.* **149**, 534–555 (2013).
62. Zaitseva, M. *et al.* Use of human MonoMac6 cells for development of in vitro assay predictive of adjuvant safety in vivo. *Vaccine* **30**, 4859–4865 (2012).

63. Chanput, W., Mes, J. J. & Wichers, H. J. THP-1 cell line: An in vitro cell model for immune modulation approach. *Int. Immunopharmacol.* **23**, 37–45 (2014).
64. Schellekens, H. Immunogenicity of therapeutic proteins: clinical implications and future prospects. *Clin. Ther.* **24**, 1720–1740 (2002).
65. Barbosa, M. D. F. S., Vielmetter, J., Chu, S., Smith, D. D. & Jacinto, J. Clinical link between MHC class II haplotype and interferon-beta (IFN- β) immunogenicity. *Clin. Immunol.* **118**, 42–50 (2006).
66. Giese, C. & Marx, U. Human immunity in vitro- Solving immunogenicity and more. *Adv. Drug Deliv. Rev.* 103–122 (2014).
67. Jiskoot, W. *et al.* Mouse Models for Assessing Protein Immunogenicity: Lessons and Challenges. *J. Pharm. Sci.* **105**, 1567–1575 (2016).
68. Zwickl, C. M. *et al.* Comparison of the immunogenicity of recombinant and pituitary human growth hormone in rhesus monkeys. *Toxicol. Sci.* **16**, 275–287 (1991).
69. Zwickl, C. M., Hughes, B. L., Pirooz, K. S., Smith, H. W. & Wierda, D. Immunogenicity of tissue plasminogen activators in rhesus monkeys: Antibody formation and effects on blood level and enzymatic activity. *Toxicol. Sci.* **30**, 243–254 (1996).
70. Zwickl, C. M., Smith, H. W., Zimmermann, J. L. & Wierda, D. Immunogenicity of biosynthetic human LysPro insulin compared to native-sequence human and purified porcine insulins in rhesus monkeys immunized over a 6-week period. *Arzneimittelforschung.* **45**, 524–528 (1995).
71. Lee, H. J. *et al.* In vivo characterization of sustained-release formulations of human growth hormone. *J. Pharmacol. Exp. Ther.* **281**, 1431–1439 (1997).
72. Katsutani, N. *et al.* Immunogenic properties of structurally modified human tissue plasminogen activators in chimpanzees and mice. *Fundam. Appl. Toxicol.* **19**, 555–562 (1992).
73. Freitag, A. J. *et al.* Investigation of the immunogenicity of different types of aggregates of a murine monoclonal antibody in mice. *Pharm. Res.* **32**, 430–444 (2015).
74. Van Beers, M. M. C. *et al.* Aggregated recombinant human interferon beta induces antibodies but no memory in immune-tolerant transgenic mice. *Pharm. Res.* **27**, 1812–1824 (2010).
75. Ratanji, K. D. *et al.* Subvisible aggregates of immunogenic proteins promote a Th1-type response. *Toxicol. Sci.* **153**, 258–270 (2016).

76. Hermeling, S. *et al.* Antibody response to aggregated human interferon alpha2b in wild-type and transgenic immune tolerant mice depends on type and level of aggregation. *J. Pharm. Sci.* **95**, 1084–1096 (2006).
77. Braun, A., Kwee, L., Labow, M. A. & Alsenz, J. Protein aggregates seem to play a key role among the parameters influencing the antigenicity of Interferon alpha in normal and transgenic mice. *Pharm. Res.* **14**, 1472–1478 (1997).
78. Hermeling, S. *et al.* Structural characterization and immunogenicity in wild-type and immune tolerant mice of degraded recombinant human interferon alpha2b. *Pharm. Res.* **22**, 1997–2006 (2005).
79. Brinks, V., Jiskoot, W. & Schellekens, H. Immunogenicity of therapeutic proteins: The use of animal models. *Pharm. Res.* **28**, 2379–2385 (2011).
80. Trunova, G. V *et al.* Morphofunctional Characteristic of the Immune System in BALB / c and C57Bl / 6 Mice. *Bull. Exp. Biol. Med.* **151**, 99–102 (2011).
81. Mills, C. D., Kincaid, K., Alt, J. M., Heilman, M. J. & Hill, A. M. M-1/M-2 Macrophages and the Th1/Th2 Paradigm. *J. Immunol.* **164**, 6166–6173 (2000).
82. Filipe, V. *et al.* Immunogenicity of different stressed IgG monoclonal antibody formulations in immune tolerant transgenic mice. *MAbs* **4**, 740–752 (2012).
83. Bessa, J. *et al.* The immunogenicity of antibody aggregates in a novel transgenic mouse model. *Pharm. Res.* **32**, 2344–2359 (2015).
84. Fradkin, A. H., Carpenter, J. F. & Randolph, T. W. Immunogenicity of aggregates of recombinant human growth hormone in mouse models. *J. Pharm. Sci.* **98**, 3247–3264 (2009).
85. Human, P. *et al.* Assessment of the immunogenicity of mechanically induced interferon aggregates in a transgenic mouse model. *J. Pharm. Sci.* **104**, 722–730 (2015).
86. Pisal, D. S., Kosloski, M. P., Middaugh, C. R., Bankert, R. B. & V., B.-I.-S. Native-like aggregates of Factor VIII (FVIII) are immunogenic von Willebrand Factor deficient and hemophilia A mice. *J. Pharm. Sci.* **101**, 2055–2065 (2012).
87. Reipert, B. M., Ahmad, R. U., Turecek, P. L. & Schwarz, H. P. Characterization of antibodies induced by human factor VIII in a murine knockout model of hemophilia A. *Thromb. Haemost.* **84**, 826–832 (2000).

88. Hermeling, S., Jiskoot, W., Crommelin, D., Bornæs, C. & Schellekens, H. Development of a transgenic mouse model immune tolerant for human interferon beta. *Pharm. Res.* **22**, 847–851 (2005).
89. van Beers, M. M. C. *et al.* Hybrid transgenic immune tolerant mouse model for assessing the breaking of B cell tolerance by human interferon beta. *J. Immunol. Methods* **352**, 32–37 (2010).
90. Van Beers, M. M. C. *et al.* Oxidized and aggregated recombinant human interferon beta is immunogenic in human interferon beta transgenic mice. *Pharm. Res.* **28**, 2393–2402 (2011).
91. Bi, V. *et al.* Development of a human antibody tolerant mouse model to assess the immunogenicity risk due to aggregated biotherapeutics. *J. Pharm. Sci.* **102**, 3545–3555 (2013).
92. Fathallah, A. M. *et al.* The Effect of Small Oligomeric Protein Aggregates on the Immunogenicity of Intravenous and Subcutaneous Administered Antibodies. *J. Pharm. Sci.* **104**, 3691–3702 (2015).
93. Cupedo, T., Stroock, A. & Coles, M. Application of tissue engineering to the immune system: Development of artificial lymph nodes. *Front. Immunol.* **3**, 1–6 (2012).
94. Giese, C. *et al.* A human lymph node in vitro-challenges and progress. *Artif. Organs* **30**, 803–808 (2006).
95. Giese, C. *et al.* Immunological substance testing on human lymphatic micro-organoids in vitro. *J. Biotechnol.* **148**, 38–45 (2010).
96. De Groot, A. S. & Moise, L. Prediction of immunogenicity for therapeutic proteins: state of the art. *Curr. Opin. Drug Discov. Devel.* **10**, 332–340 (2007).
97. Flower, D. R. Towards in silico prediction of immunogenic epitopes. *Trends Immunol.* **24**, 667–674 (2003).
98. Koren, E. *et al.* Clinical validation of the ‘in silico’ prediction of immunogenicity of a human recombinant therapeutic protein. *Clin. Immunol.* **124**, 26–32 (2007).
99. Tatarewicz, S. M. *et al.* Development of a maturing T-cell-mediated immune response in patients with idiopathic Parkinson’s disease receiving r-metHuGDNF via continuous intraputaminaal infusion. *J. Clin. Immunol.* **27**, 620–627 (2007).
100. Brinks, V. *et al.* Preclinical models used for immunogenicity prediction of therapeutic proteins. *Pharm. Res.* **30**, 1719–1728 (2013).

101. 2.9.19 Partikelkontamination- Nicht sichtbare Partikeln. *European Pharmacopoeia* 438–441 (2014).
102. United States Pharmacopeia. <788> Particulate Matter in Injections. *USP* **34**, 326–328 (2011).
103. Nejadnik, M. R. *et al.* Postproduction Handling and Administration of Protein Pharmaceuticals and Potential Instability Issues. *J. Pharm. Sci.* **107**, 2013–2019 (2018).
104. Ueda, T., Nakamura, K., Abe, Y. & Carpenter, J. F. Effects of Product Handling Parameters on Particle Levels in a Commercial Factor VIII Product: Impacts and Mitigation. *J. Pharm. Sci.* **108**, 775–786 (2018).
105. Werner, B. P. & Winter, G. Expanding bedside filtration – a powerful tool to protect patients from protein aggregates. *J. Pharm. Sci.* **107**, 2775–2788 (2018).
106. Werner, B. P. & Winter, G. Particle contamination of parenteralia and in-line filtration of proteinaceous drugs. *Int. J. Pharm.* **496**, 250–267 (2015).
107. Kijanka, G., Sauerborn, M., Boon, L., Schellekens, H. & Brinks, V. Development of ADA against recombinant human interferon beta in immune tolerant mice requires rapid recruitment of CD4⁺ T cells, induces formation of germinal centers but lacks susceptibility for (most) adjuvants. *J. Pharm. Sci.* **104**, 396–406 (2015).
108. Uchino, T., Miyazaki, Y., Yamazaki, T. & Kagawa, Y. Immunogenicity of protein aggregates of a monoclonal antibody generated by forced shaking stress with siliconized and nonsiliconized syringes in BALB/c mice. *J. Pharm. Pharmacol.* **69**, 1341–1351 (2017).
109. Fradkin, A. H., Mozziconacci, O., Schöneich, C., Carpenter, J. F. & Randolph, T. W. UV photodegradation of murine growth hormone: Chemical analysis and immunogenicity consequences. *Eur. J. Pharm. Biopharm.* **87**, 395–402 (2014).
110. Willard-Mack, C. L. Normal Structure, Function, and Histology of Lymph Nodes. *Toxicol. Pathol.* **34**, 409–424 (2006).
111. Mueller, S. N. & Germain, R. N. Stromal cell contributions to the homeostasis and functionality of the immune system. *Nat. Rev. Immunol.* **9**, 618–629 (2009).
112. Sardi, M., Lubitz, A. & Giese, C. Modeling Human Immunity In Vitro - Improving Artificial Lymph Node Physiology by Stromal Cells. *Appl. Vitro. Toxicol.* **2**, 143–150 (2016).

Chapter 2

Objectives of this thesis

2.1 Objectives of this thesis

The overall aim of this thesis was to evaluate the immunogenicity of protein aggregates of therapeutic antibodies in 2D and 3D *in vitro* models. The main focus was on the evaluation of a novel 3D artificial lymph node model, which was developed by Giese and colleagues¹, for testing the immunogenicity of protein aggregates. The human artificial lymph node model represents a complex 3D matrix assisted bioreactor system differing from the currently used *in vitro* or *in vivo* systems in several aspects: The system is based on human cells, it enables long-term cultivation including several re-stimulations, it mimics the structure of a human lymph node by forming germinal centers and lymphatic follicles, and it has a broad range of read-out parameters on the B- and T-cell level¹. The HuALN model has already been used to evaluate the immunogenicity of vaccines², but it has not been used for testing the immunogenicity of protein aggregates yet. Even though many studies exist investigating the immunogenicity of protein aggregates in *in vitro* and *in vivo*, it is still unclear which types of protein aggregates possess the strongest immunogenicity. Recently, the focus of interest has shifted in particular to submicron particles and particles with strong chemical modifications^{3,4}. However, results of these studies are often contradictory which is also due to the variety of different test models that have been used and the questionable predictiveness of immunogenicity in humans (see **Chapter 1**).

The aim of the first part of this thesis was to evaluate the novel 3D *in vitro* human artificial lymph node model for testing the immunogenicity of protein aggregates. In addition, a further aim of this thesis was to determine the types of protein aggregates that are most immunogenic. To achieve these goals, protein aggregates had to be generated by exposing the monoclonal antibodies to different stress conditions. **Chapter 4** describes the methodical approach to establish appropriate stress conditions and time points to generate protein aggregates of two monoclonal antibodies in a sustainable and reproducible amount. Moreover, a thorough analysis of the stressed protein samples is described. Based on the results of **Chapter 4**, the stress conditions and time points were selected for further studies. In addition, the stability of the selected stressed samples during storage at 2-8°C was investigated for the course of the HuALN experiment and results are described in **Chapter 4**.

Chapter 5 focuses on the evaluation of the 3D human artificial lymph node model for testing the immunogenicity of protein aggregates. A selected panel of cytokines and DC marker was analyzed and compared between a 2D *in vitro* assay and the 3D HuALN. Moreover, the analysis of anti-drug antibodies of cell culture supernatants of the 3D HuALN is described. Finally, the diffusion behavior of particles through a dextran gel matrix was investigated to ensure that the generated protein aggregates diffuse into the gel matrix in the HuALN system so that the aggregates get in contact with immobilized leukocytes in the gel matrix.

The focus of the second part of this thesis was on “in-line filtration”. In-line filtration, also known as “bedside filtration”, can be described as a filtration step directly prior to the administration of a biopharmaceutical drug to the patient. Benjamin Werner showed in the scope of his thesis that in-line filtration is a highly effective method to reduce the particle burden in biopharmaceutical products^{5,6}. He also addressed several issues that are associated with (in-line) filtration such as particle shedding from filters, leachables, protein adsorption, and conformational changes of the protein. However, it still remains to be investigated if in-line filtration has a positive effect on immunogenicity, meaning that in-line filtration is not only a tool to reduce particles but also in turn to reduce immunogenicity. Therefore, the aim of the study described in **Chapter 6** was to evaluate the effect of in-line filtration on immunogenicity in a 3D HuALN model and a 2D *in vitro* dendritic cell assay which was developed and established for this study. Differently stressed samples of a monoclonal antibody prior to and after filtration were used to stimulate the HuALN or dendritic cells in a 2D assay. Dendritic cell markers and the presence of cytokines in the cell culture supernatants were analyzed, accordingly.

Regarding particle numbers, biopharmaceutical products must comply with the limits of the Pharmacopoeias. For infusion or injection products in containers with a volume smaller than 100 mL, particles $\geq 10\ \mu\text{m}$ are limited to 6000 particles and particles $\geq 25\ \mu\text{m}$ to 600 particles per container⁷. It is without doubt, that pharmaceutical companies do their best to develop and produce biologic products of high quality. However, particles $\leq 10\ \mu\text{m}$ are not limited by the Pharmacopoeias and might also pose a risk regarding immunogenicity^{3,8,9}. Moreover, once the product has left the pharmaceutical manufacturer, the formation of particles can be triggered by transportation or inadequate post-production handling by the clinic staff in hospitals or by patients, for example. Recently, some research groups focused on this topic and observed that incorrect product handling may lead to the formation of particles which are possibly administered to patients^{10,11}. An in-line filtration step prior to the administration of the biological might provide the patient from particles in the product generated during transportation or incorrect post-production handling. To investigate particle numbers in marketed lyophilized and liquid biological products, several proteins/products were randomly selected and purchased to obtain marketed products with some shelf time. The aim of the study, described in **Chapter 7**, was to investigate if in-line filtration would be a possibility to reduce the particle burden in marketed products. Therefore, particle counts in marketed lyophilized and liquid biologics were analyzed and an in-line filtration step was performed before particle analysis was repeated. The focus hereby was on sub-visible and submicron particles.

Materials and methods that were used for this thesis are described in **Chapter 3**. A final summary of this thesis is provided in **Chapter 8**.

2.2 References

1. Giese, C. *et al.* A human lymph node in vitro-challenges and progress. *Artif. Organs* **30**, 803–808 (2006).
2. Giese, C. *et al.* Immunological substance testing on human lymphatic micro-organoids in vitro. *J. Biotechnol.* **148**, 38–45 (2010).
3. Kijanka, G. *et al.* Submicron Size Particles of a Murine Monoclonal Antibody Are More Immunogenic Than Soluble Oligomers or Micron Size Particles Upon Subcutaneous Administration in Mice. *J. Pharm. Sci.* **107**, 2847–2859 (2018).
4. Boll, B. *et al.* Extensive chemical modifications in the primary protein structure of IgG1 subvisible particles are necessary for breaking immune tolerance. *Mol. Pharm.* **14**, 1292–1299 (2017).
5. Werner, B. P. & Winter, G. Expanding bedside filtration – a powerful tool to protect patients from protein aggregates. *J. Pharm. Sci.* **107**, 2775–2788 (2018).
6. Werner, B. P. Filtration and novel polymeric containers for the improved quality of biotech drug products. (Ludwig-Maximilians-Universität München, 2017).
7. 2.9.19 Partikelkontamination- Nicht sichtbare Partikeln. *European Pharmacopoeia* 438–441 (2014).
8. Ratanji, K. D. *et al.* Subvisible aggregates of immunogenic proteins promote a Th1-type response. *Toxicol. Sci.* **153**, 258–270 (2016).
9. Joubert, M. K. *et al.* Highly aggregated antibody therapeutics can enhance the in vitro innate and late-stage T-cell immune responses. *Journal of Biological Chemistry* **287**, 25266–25279 (2012).
10. Ueda, T., Nakamura, K., Abe, Y. & Carpenter, J. F. Effects of Product Handling Parameters on Particle Levels in a Commercial Factor VIII Product: Impacts and Mitigation. *J. Pharm. Sci.* **108**, 775–786 (2018).
11. Nejadnik, M. R. *et al.* Postproduction Handling and Administration of Protein Pharmaceuticals and Potential Instability Issues. *J. Pharm. Sci.* **107**, 2013–2019 (2018).

Chapter 3

Materials and Methods

Parts of this chapter were published as research article in the Journal of Pharmaceutical Sciences as:

Teresa Kraus, Annika Lubitz, Ulrike Schließer, Christoph Giese, Jana Reuschel, Rene Brecht, Julia Engert, Gerhard Winter

Evaluation of a 3D Human Artificial Lymph Node as Test Model for the Assessment of Immunogenicity of Protein Aggregates

Journal of Pharmaceutical Sciences 108 (2019) 2358-2366

3.1 Materials

3.1.1 Monoclonal antibodies Adalimumab and Bevacizumab

Two monoclonal antibodies, Adalimumab and Bevacizumab, were kindly provided by ProBioGen (Berlin, Germany). Adalimumab was formulated in a buffer containing 14 mM phosphate, 7 mM citrate and 105 mM sodium chloride at pH 5.2. The initial concentration of the used Adalimumab batches was 45.1 mg/mL or 50.6 mg/mL. Bevacizumab was formulated in a 51 mM phosphate buffer at pH 6.2 at a concentration of 24.8 mg/mL or 16.6 mg/mL. Citric acid and sodium chloride were purchased from Bernd Kraft (Duisburg, Germany). Sodium citrate, disodium hydrogen phosphate and sodium dihydrogen phosphate were purchased from VWR International (Radnor, USA), AppliChem GmbH (Gatersleben, Germany) and Grüssing GmbH (Filsum, Germany), respectively. For the preparation of all buffers, highly purified water, generated by a PURELAB Plus instrument (USF Elga, Celle, Germany) was used. All buffers were sterile filtered using a 0.2 µm cellulose acetate filter (VWR International, Radnor, USA) before use. Prior to the exposure to different stress conditions, the antibody solutions were diluted to the desired concentration for the planned study and filled into cleaned, depyrogenized 10R vials. Finally, the vials were sealed with rubber stoppers and crimped.

The Bevacizumab batch used for the in-line filtration study (see Chapter 6) had an initial concentration of 26.1 mg/mL. For this experiment, a volume of 16 mL of the antibody solution was filled into cleaned and depyrogenized 20R vials, sealed with autoclaved rubber stoppers and crimped.

3.2 Methods used for the generation of protein aggregates

3.2.1 Light stress

For exposition of the samples to light, a Sunset CPS radiation chamber (Heraeus Holding, Hanau, Germany) was used. Radiation intensity was set to 55 ± 5 W/m². A xenon lamp was used as light source. The desired volume of the antibody solution was filled into 10R vials and positioned in the center of the radiation chamber. For the stress study (see Chapter 4), sampling was performed after 24 and 48 hours (only Adalimumab), four and seven days. For control experiments, only buffer was exposed to light as well as protein solution completely shielded with aluminum foil to control the influence of temperature increase (30-35°C) during exposure to light.

3.2.2 Stir stress

For stir stress, 10R glass vials were filled with the desired volume of the antibody solution. Polytetrafluorethylene (PTFE)–coated stir bars of a size of 10x3 mm and a Variomag multipoint stirrer

(Thermo Fisher Scientific, Schwerte, Germany) were used. Speed was set to 240 rpm, and the samples were stirred at room temperature for 4, 24 and 72 hours. For control experiments, pure buffer solution was treated using the same conditions.

3.2.3 Heat stress

Heat stress of Bevacizumab was performed in 10R glass vials filled with the desired volume of antibody solution. The vials were incubated in a cabinet dryer (Mettler, Schwabach, Germany) at a temperature of 50°C for up to 7 days. For the stress study (Chapter 4), sampling was performed after 24 hours, four, and seven days. For control experiments, pure buffer solution was exposed to heat using the same conditions.

3.2.4 Chemical oxidation stress using tert-butyl hydroperoxide (tBHP)

For the chemical oxidation, a volume of 10 mL of the antibody solution was incubated with 1 % tBHP, (Merck, Darmstadt, Germany) for 16 hours at room temperature and protected from light. The reaction was stopped by dialysis of the protein solution against a volume of 3L of the pre-cooled formulation buffer using a Slide-A-Lyzer® gamma irradiated dialysis cassette (Thermo Fisher Scientific, Waltham, USA) with a 10 kDa molecular weight cut-off. Dialysis was performed for 24 hours at room temperature. The buffer was exchanged after four and eight hours. Finally, the sample was filled into cleaned and depyrogenized vials, sealed with rubber stoppers and crimped.

3.3 Methods used for the analysis of protein aggregates

3.3.1 Turbidity

For turbidity measurements, a volume of 2 mL of the sample was measured by 90°C light scattering at $\lambda=860$ nm using a NEPHLA turbidimeter (Dr. Lange, Düsseldorf, Germany). Results are reported in formazine nephelometric units (FNU). Samples were not diluted for turbidity measurements and measured in triplicates.

3.3.2 Light Obscuration

Light obscuration was measured using a PAMAS-SVSS-C Sensor HCB-LD 25/25 (Partikelmess- und Analysensysteme GmbH, Rutesheim, Germany). Before each measurement, 0.3 mL of the sample were flushed through the system, afterwards three aliquots of 0.2 mL of each sample were analyzed. Between the measurements, the system was cleaned with highly purified water until less than 30 particles per mL could be detected. Particle numbers were calculated as mean value out of three

measurements, referring to a volume of 1 mL. Samples were not diluted for the measurements, if possible. If sample measurements were not possible due to high particle numbers, samples were diluted in order to reach the concentration range of the PAMAS.

3.3.3 Flow imaging microscopy

Particle numbers were also determined using a FlowCam® 8000 (Fluid Imaging Technologies, Inc., Scarborough, USA) with a 10x magnification. A volume of 200 µl of each sample was analyzed using a flow rate of 0.15 mL/min. After each measurement, the system was flushed with highly purified water and 2% Hellmanex® solution until the flow cell was free of particles. Particle numbers were calculated as mean value out of three measurements, referring to a volume of 1 mL. Data was evaluated using the VisualSpreadsheet® Software (Fluid Imaging Technologies, Inc., Scarborough, USA).

3.3.4 Dynamic light scattering (DLS)

A Malvern Zetasizer Nano ZS (Malvern, Herrenberg, Germany) was used for DLS measurements. Temperature was set to 25°C, and non-invasive backscattering at an angle of 173° was performed at 25°C using a Helium-neon-laser at 633 nm. The refractive index was set to 1.45 (aqueous protein solution). A volume of 700 µl of the antibody solution was measured in half-micro cuvettes made of polystyrene (Fisher Scientific, Schwerte, Germany). Some samples had to be diluted due to strong turbidity. All samples were measured in triplicates. Finally, the polydispersity index (PDI) and the Z-average diameter (Z_{ave}) were calculated using the Dispersion Technology Software (Version 7.0, Malvern).

3.3.5 Size exclusion chromatography (SEC)

Size exclusion chromatography measurements were conducted using a Waters system with UV detection (Waters GmbH, Eschborn, Germany). As solid phase a TSKgel G3000SWXL column (Tosoh Bioscience) or a YMC-Pack-Diol 300 (YMC Europe GmbH, Dinslaken) were used. The different columns provided equal resolution of the protein peaks and the change between the suppliers was justified by financial aspects. A PBS buffer containing 50 mM phosphate and 300 mM sodium chloride at pH 7.0 with a flow rate of 0.5 mL/min was used as mobile phase. In order to remove insoluble aggregates, samples were centrifuged at 5000 rpm for 10 min before injection. The injection volume for samples of the stress study described in Chapter 4 was 10 µl at a concentration of 4 mg/mL. Bevacizumab samples used for the in-line filtration study described in Chapter 6 were diluted 1 to 20 to a final concentration of 1.305 mg/mL and a volume of 20 µl was injected. Each sample was measured as duplicate. The area under the curve (AUC) of the unstressed sample was defined as 100%.

3.3.6 Protein A chromatography

Protein A chromatography measurements were conducted using a Waters system with UV detection (Waters GmbH, Eschborn, Germany). As solid phase, a PA ID Sensor cartridge (Life Technologies, Carlsbad, California, USA) was used. Solvent A was a Dulbecco's phosphate buffered saline (DPBS) 1x in water at pH 7.4. Solvent B contained 100 mM acetic acid and 150 mM NaCl at a pH of 2.8. After 10 minutes of 100% solvent A, the percentage of solvent B rose to 60% within 30 minutes. Within one minute the percentage was increased to 100% solvent B and was held for 10 minutes before the percentage of solvent B dropped again to 0% within one minute. Samples were measured at a concentration of 26.1 mg/mL. In order to remove insoluble aggregates, samples were centrifuged at 14 000 rpm for 10 min before injection. The injection volume was 10 µl and each sample was measured as triplicate. As a positive control, Bevacizumab at a concentration of 26.1 mg/mL was incubated with 2% tert-butyl hydroperoxide (tBHP) for 56 hours to create a fully oxidized sample. The area under the curve (AUC) of the unstressed sample was defined as 100%.

3.3.7 Ion exchange chromatography (IEX)

To detect the influence of heat and stir stress on the charge variants of Bevacizumab, ion exchange chromatography (IEX) was performed according to Farnan *et al.*¹. IEX was performed using a Waters 2695 Separation Module coupled to a Waters 2487 Dual λ Absorbance Detector (Waters GmbH, Eschborn, Germany). For separation, a 4 mm x 50 mm Dionex ProPac® WCX-10G guard column was connected to an analytical 4 mm x 250 mm Dionex ProPac® WCX-10 column. A volume of 50 µl of each sample at a concentration of 1 mg/mL was injected. Mobile phase A contained Trizma Base® (2.4 mM), imidazole (1.5 mM) and piperazine (11.6 mM) at a pH of 6.0. Mobile phase B contained Trizma Base® (2.4 mM), imidazole (1.5 mM), piperazine (11.6 mM), and 20 mM NaCl at a pH of 9.5. The flow rate was set to 1 mL/min. The gradient of mobile phase B is graphically illustrated in Figure 3-1.

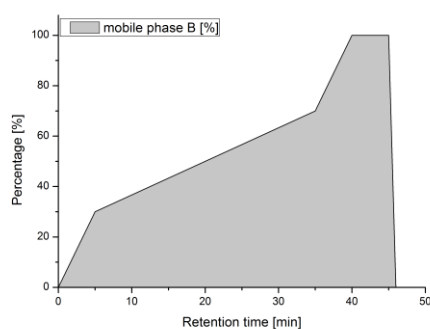


Figure 3-1 Gradient of mobile phase B for IEX measurements of Bevacizumab.

3.3.8 Fourier transform infrared spectroscopy (FT-IR)

Native and stressed protein samples were analyzed using a Bio ATR II unit of a Tensor 27 spectrometer (Bruker Optics GmbH, Ettlingen, Germany). The samples were not diluted for the measurements. Temperature was set to 20°C. Spectra were collected from 4000 cm^{-1} to 1000 cm^{-1} with a resolution of 4 cm^{-1} . Scans (120 in total) were averaged for each sample measurement. Each spectrum was background corrected and vector normalized by the OPUS software (Version 7.5, Bruker Optics, Ettlingen, Germany). Second derivatives were calculated and smoothened on 17 points.

3.3.9 Extrinsic fluorescence spectroscopy

Extrinsic protein fluorescence measurements were conducted using a Varian Cary Eclipse fluorescence spectrometer (Varian, Inc., Darmstadt, Germany). Bis-ANS (4,4'-Dianilino-1,1'-binaphthyl-5,5'-disulfonic acid) at 20 μM concentration was used as fluorescent dye. Samples were diluted to a concentration of 0.5 mg/mL or 1 mg/mL and measured in triplicates in black 96-well plates (Nunc, Denmark), using a volume of 200 μl for each well. In order to remove the insoluble aggregates, samples were centrifuged at 5000 rpm for 10 minutes before pipetting into the well plate (only for samples of the stress study (Chapter 4)). Temperature was set to 20°C. The excitation wavelength was set to 385 nm, the excitation slit was fixed at 5 nm. Emission was recorded from 395 nm to 600 nm using a 5 nm emission slit. Scanning rate was set to 120 nm/min or 30 nm/min and the voltage of the photomultiplier was set to 800V. The mean spectrum of each triplicate was calculated.

3.3.10 Intrinsic fluorescence spectroscopy

Intrinsic protein fluorescence measurements were conducted on a Varian Cary Eclipse fluorescence spectrometer (Varian, Inc., Darmstadt, Germany). Temperature was set to 20°C. The samples were diluted to a concentration of 1 mg/mL and measured in triplicates in black 96-well plates (Nunc, Denmark), using a volume of 200 μl for each well. In order to remove the insoluble aggregates, samples were centrifuged at 5000 rpm for 10 minutes before pipetting the sample into the well plate (only for samples of the stress study (Chapter 4)). The excitation wavelength was set to 295 nm and the excitation slit was fixed at 10 nm. Emission was recorded from 300 to 500 nm using a 5 nm emission slit. The scanning rate was set to 30 nm/min and the voltage of the photomultiplier was set to 800 V. The mean spectrum of each triplicate was calculated.

3.4 Endotoxins

3.4.1 Endochrome - K® Test

The endotoxin content of the samples was tested using a Limulus Amebocyte Lysate Endosafe Endochrome-K® Test (Charles River, Wilmington, USA). The samples were prepared and analyzed according to the manufacturer's instruction. The absorbance was measured at 405 nm and 37°C using a FLUOstar Omega (BMG Labtech, Ortenberg, Germany). Prior to testing in the HuALN, all samples were diluted to a concentration of 1 mg/mL and 0.5 mg/mL, respectively. Therefore, we accepted an upper limit of endotoxins of 3 EU/mL in the undiluted samples. The endotoxin levels of all samples were found to be below this limit.

3.4.2 Endosafe® - PTS Device

The endotoxin levels of the Bevacizumab samples for the in-line filtration studies were detected using an ENDOSAFE®- PTS device (Charles River, Wilmington, USA). The test was performed according to the manufacturer's instruction. The cartridges had a sensitivity range of 0.5 - 0.005 EU/mL and all samples had to be diluted 1:20 for the measurement. The endotoxin levels of all samples were found to be below the limit of 3 EU/mL.

3.5 Methods used for the evaluation of immunogenicity of protein aggregates in a 3D human artificial lymph node model (Chapter 5)

3.5.1 Generation of protein aggregates

For the generation of protein aggregates, the two monoclonal antibodies were exposed to light, mechanical and heat stress for a defined time as described in Table 3-1. A volume of 4 mL (2D *in vitro* assay) or 6 mL (HuALN) of the protein solution were filled into 10R vials (MGLas AG, Műnnerstadt, Germany), respectively, sealed with rubber stoppers (West Pharmaceutical Services, Exton, USA) and crimped. Adalimumab at a concentration of 20 mg/mL (2D *in vitro* assay) or 45.1 mg/mL (HuALN) and Bevacizumab at a concentration of 10 mg/mL (2D *in vitro* assay) or 24.8 mg/mL (HuALN) were exposed to light for 48h and 24h, respectively. Light stress was performed in a Sunset CPS radiation chamber (Heraeus Holding, Hanau, Germany) using a xenon lamp as light source. The radiation intensity was set to $55 \pm 5 \text{ W/m}^2$. To generate aggregates by mechanical stress, the samples were stirred using 10x3 mm sized polytetrafluorethylene (PTFE)–coated stir bars on a Variomag multipoint stirrer (Thermo Fisher Scientific, Schwerte, Germany) at 240 rpm for 24h. Bevacizumab was additionally exposed to heat for 4 days in a cabinet dryer (Mettmert, Schwabach, Germany) at 50°C.

Table 3-1: Overview of samples tested in the human artificial lymph node model.

Protein	Sample	Stress conditions	Duration
Adalimumab			
	Unstressed ¹	-	-
	Light stress	$55 \pm 5 \text{ W/m}^2$	48h
	Stir stress	240 rpm	24h
	Formulation buffer ²	-	-
Bevacizumab			
	Unstressed ¹	-	-
	Light stress	$55 \pm 5 \text{ W/m}^2$	24h
	Stir stress	240 rpm	24h
	Heat stress	50°C	4 days

¹ "Unstressed" = Unstressed protein solution; ² "Formulation buffer" = Formulation buffer only (no protein in sample).

3.5.2 Extrinsic fluorescence spectroscopy

Extrinsic protein fluorescence measurements were conducted using a Varian Cary Eclipse fluorescence spectrometer (Varian, Inc., Darmstadt, Germany). Bis-ANS (4,4'-Dianilino-1,1'-binaphthyl-5,5'-disulfonic acid) at 20 μM concentration was used as fluorescent dye. Samples were diluted to a

concentration of 1 mg/mL and measured in triplicates in black 96-well plates (Nunc, Denmark), using a volume of 200 µl for each well. For instrument settings see section 3.3.9.

3.5.3 Fourier transform infrared spectroscopy (FT-IR)

Native and stressed protein samples were analyzed at 24.8 mg/mL (Bevacizumab) or 45.1 mg/mL (Adalimumab) using a Bio ATR II unit of a Tensor 27 spectrometer (Bruker Optics GmbH, Ettlingen, Germany). For instrument settings see section 3.3.8.

3.5.4 Size exclusion chromatography

Size exclusion chromatography measurements were performed using a Waters system with UV detection at 280 nm (Waters GmbH, Eschborn, Germany). As solid phase a YMC-Pack-Diol 300 (YMC Europe GmbH, Dinslaken) was used. A PBS buffer containing 50 mM phosphate and 300 mM sodium chloride at pH 7.0 at a flow rate of 0.5 mL/min was used as mobile phase. Samples were diluted to a concentration of 1.24 mg/mL (Bevacizumab, 1:20 dilution) and 1.13 mg/mL (Adalimumab, 1:40 dilution), respectively. In order to remove insoluble aggregates, samples were centrifuged before injection. The injection volume was 20 µl, and each sample was measured in duplicates.

3.5.5 Cell preparation

Cells were prepared as described previously^{2,3}. Briefly, PBMCs were isolated from leukapheresis material by density gradient centrifugation. The monocytes were further isolated by CD14-magnetic bead separation and differentiated into iDCs using rhIL-4 and rhGM-CSF (Miltenyi Biotec GmbH, Bergisch Gladbach, Germany). After 6 days of cultivation, differently stressed samples of Bevacizumab and Adalimumab ('stressed antibody samples') were added to iDC culture for 24h. Generated DCs were tested by a panel of DC markers (CD80, CD83, CD86, HLA-DR, HLA-ABC; Miltenyi Biotec GmbH, Bergisch Gladbach, Germany) according to the manufacturer's protocol. The CD14-negative fraction (CD14⁻ PBMCs) was stored cryopreserved for later use.

ATSVF cells (Adipose tissue stromal vascular fraction/Human Stromal Vascular Fraction; Pelobiotec GmbH, Planegg, Germany) were differentiated into Fibroblastic reticular cells (FRC)-like cells using a 10-day protocol. ATSVF cells were stimulated with 100 ng/ml Lymphotoxin $\alpha 1\beta 2$ (R&D Systems Inc., Minnesota, USA) and 10 ng/ml TNF- α (Miltenyi Biotec GmbH, Bergisch-Gladbach, Germany) for 10 days to induce Fibroblastic reticular cells (FRC)-like development as described previously⁴.

3.5.6 2D cell culture experiments

Differently stimulated DCs and CD14⁻ PBMCs were seeded into multiwell-compartments (1:10) (n=2) at a total density of 2.75×10^6 /ml, supplemented with stressed antibody samples (0.05 mg/ml, 0.5 mg/ml, 5 mg/ml Bevacizumab and 0.1 mg/ml, 1 mg/ml, 10 mg/ml Adalimumab) and cultivated for 48h including controls lacking one of the two cell fractions as well as negative control (w/o any supplement) and positive control (IL-1 β , IL-6, TNF α at 10 ng/ml and PGE2 at 1 μ g/ml). A co-culture control was stimulated with 2 mg/mL Concanavalin A (ConA) (Sigma, Taufkirchen, Germany). Supernatant volumes of 100 μ l each were collected for cytokine analysis (see End point analysis). Cells were harvested with PBS + 2 mM EDTA (Fisher Scientific, Loughborough, UK) and analyzed by flow cytometry (DC marker: see Cell preparation; Co-culture marker: CD3, CD4, CD8, CD25, CD69 (Miltenyi Biotec GmbH) and EdU (EdU DetectPro Cell Proliferation Flow Cytometry Kit, Baseclick GmbH, Neuried, Germany, according to suppliers' protocol). Supernatant from DC culture and co-cultures were collected and analyzed for cytokine levels (IL-2, IL-4, IL-1 β , IL-6, IL-8, IL-10, IL-12p70, IL-13, IFN- γ , TNF- α) using V-PLEX Proinflammatory Panel 1 Human Kit (Meso Scale Diagnostics, Rockville, Maryland, USA) on MESO QuickPlex SQ 120 as described in the supplier's technical note.

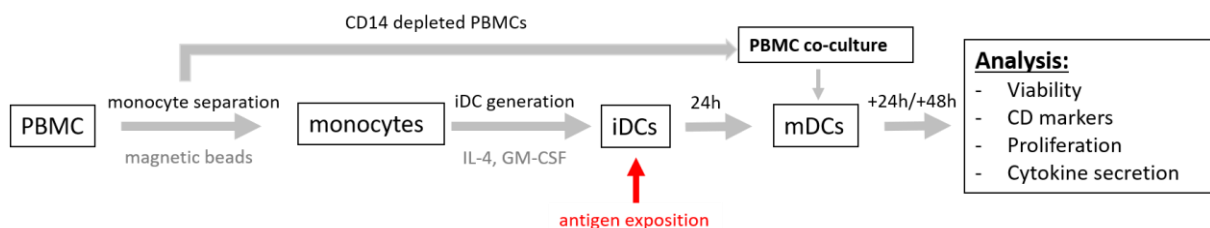


Figure 3-2: Schematic illustration of the DC/T-cell assay used in this study. PBMCs were isolated from human blood and monocytes were isolated by magnetic bead separation. Immature dendritic cells were generated by cultivation with IL-4 and GM-CSF. Finally, immature dendritic cells were stimulated with the desired antigen, incubated and CD14 depleted PBMCs were added to obtain a co-culture. After incubation, cells and culture supernatants were analyzed. PBMC: Peripheral mononuclear cells; iDC: immature dendritic cells; mDCs: mature dendritic cells.

3.5.7 Human artificial lymph node (HuALN) bioreactor experiments

The HIRISTMIII bioreactor² enables high-density matrix-assisted cultures of more than 1×10^8 cells/bioreactor including a large T cell repertoire. The bioreactor culture was already described before³. Briefly, each bioreactor was inoculated with 1×10^7 DCs, 1.5×10^8 autologous CD14⁻ PBMCs (1:15) and 5×10^5 stromal cells split in two sheets of RGD-dextran hydrogel matrix (Cellendes GmbH, Reutlingen, Germany) as recommended by the supplier. Medium perfused the bioreactor system at a rate of 1 mL/day and filled the incorporated sample reservoir. The HuALN system was initially stimulated with unstressed or stressed antibody samples (0.5 mg/ml Bevacizumab, 1 mg/ml Adalimumab) and re-stimulation on day 7, 14, and 21 included in addition freshly prepared dendritic cells. Bioreactor culture time was 28 days.

3.5.8 In-process controls and end point analyses

Cell culture supernatant was collected daily from the bioreactor reservoir, subsequently aliquoted, and stored at -20°C. Samples were subject to cytokine analysis (as described above). On the day of harvest, matrix sheets were removed from the bioreactor and digested by dextranase 1:200 in PBS (Cellendes GmbH, Reutlingen, Germany) for 1h at 37°C. Cell number and viability was determined (ViCell, Beckman Coulter) as well as CD marker expression using flow cytometry (MACS Quant, Miltenyi Biotec GmbH, Bergisch Gladbach, Germany).

3.5.9 Analysis of HuALN culture experiments

Analyzed supernatant cytokine levels were displayed as time response over the entire culture time of 28 days. The area under curve was calculated using the linear trapezoidal rule method for every single cytokine profile over the time (OriginLab Version 8.1 Integration). The curve was divided into pieces and the software calculates the sum of each trapezoid to estimate the integral by

$$\int_{x_1}^{x_n} f(x)dx \approx \sum_{i=1}^{n-1} (x_{i+1} - x_i) \frac{1}{2} [f(x_{i+1}) + f(x_i)]$$

This AUC value was calculated for each run, and each cytokine profile and subsequently normalized to the control run, which was in this case the unstressed antibody sample. Values below 1 indicate downregulation of the particular cytokine compared to the control, whereas values larger than 1 imply an upregulation. In a next step, the sum of the normalized values (AUC*) from different cytokines belonging to one or more of 4 selected groups as shown in Table 3-2 which are pro-inflammatory immune response (Pro-inf), anti-inflammatory immune response (Anti-inf), T helper cell 1 (TH1) and T helper cell 2 (TH2) immune response, was calculated. Afterwards the sums were divided by the number of cytokines within the current group resulting in values of 1 for the control run and values larger or smaller than 1 for every other run. Visualizing these values in a spider grid diagram allows recognizing the overall effect of the drug in a simplified way. The drug either promotes or suppresses the immune reaction of the HuALN in a specific direction. For further explanation, see Figure 3-3.

Table 3-2: Cytokine groups: analyzed cytokines are classified to groups based on their immunological function for a simplified analysis of immune responses in HuALN bioreactors.

Groups	Assorted cytokines
Pro-inflammatory	IL-1 β
	IL-6
	IFN- γ
	TNF- α
Anti-inflammatory	IL-6
	IL-10
TH1	IL-2
	IL-12p70
	IFN- γ
	TNF- α
TH2	IL-4
	IL-6
	IL-10
	IL-13

$^{IFN}AUC_c$ $^{IFN}AUC_{drug1}$ $AUC^*_c = ^{IFN}AUC_c / ^{IFN}AUC_c = 1$ $AUC^*_{drug1} = ^{IFN}AUC_{drug1} / ^{IFN}AUC_c = x$ <p>Example:</p> $q_{Th1} = (IL-1\beta AUC^*_{drug1} + IL-6 AUC^*_{drug1} + IFN\gamma AUC^*_{drug1} + TNF\alpha AUC^*_{drug1}) / z_{Th1}$	<p>c = control run (unstressed antibody sample)</p> <p>AUC = area under curve of the specified cytokine</p> <p>AUC* = normalized AUC</p> <p>z = number of cytokines in group</p> <p>q = extent of immune response</p>
--	---

Figure 3-3: Additional formula for the explanation of the applied method for cytokine evaluation. AUCs are derived from cytokine profiles over time, which are normalized and then merged into groups before visualization.

3.5.10 Analysis of anti-drug antibodies (ADAs)

Anti-drug antibodies were analyzed via a bridging ELISA assay (see Figure 3-4), which was performed using MSD Gold 96-well-Streptavidin Quickplex plates (MSD, Kenilworth, USA). The ADA assays for Adalimumab and Bevacizumab were established according to the manufacturer's instructions (MSD, Kenilworth, USA) and performed at ProBioGen (Berlin, Germany). For analyzing ADAs in the cell culture supernatants, a volume of 50 μ l of master mix (containing biotinylated drug and SULFO-TAG labeled drug mixture) and 25 μ l of sample or standard were added to each well of a non-binding 96-well plate,

accordingly. The plate was sealed and incubated for 1-2 hours at room temperature with moderate shaking or incubated overnight at 4°C. During the master mix incubation, a volume of 150 µl of blocking solution was added to each well of the streptavidin gold plate. The plate was sealed and incubated for at least 30 minutes at room temperature. Subsequently, the blocking solution was removed from the streptavidin gold plate and the plate was washed with washing buffer. A volume of 50 µl from each well of the “pre-incubation” plate with the master mix was transferred to the streptavidin gold plate. The plate was sealed and incubated for one hour at room temperature shaking at 300-700 rpm. Subsequently, the plate was washed three times with at least 200 µl of wash buffer per well. A volume of 150 µl per well of 2x read buffer T was added and finally, the electrochemoluminescence was measured on a Meso Quickplex SQ120 (MSD, Kenilworth, USA). A standard curve with concentrations of 2500 ng/mL, 625 ng/mL, 156.25 ng/mL, 39.06 ng/mL, 9.77 ng/mL, 2.44 ng/mL and 0.61 ng/mL for Adalimumab and Bevacizumab was monitored, accordingly, and concentrations of anti-drug antibodies were calculated using DISCOVERY WORKBENCH 4.0.

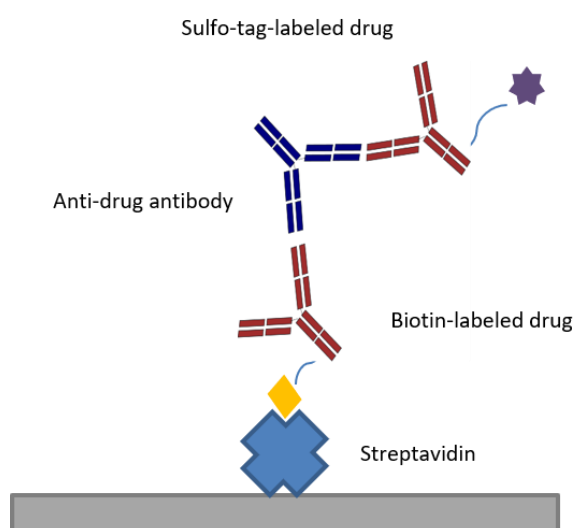


Figure 3-4: Schematic overview of a bridging ELISA assay.

3.5.11 Investigations on the diffusion behavior of fluorescent particles through a 3D Life dextran-CD hydrogel using a Franz Cell model

3.5.11.1 Materials and set-up

Green fluorescence microsphere suspensions of particles at a concentration of 10 mg/mL and a size of 26 nm and 2 µm (Distrilab Particle Technology B.V., Leusden, Netherlands) were used as model particles. The experiment was performed using a Franz Cell model (see Figure 3-5) with PBS Buffer (SIGMA Aldrich, St. Louis, Missouri, USA) as acceptor medium. The Franz Cell was tempered at 37°C and sampling was performed after 24, 48, 72 hours and 4 days or after 24, 48, 72 hours, 6 and 7 days. As controls, cellulose acetate membranes with a cut-off of 0.2 µm and 5 µm were used. An amount of

5 mg of particles was pipetted on top of the membrane or gel, respectively. In order to obtain a homogenous distribution of particles in the acceptor medium, a stir bar was added to the Franz Cell. The Franz Cells were placed on a magnetic stirrer (Thermo Fisher Scientific, Waltham, USA), and rotation speed was set to 200 rpm.

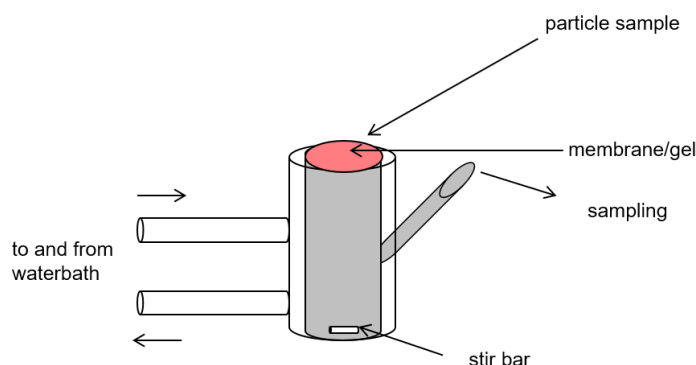


Figure 3-5: Schematic drawing of a Franz Cell model used for this experiment.

3.5.11.2 Preparation of 3D Life Dextran–CD hydrogel SG

The components and its concentrations of the used 3D Life Dextran-CD Hydrogel (Cellendes, GmbH, Reutlingen, Germany) are listed in Table 3-3. According to the manufacturer's instructions, water, 10xCB and the SG-polymer (SG-Dextran) were pipetted into a reaction tube and mixed well by pipetting up and down. The RGD-peptide (thiol-peptide) was added and mixed immediately. The sample was incubated for 20 minutes at room temperature. Finally, the cross-linker (CD-Link) was added and the mixture was pipetted up and down few times before the gel was placed in a custom-made teflon mold within one minute. The diameter of the dextran gel was 30 mm with a height of 2 mm. The gel was incubated at least for 10 minutes at room temperature to allow the gel to solidify. The solidified gel was subsequently used for the experiment.

Table 3-3: Overview of components and concentrations used for the preparation of the 3D Life dextran-CD hydrogel SG.

Component	Stock concentration [mMol/L]	Final concentration [mMol/L]
Thiol-reactive polymer	30	2.5
Crosslinker	20	2
Thiol-peptide	20	0.5
Thioglycerol	0	-

3.5.11.3 Analysis of acceptor medium by fluorimetry

The concentration of fluorescent particles diffused to the acceptor medium was determined using fluorescence spectroscopy. Measurements were performed on a Varian Cary Eclipse fluorescence spectrometer (Varian, Inc., Darmstadt, Germany). The excitation wavelength was set to 468 nm and the excitation slit was fixed at 5 nm. The emission wavelength was set to 508 nm using a 2.5 nm

emission slit. The voltage of the photomultiplier was set to 600V. Samples were measured in triplicates. In order to calculate the particle concentration in the samples, calibration curves were measured for 26 nm and 2 μ m particles, respectively (Figure 3-6). Finally, the yield was calculated and displays the particle concentration in % relative to the applied particle amount in mg.

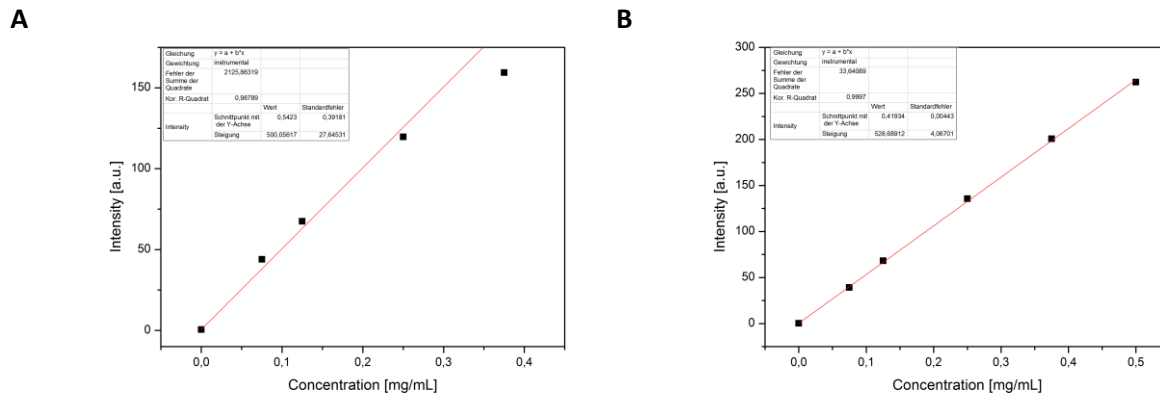


Figure 3-6: Calibration curves for 2 μ m (A) and 26 nm (B) fluorescent particles in PBS.

3.5.11.4 Analysis of 3D Life Dextran-CD hydrogel SG by microscopy

On the last day of the experiments, the hydrogels were washed with PBS until the washing solution was clean (determined by fluorescence spectroscopy, see 3.5.11.3) and analyzed using a Keyence BZ8100 Fluorescence microscope (Keyence, Osaka, Japan) equipped with a Nikon SPlan Fluor 20x/0.45 objective (Nikon, Japan). The gel was screened from the top to the bottom and photographs were taken.

3.6 Methods used for investigating the effect of in-line filtration on immunogenicity (Chapter 6)

3.6.1 In-line filtration process used for the evaluation of immunogenicity in a 3D human artificial lymph node model

For the analysis of the filtered samples, a volume of 4 mL of the heat stressed and stir stressed samples was filtered using PharmAssure® syringe filters (Pall Corporation, New York, USA) with a pore size of 0.2 μ m. For evaluating the effect of in-line filtration in the human artificial lymph node model, a volume of about 1 mL was filtered directly prior to the stimulation of the dendritic cells or the human artificial lymph node model using PharmAssure® syringe filters (Pall Corporation, New York, USA) with a pore size of 0.2 μ m. The unstressed protein solution was also filtered using a PharmAssure® filter (Pall Corporation, New York, USA) with a pore size of 0.2 μ m.

3.6.2 In-line filtration process used for the evaluation of immunogenicity in a 2D dendritic cell assay

For the analysis of unstressed and stressed Bevacizumab and for testing the effect of in-line filtration in a 2D dendritic cell assay, the desired samples were filtered using an Acrodisc® syringe filter (Pall Corporation, New York, USA) with a pore size of 0.2 µm directly prior to cell stimulation or analysis of the filtered samples.

3.6.3 Hold-up volume PharmAssure® filter

In order to determine the hold-up volume of the used PharmAssure® syringe filter (Pall Corporation, New York, USA), a volume of 2 mL formulation buffer was filtered by a PharmAssure® filter. The filtrate was weighed prior to and after filtration. To optimize the hold-up volume, 6 mL of air were filtered through the used filter and the mass of the filtrate was determined again after purging a volume of 3 mL of air and after reaching the bubble point.

3.6.4 Hold-up volume Acrodisc® filter

The hold-up volume was also determined for the Acrodisc® syringe filter (Pall Corporation, New York, USA). A volume of 2 mL formulation buffer was filtered by an Acrodisc® filter and the filtrate was weighed prior to and after filtration. To optimize the hold-up volume, a volume of 1 mL of air was purged through the used filter and the mass of the filtrate was determined again.

3.6.5 Filter quality PharmAssure® filter

To ensure the quality of the PharmAssure® filters (Pall Corporation, New York, USA), a solution of a monoclonal antibody at a concentration of 25 mg/mL was stirred with a 10x3 mm sized PTFE-coated stir bar and a Variomag multipoint stirrer (Thermo Fisher Scientific, Schwerte, Germany) for 24 hours. The speed was set to 240 rpm. The stressed protein solution was subsequently filtered with ten PharmAssure® filters (Pall Corporation, New York, USA) and particle numbers were determined by light obscuration using a PAMAS-SVSS-C Sensor HCB-LD 25/25 (Partikelmess- und Analysensysteme GmbH, Rutesheim, Germany). Before each measurement, 0.3 mL of the sample were flushed through the system, afterwards three aliquots of 0.2 mL of each sample were analyzed. Between the measurements, the system was flushed with highly purified water until the system was clean. Particle counts were calculated as mean value out of three measurements, referring to a volume of 1 mL.

3.6.6 Methods used for the evaluation of immunogenicity using a 2D dendritic cell assay

3.6.6.1 Isolation of mononuclear cells from human peripheral blood by density gradient centrifugation

Human blood (approx. 7.5 mL) was transferred to a 50 mL falcon tube and diluted with 27.5 mL (total volume of diluted blood sample 35 mL) of pre-cooled (2-8°C) PBS buffer containing 2 mM EDTA at pH 7.2. The diluted cell suspension was carefully layered over 5 mL Ficoll-Paque® Reagent (GE Healthcare, Uppsala, Sweden) and centrifuged at 400xg for 30 minutes at 20°C in a swinging-bucket rotor without brake. After aspirating the upper layer, the interphase containing lymphocytes, monocytes and thrombocytes was transferred to a new Falcon tube (50 mL). The tube was filled with PBS buffer containing 2 mM EDTA to a total volume of 50 mL and centrifuged at 300xg for 10 minutes at 20°C. The supernatant was removed completely. For the removal of platelets, the cell pellet was resuspended in 50 mL of PBS buffer containing 2 mM EDTA and subsequently centrifuged at 200xg for 10 minutes at 20°C. The washing step was repeated once, and the supernatant was removed completely. Finally, the cell pellet was resuspended in 20 mL of MACS buffer (PBS incl. 2 mM EDTA and 0.5% BSA at pH 7.2) for the isolation of CD14 positive cells from PBMCs.

3.6.6.2 Isolation of CD14 positive cells from PBMCs and differentiation of Mo-DCs

After determining the cell number, the cell suspension was centrifuged at 300xg for 10 minutes and the supernatant was removed completely. The cell pellet was resuspended in 80 µl of buffer containing 2 mM EDTA and 0.5% BSA at pH 7.2 per 10^7 total cells. A volume of 20 µl of CD14 Microbeads (Miltenyi Biotech, Bergisch-Gladbach, Germany) per 10^7 total cells was added, mixed well and incubated for 15 minutes at 2-8°C. Finally, cells were washed by adding 1 mL of MACS buffer per 10^7 cells and centrifuged at 300xg for 10 minutes. The supernatant was removed completely and up to 10^8 cells were resuspended in 500 µl of buffer. The magnetic separation was performed using LS columns (Miltenyi Biotech, Bergisch-Gladbach, Germany). The column was placed in the magnetic field and washed with 3 mL MACS buffer. Subsequently, the cell suspension was added to the column. To collect the unlabeled fraction, 3x3 mL MACS buffer were passed through the column. Finally, the column was removed from the magnetic field and placed on a 15 mL falcon tube. A volume of 5 mL of MACS buffer was pipetted onto the column and immediately flushed out by pushing the plunger into the column. The cell number was determined, and cells were seeded at a density of 10^7 cells per 10 mL Mo-DC differentiation medium (Miltenyi Biotech, Bergisch-Gladbach, Germany) in T-75 flasks (10 mL cell suspension per T-75 flask). Cells were incubated for two days at 37°C and 5% CO₂. After two days, a volume of 10 mL of Mo-DC Differentiation medium (Miltenyi Biotech, Bergisch-Gladbach, Germany) was added to each flask and mixed well. Cells were incubated for further four days at 37°C and 5% CO₂. On day 6, cells were used for cell experiments.

3.6.6.3 Activation of iDCs for analysis of cytokines and DC Marker

Immature Mo-DCs were harvested on day 6. The cell suspension of the flasks was transferred into a 50 mL Falcon tube. In order to remove adherent cells, a volume of 20 mL of PBS buffer containing 2 mM EDTA was added to the flask and incubated for 15 minutes at 37°C. Cells were centrifuged at 300xg for 5 minutes. The supernatant was removed, and cell pellets were resuspended in cell culture medium (RPMI 1640 medium containing 10 % Human AB serum). The cell number was determined. 200 000 cells per well were seeded in a 96-well plate (200 µl of a 10⁶ cells/mL suspension). Cells were stimulated with different formulations at a concentration of 0.5 mg/mL. LPS at concentration of 3 µg/mL was used as a positive control and cell culture medium only was used as negative control. The well plate was incubated at 37°C and 5% CO₂ for 22 hours.

3.6.6.4 Analysis of DC Marker

After 22 hours of incubation, cell supernatants were transferred into 1.5 mL tubes and centrifuged at 300xg for 10 minutes. In order to remove adherent cells 200 µl/well of PBS buffer containing 2 mM EDTA were added to the flask and incubated for 15 minutes at 37°C. The supernatants of the centrifuged samples were transferred into new 1.5 mL tubes and subsequently stored at -80°C for cytokine analysis. The cell pellets were washed with a PBS buffer containing 2 mM EDTA and centrifuged at 300xg for 10 minutes. Supernatants were carefully discarded, and cell pellets were resuspended in 100 µl of a PBS buffer containing 0.5% BSA and 2 mM EDTA. Finally, the antibodies CD 80, CD 83, CD 86 and HLA –DR were added in amounts recommend by the manufacturer (Miltenyi Biotech, Bergisch-Gladbach, Germany). All samples were mixed well and incubated in the dark a 2-8°C for 10 minutes. After incubation a volume of 1 mL of buffer was added to each tube and centrifuged at 300xg for 10 minutes. The supernatant was aspirated completely, and the cell pellets were resuspended in 500 µl of buffer and stored at 2-8°C until measurement (samples were measured on the same day).

3.6.6.5 Analysis of cytokines using MACSPlex Cytokine Basic Kit

Cytokines were analyzed using a MACSPlex Cytokine Basis Kit (Miltenyi Biotech, Bergisch Gladbach, Germany). First, the MPx Cytokine 12 Standard was prepared. The stock solution had a concentration of 10 000 pg/mL and was diluted with MACSPlex buffer, respectively, to obtain different concentrations: 2 000 pg/mL, 400 pg/mL, 80 pg/mL, 16 pg/mL, 3.2 pg/mL. MACSPlex buffer was kept as blank control (0 pg/mL). Cell culture supernatants were centrifuged at 10 000xg for 10 minutes at 4°C and transferred into a new tube. A volume of 50 µl of each standard and sample was pipetted into the corresponding 1.5 mL tubes. MPx Capture Beads (Miltenyi Biotech, Bergisch Gladbach, Germany) of IL-10, IL-6, TNF-α and IFN-γ were mixed and diluted according to the manufacturer's instructions and a volume of 20 µl of diluted MPx Capture Beads (Miltenyi Biotech, Bergisch Gladbach, Germany)

was added to each tube. The samples were incubated for two hours protected from light on an orbital shaker (450 rpm). After washing twice with 500 μ l MACSPlex buffer, 80 μ l of diluted MACSPlex detection reagent were added to each tube (mixed and diluted according to manufacturer's instructions). The samples were incubated for one hour protected from light on an orbital shaker (450 rpm). The washing steps were repeated and a volume of 400 μ l of MACSPlex buffer was added to each tube. Samples were analyzed by flow cytometry (Attune NxT flow cytometer, Thermo Fisher Scientific, Waltham, USA). Data was evaluated using Flowlogic™ and Beadlogic™ Softwares (Miltenyi Biotech, Bergisch Gladbach, Germany).

3.7 Methods used to investigate the particle burden in biologics (Chapter 7)

3.7.1 Materials

3.7.1.1 Monoclonal antibody IgG₁

A lyophilized monoclonal antibody IgG₁ was used as model protein. The antibody was formulated in a buffer containing 0.02 mol/L histidine, 0.21 mol/L trehalose, 0.01 mol/L methionine and 0.04% polysorbate. A volume of 1.25 mL of the stock solution (equal to 150 mg antibody) of the monoclonal antibody was lyophilized on a Christ Epsilon 2-6D freeze dryer (Martin Christ Gefriertrocknungsanlagen GmbH, Osterode am Harz, Germany) using a conventional lyophilization cycle (see Figure 3-7). The lyophilized antibody was reconstituted by adding 7.2 mL water for injections and waiting for five minutes. Subsequently, the turbidity and the number of particles in the reconstituted solution was measured. Finally, the reconstituted antibody was filtered using a 0.2 μ m Acrodisc® filter (Pall Corporation, New York, USA) and turbidity and particles numbers were analyzed again. In addition, the lyophilized monoclonal antibody was stored at 2-8°C for six months and particle numbers directly after reconstitution and after an additional in-line filtration step were analyzed again.

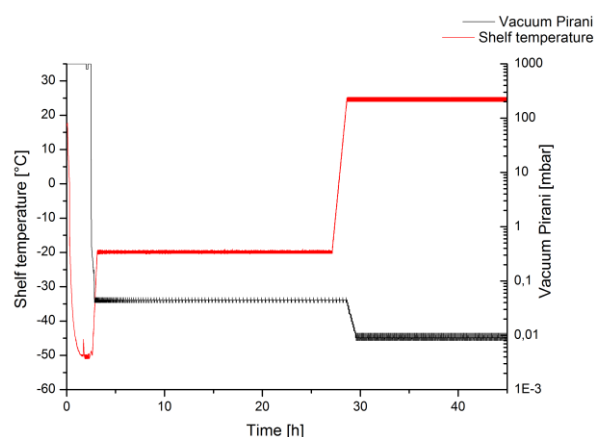


Figure 3-7 Lyophilization cycle applied to the solution of the model monoclonal antibody IgG₁.

3.7.1.2 Marketed lyophilized products

3.7.1.2.1 Actilyse®

Actilyse® (Boehringer Ingelheim, Ingelheim am Rhein, Germany) contains an amount of 10 mg of lyophilized Alteplase. The product was reconstituted in a volume of 10 mL of water for injection according to the manufacturer's technical information. The final concentration of the reconstituted Alteplase solution was 1 mg/mL. After analyzing the turbidity and the number of subvisible and submicron particles of the reconstituted protein, the solution was filtered using an Acrodisc® syringe filter with a diameter of 13 mm and a pore size of 0.2 µm (Pall Corporation, New York, USA), and turbidity and particles numbers were analyzed again.

3.7.1.2.2 Gammagard®

Gammagard® (Shire Pharmaceuticals, Lexington, Massachusetts, USA) contains an amount of 5 g of human immunoglobulin per vial. The protein was reconstituted according to the technical information. A volume of 96 mL water for injection was added to achieve a final protein concentration of 50 mg/mL. After analyzing the turbidity and the number of subvisible and submicron particles of the reconstituted protein, the solution was filtered using an Acrodisc® syringe filter with a diameter of 13 mm and a pore size of 0.2 µm (Pall Corporation, New York, USA) and turbidity and particles numbers were analyzed again.

3.7.1.2.3 Flixabi®

Flixabi® (Samsung Bioepis NL B.V., Delft, Netherlands) contains an amount of 100 mg of the monoclonal antibody Infliximab. The protein was reconstituted according to the technical information by adding a volume of 10 mL water for injection and waiting for five minutes. After analyzing the turbidity and the number of subvisible and submicron particles of the reconstituted protein, the solution was filtered using an Acrodisc® syringe filter with a diameter of 13 mm and a pore size of 0.2 µm (Pall Corporation, New York, USA) and turbidity and particles numbers were analyzed again.

3.7.1.3 Marketed liquid products

The products Pulmozyme®, containing Dornase alfa at a concentration of 1 mg/mL (Genentech, South San Francisco, California, USA), Beriglobin®, containing human immune globulin at a concentration of 160 mg/mL (CSL Behring, Pennsylvania, USA), and Truxima®, containing the monoclonal antibody Rituximab at a concentration of 10 mg/mL (Mundipharma, Frankfurt am Main, Germany) were used to determine the particle numbers in liquid products. The turbidity and the number of subvisible and submicron particles was analyzed prior to and after an in-line filtration step using an Acrodisc® syringe filter with a diameter of 13 mm and a pore size of 0.2 µm (Pall Corporation, New York, USA).

3.7.2 Methods to determine the number of subvisible and submicron particles in biologics

Methods used for turbidity, light obscuration and flow imaging measurements are described in sections 3.3.1, 3.3.2 and 3.3.3, respectively.

3.7.2.1 Tunable resistive pulse sensing (TRPS)

The number of submicron particles was measured by tunable resistive pulse sensing (TRPS) on a qNano Gold instrument (IZON, Oxford, UK). The samples prior to and after filtration were prepared as described in Table 3-4. Prior to the measurements, a nanopore NP300 with a size range of 150-900 nm was fitted into the qNano Gold and a stretch of 47 mm was applied. A volume of 70 µl and of 35 µl of filtered (0.22 µm) coating solution was loaded to the lower and upper fluid level. Subsequently, a pressure of +20 mbar was applied for 30 minutes, followed by applying a pressure of -20 mbar for 15 minutes. The coating solution was removed from the upper and lower fluid level which were both rinsed with highly purified water and the upper fluid level was additionally dried with pressurized air. A volume of 70 µl of electrolyte (60 mM NaCl + 0.05% polysorbate 80) was added to the lower fluid level. The electrolyte was identical to the sample, if applicable. If the exact composition was not known, the ionic strength was matched as close as possible by adjusting the concentration of NaCl in the electrolyte using a 1 M NaCl stock solution. Calibration beads (CPC400) were diluted twice 1 to 100 in filtered electrolyte for a final dilution of 1/10000 in electrolyte. For the measurements, a volume of 35 µl of electrolyte was added to the upper fluid level and a pressure of +10 mbar was applied to check the cleanliness of the system (less than 10 particles/10 minutes were required). After cleaning the upper fluid level, a volume of 35 µl of the sample (calibration beads or protein sample) was added to the upper fluid level and a pressure of 10 mbar was applied. Finally, the measurement was started. A particle read of > 500 particles or a maximum recording time of 10 minutes were chosen as limits. For calibration beads measurements, the limit was set to a particle rate of 250-400 particles/min for a 1/10000 dilution. The recording was paused if blockages occurred and the nanopore was unblocked according to the manufacturer's advice.

Table 3-4: Sample preparation of tested products for the analysis of submicron particles using a qNano Gold TRPS. Measurements were performed by Andreas Stelzl.

	Product	Sample preparation	Reason for sample preparation	Pipetted volumes	Calibration beads
Lyo-Products	Gammagard®	diluted 1/10 in 60 mM electrolyte ¹	high viscosity in undiluted samples caused instable baseline	100 µl Gammagard® + 900 µl 60 mM NaCl	CPC400 in 60 mM NaCl
	Actilyse®	no dilution, no spiking	electrolyte concentration sufficient for analysis	200 µl Actilyse®	CPC400 in 60 mM NaCl
	Flixabi®	50 mM electrolyte spiked in from 1M NaCl stock solution ¹	increase electrolyte concentration without large dilution	190 µl Flixabi® + 10 µl 1M NaCl	CPC400 in 60 mM NaCl
	IgG ₁	50 mM electrolyte spiked in from 1M NaCl stock solution ¹	increase electrolyte concentration without large dilution	190 µl IgG ₁ + 10 µl 1M NaCl	CPC400 in 60 mM NaCl
	Beriglobin®	diluted 1/10 in 60 mM electrolyte ¹	high viscosity in undiluted samples caused instable baseline	100 µl Beriglobin® + 900 µl 60 mM NaCl	CPC400 in 60 mM NaCl
Liquid-Products		after dilution: 5 µm filtration step applied (Acrodisc® 32 mm syringe filter with 5 mm Supor® membrane, Pall Corporation)	high number of blockages through larger particles, if 5 µm filtration was not applied		
	Pulmozyme®	no dilution, no spiking	electrolyte concentration sufficient for analysis	200 µl Pulmozyme®	CPC400 in 120 mM NaCl
	Truxima®	no dilution, no spiking	electrolyte concentration sufficient for analysis	100 µl Truxima® + 900 µl 60 mM NaCl	CPC400 in 60 mM NaCl

¹The electrolyte solution was filtered using an inorganic membrane filter Anotop®25 Whatman® with a pore size of 0.02 µm.

3.8 References

1. Farnan, D. & Moreno, G. T. Multiproduct high-resolution monoclonal antibody charge variant separations by pH gradient ion-exchange chromatography. *Anal. Chem.* **81**, 8846–8857 (2009).
2. Giese, C. *et al.* A human lymph node in vitro-challenges and progress. *Artif. Organs* **30**, 803–808 (2006).
3. Giese, C. *et al.* Immunological substance testing on human lymphatic micro-organoids in vitro. *J. Biotechnol.* **148**, 38–45 (2010).
4. Sardi, M., Lubitz, A. & Giese, C. Modeling Human Immunity In Vitro - Improving Artificial Lymph Node Physiology by Stromal Cells. *Appl. Vitro. Toxicol.* **2**, 143–150 (2016).

Chapter 4

Aggregation studies on the human monoclonal antibodies Adalimumab and Bevacizumab

4.1 Introduction

The introduction was published as part of the review article “Test Models for the Evaluation of Immunogenicity of Protein Aggregates” in International Journal of Pharmaceutics 559 (2019) 192-200.

Protein aggregation is a well-known instability of protein drugs and poses a major challenge to the development and manufacturing of biopharmaceuticals¹. Protein aggregation can occur during development, manufacturing, shipment, and storage of the protein drug product^{2,3}. It leads not only to a compromised product quality, but it may also increase the risk of immunogenic side events when administered to patients⁴. Protein aggregates can be formed by different pathways and can therefore result in a variety of different types of protein aggregates. Mahler *et al.*³ suggested a classification of protein aggregates by (a) the type of bond: non-covalent vs. covalent protein aggregates; (b) reversibility: reversible vs. irreversible protein aggregates; (c) size: small soluble vs. larger insoluble aggregates and (d) protein conformation: protein aggregates with native structure vs. protein aggregates with a non-native structure. Irreversible aggregates often involve covalent cross-linking. According to Narhi *et al.*⁵ there are two types of reducible disulfide crosslinking which are intermolecular and intramolecular crosslinking of the proteins. Also, non-reducible crosslinks such as thioether and dityrosine covalent bonds can be present in protein aggregates. Protein aggregates can also be classified due to their reversibility^{3,5}. Irreversible protein aggregates are mostly higher molecular weight species and the aggregation process cannot be reversed without the addition of a denaturant or reducing agent⁵. On the contrary, reversible aggregates can dissociate into their “native” form again. According to Narhi *et al.*⁵ reversible aggregates “exist in equilibrium with the native monomeric form”. A common way to classify protein aggregates is according to their size^{3,5,6}. Aggregates in the nanometer range < 100 nm are usually referred to as soluble aggregates or oligomers, whereas aggregates in the range of 100 – 1000 nm are usually referred to as submicron particles. Aggregates in the range of 1 – 100 µm can be classified as subvisible particles and aggregates larger than 100 µm are referred to as visible particles^{5,7}. Finally, protein aggregates can be classified according to the conformation of the protein in aggregates. A protein can be present in its native structure, it can be partially unfolded, misfolded, unfolded or amyloid, for example⁵.

Aggregation mechanisms can be differentiated into physical and chemical aggregation. According to the Lumry-Eyring model (Figure 4-1), changes in the conformation of a protein lead to an intermediate state of the protein, which is then prone to aggregate and subsequently, irreversible (or reversible) protein aggregates are formed⁸. This model suggests that aggregation is based on conformational changes. However, aggregation can also be induced by chemical instabilities such as crosslinking of protein chains or changes of the hydrophilicity of the protein⁹. Chemical modifications are usually

based on modifications of amino acid residues. The most commonly described chemical reactions are oxidation, reduction, deamidation, hydrolysis, arginine conversion, β -elimination, and racemization¹⁰.

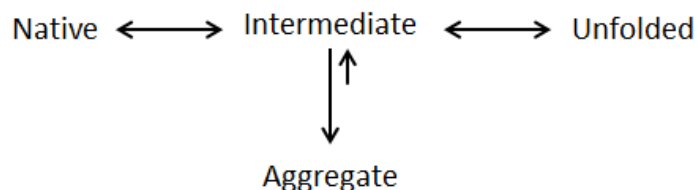


Figure 4-1: The Lumry-Eyring model of protein aggregation. A protein in a native state can form an intermediate, which can either reversibly unfold or lead to irreversible or reversible protein aggregates (adopted from Wang et al.⁹).

Besides the “natural occurrence”, protein aggregation can also be intentionally triggered by the exposure to various stress conditions such as elevated temperature^{11,12}, freezing and thawing^{11,13}, agitation stress, such as stirring and shaking^{12,14}, high protein concentration¹⁵, solvent and surface effects like changes in the pH or ionic strength and chemical modifications^{3,9,16,17}. Different stress conditions may lead to different kinds of protein aggregates. To distinguish between different protein aggregates a variety of analytical methods is available^{3,9}. In fact, there is no analytical method available covering the complete size range of protein aggregates, making the analysis of protein aggregates rather complex^{6,14}. Chromatographic methods such as size exclusion or reversed phase chromatography, for example, are used to analyze soluble aggregates in the nanometer range. Further commonly used methods for the analysis of subvisible aggregates are light obscuration, coulter counter or flow imaging and other microscopy techniques. Spectroscopic methods such as fluorescence spectroscopy, (FT-)IR spectroscopy, Raman spectroscopy or circular dichroism are used to analyze the structure and conformation of proteins and protein aggregates^{3,7}. Due to the different information gained by such methods, it is recommended to apply several methods. At that point it is particularly favorable and recommended by the authorities to use orthogonal methods, hence methods with different underlying mechanisms, to reduce artefacts and misinterpretations as far as possible⁷.

The aim of the study described in this chapter was to generate different types of protein aggregates by exposing two monoclonal antibodies, Adalimumab and Bevacizumab, to various stress conditions. Moreover, we aimed at finding appropriate time points and stress conditions for the two investigated monoclonal antibodies with the further aim of evaluating the immunogenicity of the generated protein aggregates in a human artificial lymph node model. Therefore, samples of Bevacizumab and Adalimumab were exposed to light, stir and heat stress (Bevacizumab only) for different periods of time and the samples were subsequently analyzed by light obscuration, turbidity, dynamic light scattering, size exclusion chromatography, Fourier-transform infrared spectroscopy and intrinsic and

extrinsic fluorescence spectroscopy. Based on the results of this chapter, stress conditions and time points for following experiments were selected. Once the selection was made, we investigated the stability of the desired samples during storage at 2-8°C to ensure the stability and a consistent composition of the aggregated samples over the run time of the human artificial lymph node model. Additionally, we also tested the stability of the samples stored at 2-8°C for six weeks after storage at - 80°C prior to the experiment.

4.2 Results

4.2.1 Turbidity

Turbidity measurements can be a helpful tool to assess protein aggregation. Even though the method cannot provide quantitative information about aggregate size or particle counts, it can be a helpful qualitative method to estimate if aggregation occurred¹⁸. The results of turbidity measurements of Adalimumab and Bevacizumab after exposition to different stress conditions are displayed in Figure 4-2. In general, stir stress of both monoclonal antibodies led to the strongest increase and highest turbidity values. Compared to the unstressed proteins and the buffer controls, turbidity increased already after 4 hours of stirring. This trend continued until the detection limit of 1300 FNU was reached after 24 hours stirring of Adalimumab and 72 hours stirring of Bevacizumab. Exposing Adalimumab to light stress also resulted in an increase of turbidity starting after 48 hours of light exposition. After 7 days of light exposure, the turbidity increased to > 1000 FNU. The same is true for Bevacizumab where no major increase in turbidity was detectable after 24 hours of light stress but after 4 days of light exposition turbidity rose to approximately 140 FNU. Remarkably, a decreased turbidity value was determined after 7 days of light stress. This is probably due to the fact, that the protein was completely aggregated and precipitated after 7 days of exposure to light while the supernatant was relatively clear. The exposure of Bevacizumab to elevated temperature also resulted in increased turbidity values. However, values were in general much lower than after stir stress for example. After 7 days of incubation at 50 °C, a turbidity of 14 FNU was measured. In summary, it can be found that turbidity increased with increasing exposure times to the distinct stress conditions.

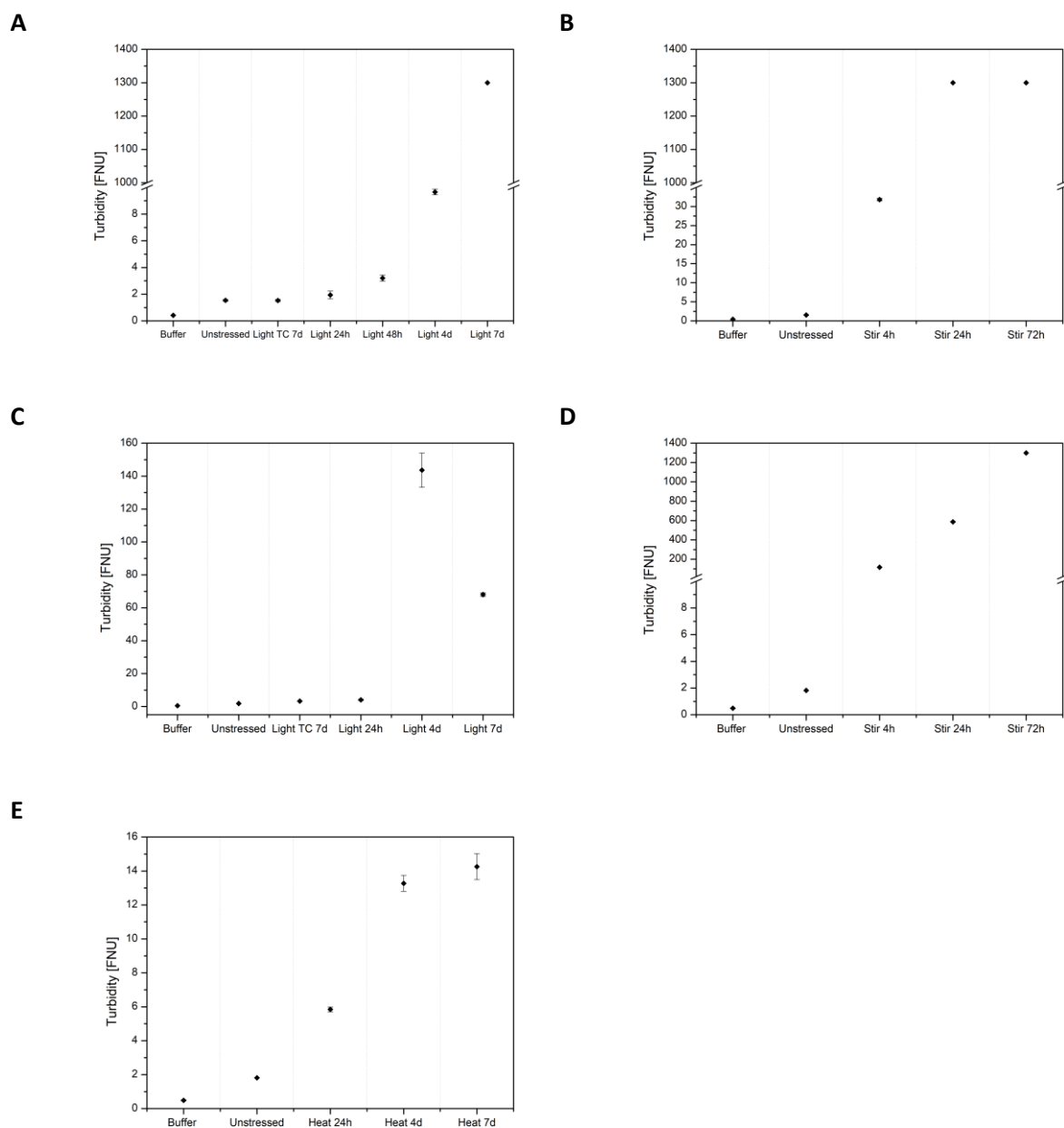
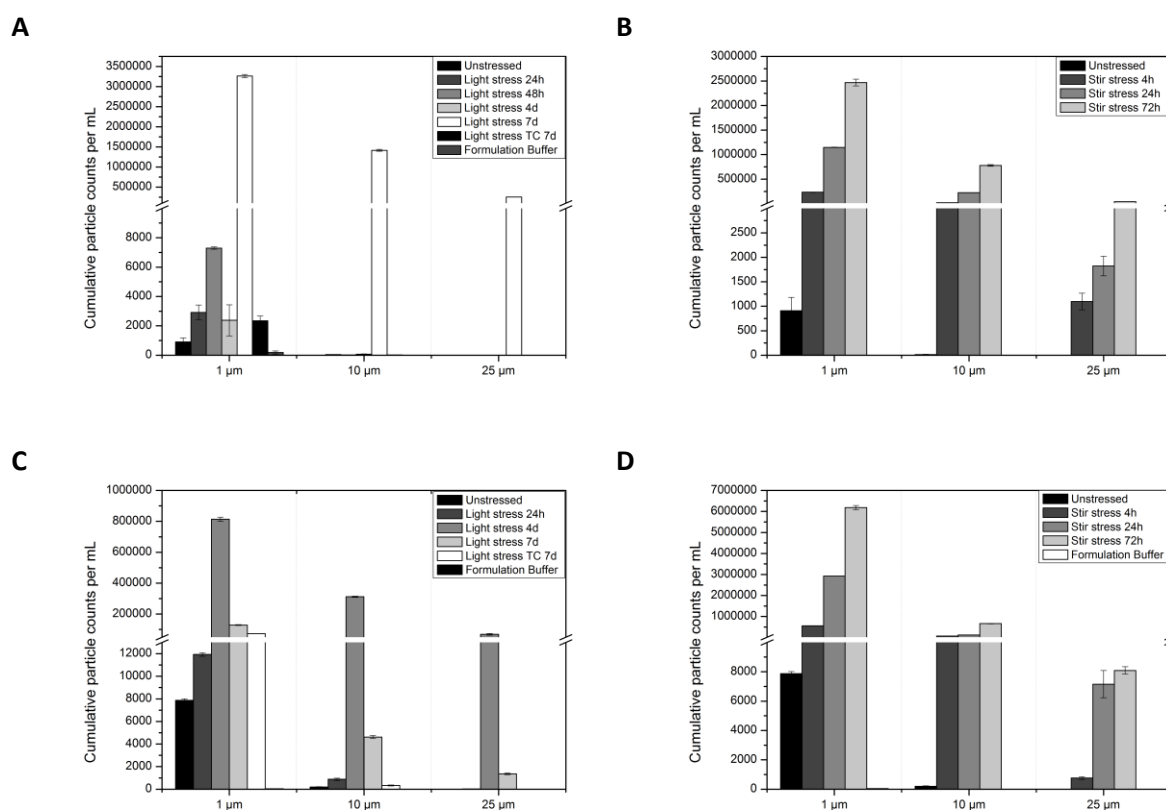


Figure 4-2: Results of turbidity measurements displayed in FNU of Adalimumab after light stress (A) and after stir stress (B) and Bevacizumab after light stress (C), after stir stress (D) and after heat stress (E). Note the different y-axes in (C) and (E).

4.2.2 Light obscuration

Subvisible particles were detected using light obscuration. The European Pharmacopoeia limits the number of particles larger than 10 μm to 6000 and of particles larger than 25 μm to 600 particles per container for infusion and injection products filled in a container with a volume of $\leq 100 \text{ mL}$ ¹⁹. The cumulative particle counts of particles $\geq 1 \mu\text{m}$, $\geq 10 \mu\text{m}$ and $\geq 25 \mu\text{m}$ of Bevacizumab and Adalimumab after exposure to the different stress conditions are displayed in Figure 4-3. The results show that stir stress strongly triggered the formation of particles of Adalimumab and Bevacizumab. After 4 hours of stirring there was already a strong increase in particles $\geq 1 \mu\text{m}$ and $\geq 10 \mu\text{m}$ compared to the particle burden of the unstressed antibodies. The number of particles of those $\geq 25 \mu\text{m}$, increased with longer

exposure times. In contrast, light stress led to lower particle counts. In the case of Adalimumab, the total particle count was only slightly increased after 24 hours and 4 days, but after 7 days there was a sudden increase in particle numbers of particles $\geq 1 \mu\text{m}$, $\geq 10 \mu\text{m}$ and $\geq 25 \mu\text{m}$. Bevacizumab appeared to be more sensitive to light stress regarding the particle increase. A strong increase in particle counts of particles $\geq 1 \mu\text{m}$, $\geq 10 \mu\text{m}$ and $\geq 25 \mu\text{m}$ was already detected after 4 days of exposure to light. The lower particle counts for the Bevacizumab sample that was exposed to light for 7 days is again explainable with a total precipitation of the protein after 7 days of light exposure as mentioned before. The exposure of Bevacizumab to elevated temperature for 24 hours resulted in an increase in particles in the range of $1 - 10 \mu\text{m}$. The number of particles $\geq 10 \mu\text{m}$ was slightly elevated compared to the unstressed protein. After 4 days of incubation at 50°C , particle numbers $\geq 1 \mu\text{m}$ and $\geq 10 \mu\text{m}$ increased strongly and particles $\geq 25 \mu\text{m}$ were formed. As reported for 7 days of light stress, the exposure to heat for 7 days also resulted in a decrease of particles $\geq 1 \mu\text{m}$ and $\geq 10 \mu\text{m}$ and in this case, a slight increase in particles $\geq 25 \mu\text{m}$. Due to the precipitation of the protein after 7 days of heat stress, the smaller particles might have agglutinated, and no more smaller particles could be detected.



E

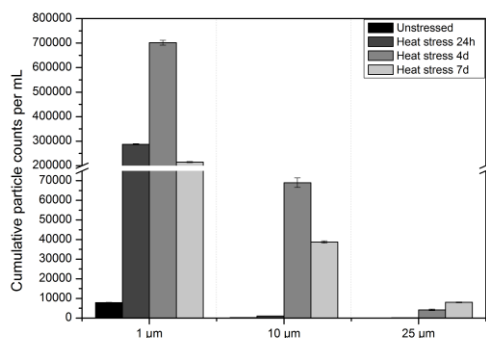


Figure 4-3: Cumulative particle counts per mL of Adalimumab after exposure to light (A) and stir stress (B) and of Bevacizumab after exposure to light (C), stir stress (D) and to elevated temperature (E).

4.2.3 Dynamic light scattering (DLS)

Dynamic light scattering is used to determine the hydrodynamic size of proteins and protein aggregates within a size range from 1 nm – 10 µm, whereby DLS is especially suitable for the analysis of smaller aggregates in the nanometer range⁷. The hydrodynamic diameter is reported as Z-average (Z_{ave}) diameter and represents the mean diameter. Results of DLS measurements of Adalimumab and Bevacizumab after exposure to different stress conditions are shown in Figure 4-4 and Table 4-1 and Table 4-2. The intensity peaks of Adalimumab and Bevacizumab after light stress shifted towards larger particle sizes after exposure to light. Longer exposure times resulted in larger Z_{ave} diameter values and the polydispersity indexes also increased (Table 4-1 and Table 4-2). After 7 days of light stress of Adalimumab, the Z_{ave} diameter increased to 1163 ± 113 nm and the PDI to 0.92 ± 0.06 . This is also true for Bevacizumab. The intensity graph of Bevacizumab after light stress (Figure 4-4C) shows a clear shift of the monomer peak towards larger particle sizes over the exposure time. Stir stress triggered the formation of rather large particles. After 4 hours of stirring of Adalimumab, parts of the monomer peak were still detectable. In contrast, 24 hours of stirring already led to a complete shift of the monomer peak towards particle sizes larger than 1000 nm. The PDI values, representing the homogeneity of the particle sizes, of the stirred samples increased to values larger than 0.3 in the case of Bevacizumab and larger than 0.8 for Adalimumab. The exposure of Bevacizumab to heat triggered the formation of submicron particles as displayed in Figure 4-4E. The Z_{ave} diameter increased from 11.62 ± 0.09 nm of the unstressed antibody to 61.53 ± 9.73 nm after 24 hours of heat stress, to 74.87 ± 11.09 nm after 4 days of heat stress and to 393 ± 94 nm after 7 days of heat stress and PDI values rose again to values larger than 0.3.

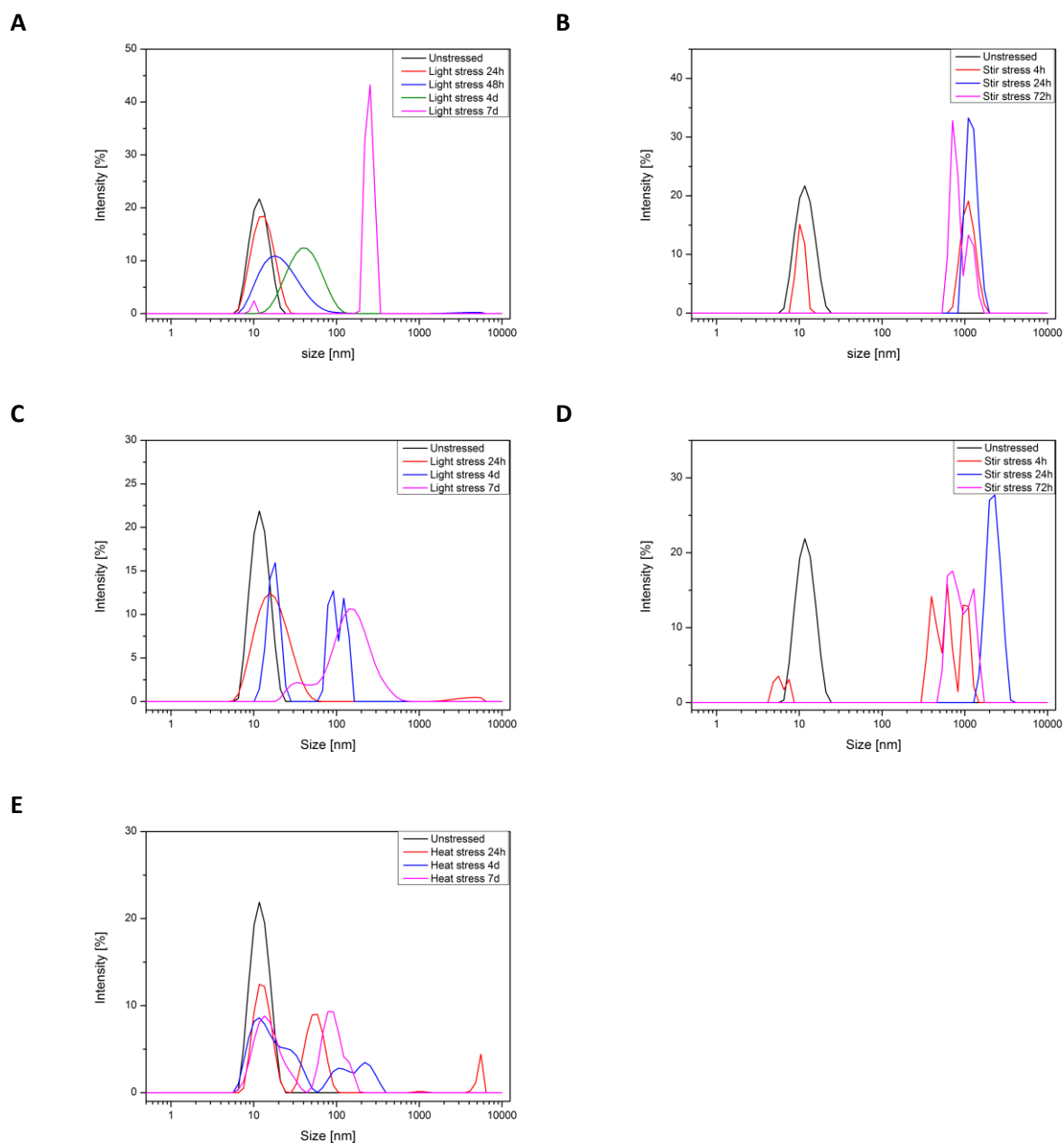


Figure 4-4: Results of DLS measurements of Adalimumab after exposure to light (A) and stir stress (B) and of Bevacizumab after exposure to light (C), stir stress (D) and elevated temperature (E).

Table 4-1: Values for Z_{ave} diameter and PDI of Adalimumab after light and stir stress.

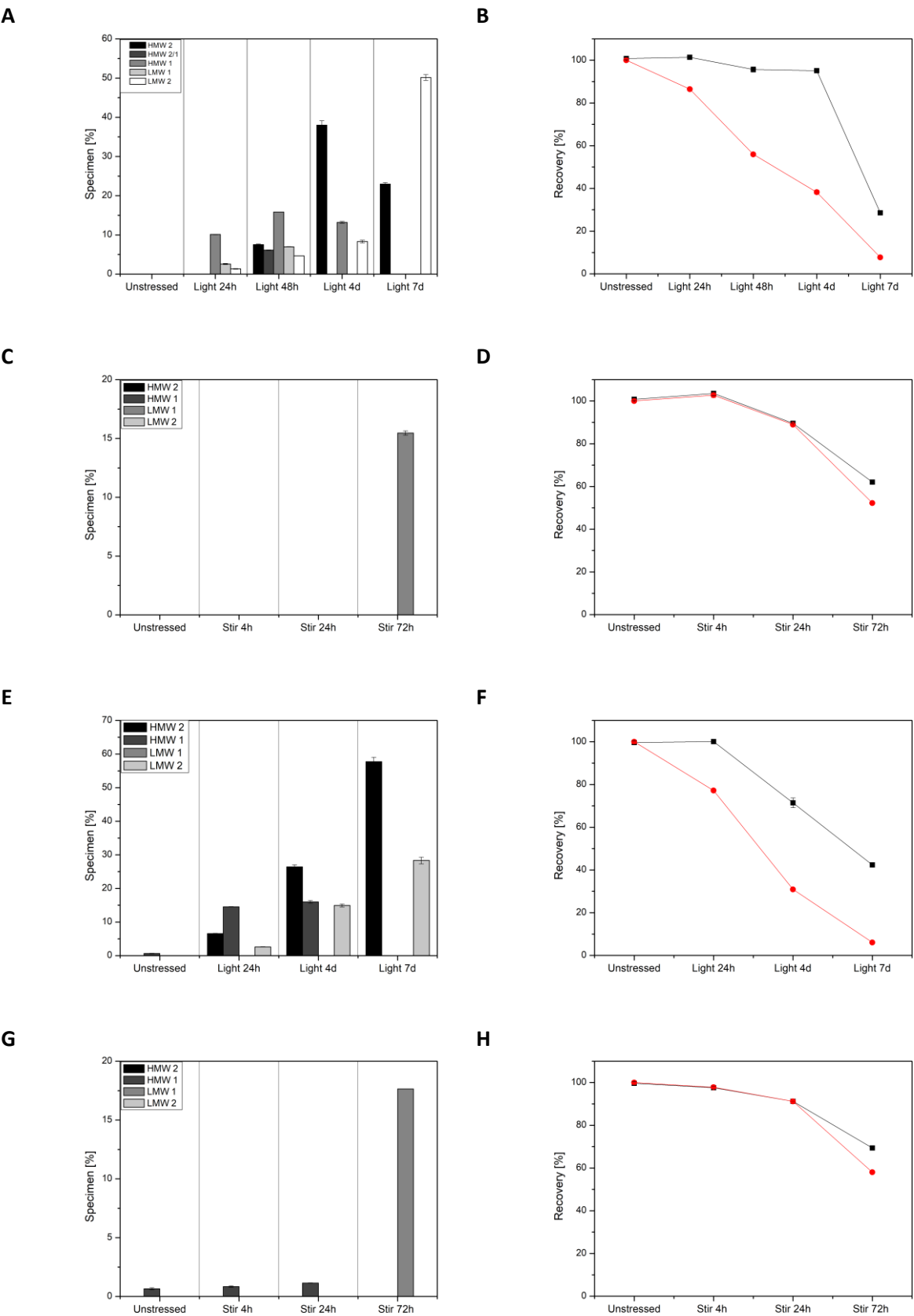
	Unstressed	Light 24h	Light 48h	Light 4d	Light 7d
Z_{ave} [nm]	11.40 ± 0.09	12.37 ± 0.08	18.72 ± 0.2	35.72 ± 0.13	1163 ± 113
PDI	0.04 ± 0.02	0.07 ± 0.01	0.2 ± 0.01	0.18 ± 0.01	0.92 ± 0.06
		Stir 4h	Stir 24h	Stir 72h	
Z_{ave} [nm]		296 ± 77	2334 ± 597	1898 ± 326	
PDI		0.92 ± 0.07	0.83 ± 0.29	1 ± 0	

Table 4-2: Values for Z_{ave} diameter and PDI of Bevacizumab after light, stir and heat stress.

	Unstressed	Light 24h	Light 4d	Light 7d
Z_{ave} [nm]	11.62 ± 0.09	15.78 ± 0.12	874 ± 224	111 ± 1
PDI	0.03 ± 0.01	0.19 ± 0.01	0.87 ± 0.06	0.28 ± 0.03
		Stir 4h	Stir 24h	Stir 72h
Z_{ave} [nm]		1236 ± 442	2660 ± 243	2141 ± 919
PDI		0.58 ± 0.28	0.36 ± 0.04	0.91 ± 0.16
		Heat 24h	Heat 4d	Heat 7d
Z_{ave} [nm]		61.53 ± 9.73	74.87 ± 11.09	393 ± 94
PDI		0.34 ± 0.06	0.56 ± 0.32	0.42 ± 0.05

4.2.4 Size exclusion chromatography (SEC)

To analyze soluble aggregates, size exclusion chromatography was performed. The distribution of protein species of Adalimumab and Bevacizumab and the protein recovery is displayed in Figure 4-5. In the case of both monoclonal antibodies, light stress strongly triggered the formation of soluble aggregates of different sizes as displayed in Figure 4-5A and E. The longer the proteins were exposed to light, the larger the amount of high and low molecular weight species was in the samples. This increase in high and low molecular weight species correlated with a strong decrease in total protein and monomer recovery (Figure 4-5B and F). Exposure to light for 7 days resulted in a monomer recovery of less than 10%. On the contrary to light stress, stir stress did not lead to the formation of soluble aggregates of Adalimumab after 4 and 24 hours of stirring. In the case of Bevacizumab, the amount of high molecular weight species increased slightly during stirring compared to the unstressed monoclonal antibody. It is notable, that after 72 hours of stirring the number of fragments suddenly increased to more than 15% for both antibodies. Moreover, there is a decrease in total protein and monomer recovery over time (Figure 4-5D and H). The exposure of Bevacizumab to elevated temperature resulted in the formation of soluble aggregates and fragments at the same time (Figure 4-5I) and longer exposure times led to larger amounts of the high and low molecular weight species. After 7 days of heat stress the number of fragments (LMW1 and LMW2) increased to more than 15%. The total protein and monomer recovery decreased slightly over time.



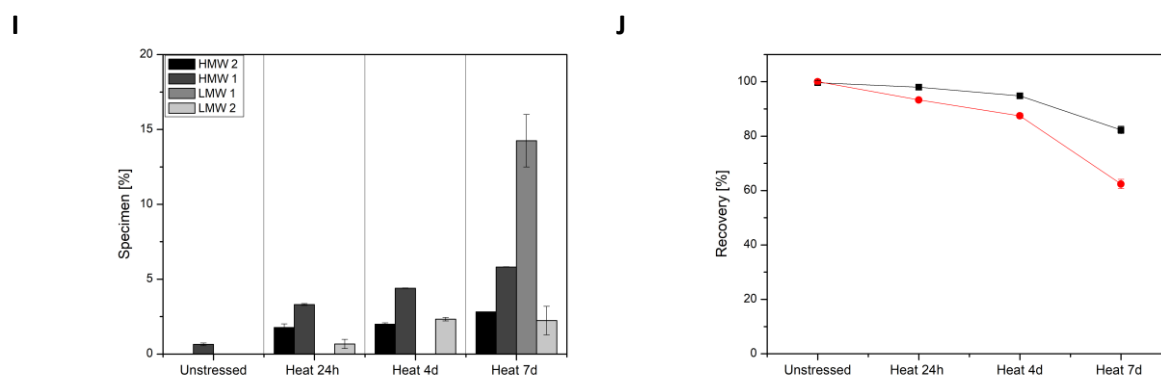


Figure 4-5: Distribution of protein species of Adalimumab after light stress (A) and after stir stress (C) and of Bevacizumab after light stress (E), stir stress (G) and heat stress (I). Corresponding recovery data is displayed in graphs (B), (D), (F), (H) and (J). The black line represents the total recovery and the red line displays the monomer recovery. HMW 2 > HMW 1; LMW 1 > LMW 2.

4.2.5 Extrinsic fluorescence

Fluorescence spectroscopy techniques were used to analyze possible changes in the tertiary structure of Bevacizumab and Adalimumab after exposure to different stress conditions. In Figure 4-6, the results of extrinsic fluorescence measurements using Bis-ANS as noncovalent dye are displayed. Noncovalent fluorescence dyes are usually non-fluorescent in aqueous medium, but become highly fluorescent in a hydrophobic environment^{20,21}. Additionally, the spectra showed a blue shift, meaning that the fluorescence spectra shifted to smaller wavelengths. The emission maxima of the fluorescence spectra of Adalimumab and Bevacizumab after exposure to different stress conditions are presented in Table 4-3 and Table 4-4. The fluorescence intensity of the Adalimumab samples exposed to light for 24 hours or 4 days increased with longer exposure times indicating a more hydrophobic environment compared to the unstressed antibody. This was also confirmed by a blue shift of the spectra that increased after 4 days of light exposure. However, after 7 days of light stress, fluorescence intensity was smaller than after 4 days and, there was no further blue shift compared to the sample that was exposed to light for 4 days. This could be due to the precipitation of the protein after 7 days of light exposure and therefore, the aggregated protein was not in solution anymore. The spectra of Bevacizumab after light stress (Figure 4-6C) show increasing fluorescence intensity with increasing exposure times to light and the blue shifts of the spectra also increased corresponding to the exposure times. This indicates an increasing hydrophobic environment upon light stress. No remarkable increase in fluorescence intensity and only a blue shift after 72 hours of stirring could be detected after stir stress of Bevacizumab. In contrast, after stirring of Adalimumab a decrease in fluorescence intensity was seen. However, one must keep in mind, that the stirred stressed samples had high counts of particles that possibly interfered with the measurement. Therefore, one must be cautious with interpreting the data after stir stress. For Bevacizumab after heat stress, there was a small increase in fluorescence intensity compared to the unstressed protein, but also here increasing particle counts make it difficult to

determine a trend. In summary, light stress had the largest influence on the extrinsic fluorescence. However, it should be mentioned that the data of the latest time points of both proteins was difficult to interpret, because of the presence of large amounts of particles or the precipitation/denaturation of the antibodies after 7 days of light stress, for example.

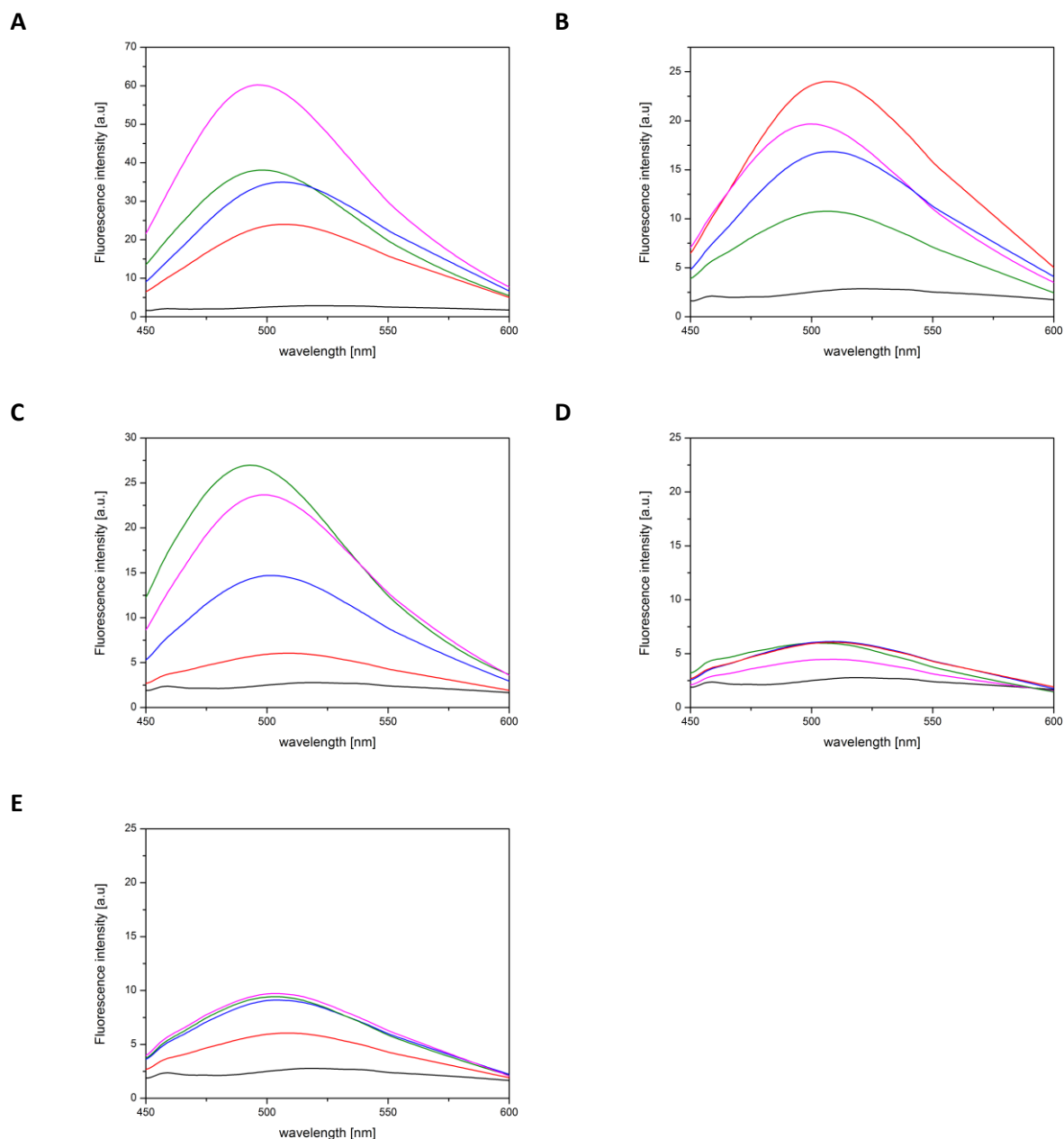


Figure 4-6: Extrinsic fluorescence emission spectra of Adalimumab at a concentration of 1 mg/mL after exposure to light (A) and stir stress (B) and of Bevacizumab after exposure to light (C), stir stress (D) and elevated temperature (E). The black line represents the formulation buffer, the red line represents the unstressed protein, the blue line represents Adalimumab/Bevacizumab after 4h of stir stress or 24h of light stress or 24h of heat stress; the pink line represents Adalimumab/Bevacizumab after 24h of stir stress or 4d of light stress or 4d of heat stress and the green line represents Adalimumab/Bevacizumab after 72h of stir stress or 7d of light stress or 7d of heat stress, respectively.

Table 4-3: Peak positions of Bis-ANS fluorescence emission spectra of Adalimumab after light and stir stress.

Light stress	Unstressed	24h	4 days	7 days
Peak position [nm]	507.01	505.97	495.97	498.05
Stir stress	Unstressed	4h	24h	72h
Peak position [nm]	507.01	508.05	500	505.97

Table 4-4: Peak positions of Bis-ANS fluorescence emission spectra of Bevacizumab after light, stir and heat stress.

Light stress	Unstressed	24h	4 days	7 days
Peak position [nm]	508.95	501.04	498.95	492.98
Stir stress	Unstressed	4h	24h	72h
Peak position [nm]	508.95	508.95	508.95	501.94
Heat stress	Unstressed	24h	4 days	7 days
Peak position [nm]	508.95	504.02	502.98	504.02

4.2.6 Intrinsic fluorescence

The results of intrinsic fluorescence spectroscopy are displayed in Figure 4-7. The most substantial alterations in fluorescence intensity were detected after light stress. One can state that with increasing exposure times to light, the fluorescence intensity decreased, except for Adalimumab after 24 hours of light stress where no decrease was detectable. This reduced fluorescence intensity may be due to quenching of fluorescence intensity of tryptophan by intrinsic quenchers such as amine, carboxylic acids, disulfide or histidine groups²¹ and implies conformational changes such as unfolding. The same is true for Bevacizumab after exposure to elevated temperature. The fluorescence intensity decreased slightly after 4 and 24 hours of exposure to 50°C and decreased even stronger after 7 days of heat stress. Also stirring had an impact on the fluorescence intensity. In case of Bevacizumab, the intensity decreased again with longer stirring times. It is remarkable, that 72 hours of stirring led to a very strong decrease of fluorescence intensity, comparable with the level of intensity after 7 days of light stress. In contrast, the intensity of Adalimumab after 72 hours of stirring dropped to a lesser extent, after 24 hours of stirring the intensity was not changed compared to the unstressed protein and after 4 hours of stirring, fluorescence intensity even increases slightly compared to unstressed Adalimumab. However, as mentioned before, the stir stressed samples contained high numbers of particles which could possibly have interfered with the fluorescence measurements.

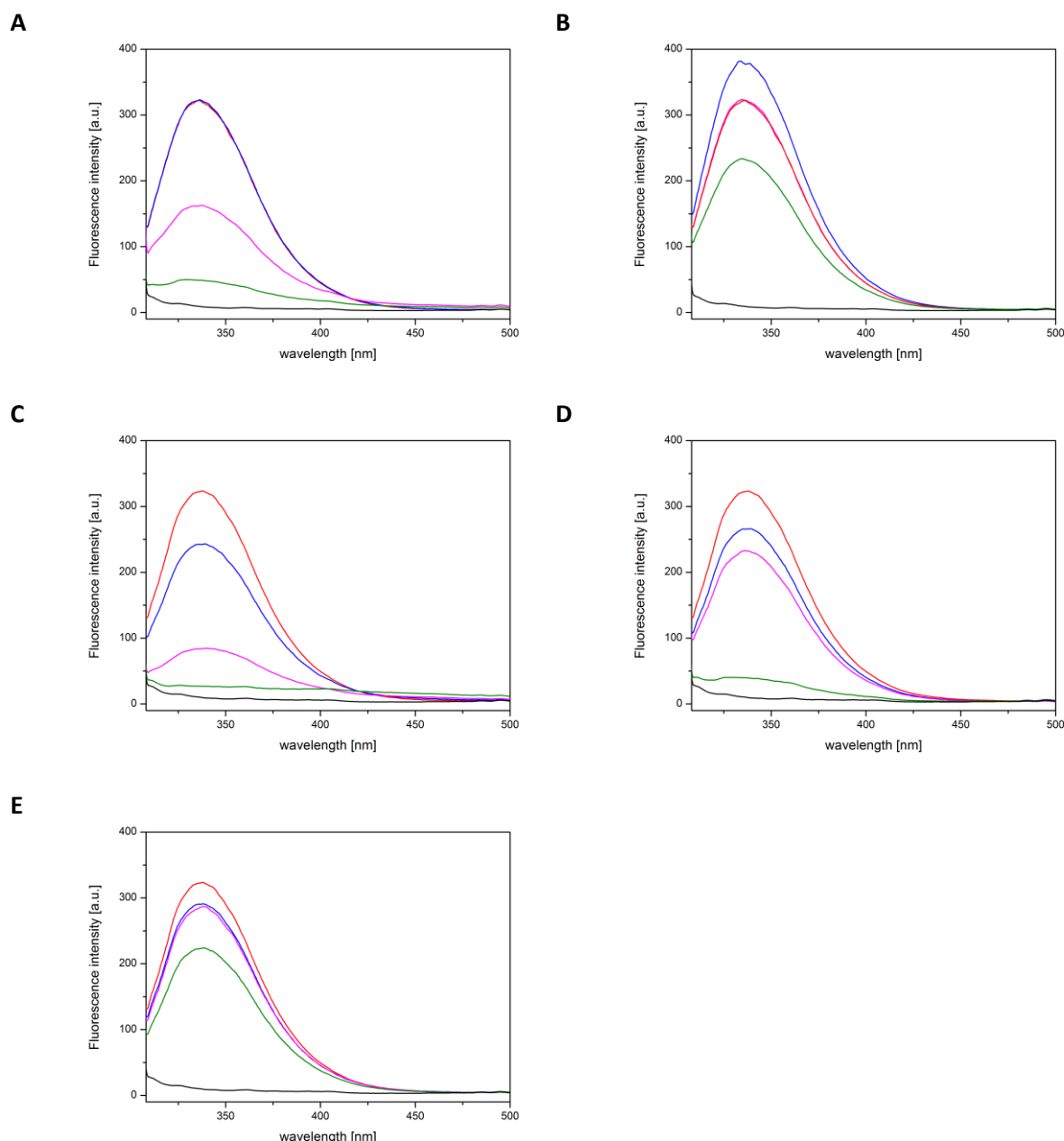


Figure 4-7: Intrinsc fluorescence emission spectra of 1 mg/mL of Adalimumab after exposure to light (A) and stir stress (B) and of Bevacizumab after exposure to light (C), stir stress (D) and elevated temperature (E). The black line represents the formulation buffer, the red line represents the unstressed protein, the blue line represents Adalimumab/Bevacizumab after 4h of stir stress or 24h of light stress or 24h of heat stress; the pink line represents Adalimumab/Bevacizumab after 24h of stir stress or 4d of light stress or 4d of heat stress and the green line represents Adalimumab/Bevacizumab after 72h of stir stress or 7d of light stress or 7d of heat stress, respectively.

4.2.7 Fourier transform infrared spectroscopy (FT-IR)

FT-IR measurements have been widely used to investigate alterations in the secondary structure of protein samples^{22,23,24}. Usually, amide band I with its spectral region is between 1700 and 1600 cm^{-1} is used to detect conformational changes. The 2nd derivative spectra of the unstressed and stressed antibody samples are displayed in Figure 4-8A-E. In the case of Adalimumab alterations of amide band I were detected after light stress. Slight decreases of the main valley around 1638 cm^{-1} were already

seen after 24 and 48 hours. The changes increased after 4 days and after 7 days of exposure to light, the valley significantly decreased and shifted towards 1630 cm^{-1} . Moreover, a second valley between 1640 and 1650 started to form. The same is true for Bevacizumab after light stress. Stirring for 4 to 24 hours only led to minor decreases of the amide band I of Bevacizumab and Adalimumab, but 72 hours of stirring resulted in clear decreases of the valley and a shift towards 1630 cm^{-1} . In the case of Bevacizumab after heat stress, again increasing exposure times to heat led to increasing alterations in the shape of the spectra, whereas after 24 hours and 4 days of heat stress the alterations of the spectra were based on a decreasing main valley.

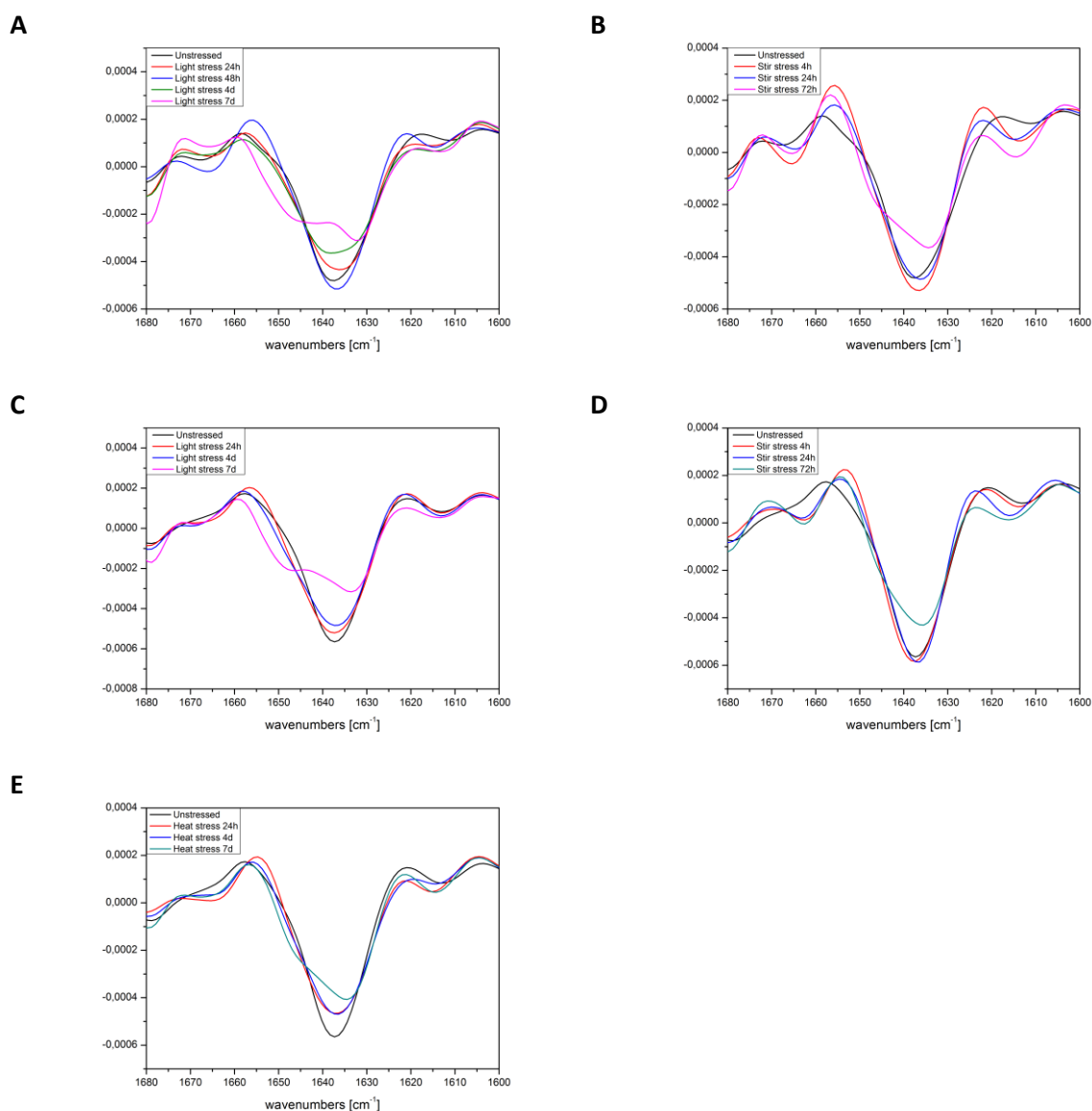


Figure 4-8: 2nd derivative FT-IR spectra of Adalimumab after exposure to light (A) and stir stress (B) and of Bevacizumab after exposure to light (C), stir stress (D) and elevated temperature (E).

4.2.8 Stability of aggregated samples of Adalimumab and Bevacizumab after storage at 2 - 8°C over a period of 6 weeks

As the immunogenicity of the aggregated samples of Adalimumab and Bevacizumab was investigated in a human artificial lymph node model over a period of 4 weeks, it was essential to show that the samples were stable after storage at 2-8°C. The composition of the aggregated samples was investigated by size exclusion chromatography and samples were analyzed weekly. We chose a period of 6 weeks to show the stability during the experiment running for 28 days but also some additional days for transportation or in case the start of the experiment had to be delayed, for example. The results for aggregated Adalimumab and Bevacizumab samples are shown in Figure 4-9 and Figure 4-10, respectively. The distribution of protein species of Adalimumab and Bevacizumab did not change dramatically during storage. Moreover, no additional or new protein species such as aggregates or fragments of different sizes were formed upon storage. On day 42, slight changes in the distribution of the protein species of Bevacizumab could be detected. There was a small increase in HMW 1 species after heat stress and alterations in the aggregate content after light stress. However, alterations were rather small. Therefore, it can be stated, that all samples were stable during storage at 2-8°C over a period of 6 weeks.

4.2.9 Stability of aggregated samples of Adalimumab and Bevacizumab after storage at – 80°C for 6 months and further storage at 2-8°C for 6 weeks after thawing

The stability of the aggregated samples of Adalimumab and Bevacizumab was also investigated after storage at -80°C for 6 months. After thawing, the samples were further stored at 2-8°C for 6 weeks and analyzed weekly by size exclusion chromatography. The distribution of the protein species of Adalimumab and Bevacizumab after thawing and storage at 2-8°C is displayed in Figure 4-11 and Figure 4-12. The composition of the Bevacizumab samples did not change dramatically during 6 weeks of storage at 2-8°C after thawing. In contrast, there were changes in the composition of the aggregated Adalimumab samples after light stress starting at day 14. Figure 4-11C displays the distribution of protein species of Adalimumab after light and stir stress after thawing and storage at 2-8°C for 14 days. The percentage of HMW 2 aggregates and the total recovery decreased compared to day 9 (Figure 4-11B). This trend continued until day 42 and might indicate increasing particle formation during storage at 2-8°C after thawing.

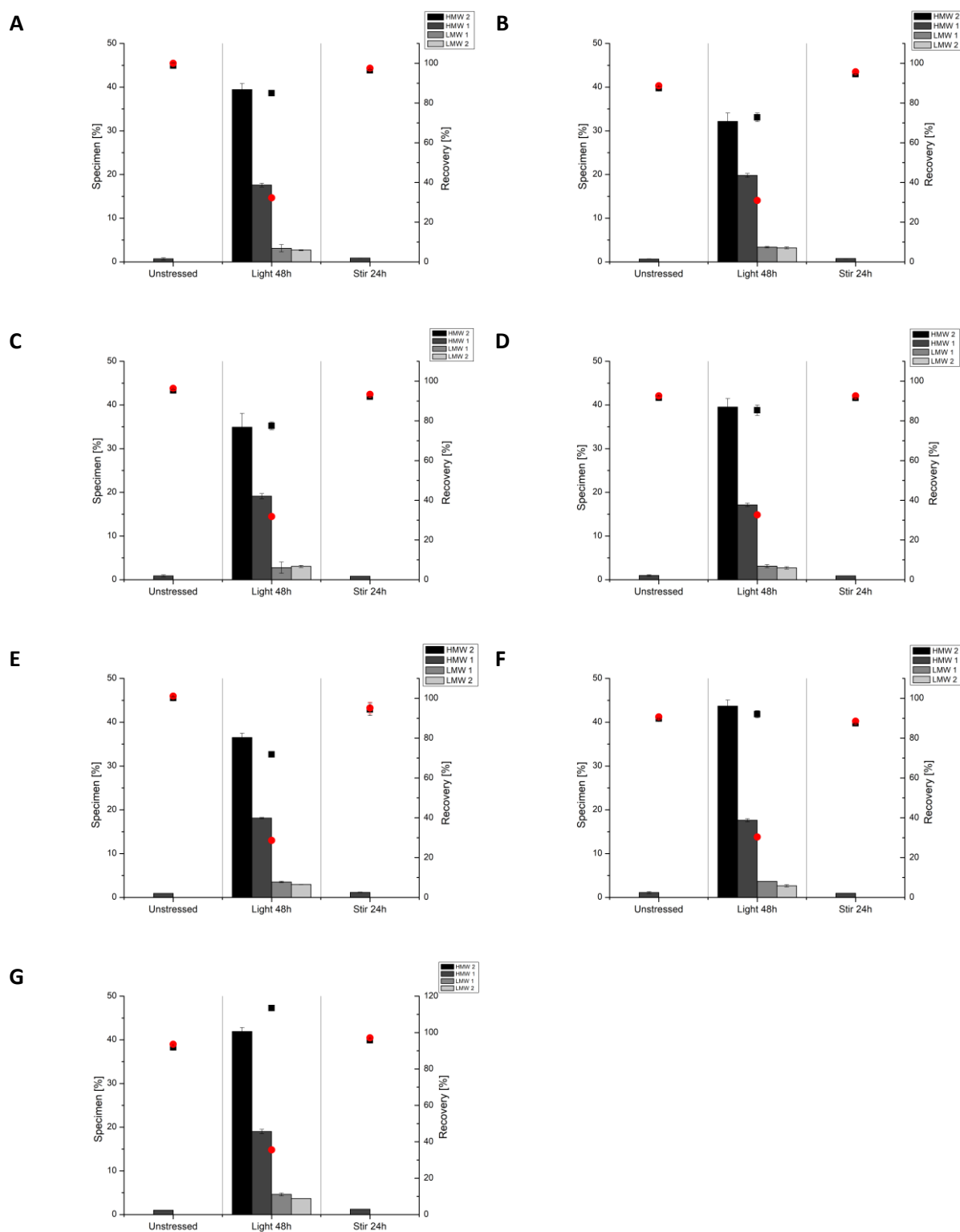


Figure 4-9: Distribution of protein species of Adalimumab after 48 hours of light and 24 hours of stir stress directly after production (A) and after storage at 2-8°C for 7 days (B), 14 days (C), 21 days (D), 28 days (E), 35 days (F) and 42 days (G). The black squares represent the total recovery of the protein, the red dots represent the monomer recovery; HMW 2 > HMW 1; LMW 1 > LMW 2.

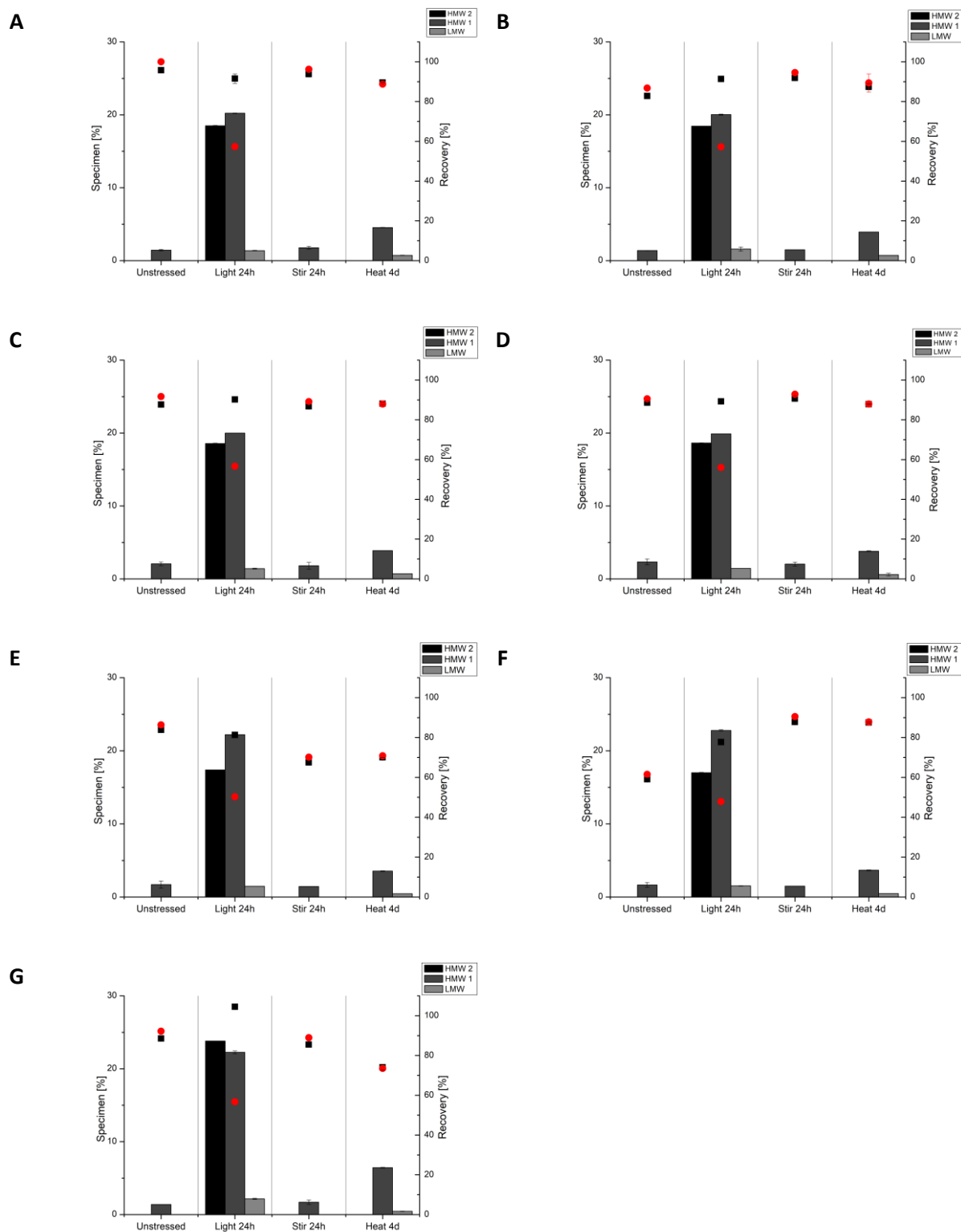


Figure 4-10: Distribution of protein species of Bevacizumab after 24 hours of light, 24 hours of stir and 4 days of heat stress directly after production (A) and after storage at 2-8°C for 7 days (B), 14 days (C), 21 days (D), 28 days (E), 35 days (F) and 42 days (G). The black squares represent the total recovery of the protein, the red dots represent the monomer recovery; HMW 2 > HMW 1 > LMW.

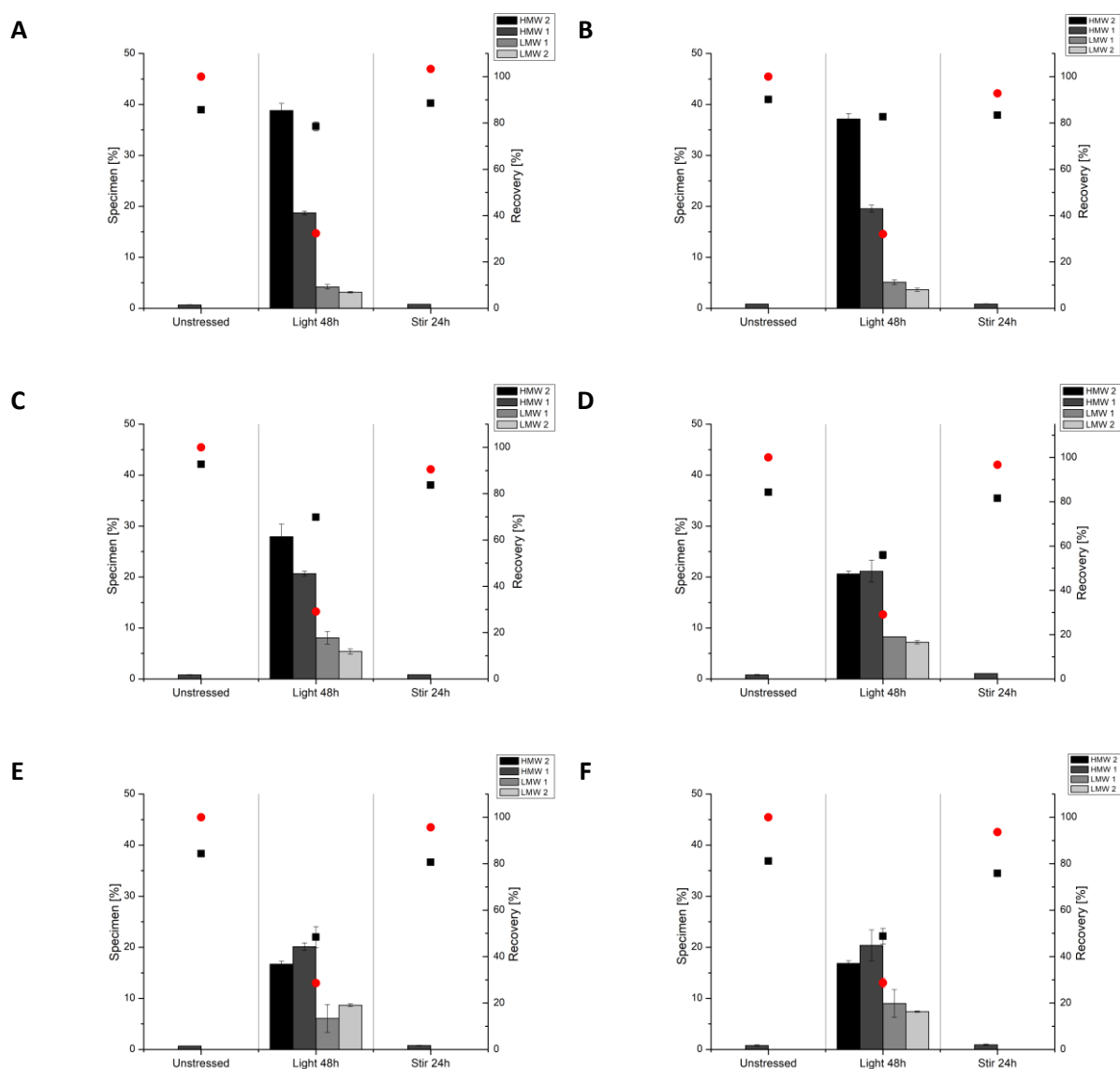


Figure 4-11: Distribution of protein species of Adalimumab after 48 hours of light and 24 hours of stir stress after storage at -80°C for 6 months directly after thawing (A) and after further storage at 2-8°C for 9 days (B), 14 days (C), 21 days (D), 28 days (E) and 42 days (F). The black squares represent the total recovery of the protein, the red dots represent the monomer recovery; HMW 2 > HMW 1; LMW 1 > LMW 2.

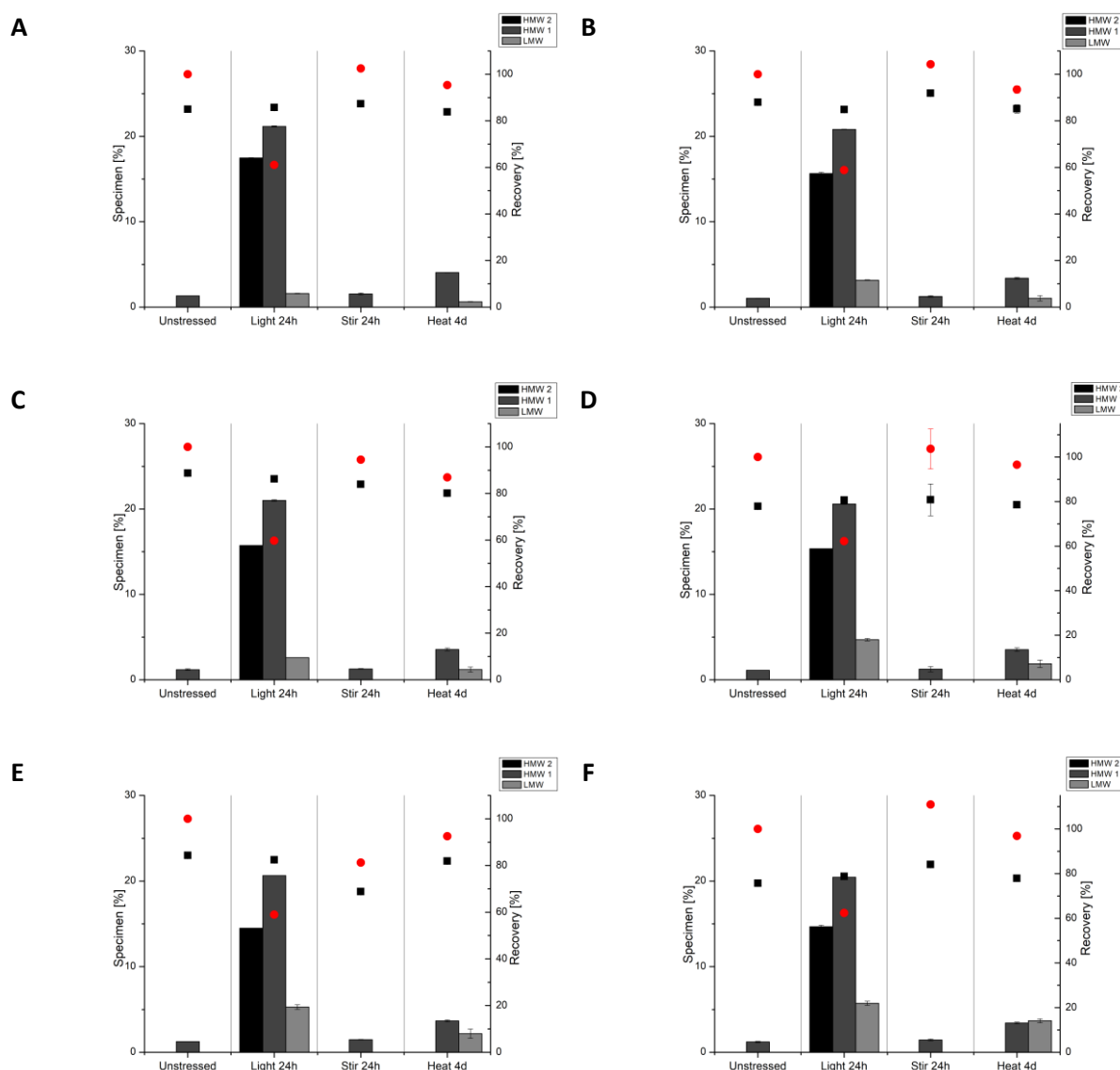


Figure 4-12: Distribution of protein species of Bevacizumab after 24 hours of light, 24 hours of stir stress and 4 days of heat stress after storage at -80°C for 6 months directly after thawing (A) and after further storage at $2-8^{\circ}\text{C}$ for 9 days (B), 14 days (C), 21 days (D), 28 days (E) and 42 days (F). The black squares represent the total recovery of the protein, the red dots represent the monomer recovery; $\text{HMW } 2 > \text{HMW } 1 > \text{LMW}$.

4.3 Discussion

In this study, we evaluated different stress conditions and time points with the aim to generate different types of protein aggregates in a reasonable amount for further experiments. Therefore, we used common stress conditions such as elevated temperature, light and mechanical stress that can possibly occur during the entire development, production, storage and handling of therapeutic proteins. It has been shown in many studies that different stress conditions lead to different protein aggregates^{3,25,26}. Stirring, for example, is known as a rather harsh stress condition to trigger protein aggregation^{14,27,28}. Also, in our study, stir stress strongly triggered the formation of subvisible particles as indicated by very high particle counts measured by light obscuration. According to the literature,

the mechanism of particle formation upon stirring is based on a mixture of shear and interfacial effects, cavitation, local thermal effects during stirring and accelerated transportation of aggregates or adsorbed protein species into the solution possibly leading to further aggregation^{14,27}. In the case of Adalimumab and Bevacizumab stirring especially led to the formation of particles larger than 1, 10 and 25 μm and less to the formation of soluble aggregates as indicated by size exclusion chromatography. It is remarkable, that stirring for more than 24 hours led to fragmentation of Bevacizumab and Adalimumab, since the percentage of fragments after 72 hours of stirring was increased for both proteins. This might be explained by the increasing exposure time to mechanical stress.

Light stress is known to trigger the formation of soluble aggregates and oxidation^{17,29–33}. Amino acid residues such as of methionine, cysteine, histidine, tryptophan and tyrosine are prone to undergo photooxidation³⁰, which may lead to protein aggregation. In our study, light exposure of the monoclonal antibodies was the most effective way to generate soluble aggregates as shown by size exclusion chromatography. The exposure to elevated temperature is also a well-known method to trigger protein aggregation^{11,34}. Higher temperatures promote chemical modifications such as oxidation and deamidation leading to increasing protein aggregation^{34,35}. In this study, we only exposed Bevacizumab to heat; since we knew from preliminary studies (data not shown) that heat stress of Adalimumab did not lead to a sustainable amount of protein aggregates within an acceptable period of time (7 days). The exposure of Bevacizumab to heat led to the formation of soluble aggregates and fragments on the one side, but also to the formation of insoluble protein aggregates, thus particles. Compared to light stressed Bevacizumab less soluble aggregates were formed upon heat stress. However, the heat stressed samples contained a moderate number of particles, soluble aggregates and fragments at the same time.

Dynamic light scattering was used to determine the hydrodynamic radius of the generated protein aggregates in the range of 1 nm – 10 μm . The data show that in case of both monoclonal antibodies, stir stress triggered protein aggregates with hydrodynamic diameters > 1000 nm. In contrast protein aggregates generated by the exposure to light and elevated temperature revealed to have hydrodynamic diameters smaller than 1000 nm. Since protein aggregates have various shapes and are usually not of perfect spherical form, data obtained from DLS measurements of protein aggregates should be interpreted with care. This is especially true for samples with a high polydispersity index. Moreover, DLS measurements are intensity-based measurements. Regarding the fact that the scattering intensity depends on the diameter of the protein aggregates to the power of six according to the Rayleigh approximation, the resulting intensity-based size distribution can be biased to larger aggregates.⁷ Despite these disadvantages, dynamic light scattering is a helpful complementary method to characterize aggregated protein samples.

Conformational changes of the proteins were investigated by intrinsic fluorescence, extrinsic fluorescent dyes and FT-IR spectroscopy. The latter was used to detect alterations in the secondary structure of the proteins which are characterized by changes in the amide band I of the spectra²². The most pronounced alterations in the 2nd derivative spectra of Adalimumab and Bevacizumab were detected after 7 days of light exposure. The main peak shifted towards 1630 cm⁻¹ and a second valley arose around 1648 cm⁻¹. The latter is, according to Yang *et al.*²² a characteristic band for random coil structures whereas bands between 1624 and 1642 cm⁻¹ are assigned to β -sheet structures^{24,36}. Alterations in the spectra for the other light stress time points were rather small with exception of Adalimumab after 4 days of light stress where alterations were already more pronounced. Stir stress affected the secondary structure only after 72 hours of stirring, since similar trends as for the light stressed samples in alterations of the 2nd derivative spectra could be detected, to a lower extent though. Less hours of stirring (4 and 24 hours) did not lead to remarkable changes in the spectra. The same can be stated for heat stressed Bevacizumab. After incubating the antibody at 50°C for 7 days similar changes in the spectra as after 7 days of light stress could be detected. In summary, it can be said that the secondary structure was affected only under rather harsh and long exposure times to the respective stress conditions. Thus, the extent of the changes in secondary structure increased with longer exposure times. Among the different stress methods, light stress triggered alterations in the secondary structure most, followed by heat and stir stress.

Alterations in the tertiary structure of proteins can lead to protein aggregation as described by the Lumry-Eyring theory⁸. Changes in the tertiary structure were investigated by fluorescence spectroscopy (intrinsic and extrinsic). Intrinsic fluorescence measurements of proteins are based on the fluorescent amino acid residues of tryptophan, phenylalanine and tyrosine. Among these amino acids, the fluorescence spectrum of tryptophan is decisively dependent on its environment and the spectrum can be blue shifted to shorter wavelengths when the environment gains hydrophobicity or when residues are buried in hydrophobic cores due to protein aggregation²¹. Furthermore, quenching of the tryptophan fluorescence can be induced by the interaction with intrinsic quenchers such as amine, carboxyl acid, disulfide or histidine groups or by addition of various other substances such as iodide, hydrogen peroxide, acrylamide^{21,37}. A drawback of measuring the intrinsic fluorescence is the relatively small quantum yield in comparison to the usage of extrinsic dyes²¹. Therefore, the extrinsic fluorescence using Bis-ANS as non-covalent fluorescence dye of the monoclonal antibodies was also determined. The principle of measuring extrinsic fluorescence is because non-covalent extrinsic fluorescence dyes such as ANS and Bis-ANS are non-fluorescent in a polar environment, but get strongly fluorescent in an apolar, hydrophobic surrounding. The spectra often show a blueshift and fluorescence intensity is clearly increased^{20,21}. In summary, changes in the fluorescence intensity

indicate alterations in the surrounding environment of the protein, thus indicating unfolding processes. Among all applied stress methods light stress led to the strongest alterations in fluorescence intensity. With longer exposure times to light, the intrinsic fluorescence decreased strongly indicating tryptophan quenching. Extrinsic fluorescent measurements confirmed these assumptions. The fluorescence intensity of Bis-ANS increased with longer exposure times to light (except for Adalimumab after 7 days of exposure to light) and spectra were blue shifted indicating an increasing presence of hydrophobic regions which may be caused by protein aggregation or unfolding processes. Due to high particle counts the interpretation of the intrinsic fluorescence measurements after stir stress was difficult. However, after 72 hours of stirring a remarkable decrease in fluorescence intensity for Bevacizumab and a smaller decrease for Adalimumab could be shown. As mentioned above, mechanical stress such as stirring is mixture of shear, interfacial effects between the protein and the stir bar e.g., cavitation and local thermal effects¹⁴. These effects might also lead to conformational changes such as unfolding and it is known from literature that heat stress can lead to conformational changes^{3,11,34}. The exposure of Bevacizumab to elevated temperature also resulted in a decrease of intrinsic fluorescence intensity indicating unfolding processes. The extent of the decrease elevated with longer exposure times. The extrinsic fluorescence measurements of the heat stressed Bevacizumab revealed no remarkable changes in fluorescence intensity compared to the unstressed protein. A blueshift of the spectra after 24 hours and 4 days of heat exposure could be shown. However, the particle burden in the sample was elevated which might have interfered with the extrinsic fluorescent dye.

The current study had two principal aims: First, we determined suitable stress conditions for Adalimumab and Bevacizumab to generate different types of protein aggregates; and second, to find respective time points to generate samples with a sustainable amount of protein aggregates but still contain enough monomer, thus are not fully denatured. Table 4-5 and Table 4-6 represent an overview of the selected stress methods and time points for following experiments using the human artificial lymph node model for the evaluation of immunogenicity of protein aggregates. For Adalimumab we selected light stress for 48 hours and stir stress for 24 hours. The latter represents a sample containing primarily insoluble aggregates, thus particles. Due to the high particle burden the monomer recovery was decreased slightly to 88.94 %. Contrarily, the light stressed sample especially contained various high and low molecular species coinciding with a decreased monomer recovery of 55.93%. The number of particles was also increased but to a lower extent than after stirring. The same is true for Bevacizumab after stir and light stress with the difference that 24 hours of light exposure were enough to generate protein aggregates of different sizes. For the heat stressed sample we chose 4 days as an appropriate time point, since this sample contained soluble aggregates, fragments and particles at the

same time and a monomer recovery of 87.44% was acceptable. The secondary structure of the stir stressed antibodies was preserved, for the light and heat stressed sample(s) we detected small modifications. The tertiary structure of the Bevacizumab was especially influenced by light stress. Since the time point after 48 hours was analyzed later, no fluorescence data was available for the current study. In the following studies we applied fluorescence spectroscopy to all stressed samples.

Moreover, we investigated the stability of the aggregated samples of Adalimumab and Bevacizumab after storage at 2-8°C and after storage at -80°C for 6 months and subsequent storage at 2-8°C for 6 weeks after thawing. The aim of this stability study was to ensure the quality of the generated samples during the reactor run time over 4 weeks. The results revealed that the composition of the aggregated samples of Bevacizumab and Adalimumab did not change dramatically when stored at 2-8°C directly after production. When the samples were frozen at -80°C for 6 months before they were thawed and again stored at 2-8°C for 6 weeks, a trend towards the generation of larger molecular weight species in Adalimumab samples after light stress was detectable. In combination with a decrease in total recovery, this might indicate particle formation. Thus, it can be assumed that, aggregated Adalimumab samples are less stable once they were stored at -80°C prior to the experiment. In contrast, aggregated Bevacizumab samples did not show any changes in the composition after thawing and storage at 2-8°C. Therefore, aggregated Bevacizumab samples can be stored at -80°C prior to the start of the reactor run, while it is recommended for aggregated Adalimumab samples to be used within 6 weeks after production and storage at 2-8°C. However, it is possible to store all aggregated samples of Adalimumab and Bevacizumab at 2-8°C for a period of 6 weeks. Thus, the quality of the samples remains consistent during the reactor run time.

Table 4-5: Overview of selected stress methods and time points for Adalimumab. HMW= High molecular weight species, LMW= Low molecular weight species; HMW 2 > HMW 2/1 > HMW 1; LMW 1 > LMW 2; - no significant changes; + moderate changes; ++ strong changes.

Adalimumab	Turbidity	Increased number of particles	Formation of soluble aggregates	Formation of fragments	Monomer recovery (SEC)	Altered secondary structure (FT-IR)	Altered tertiary structure (Fluorescence)
Unstressed	1.54 FNU	-	-	-	100%	-	-
Light stress 48h	3.21 FNU	+	++ 7.53% HMW2 6.12% HMW2/1 15.83% HMW1	+ 6.97% LMW1 4.65% LMW2	55.93%	+	n.d.
Stir stress 24h	>1300 FNU	++	-	-	88.94%	-	n.d.

Table 4-6: Overview of selected stress methods and time points for Bevacizumab. HMW= High molecular weight species, LMW= Low molecular weight species; HMW 2 > HMW 1; LMW 1 > LMW 2; - no significant changes; + moderate changes; ++ strong changes.

Bevacizumab	Turbidity	Increased number of particles	Formation of soluble aggregates	Formation of fragments	Monomer recovery (SEC)	Altered secondary structure (FT-IR)	Altered tertiary structure (Fluorescence)
Unstressed	1.82 FNU	-	+	-	99.64%	-	-
Light stress 24h	4.04 FNU	+	++ 6.55% HMW2 14.54% HMW1	+ 2.61% LMW2	77.16%	+	++
Stir stress 24h	587.0 FNU	++	+ 1.14% HMW1	-	91.19%	-	n.d.
Heat stress 4d	13.27 FNU	++	+ 1.99% HMW2 4.39% HMW1	+ 2.32% LMW2	87.44%	+	n.d.

4.4 References

1. Wang, W. Instability, stabilization, and formulation of liquid protein pharmaceuticals. *Int. J. Pharm.* **185**, 129–188 (1999).
2. Elvin, J. G., Couston, R. G. & Van Der Walle, C. F. Therapeutic antibodies: Market considerations, disease targets and bioprocessing. *Int. J. Pharm.* **440**, 83–98 (2013).
3. Mahler, H.-C., Friess, W., Grauschopf, U. & Kiese, S. Protein aggregation: Pathways, induction factors and analysis. *J. Pharm. Sci.* **98**, 2909–2934 (2009).
4. Rosenberg, A. S. Effects of protein aggregates: an immunologic perspective. *AAPS J.* **8**, E501–E507 (2006).
5. Narhi, L. O., Schmit, J., Bechtold-Peters, K. & Sharma, D. Classification of Protein Aggregates. *J. Pharm. Sci.* **101**, 493–498 (2012).
6. Philo, J. S. Is any measurement method optimal for all aggregate sizes and types? *AAPS J.* **8**, E564–E571 (2006).
7. Zölls, S. *et al.* Particles in Therapeutic Protein Formulations, Part 1: Overview of Analytical Methods. *J. Pharm. Sci.* **101**, 914–935 (2012).
8. Lumry, R. & Eyring, H. Conformation changes of proteins. *J. Phys. Chem* **58**, 110–120 (1954).
9. Wang, W. Protein aggregation and its inhibition in biopharmaceutics. *Int. J. Pharm.* **289**, 1–30 (2005).
10. Reubsaet, J. L. *et al.* Analytical techniques used to study the degradation of proteins and peptides: chemical instability. *J. Pharm. Biomed. Anal.* **17**, 955–978 (1998).
11. Hawe, A., Kasper, J. C., Friess, W. & Jiskoot, W. Structural properties of monoclonal antibody aggregates induced by freeze-thawing and thermal stress. *Eur. J. Pharm. Sci.* **38**, 79–87 (2009).
12. Ratanji, K. D. *et al.* Subvisible aggregates of immunogenic proteins promote a Th1-type response. *Toxicol. Sci.* **153**, 258–270 (2016).
13. Fradkin, A. H., Carpenter, J. F. & Randolph, T. W. Immunogenicity of aggregates of recombinant human growth hormone in mouse models. *J. Pharm. Sci.* **98**, 3247–3264 (2009).
14. Kiese, S., Pappenberg, A., Friess, W. & Mahler, H.-C. Shaken, not stirred: Mechanical Stress Testing of an IgG1 Antibody. *J. Pharm. Sci.* **97**, 4347–4366 (2008).

15. Shire, S. J., Shahrokh, Z. & Liu, J. Challenges in the development of high protein concentration formulations. *J. Pharm. Sci.* **93**, 1390–1402 (2004).
16. Narhi, L. O. *et al.* Chemical and Biophysical Characteristics of Monoclonal Antibody Solutions Containing Aggregates Formed during Metal Catalyzed Oxidation. *Pharm. Res.* **34**, 2817–2828 (2017).
17. Bessa, J. *et al.* The immunogenicity of antibody aggregates in a novel transgenic mouse model. *Pharm. Res.* **32**, 2344–2359 (2015).
18. Chaudhuri, R., Cheng, Y., Middaugh, C. R. & Volkin, D. B. High-Throughput Biophysical Analysis of Protein Therapeutics to Examine Interrelationships Between Aggregate Formation and Conformational Stability. *AAPS J.* **16**, 48–64 (2014).
19. 2.9.19 Partikelkontamination- Nicht sichtbare Partikeln. *European Pharmacopoeia* 438–441 (2014).
20. Hawe, A., Sutter, M. & Jiskoot, W. Extrinsic fluorescent dyes as tools for protein characterization. *Pharm. Res.* **25**, 1487–1499 (2008).
21. Poole, R. A., Hawe, A. & Jiskoot, W. in *Analysis of Aggregates and Particles* (eds. Mahler, H.-C. & Jiskoot, W.) 201–226 (2012).
22. Yang, H., Yang, S., Kong, J., Dong, A. & Yu, S. Obtaining information about protein secondary structures in aqueous solution using Fourier transform IR spectroscopy. *Nat. Protoc.* **10**, 382–96 (2015).
23. Arrondo, J. L., Muga, a, Castresana, J. & Goñi, F. M. Quantitative studies of the structure of proteins in solution by Fourier-transform infrared spectroscopy. *Prog. Biophys. Mol. Biol.* **59**, 23–56 (1993).
24. Kong, J. & Yu, S. Fourier transform infrared spectroscopic analysis of protein secondary structures. *Acta Biochim. Biophys. Sin. (Shanghai)*. **39**, 549–559 (2007).
25. Paul, R. *et al.* Structure and function of purified monoclonal antibody dimers induced by different stress conditions. *Pharm. Res.* **29**, 2047–2059 (2012).
26. Joubert, M. K., Luo, Q., Nashed-Samuel, Y., Wypych, J. & Narhi, L. O. Classification and characterization of therapeutic antibody aggregates. *J. Biol. Chem.* **286**, 25118–25133 (2011).
27. Telikepalli, S. N. *et al.* Structural characterization of IgG1 mAb aggregates and particles

- generated under various stress conditions. *J. Pharm. Sci.* **103**, 796–809 (2014).
28. Mahler, H. C., Müller, R., Frieß, W., Delille, A. & Matheus, S. Induction and analysis of aggregates in a liquid IgG1-antibody formulation. *Eur. J. Pharm. Biopharm.* **59**, 407–417 (2005).
29. Freitag, A. J. *et al.* Investigation of the immunogenicity of different types of aggregates of a murine monoclonal antibody in mice. *Pharm. Res.* **32**, 430–444 (2015).
30. Li, S., Schöneich, C. & Borchardt, R. T. Chemical Instability of Protein Pharmaceuticals : Mechanisms of Oxidation and Strategies for Stabilization. *Biotechnol. Bioeng.* **48**, 490–500 (1995).
31. Davies, M. J. Singlet oxygen-mediated damage to proteins and its consequences. *Biochem. Biophys. Res. Commun.* **305**, 761–770 (2003).
32. Boll, B. *et al.* Extensive chemical modifications in the primary protein structure of IgG1 subvisible particles are necessary for breaking immune tolerance. *Mol. Pharm.* **14**, 1292–1299 (2017).
33. Lam, X. M., Yang, J. Y. & Cleland, J. L. Antioxidants for prevention of methionine oxidation in recombinant monoclonal antibody HER2. *J. Pharm. Sci.* **86**, 1250–1255 (1997).
34. Luo, Q. *et al.* Chemical modifications in therapeutic protein aggregates generated under different stress conditions. *J. Biol. Chem.* **286**, 25134–25144 (2011).
35. Chumsae, C., Gaza-Bulseco, G., Sun, J. & Liu, H. Comparison of methionine oxidation in thermal stability and chemically stressed samples of a fully human monoclonal antibody. *J. Chromatogr. B Anal. Technol. Biomed. Life Sci.* **850**, 285–294 (2007).
36. Dong, A., Huang, P. & Caughey, W. S. Redox-Dependent Changes in beta-extended Chain and Turn Structures of Cytochrome C in Water Solution Determined by Second Derivative Amide I Infrared Spectra. *Biochemistry* **31**, 182–189 (1992).
37. Ladokhin, A. S. in *Encyclopedia of Analytical Chemistry* (ed. Meyers, R. A.) 5762–5779 (John Wiley&Sons Ltd, 2000).

Chapter 5

The evaluation of immunogenicity of protein aggregates in a 3D human artificial lymph node model

Parts of this chapter were published as research article in the Journal of Pharmaceutical Sciences as:

Teresa Kraus, Annika Lubitz, Ulrike Schließer, Christoph Giese, Jana Reuschel, Rene Brecht, Julia Engert, Gerhard Winter

Evaluation of a 3D Human Artificial Lymph Node as Test Model for the Assessment of Immunogenicity of Protein Aggregates

Journal of Pharmaceutical Sciences 108 (2019) 2358-2366

The publication includes work that was performed in collaboration with ProBioGen AG in Berlin. The planning of the study, the production and analysis of all stressed protein samples was accomplished by the main author Teresa Kraus; all HuALN bioreactor experiments including cytokine and ADA analysis were performed by ProBioGen AG, Berlin.

5.1 Introduction

Biopharmaceuticals are a steadily growing group of drugs to treat severe diseases such as cancer, multiple sclerosis, Crohn's disease and rheumatoid arthritis¹. However, it is known, that biopharmaceuticals bear the risk to elicit immunogenicity in patients e.g. resulting in the formation of anti-drug antibodies (ADAs). Clinical consequences can be severe allergic reactions such as anaphylaxis or the loss of efficacy of the drug²³. Besides patient-related factors like the immunological status, the history of allergy of patients, the route and frequency of administration and the dosing that are likely to modulate immunogenicity, product related factors may also contribute to immunogenicity substantially. These include the product origin, the primary structure of the protein, containers, additives, impurities from the manufacturing process and in particular protein aggregates³⁻⁶. The effect of protein aggregates on the immune system has been discussed and investigated for a long time⁷. In various studies, protein aggregates were generated by exposure of the protein to various stress conditions such as light, mechanical, thermal and chemical stress, and the immunogenicity was evaluated using either *in vitro* or *in vivo* models⁸⁻¹³. Some groups tested a mix of different sized protein aggregates^{9,10}, while others used fractionation methods such as asymmetrical flow field flow fractionation (AF4) or fluorescence-activated cell sorting (FACS) to evaluate the immunogenicity of a distinct group of protein aggregates^{12,14,15}. Despite all these studies it remains uncertain, which types of protein aggregates pose the greatest risk to elicit immunogenicity. Recently, research focused especially on subvisible particles in the size range of 0.1-10 μm and protein aggregates with considerable chemical modifications^{14,16-18}. It is a challenge to establish an appropriate test system to evaluate and predict immunogenicity in humans. For the evaluation of immunogenicity of protein aggregates, *in vitro* and *in vivo* models are used¹⁹. *In vitro* models are often based on the interaction of protein aggregates with antigen presenting cells and T-cells isolated from human peripheral blood mononuclear cells (PBMCs). Several DC markers, cytokine profiles and T-cell proliferation can be analyzed^{1,20}. However, it needs to be considered that only specific immune cells are investigated, and that cell assays represent only a small part of the human immune system¹. In contrast, *in vivo* models enable to evaluate immunogenicity in an organism with a fully trained immune system and to investigate the formation of anti-drug antibodies²¹. The most common *in vivo* models used for the assessment of immunogenicity of protein aggregates are mouse models^{12,14,22-25}. Yet, the choice of an appropriate mouse strain is complex and may influence immunogenic answers²¹. Furthermore, the assessment of immunogenicity in mouse models is not necessarily predictive of immune responses in humans^{1,26}. Recently, the development of various 3D models of human organs to mimic human immunity attracted great interest. Generally, these models can be divided into non-lymphoid organs imitating innate immunity and lymphoid human organs mimicking adaptive immunity²⁰. Among

lymphoid organs, the development of lymph node models is a key aspect, since lymph nodes play a major role in an immune response²⁰. Giese and colleagues developed and optimized a 3D human artificial lymph node (3D HuALN) model to mimic the interface between the innate and adaptive immune response *in vitro*^{20,27,31}. The HuALN is a miniaturized, disposable 3D *in vitro* culture model based on cells from human donors. Continuous perfusion of the bioreactor device ensures long-term cultivation under steady-state conditions and allows repeated drug exposition as well as a broad range of read-out parameters on T- and B-cell levels. The system was already successfully used for testing albumins and vaccines²⁸, but has not yet been utilized for evaluating the immunogenicity of protein aggregates.

In this chapter, a HuALN model was used to evaluate the immunogenicity of preparations of two monoclonal antibodies. Protein aggregates were formed by exposing two monoclonal antibodies to different stress conditions. The protein aggregates were thoroughly analyzed regarding their size and structure, tested in a 2D co-culture assay format (DC/T cell assay) and finally the HuALN was stimulated with the generated samples. Cell culture supernatants were harvested daily and analyzed for the presence of various cytokines. Moreover, some additional data regarding the presence of anti-drug antibodies (ADAs) in the cell culture supernatants of the HuALN culture and the diffusion behavior of particles through a dextran gel matrix was collected.

5.2 Evaluation of a 3D human artificial lymph node model as test model for the assessment of immunogenicity of protein aggregates

5.2.1 Results and Discussion

5.2.1.1 Analysis of prepared protein aggregates after stir, light and heat stress

Adalimumab and Bevacizumab were exposed to different stress conditions (see Materials and Methods, Chapter 3) and analyzed using turbidity, light obscuration, size exclusion chromatography, FT-IR, and extrinsic fluorescence spectroscopy to characterize the aggregated samples. The turbidity of Adalimumab and Bevacizumab increased after exposure to different stress conditions (Table 5-1) indicating changes in the aggregation status of the proteins. The strongest increase was detected for the samples after stir stress, when turbidity reached values of 313 FNU for Adalimumab and 848 FNU for Bevacizumab. After the exposure of the antibodies to light stress, turbidity values of 66.37 FNU (Adalimumab) and 25.87 FNU (Bevacizumab) were detected. Heat stressed Bevacizumab led only to a small increase in turbidity (12.19 FNU) compared to unstressed Bevacizumab (8.76 FNU). To detect subvisible particles larger than 1 μm , light obscuration measurements were performed. The

cumulative particle counts per mL of Adalimumab and Bevacizumab after exposure to different stress conditions are summarized in Table 5-1. High particle numbers were observed for Adalimumab and Bevacizumab after stir stress which strongly triggered the formation of particles between 1 μ m and 25 μ m. After light stress a moderate increase in particles sized between 1-10 μ m was observed for both proteins. Particles larger than 10 μ m also increased, but standard deviations were high making a statement difficult. Heat stress of Bevacizumab predominantly triggered the formation of subvisible particles in the range of 1-10 μ m. The presence of soluble aggregates was investigated by size exclusion chromatography. The distribution of protein species of Adalimumab and Bevacizumab is displayed in Table 5-2. It is apparent that light stress strongly induced the formation of soluble aggregates and fragments of different sizes (HMW 2 > HMW 1; LMW 1 > LMW 2). As a result, the monomer content was reduced significantly to $37.13 \pm 0.25\%$ for Adalimumab and $59.91 \pm 0.02\%$ for Bevacizumab. In contrast, stir stress did not lead to an increase in the content of soluble aggregates or to the formation of fragments compared to the unstressed antibody solutions. Heat stress of Bevacizumab moderately triggered the formation of soluble aggregates ($4.54 \pm 0.04\%$) and fragments ($0.72 \pm 0.03\%$). FT-IR measurements were performed to detect alterations in the secondary structure. Second derivative FT-IR spectra of unstressed Adalimumab and Bevacizumab and after light, stir and heat stress are shown in Figure 5-1. Light, stir and heat stress did not lead to significant changes of the amide I band. However, already minimal changes in the intensities of the second derivatives indicate that the contents of the secondary structure components may have changed, although the local secondary structural geometry may not have changed.

Table 5-1: Summary of turbidity measurements and cumulative particle counts per mL of Adalimumab and Bevacizumab samples tested in the current study. Values are reported as the mean of three aliquots \pm standard deviation.

Adalimumab	Sample	Turbidity [FNU]	Particle counts $\geq 1 \mu\text{m}$	Particle counts $\geq 10 \mu\text{m}$	Particle counts $\geq 25 \mu\text{m}$
	Unstressed	15.81 \pm 0.98	14673 \pm 4676	225 \pm 224	8 \pm 12
	Light stress 48h	66.37 \pm 2.61	344683 \pm 230493	27617 \pm 24702	292 \pm 271
	Stir stress 24h	313.00 \pm 3.46	6429000 \pm 205533	22334 \pm 1179	250 \pm 354
	Formulation buffer	0.45 \pm 0.03	78 \pm 29	2 \pm 2	0 \pm 0
Bevacizumab	Sample	Turbidity [FNU]	Particle counts $\geq 1 \mu\text{m}$	Particle counts $\geq 10 \mu\text{m}$	Particle counts $\geq 25 \mu\text{m}$
	Unstressed	8.76 \pm 1.0	34742 \pm 1214	1008 \pm 907	8 \pm 12
	Light stress 24h	25.87 \pm 3.82	173242 \pm 47412	11300 \pm 10583	117 \pm 94
	Stir stress 24h	848.33 \pm 21.01	15732667 \pm 181491	74250 \pm 12138	2500 \pm 236
	Heat stress 4d	12.19 \pm 1.43	840000 \pm 61943	2200 \pm 141	50 \pm 71

Table 5-2: Summary SEC results: Distribution of protein species of Adalimumab and Bevacizumab after exposure to different stress conditions (n=2). ¹ The total protein recovery represents the total eluted protein normalized to the injected protein amount.

Adalimumab	Sample	HMW 2 [%]	HMW 1 [%]	Monomer [%]	LMW 1 [%]	LMW 2 [%]	Total protein recovery [%] ¹
	Unstressed	-	0.71 \pm 0.24	99.29 \pm 0.24	-	-	98.82 \pm 1.33
	Light stress 48h	39.44 \pm 1.40	17.59 \pm 0.43	37.13 \pm 0.25	3.13 \pm 0.83	2.71 \pm 0.11	84.98 \pm 0.76
	Stir stress 24h	-	0.88 \pm 0.05	99.12 \pm 0.05	-	-	96.46 \pm 0.43
Bevacizumab		HMW 2 [%]	HMW 1 [%]	Monomer [%]	LMW [%]		
	Unstressed	-	1.44 \pm 0.11	98.56 \pm 0.11	-	-	95.76 \pm 0.78
	Light stress 24h	18.50 \pm 0.06	20.21 \pm 0.04	59.91 \pm 0.02	1.38 \pm 0.04	-	91.54 \pm 2.40
	Stir stress 24h	-	1.77 \pm 0.19	98.23 \pm 0.19	-	-	93.77 \pm 1.35
	Heat stress 4 days	-	4.54 \pm 0.04	94.74 \pm 0.07	0.72 \pm 0.03	-	89.59 \pm 0.35

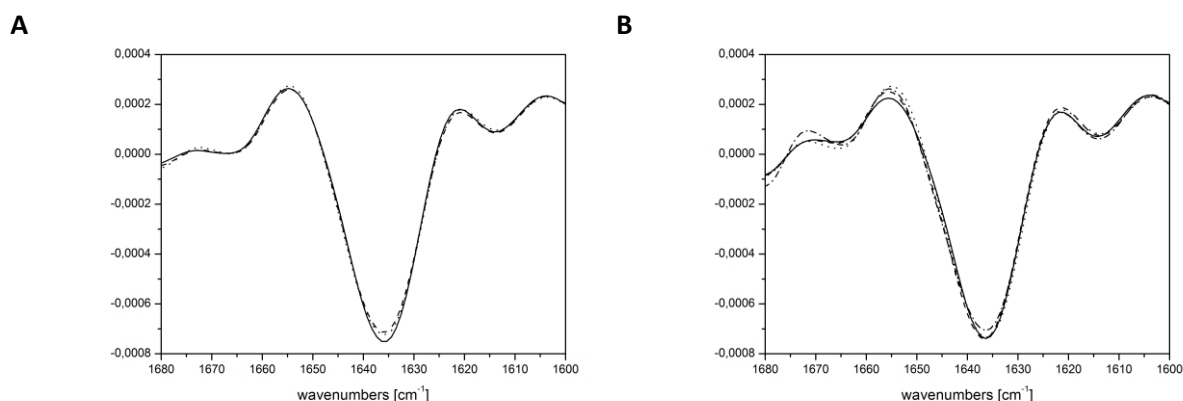


Figure 5-1: Second derivative FT-IR spectra of A) Adalimumab and B) Bevacizumab: The black line represents the spectrum of unstressed Adalimumab/Bevacizumab, the dotted line represents the spectrum of stir stressed Adalimumab/Bevacizumab, the dashed line represents the spectrum of Adalimumab/Bevacizumab after light stress and the dashed/dotted line represents the spectrum of heat stressed Bevacizumab.

The extrinsic fluorescence emission spectra of Adalimumab and Bevacizumab using 20 μ M Bis-ANS as fluorescence dye are displayed in Figure 5-2. The fluorescence intensity of Adalimumab increased clearly after light exposition indicating a more hydrophobic environment and therefore unfolding processes²⁹. Moreover, the emission maxima after light stress clearly shifted to a smaller wavelength (495.97 nm) compared to the unstressed sample (503.43 nm). After exposure of Adalimumab to stir stress, fluorescence intensity also increased slightly, but to a lower extent than after light stress. The emission maxima after stir stress shifted to a wavelength of 502.98 nm. Thus, only a minimal blue shift was observed. A strong increase in fluorescence intensity and a blue shift of the emission spectra was also observed for Bevacizumab after light stress as shown in Figure 5-2 and Table 5-3. No shift of the emission maxima of Bevacizumab after stir stress was detected, but an increase in fluorescence intensity was observed (see Figure 5-2). No increase in fluorescence intensity could be detected for Bevacizumab after heat stress. Conversely, there was a blue shift of the spectra to a wavelength of 499.55 nm, as displayed in Figure 5-2 and Table 5-3. It can be assumed that particularly light stress altered the tertiary structure of Adalimumab and Bevacizumab. Changes were also detectable after stir stress, to a lesser extent though.

Table 5-3: Maxima of extrinsic fluorescence emission spectra of Adalimumab and Bevacizumab after exposure to different stress conditions.

Adalimumab	Unstressed	Light stress 48h	Stir stress 24h	-
Peak position [nm]	503.43	495.97	502.98	-
Bevacizumab	Unstressed	Light stress 24h	Stir stress 24h	Heat stress 4d
Peak position [nm]	501.94	498.05	498.05	499.55

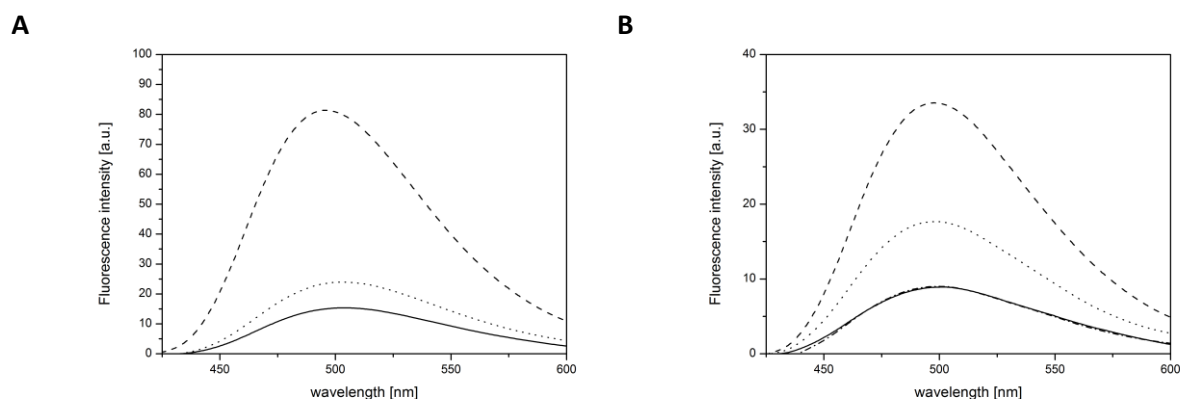


Figure 5-2: Extrinsic fluorescence emission spectra of A) Adalimumab and B) Bevacizumab at 1 mg/mL using 20 μ M Bis-ANS excited at 385 nm: The black line represents the spectrum of unstressed Adalimumab/Bevacizumab, the dotted line represents the spectrum of stir stressed Adalimumab/Bevacizumab, the dashed line represents the spectrum of Adalimumab/Bevacizumab after light stress and the dashed/dotted line represents the spectrum of heat stressed Bevacizumab.

The aim was to generate aggregated protein samples by exposure of the monoclonal antibodies to different stress conditions that biopharmaceuticals possibly face during production, handling and transportation³⁰. The stress conditions were carefully selected during a pre-study to obtain reproducible amounts and types of protein aggregates (data not shown). In our study, light stress primarily led to the formation of soluble aggregates whereas stir stress strongly triggered the formation of particles but not of soluble aggregates. Bevacizumab was additionally exposed to elevated temperatures which resulted in a sample containing moderate amounts of soluble and insoluble aggregates and fragments at the same time. According to light obscuration data heat stress primarily triggered the formation of particles in the size range between 1 - 10 μ m which are in particular of interest due to their immunogenic risk^{16,31}. It has been shown before that subvisible aggregates can promote a TH1-type immune response *in vivo*³². Heat stress was not applied to Adalimumab in our study, since the reasonable conditions applied in pre-studies did not lead to a considerable amount of protein aggregates. The scope of our work focused particularly on the “proof of concept” of using a 3D HuALN model for testing the immunological risk of protein aggregates; therefore, no further analytics were applied. Moreover, it should be considered that the levels of generated protein aggregates in the stressed sample do not represent levels of protein aggregates in marketed drug products.

5.2.1.2 Analysis of 2D Cell Culture Experiments and HuALN Culture Experiments

The aim of testing the stressed samples in a 2D *in vitro* assay was first the comparison of results with a 3D *in vitro* model and, second to find an appropriate test concentration of the samples for the evaluation of immunogenicity in the human artificial lymph node model. Stressed samples of Bevacizumab and Adalimumab were tested at concentrations of 0.05, 0.5 and 5 mg/mL and 0.1, 1 and 10 mg/mL, respectively. Selected data of cytokine analysis is exemplarily shown in Figure 5-3.

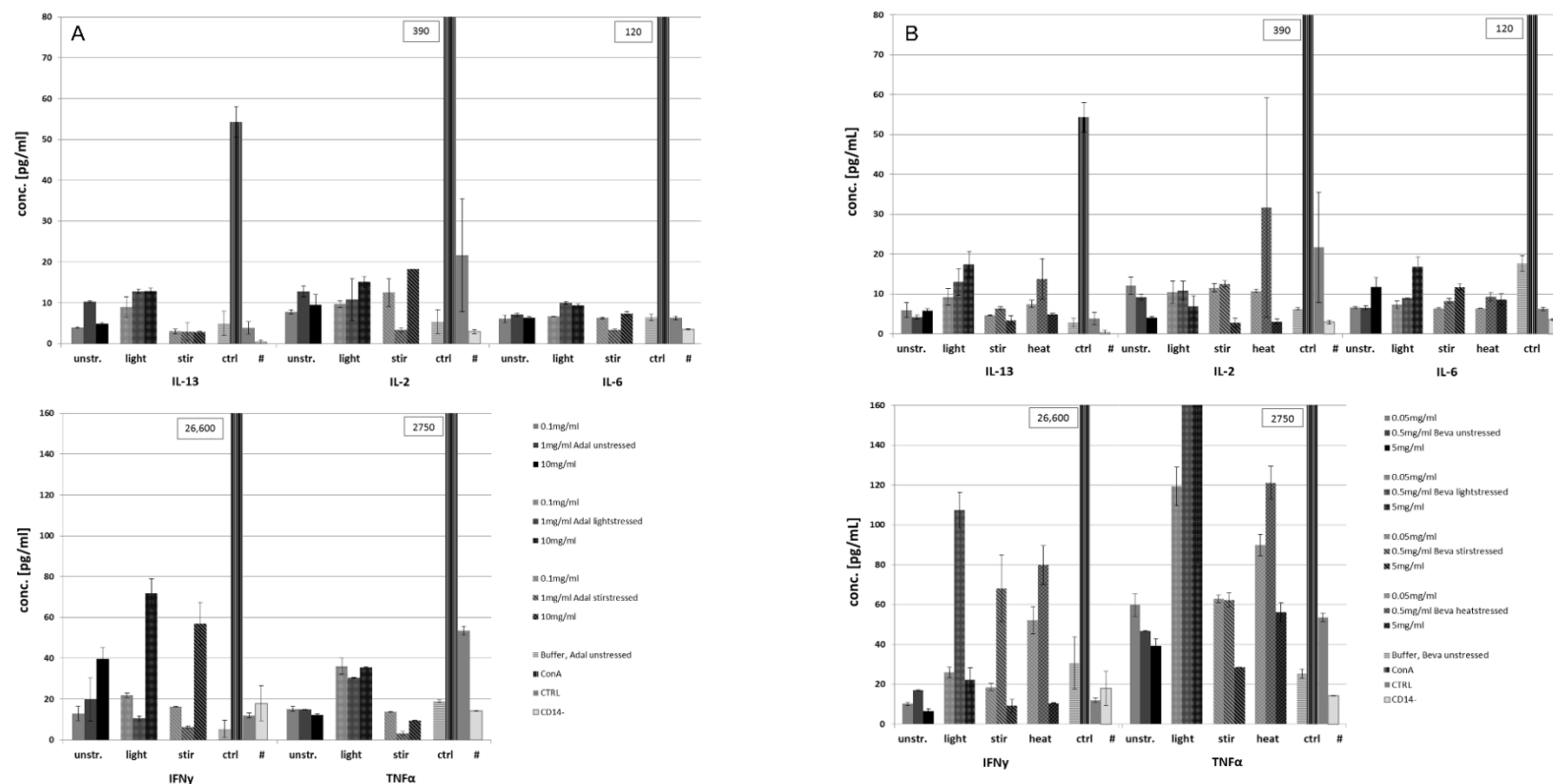


Figure 5-3: Cytokine secretion in 2D co-cultures treated with three different doses of variously stressed antibody samples in duplicates. ConcavalinA (ConA, vertically striped black line) was used as positive control, then grey and the light grey bar display negative controls. Where bars are out of display, concentration is displayed in boxes [pg/mL]. A) Results for Adalimumab: unstressed Adalimumab (solid bars), Adalimumab after light stress (dotted bars) and after stir stress (striped bars). Buffer is displayed in dark grey bars. B) Results for Bevacizumab: unstressed Bevacizumab (solid bars), Bevacizumab after light stress (dotted bars), stir stress (striped bars) and after heat stress (chessboard bars). Buffer is displayed in vertically striped bars. This data was provided by ProBioGen AG, Berlin.

Five cytokines (IFN- γ , TNF- α , IL-2, IL-13, IL-6) were selected out of the panel of ten cytokines since these cytokines showed levels above 5 pg/mL, dose-dependency, and differences between stress conditions. Cytokine analysis of supernatants revealed enhancement of IFN- γ induction by light-, heat-, and stir-stressed Bevacizumab (0.5 mg/ml). The secretion of TNF- α was elevated by stressed Bevacizumab and light-stressed Adalimumab samples, to a lower extent though. In contrast, stir-stressed Adalimumab samples reduced TNF- α secretion. This reduced TNF- α secretion can be explained by the mechanism of action of Adalimumab as a member of the group of TNF- α – blockers binding to TNF- α to prevent its effect³³. According to the cytokine data stressed Adalimumab was still able to bind its target. However, it remains unclear, whether the TNF- α binding refers to protein aggregates of Adalimumab or to the remaining non-denatured molecules present in the stressed antibody sample. Only Adalimumab after light stress showed a small increase in TNF- α secretion compared to the unstressed protein. Slight, but dose-dependent increase of IL-13 and IL-6 secretion for both light-stressed antibody samples was observed. Levels of CD86, CD83, CD80 and other DC markers were not increased by exposure with stressed antibody samples, even high doses of stir- and heat-stressed samples strongly decreased all markers (see Figure 5-5). Only high dose of stir-stressed samples reduced the expression of CD3, CD4 and CD8 on T cells (data not shown). Proliferation of T-cells (CD3+/Edu+) in co-cultures treated with stressed samples compared to control was not enhanced (data not shown). Due to a down-regulation of DC markers with the highest concentration and no response of cells with the lowest concentration, 0.5 and 1 mg/mL were selected as test concentrations for Bevacizumab and Adalimumab for the HuALN experiment, respectively. The results of cytokine analysis after stimulation of the HuALN with the generated samples of Bevacizumab and Adalimumab are displayed in Figure 5-4. Stimulating the HuALN with Adalimumab after stir and light stress resulted in a cytokine profile comparable to unstressed Adalimumab. Thus, no differences in cytokine secretion profiles were seen between unstressed and stressed samples. In contrast, Bevacizumab after exposure to heat enhanced a pro-inflammatory (Pro-inf), T-helper 1 (TH1) as well as a slight T-helper 2 (TH2) immune response. The same trends were seen for light- and stir-stressed Bevacizumab, even though to a lower extent.

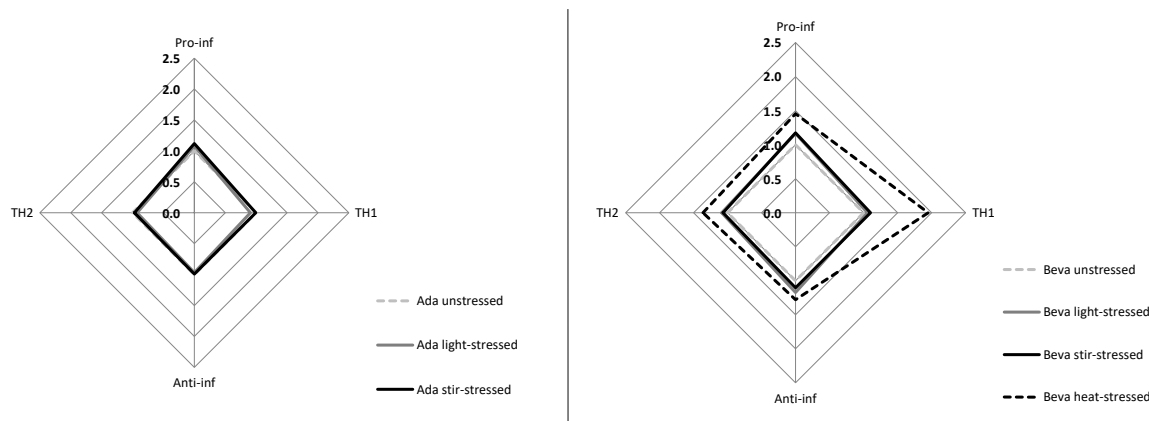


Figure 5-4: Spider grid diagrams for tested antibody samples: spider grid diagram of Adalimumab samples (left); spider grid diagram of Bevacizumab samples (right)). The mean of three independent HuALN runs each is displayed: Left: Adalimumab: unstressed (dashed grey line), light stress (grey line), stir stress (black line) and right: Bevacizumab: unstressed (dashed grey line), light stress (grey line), stir stress (black line) and heat stress (dashed black line). In brief: AUC values displaying the overall amount of each cytokine secreted during the entire bioreactor run are normalized to the control run, combined with respect to cytokine groups (TH1, TH2, Pro-inf, Anti-inf), and displayed in spider grids. Values larger/smaller than 1 display up-/downregulation in direct comparison to control run. This data was provided by ProBioGen AG, Berlin.

The 2D DC assay as well as the 3D HuALN model represents an *in vitro* model based on cells from human donors. Whereas the 2D *in vitro* assay is performed in a standard well-plate format, the human artificial lymph node model is a complex 3D matrix assisted model operated with PBMCs and DCs in combination with allogeneic MSC-derived stromal cells. By combination of functional and structural cells lymphatic follicles and germinal centers form and mimic the 3D structure of human lymph nodes^{28,34}. Continuous perfusion of the bioreactor device ensures cultivation under steady-state conditions enabling a long-term exposition of the drug including multiple re-stimulations. In the present study, the HuALN experiment was performed for 28 days including an initial stimulation with the stressed samples on day 0 followed by three re-stimulations on day 7, 14 and 21. The possibility of a long-term exposure up to four weeks including the mentioned re-stimulations of the stressed protein samples represents a major advantage of the HuALN system compared to conventional 2D *in vitro* experiments. Exposure times during 2D *in vitro* experiments are rather short varying from several hours until up to a few days^{18,35}. By re-stimulating the model weekly, delayed immune reactions can be monitored as well which is an important aspect for therapies with weekly applications, for example³⁶. Due to its continuous perfusion the lymph node model also mimics the dilution of protein aggregates that occurs *in vivo* following an application more closely than 2D *in vitro* assays. Comparing the results from the 2D *in vitro* assay and the HuALN experiment, it is noticeable that primarily light – and heat stressed Bevacizumab triggered the secretion of IFN- γ and TNF- α whereby light stress had a stronger effect than heat stress in 2D experiments. According to the HuALN data, heat stress led to a TH1 and pro-inflammatory answer which is also characterized by the secretion of IFN- γ and TNF- α (see Table 5-4).

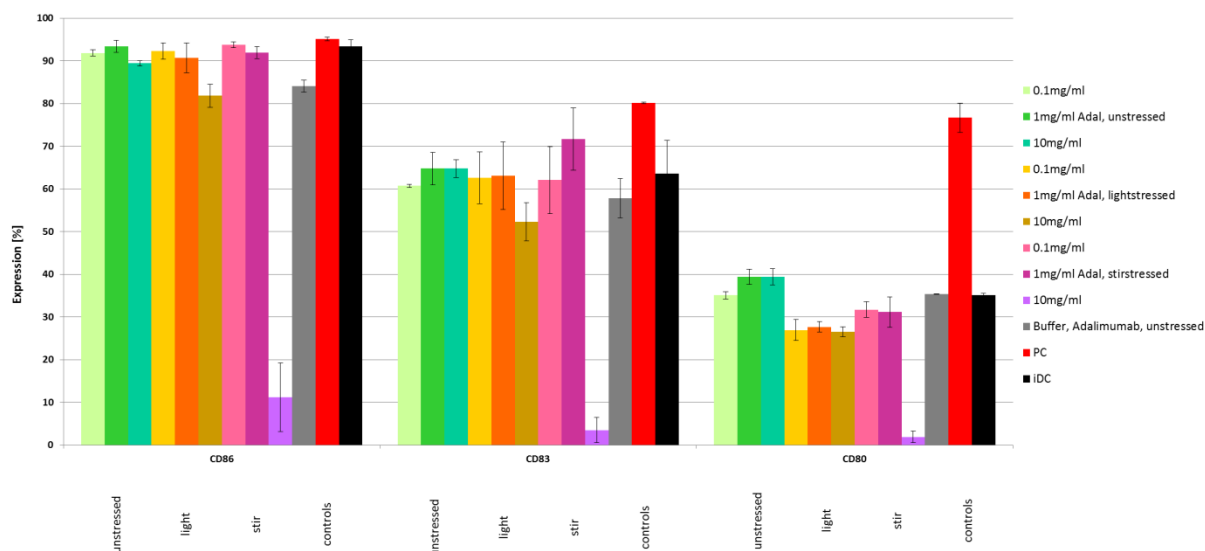
Table 5-4: Cytokine groups: analyzed cytokines are classified to groups based on their immunological function for a simplified analysis of immune responses in HuALN bioreactors.

Groups	Assorted cytokines
Pro-inflammatory	IL-1 β
	IL-6
	IFN- γ
	TNF- α
Anti-inflammatory	IL-6
	IL-10
TH1	IL-2
	IL-12p70
	IFN- γ
	TNF- α
TH2	IL-4
	IL-6
	IL-10
	IL-13

For better understanding the results of cytokine analysis of the 2D *in vitro* assay were also displayed as spider grid diagrams (see Figure 5-6). In comparison to the spider grid diagrams of the HuALN experiment, there was a slight trend towards a pro - inflammatory and TH2 immune response of light stressed Adalimumab, whereas no differences between the differently stressed Adalimumab samples were observed according to the cytokine analysis of the HuALN experiment. Differences between the induced cytokine responses were also found for Bevacizumab. The spider grid of the 2D *in vitro* assay revealed that light stressed Bevacizumab resulted in a larger effect than heat stress, both triggering a pro-inflammatory and TH1 immune response. However, evaluating the cytokine data over a period of four weeks, heat stress resulted in having the stronger effect on the cytokine secretion. For a more detailed analogy observation between the 2D assay and the 3D HuALN experiment, the cytokine secretion of similar time points of the 3D assay was analyzed. Comparison of the cytokine levels in bioreactor samples of day three (Figure 5-7) with the results from the 2D DC assay (see Figure 5-3 and Figure 5-8) revealed similar absolute levels of IL-13, IL-2, and IFN- γ . Irrespective of minimal differences which should not be overrated, these levels were independent from stress conditions of the applied antibodies in the 3D HuALN experiment, at this early stage. In the 2D assay, slight increases in cytokine levels could be observed for Adalimumab (especially light-stressed) and Bevacizumab (all stress conditions). No significant differences between the stressed samples were observed on day three of the 3D bioreactor culture. However, TNF- α , IFN- γ and IL-6 levels were increased in 3D compared to 2D

experiments (except from TNF- α for Adalimumab). Common for both methods was that Bevacizumab induced higher secretion of TNF- α and slightly of IFN- γ than Adalimumab.

A



B

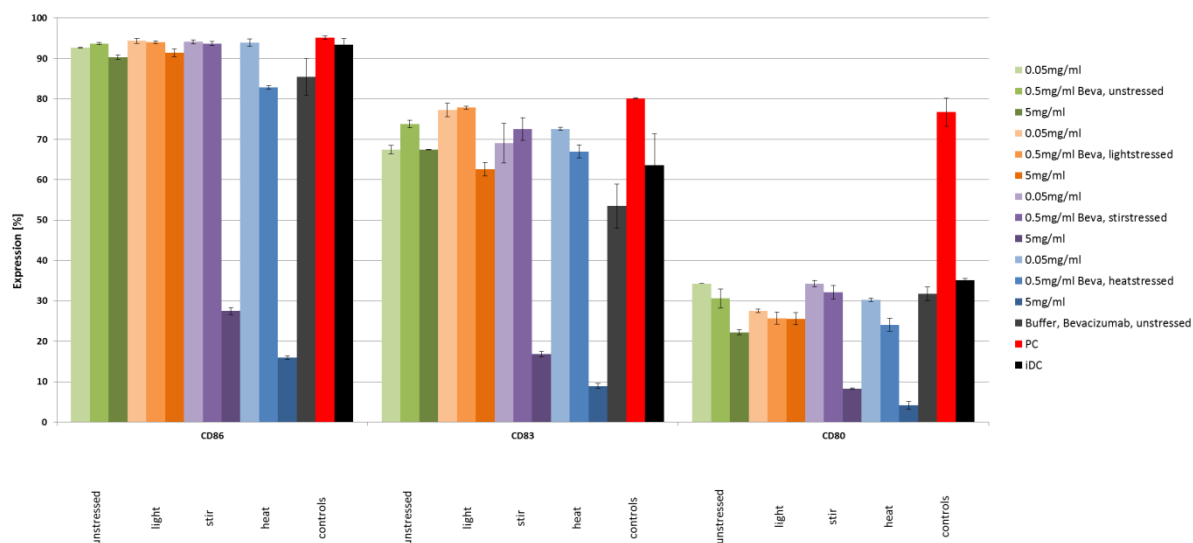


Figure 5-5: Diagram displaying the marker expression (CD86, CD83, CD80) of DCs exposed to different concentrations of stressed antibodies Adalimumab (A) and Bevacizumab (B). For the highest concentration of stressed samples, a drop-down of marker expression was observed (to a lower extent for light-stressed material and to higher extent for stir- and heat-stressed material). The mid dose shows comparable expression or higher levels than the low dose, this is why the mid dose was selected for use in the HuALN study. This data was provided by ProBioGen AG, Berlin.

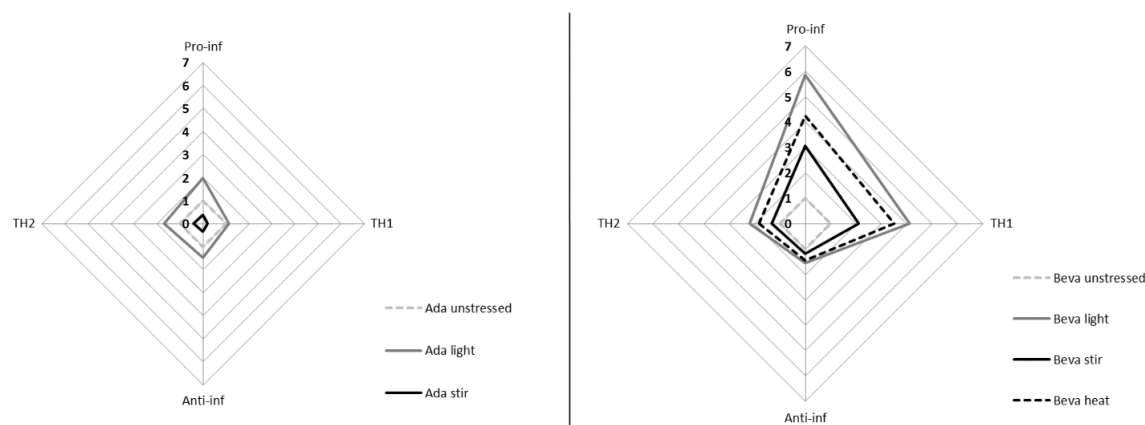
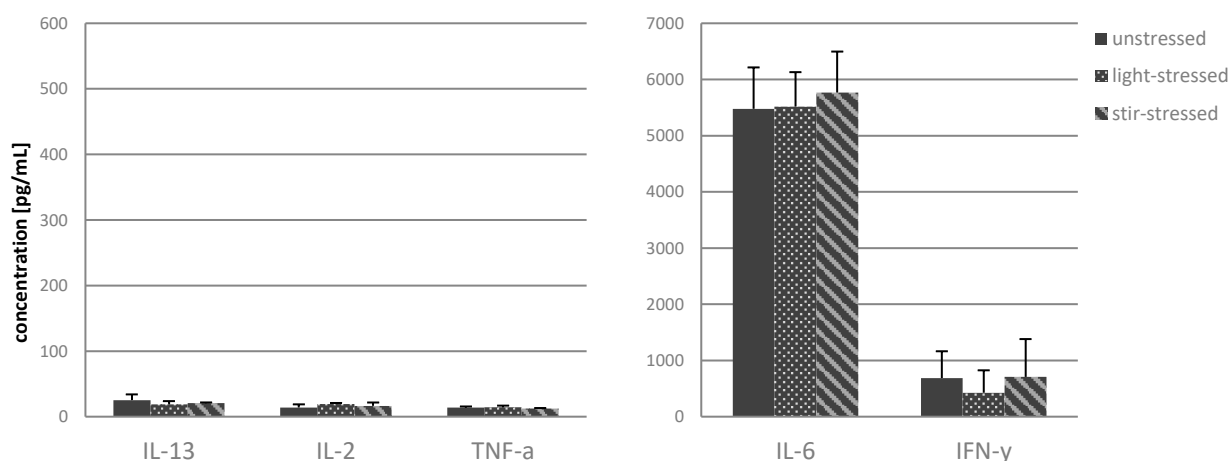


Figure 5-6: Diagram showing spider grids for the 2D assay (for 3D assay see Fig. 4) of Adalimumab (left) and Bevacizumab (right). The cytokine values were directly normalized to control run (unstressed), combined with respect to cytokine groups (TH1, TH2, Pro-inf, Anti-inf), and displayed in spider grids. Values larger/smaller than 1 are displaying up-/downregulation in direct comparison to control run. This data was provided by ProBioGen AG, Berlin.

Even though the applied methods (static DC/T cell assay (2D) and perfused HuALN (3D)) are different systems, also regarding cell numbers and culture volume, absolute levels of IL-13 and IL-2 were similar and, differences between the two antibodies were replicable. Neither the cytokine release of the 3D HuALN experiment on day three nor the spider grid evaluation could confirm the slight increase induced by light stressed Adalimumab compared to unstressed Adalimumab in the 2D assay. For Bevacizumab the immunogenic potential of heat-stressed material could be confirmed, whereas light- and stir-stressed Bevacizumab revealed no immunogenic potential in bioreactor experiments. This leads to the assumption that the 2D assay may be more sensitive than the 3D HuALN model, but not relevant regarding long-term immune responses. In addition, these results indicate that it is important not to monitor short-term immune reactions only, but also to investigate the long-term exposition of the drug, since the type of immune responses might change or develop over time. This could be primarily important for biopharmaceuticals which are applied several times during drug therapy. Even though numerous groups investigated the immunogenicity of protein aggregates using *in vitro* and *in vivo* test models^{10,12,13,18}, still little is known about the underlying mechanisms. Often the predictability of immunogenicity in humans by the used test models is questionable. Thus, there is a need to improve the currently used test models regarding the simulation of the human immune system. Lymph nodes belong to the secondary lymphatic tissues and play a major role in human immunity. Antigen presenting cells such as dendritic cells take up antigens in the periphery of the human body and transport them to lymph nodes where they present the antigen to lymphocytes. Thus, the stimulation of the primary immune responses occurs in lymph nodes^{37,38}.

A



B

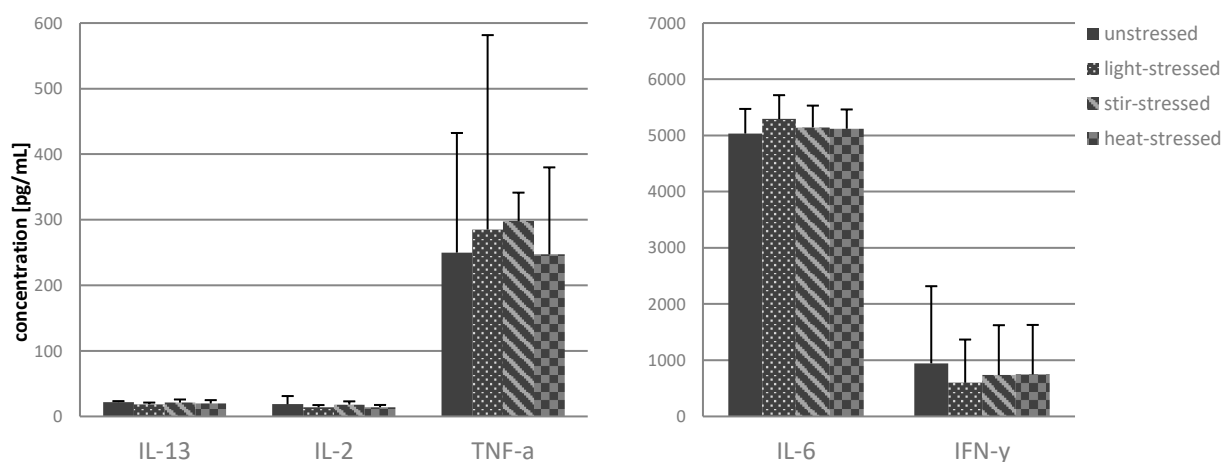


Figure 5-7: Diagram showing the cytokine values (mean of day 3 of all three bioreactor runs) for the 5 selected cytokines, which are also displayed for the 2D assay (see Figure 5-3). This is supplied for comparison of 2D and 3D data at a single data point for Adalimumab (A) and Bevacizumab (B). This data was provided by ProBioGen AG, Berlin.

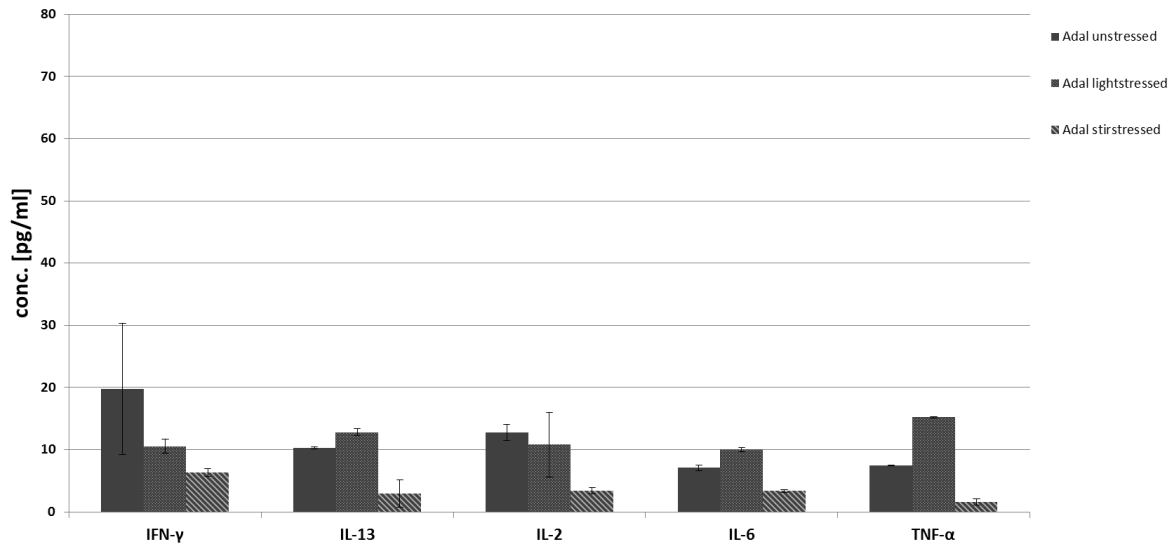
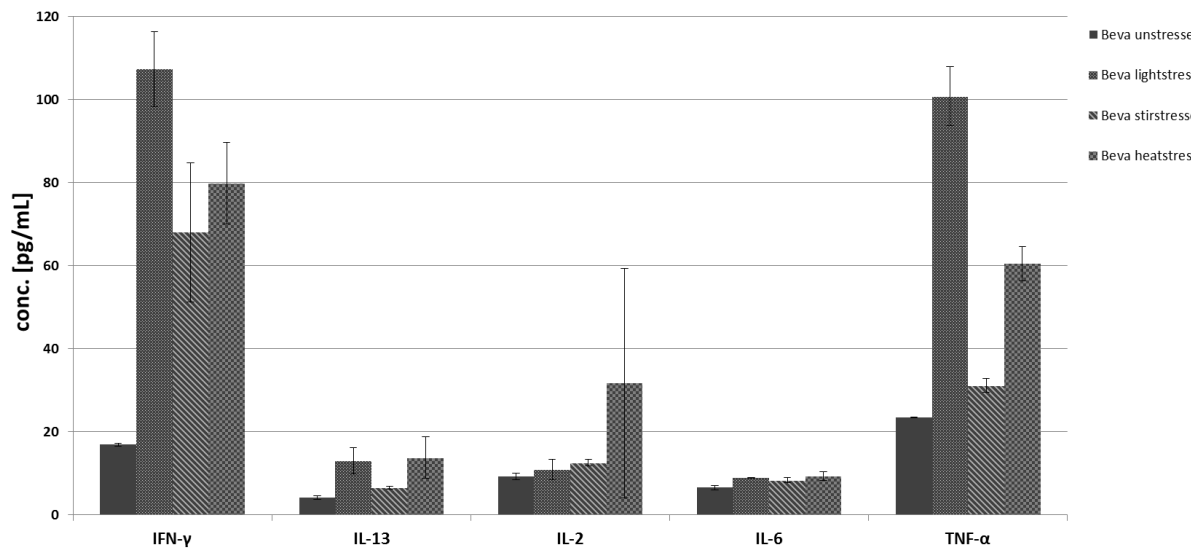
A**B**

Figure 5-8: Extract of Figure 5-3. Cytokine data from DC/T cell assay (48h time point) displayed in Figure 5-3 reduced to the selected concentration (1 mg/mL Adalimumab (A) and 0.5 mg/mL Bevacizumab (B)), which was used for 3D HuALN experiments. This is supplied for comparison of additional 3D data (Figure 5-7) with 2D data for the selected concentration. This data was provided by ProBioGen AG, Berlin.

The approach to use a human artificial lymph node model as an immunologically relevant organ to test the immunogenicity of protein aggregates is therefore a first step in the theoretically relevant direction. While 2D *in vitro* assays enable us to investigate the first contact of antigens with dendritic cells; the HuALN model is capable to monitor the next step, the interaction of dendritic cells with B- and T-cells in a secondary lymphatic organ. The fact that the HuALN model is not only stimulated by the antigen itself but also with antigen matured dendritic cells makes it possible to mimic the *in vivo* situation in patients. The HuALN model has already been used to show immunogenicity of vaccines²⁸,

but was not yet applied for testing the immunogenicity of protein aggregates. Although our study is only the beginning of qualifying this model for its new application, we could show that the human artificial lymph node model is able to differentiate the immunogenicity of different types of protein aggregates and proteins.

5.3 Additional Data

Besides section 5.2, which was published as research article “Evaluation of a 3D human artificial lymph node model as test model for the assessment for immunogenicity of protein aggregates” in the Journal of Pharmaceutical Sciences³⁹, additional data was collected. First, the cell culture supernatants of the 3D HuALN culture were analyzed for the presence of anti-drug antibodies against Adalimumab and Bevacizumab, respectively. The results are represented in section 5.3.1. In addition, stressed Bevacizumab samples were analyzed for the presence of submicron particles, since the focus was recently on submicron particles as potential trigger for immunogenicity⁴⁰. The number of submicron particles in stressed Bevacizumab samples was analyzed after exposure to light, stir and heat stress using the Tunable Resistive Pulse Sensing (TRPS) technique. Since the stimulation of the HuALN with stressed Bevacizumab samples resulted in a more pronounced immune response than stressing with Adalimumab samples, only Bevacizumab after exposure to light, stir and heat stress was analyzed and results are displayed in section 5.3.2.

5.3.1 The analysis of anti-drug antibodies (ADAs)

5.3.1.1 Results

The cell culture supernatants of the HuALN culture after stimulation with differently stressed samples of Adalimumab and Bevacizumab were analyzed for the presence of anti-drug antibodies (ADAs) via a bridging ELISA assay. In addition, the total IgM levels were analyzed. The results of analysis of anti-drug antibodies for all donors of Adalimumab and Bevacizumab are displayed in Figure 5-9A-F, accordingly. The pink and green line represent the signal for the negative control which was media only. The graphs show that the signal of all samples was nearly on the same level as the negative control. Thus, no anti-drug antibodies could be found in any of the HuALN cell culture supernatants after stimulation with differently stressed Adalimumab or Bevacizumab samples. The analysis of ADAs in culture supernatants of the bioreactor with cells of donor 1 revealed a strong signal for stir stressed Adalimumab on day 19. However, this signal could only be observed for one donor and can therefore be defined as outlier. The investigation of further donors would be necessary to future evaluations. Besides ADAs, the titer of IgM antibodies was investigated, and results are displayed in Figure 5-10 and

Figure 5-11. The graphs showed reasonable and unspecific IgM release profiles and did not indicate major differences between the unstressed antibodies and the stressed protein samples, accordingly.

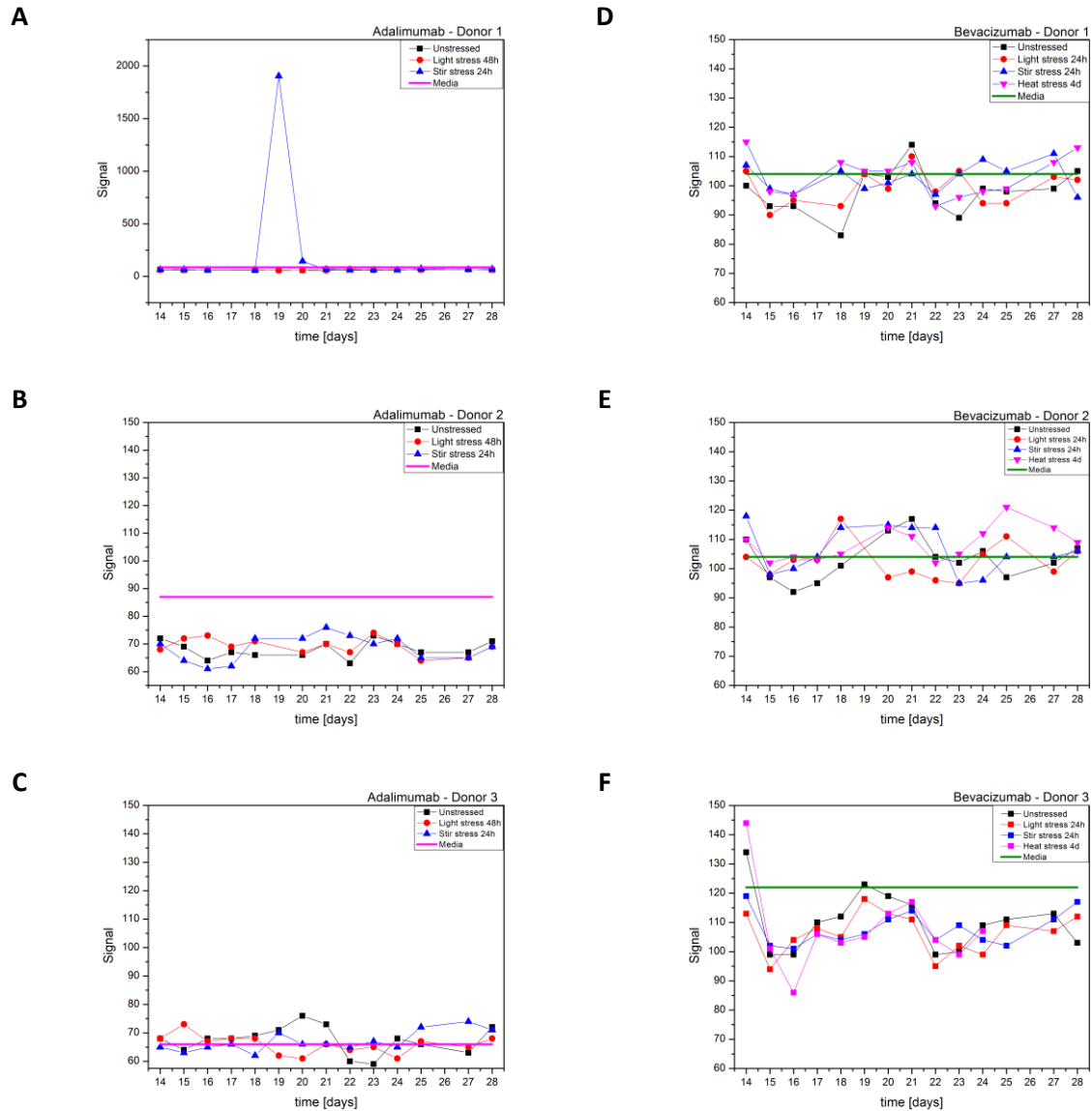


Figure 5-9: Results of anti-drug antibody analysis after stimulation of the human artificial lymph node model with unstressed and stressed samples of Adalimumab and Bevacizumab. Graphs A-C: Results for Adalimumab, donor 1-3; Graphs D-F: Results for Bevacizumab, Donor 1-3. This data was provided by ProBioGen AG, Berlin.

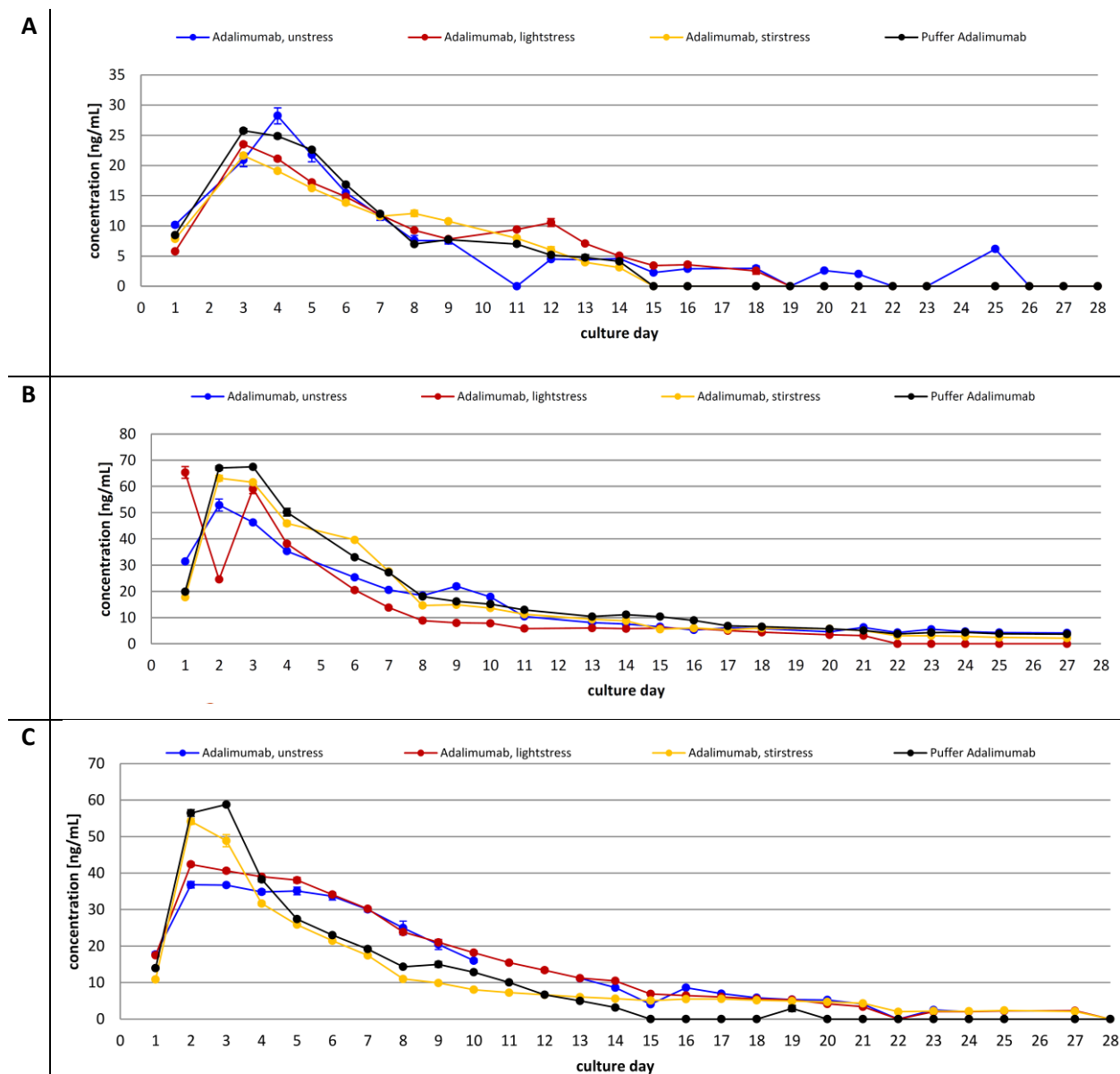


Figure 5-10: Secretion of IgM over a HuALN run period of 28 days of donor 1 (A), donor 2 (B) and donor 3 (C). Blue line: Unstressed Adalimumab, red line: Adalimumab after 48h light stress, yellow line: Adalimumab after 24h stir stress, black line: Formulation Buffer. This data was provided by ProBioGen AG, Berlin.

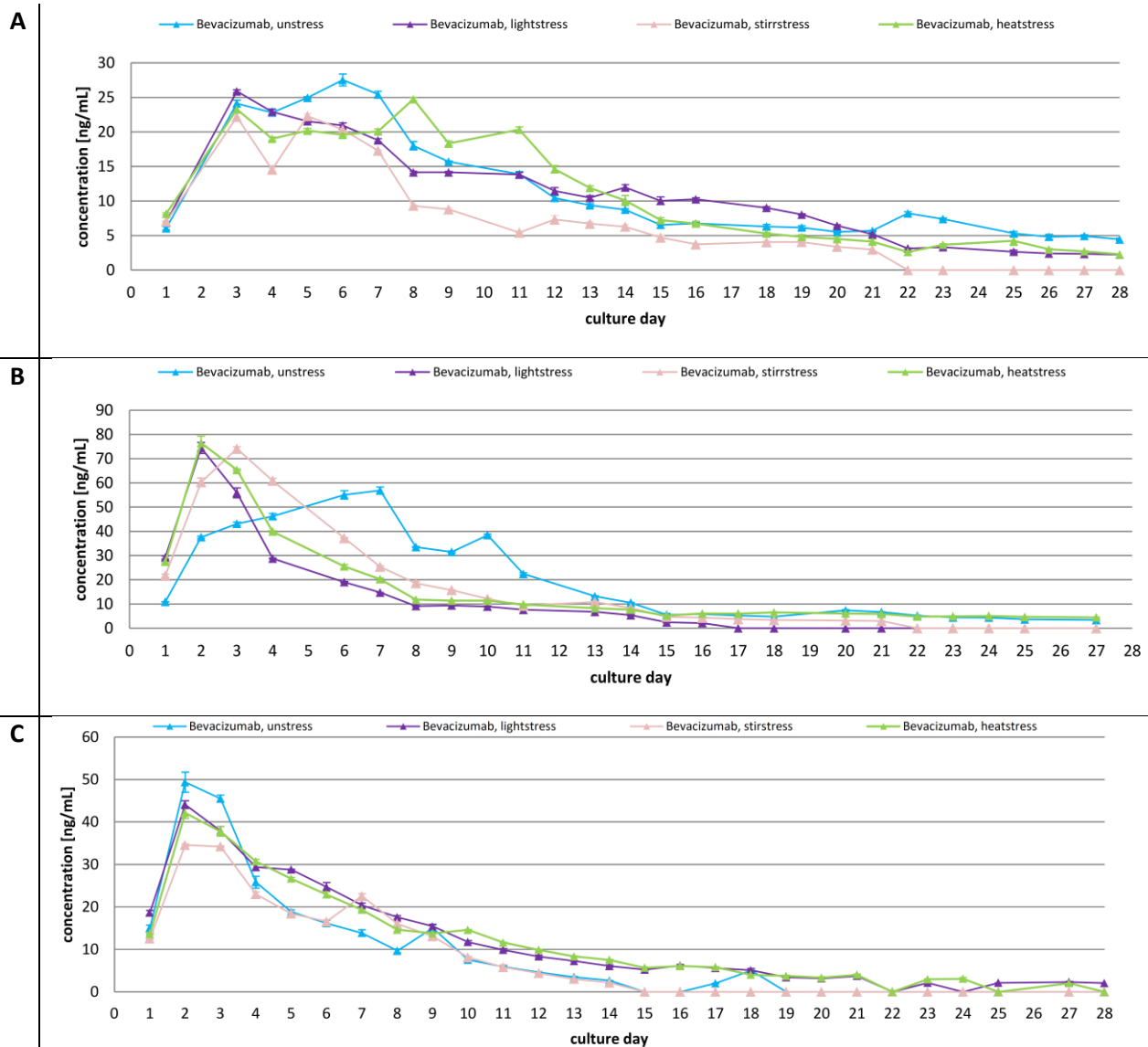


Figure 5-11: Secretion of IgM over a HuALN run period of 28 days of donor 1 (A), donor 2 (B) and donor 3 (C). Blue line: Unstressed Bevacizumab, purple line: Bevacizumab after 24h light stress, rose line: Bevacizumab after 24h stir stress, light green line: Bevacizumab after 4d heat stress. This data was provided by ProBioGen AG, Berlin.

5.3.1.2 Discussion

The analysis of anti-drug antibodies is complex⁴¹. Often the presence of free drug in the samples falsifies results due to the generation of so-called anti-drug antibody-drug complexes preventing ADAs to be detected in ELISA assays. In order to exclude false negative results, an acid dissociation step was performed for single samples. Several groups used this technique to detect anti-drug antibodies in the presence of free drug^{12,42,43}. However, also after an acid dissociation step, no ADAs could be detected (data not shown). Therefore, it can be assumed that Adalimumab and Bevacizumab after light, stir and heat stress (only Bevacizumab) did not lead to the formation of anti-drug antibodies in the HuALN model. There are different types and subclasses of anti-drug antibodies. Involvement of T-cells usually requires higher affinity ADAs of the IgG isotype, whereas IgM ADAs have a lower affinity and are

temporary⁴⁴. However, the formation of immune complexes between the drug and the anti-drug antibody may lead to a loss of efficacy of the drug, changes in the pharmacokinetic profile or to severe clinical complications^{41,44}. In our study, no Ig-type ADAs could be detected, and total IgM levels were unspecific. It is described that the drug therapy of up to 40% of patients with rheumatoid arthritis treated with anti-TNF- α drugs shows reduced efficacy, thus disease symptoms are not mitigated efficiently⁴⁵. The reason therefore might be the generation of anti-drug antibodies⁴⁵. It also has been shown that for example Adalimumab triggered the formation of anti-drug antibodies in patients with rheumatoid arthritis^{33,46–48}. However, in the current study, cells from healthy donors not suffering from any auto-immune disease were used for the HuALN model. The health status of the patient might play an important role regarding immunogenicity³. For Bevacizumab, there is barely any data focusing on immunogenicity and the formation of ADAs for Bevacizumab has not been described in literature⁴⁹. A critical point concerning the analysis of ADAs in this study is, that there was no positive control that confirmed the ability of the HuALN to be able to produce ADAs. According to ProBioGen who developed the HuALN system, it has been demonstrated during development that the HuALN model is able to secrete anti-drug antibodies. However, for further studies, it is indispensable to include such control runs into the experiment. In conclusion, no anti-drug antibodies were detected for Adalimumab or Bevacizumab in this study. Further investigations are needed to improve the analysis of anti-drug antibodies using the HuALN system as model for testing the immunogenicity of different protein aggregates.

5.3.2 The analysis of submicron particles in stressed Bevacizumab samples using Tunable Resistive Pulse Sensing (TRPS)

The analysis of submicron particles has always been a challenge in the development of biotech drugs⁵⁰. For the analysis of subvisible particles $\geq 1\ \mu\text{m}$, methods such as light obscuration and flow imaging are available and limits for particles ≥ 10 and $25\ \mu\text{m}$ are set by the Pharmacopoeia⁵¹. Recently, the regulatory agencies laid their focus on particles $\leq 10\ \mu\text{m}$, and even more recently submicron particles smaller than $1\ \mu\text{m}$ are regarded as relevant. There are several techniques available to analyze submicron particles in protein solutions such as nanoparticle tracking analysis (NTA)⁵², dynamic light scattering (DLS)⁵² or resonant mass measurement (RMM)^{53,54}. A relatively new technique for the analysis of submicron particles is tunable resistive pulse sensing (TRPS). This technique is based on the principle of the coulter counter with the difference that TRPS uses a tunable pore. There are two chambers filled with electrolyte solution and an ionic current is passed. The sample is added at the top chamber and passes through the pore. If particles pass the pore, they cause a decrease in current which is registered as blocking event. The dimension of the blockage determines the size of the particles and the frequency of blockage events is used to determine the particle concentration^{52,55}. In this study, TRPS was used to determine the number of submicron particles of unstressed Bevacizumab and Bevacizumab after exposure to stir, light and heat stress. Figure 5-12 and Figure 5-13 display the results of TRPS measurements of unstressed Bevacizumab and Bevacizumab after heat, stir and light stress. When the samples were filtered using a syringe filter with a pore size of $5\ \mu\text{m}$ (Figure 5-12), the heat stressed sample showed the highest number of submicron particles followed by the stir stressed sample. After light stress, the number of submicron particles was also increased compared to the unstressed protein. When the samples were filtered using a syringe filter with a pore size of $1.2\ \mu\text{m}$, the heat stressed sample still contained the highest amount of submicron particles. However, the concentration of the measured submicron particles was lower. The same was true for the stir stressed sample. This might be due to the different filtration processes. After the pre-filtration using a $5\ \mu\text{m}$ cut-off, the samples still contained many particles in the range of $1\text{-}5\ \mu\text{m}$ (compare also light obscuration data), which resulted in high particle counts and at times also in a blockage of the nanopore. When a $1.2\ \mu\text{m}$ cut-off was used, many particles larger than $1.2\ \mu\text{m}$ were removed and therefore, total particle numbers were smaller. However, heat stress seemed to trigger the formation of submicron particles most. This is an interesting fact, since Bevacizumab after heat stress resulted in a pro-inflammatory/TH1 helper immune answer when injected into the human artificial lymph node model. However, further investigations are needed to evaluate the immunogenic effect of submicron particles in the HuALN model.

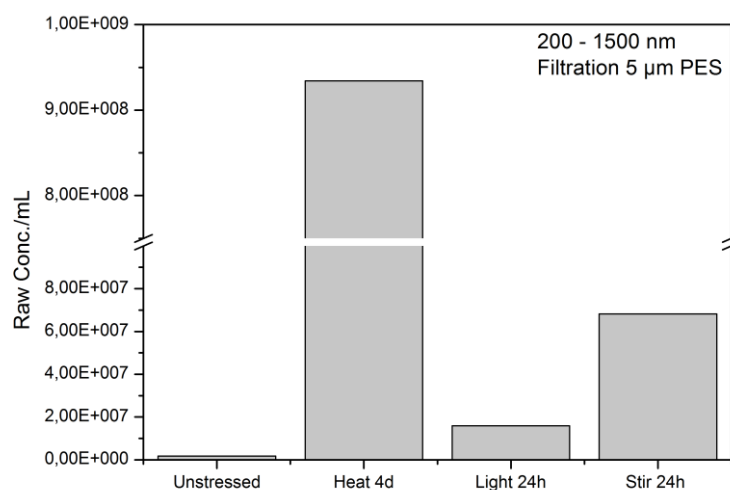


Figure 5-12: Total count of submicron particles/mL determined by TRPS of unstressed Bevacizumab and Bevacizumab after heat, light and stir stress using a syringe filter made of PES with a 5 µm cut-off.

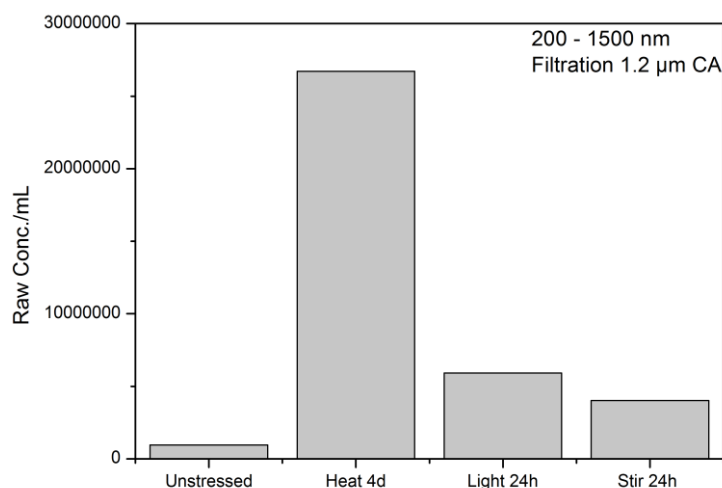


Figure 5-13: Total count of submicron particles/mL determined by TRPS of unstressed Bevacizumab and Bevacizumab after heat, light and stir stress after filtration using a syringe filter made of cellulose acetate with a 1.2 µm cut-off.

5.4 Investigations on the diffusion behavior of fluorescent particles through a 3D life dextran-CD hydrogel using a Franz Cell model

5.4.1 Abstract

Recently, a lot of effort has been put in the development of 3D *in vitro* models to improve the simulation of human organs²⁰. Besides *in vitro* skin models⁵⁶, also *in vitro* gut⁵⁷, lung⁵⁸ and bone marrow models⁵⁹ have been developed. The development of human artificial lymph nodes offers great opportunities to test the wanted or unwanted immunogenicity of vaccines or biopharmaceuticals, for example. However, the development of 3D *in vitro* models is complex and challenging. Several parameters such as biomaterials, culture systems, stromal cells to simulate the functional network of an organ must be taken into consideration⁶⁰. Also, the development of the human artificial lymph node model HIRIS III, developed by Giese *et al.*²⁷, had to undergo various development stages until the development of the currently used model HIRIS III was established. According to Giese *et al.*²⁷, the key aspects of the development were a) the qualification and source of human cells; b) the design and prototyping of the bioreactor; c) the qualification of in-process and end-point analyses and d) the evaluation of different materials for the matrix-assisted cell culture. The gel matrix is necessary for the stromal cells to build a network and cell clusters in combination with the immune cells. The matrix-based system enables the cells to form follicles and germinal centers, which are indispensable for the functionality of the lymph node model. During development of the HuALN model, a variety of different materials for the matrix was tested. Criteria such as cell attachment, macroporosity, stability, cell growth, sterilization and handling of the material were taken into account²⁷. At present, a hydrogel based on dextran including several factors that are important for cell culturing is used as hydrogel matrix (see Materials and Methods, Chapter 3).

In order to investigate the immunogenicity of substances, in this case of protein aggregates, it is necessary that the investigated antigen gets in contact with the embedded immune cells. Thus, it is essential to show that the protein aggregates diffuse into the hydrogel matrix to interact with the cultured immune cells. In this study, the immunogenicity of protein aggregates varying in size from several nanometers to several micrometers was tested. The aim of this study was to investigate the diffusion behavior of particles of different sizes through a 3D Life dextran-CD hydrogel matrix. Therefore, we used green fluorescent polystyrene model particles at a size of 2 μm and 26 nm to mimic protein aggregates of different size ranges. A Franz Cell was used as model and the acceptor medium as well as the gel itself was analyzed for the presence of fluorescent particles by fluorescence spectroscopy or microscopy methods. For a detailed description of the used methods see Chapter 3 (Materials and Methods).

5.4.2 Results

5.4.2.1 Diffusion of 2 μm fluorescent particles

The results of the quantification of fluorescent particles present in the acceptor medium by fluorimetry are displayed in Figure 5-14. Graphs A and C revealed that no fluorescent particles at a size of 2 μm could be found in the acceptor medium. Graphs B and D display enlargements of Graphs A and C and show that the fluorescence intensity of the acceptor medium of the Franz Cell with the dextran hydrogel as membrane was on the same level as the negative control, a cellulose acetate membrane with a cut-off of 0.2 μm . It is noticeable that the intensity of the acceptor medium of the positive control, a cellulose acetate membrane with a cut-off of 5 μm , did also not show any increase. This was probably due to aggregation of the model particles in PBS. The cut-off of 5 μm for particles with a diameter of 2 μm was very low, but no other membranes at the desired size were available. However, the membranes should serve as a “proof of concept” model to develop the analytical method and it worked fine using highly purified water as acceptor medium or using smaller particles. However, no increase in fluorescence intensity could be detected in the acceptor medium of the Franz Cell with the dextran hydrogel and therefore it can be assumed, that the particles did not diffuse through the gel within the investigated time of four days. At the end of the experiment after four days, the hydrogel was washed thoroughly with PBS buffer and analyzed by microscopy to investigate if particles diffused into the hydrogel and how the particles were distributed within the hydrogel matrix. The photographs are displayed in Figure 5-15, showing that many of the particles diffused into the upper layer of the gel, but only few particles diffused to the bottom of the gel.

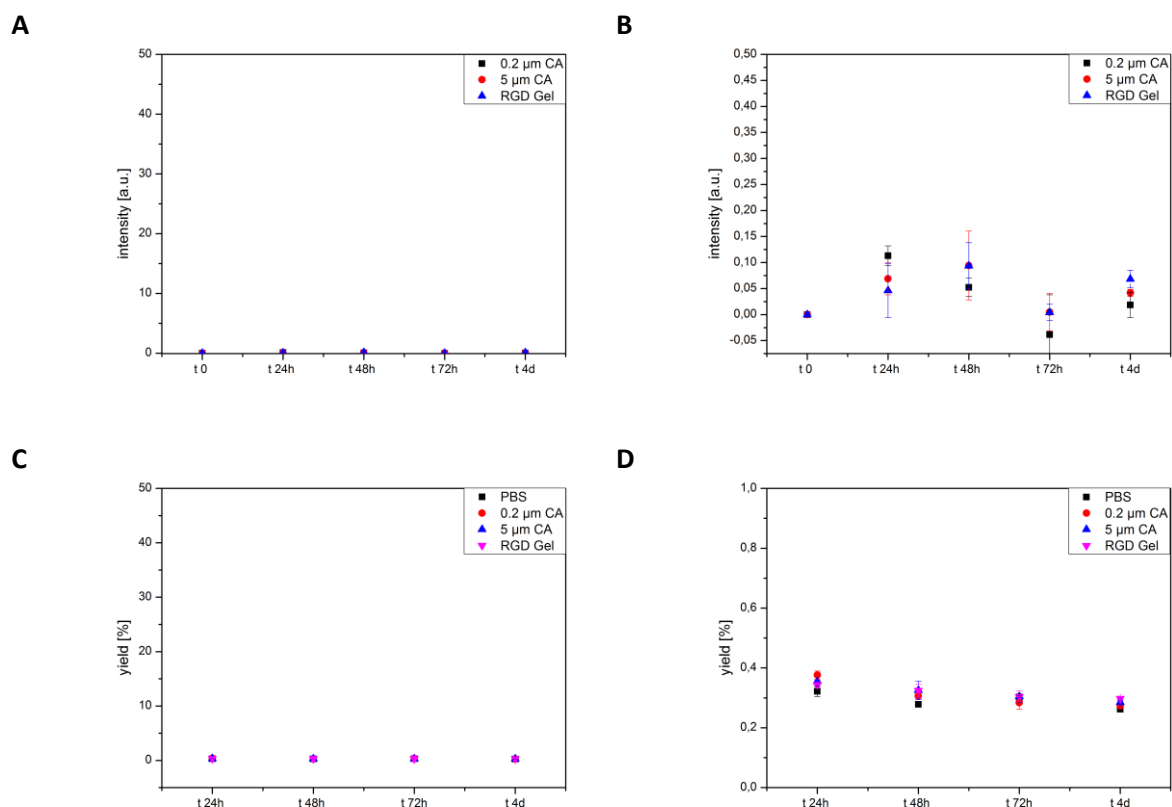


Figure 5-14: Concentration of particles in the acceptor medium reported as fluorescence intensity (A and B) and as yield (C and D). Graphs B and D represent enlargements of graphs A and C, respectively.

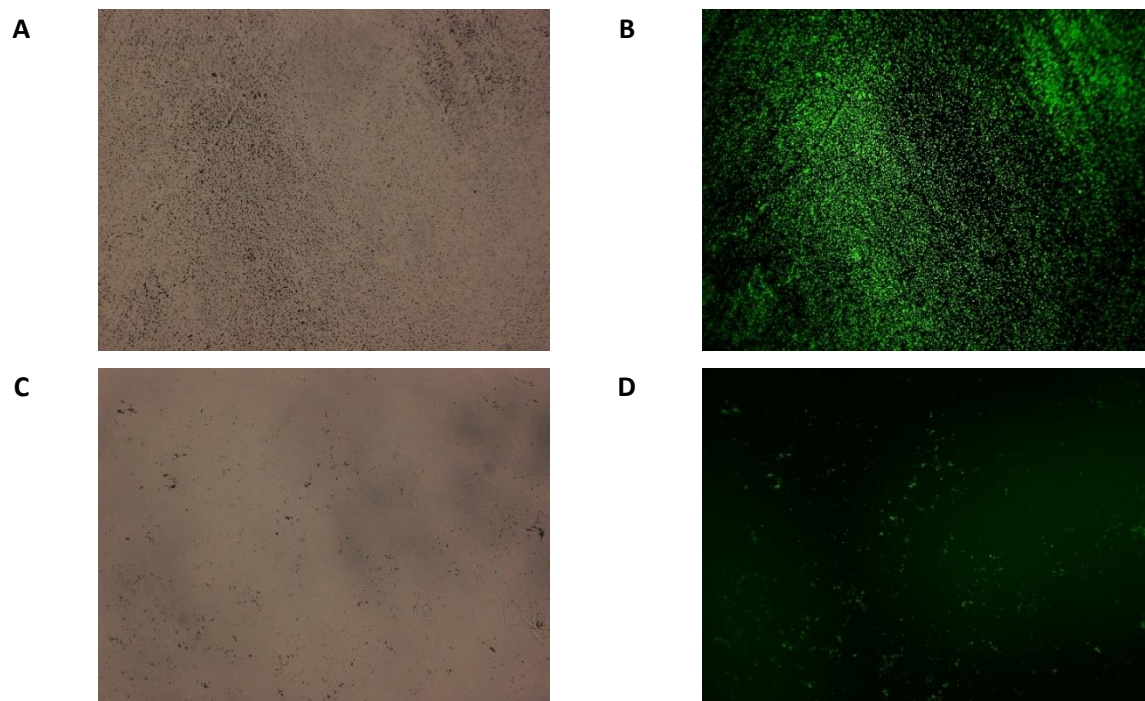


Figure 5-15: Images taken from the 3D Life Dextran – CD hydrogel at the end of the experiment; 20x magnification; A-B: Pictures display the upper layer of the gel. C-D: Pictures display the bottom layer of the gel.

5.4.2.2 Diffusion of 26 nm fluorescent particles

Figure 5-16 displays the results of the analysis of the acceptor medium using 26 nm fluorescent particles. In contrast to the particles with a size of 2 μm , there was a slight increase in fluorescence intensity in the acceptor medium using 26 nm particles. The yield on day 7 is about 0.25%, which was still very small, but a continuous increase in particle concentration in the acceptor medium during 7 days of investigation could be shown. A cellulose acetate membrane with a cut-off of 5 μm was again used as positive control and the 26 nm particles could diffuse to the acceptor medium. A yield of about 40 % was reached after 24 hours already and no further increase was detectable. After day 7 there was even a small decrease in intensity and yield which might be due to a slight loss of fluorescence intensity of the particles. The fluorescent particles at a size of 26 nm were too small to be detected in the microscope. However, it was clearly visible that the gel was coloured with the green fluorescence (Figure 5-17). There was a strong green fluorescence distributed all over the hydrogel, most intense at the top of the gel, slightly decreased in the centre of the hydrogel and smaller at the bottom of the hydrogel (Figure 5-17A-C). However, these results suggest that the particles diffused into the hydrogel matrix and were equally distributed within the hydrogel.

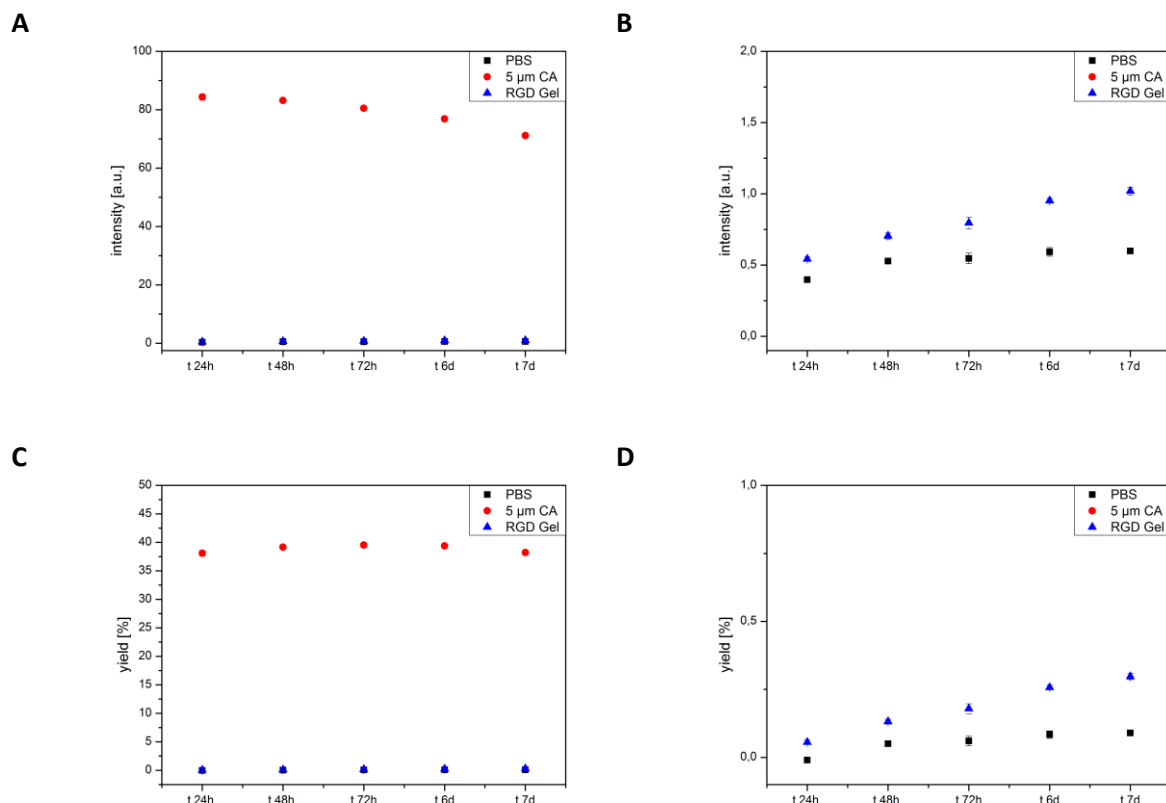


Figure 5-16: Concentration of particles in the acceptor medium reported as fluorescence intensity (A and B) and as yield (C and D). Graphs B and D represent enlargements of graphs A and C, respectively.

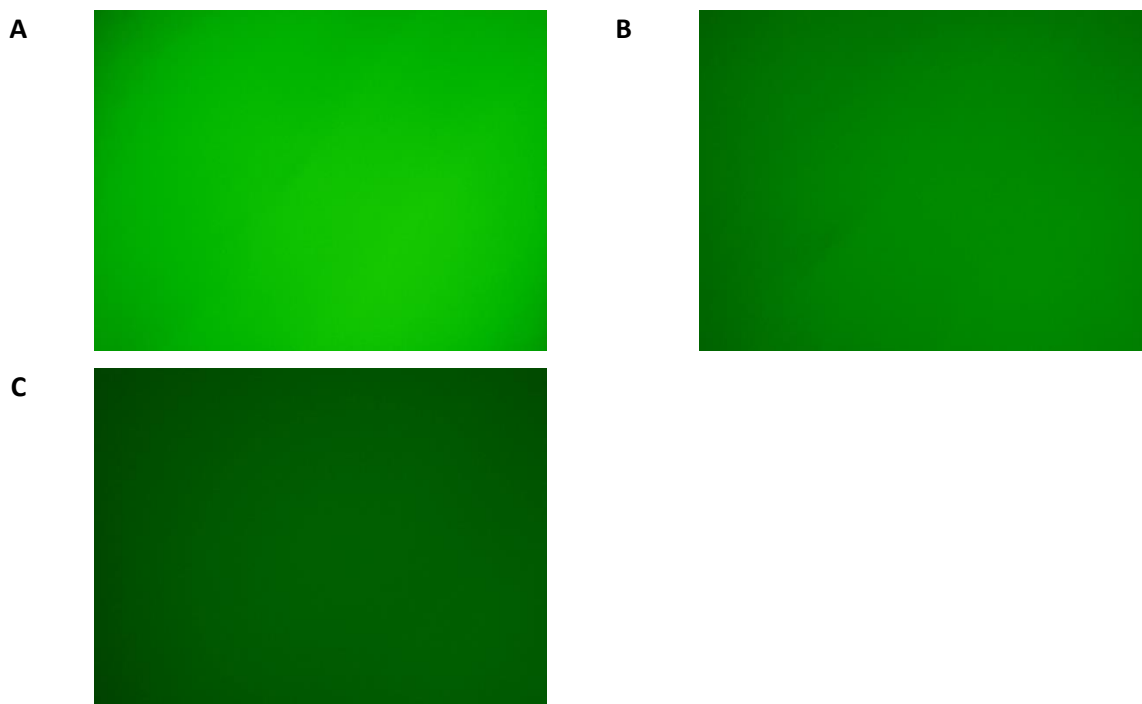


Figure 5-17: Images taken from the 3D Life Dextran -CD hydrogel at the end of the experiment; 20x magnification; A-C: Photographs from the top (A), center (B) and bottom of the gel (C).

5.4.3 Discussion

The results showed clear differences between the diffusion behavior of particles at a size of $2\ \mu\text{m}$ or $26\ \text{nm}$. While $26\ \text{nm}$ particles are distributed equally within the hydrogel, most of the $2\ \mu\text{m}$ particles diffused only into the upper layer of the hydrogel and only few particles diffused to the bottom of the gel (Figure 5-18). This leads to the assumption that larger particles cannot diffuse through the dextran hydrogel matrix and therefore cannot get in contact with immune cells that are embedded in the dextran gel matrix in the human artificial lymph node model. Thus, the human artificial lymph node model might be “self-selecting” by filtering larger particles. However, further investigations of the diffusion behavior of differently sized particles ($26\ \text{nm}$, $500\ \text{nm}$ and $2\ \mu\text{m}$) using the human artificial lymph node model are necessary to confirm this assumption, since conditions in the human artificial lymph node differ in several issues such as media and gas flow from the used Franz Cell model.

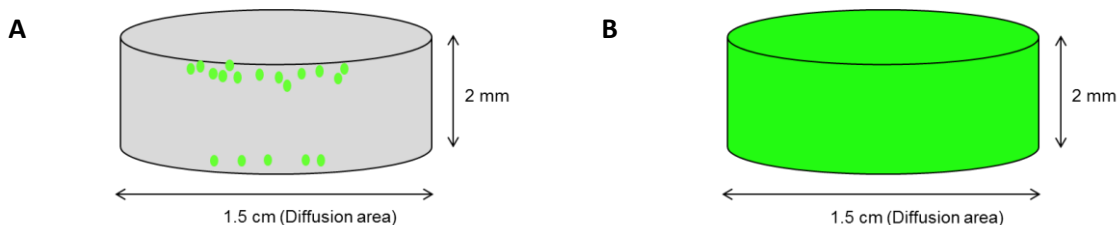


Figure 5-18: Schematic drawing of diffusion behavior of fluorescent particles at a size of $2\ \mu\text{m}$ (A) and $26\ \text{nm}$ (B).

5.5 Conclusion

The aim of this study was to use a complex human artificial lymph node model to test the immunogenic risk of protein aggregates of two monoclonal antibodies. In contrast to the currently used *in vitro* test models, the human artificial lymph node represents a complex 3D matrix assisted culture model mimicking the key structures of a human lymph node such as lymphatic follicles and germinal centers. The immunogenicity of differently produced protein aggregates of two monoclonal antibodies was evaluated. Even if the 2D assay indicates the immunogenic potential of stressed antibodies, the 3D model revealed that Bevacizumab after exposure to heat triggered a TH1 and pro-inflammatory immune response. The analysis of anti-drug antibodies (ADAs) revealed that no ADAs could be found against Adalimumab or Bevacizumab. Investigating the diffusion behavior of model particles through the dextran gel matrix used in the HuALN model indicated that the HuALN might be “self-selecting” by filtering larger particles so that larger particles cannot get in contact with embedded immune cells in the gel matrix. In summary, the human artificial lymph node model represents a new model to test the immunogenicity of protein aggregates. However, further development of the HuALN is needed to improve the predictive power of the system regarding immunogenicity in humans.

5.6 References

1. Brinks, V. *et al.* Preclinical models used for immunogenicity prediction of therapeutic proteins. *Pharm. Res.* **30**, 1719–1728 (2013).
2. Porter, S. Human Immune Response to Recombinant Human Proteins. **90**, 1–11 (2001).
3. U.S. Department of Health and Human Services, FDA, CDER, C. Guidance for Industry Immunogenicity Assessment for Therapeutic Protein Products. (2014).
4. Schellekens, H. Immunogenicity of therapeutic proteins: clinical implications and future prospects. *Clin. Ther.* **24**, 1720–1740 (2002).
5. Deehan, M. *et al.* Managing unwanted immunogenicity of biologicals. *Autoimmun. Rev.* **14**, 569–574 (2015).
6. Kessler, M., Goldsmith, D. & Schellekens, H. Immunogenicity of biopharmaceuticals. *Nephrol. Dial. Transplant.* **21**, 9–12 (2006).
7. Rosenberg, A. S. Effects of protein aggregates: an immunologic perspective. *AAPS J.* **8**, E501–E507 (2006).
8. Rombach-Riegraf, V. *et al.* Aggregation of human recombinant monoclonal antibodies influences the capacity of dendritic cells to stimulate adaptive T-cell responses in vitro. *PLoS One* **9**, e86322 (2014).
9. Moussa, E. M., Kotarek, J., Blum, J. S., Marszal, E. & Topp, E. M. Physical Characterization and Innate Immunogenicity of Aggregated Intravenous Immunoglobulin (IGIV) in an In Vitro Cell-Based Model. *Pharm. Res.* **33**, 1736–1751 (2016).
10. Joubert, M. K. *et al.* Highly aggregated antibody therapeutics can enhance the in vitro innate and late-stage T-cell immune responses. *J. Biol. Chem.* **287**, 25266–25279 (2012).
11. Fathallah, A. M. *et al.* The Effect of Small Oligomeric Protein Aggregates on the Immunogenicity of Intravenous and Subcutaneous Administered Antibodies. *J. Pharm. Sci.* **104**, 3691–3702 (2015).
12. Freitag, A. J. *et al.* Investigation of the immunogenicity of different types of aggregates of a murine monoclonal antibody in mice. *Pharm. Res.* **32**, 430–444 (2015).
13. Bessa, J. *et al.* The immunogenicity of antibody aggregates in a novel transgenic mouse model.

- Pharm. Res.* **32**, 2344–2359 (2015).
14. Boll, B. *et al.* Extensive chemical modifications in the primary protein structure of IgG1 subvisible particles are necessary for breaking immune tolerance. *Mol. Pharm.* **14**, 1292–1299 (2017).
 15. Telikepalli, S. *et al.* Physical characterization and in vitro biological impact of highly aggregated antibodies separated into size-enriched populations by fluorescence-activated cell sorting. *J. Pharm. Sci.* **104**, 1575–1591 (2015).
 16. Carpenter, J. F. *et al.* Overlooking Subvisible Particles in Therapeutic Protein Products: Gaps That May Compromise Product Quality. *J. Pharm. Sci.* **98**, 1201–1205 (2009).
 17. Van Beers, M. M. C. *et al.* Oxidized and aggregated recombinant human interferon beta is immunogenic in human interferon beta transgenic mice. *Pharm. Res.* **28**, 2393–2402 (2011).
 18. Ahmadi, M. *et al.* Small amounts of sub-visible aggregates enhance the immunogenic potential of monoclonal antibody therapeutics. *Pharm. Res.* **32**, 1383–1394 (2015).
 19. Moussa, E. M. *et al.* Immunogenicity of Therapeutic Protein Aggregates. *J. Pharm. Sci.* **105**, 417–430 (2016).
 20. Giese, C. & Marx, U. Human immunity in vitro- Solving immunogenicity and more. *Adv. Drug Deliv. Rev.* **69–70**, 103–122 (2014).
 21. Jiskoot, W. *et al.* Mouse Models for Assessing Protein Immunogenicity: Lessons and Challenges. *J. Pharm. Sci.* **105**, 1567–1575 (2016).
 22. Filipe, V. *et al.* Immunogenicity of different stressed IgG monoclonal antibody formulations in immune tolerant transgenic mice. *MAbs* **4**, 740–752 (2012).
 23. Shomali, M. *et al.* Dose levels in particulate-containing formulations impact anti-drug antibody responses to murine monoclonal antibody in mice. *J. Pharm. Sci.* **104**, 1610–1621 (2015).
 24. Van Beers, M. M. C. *et al.* Aggregated recombinant human interferon beta induces antibodies but no memory in immune-tolerant transgenic mice. *Pharm. Res.* **27**, 1812–1824 (2010).
 25. Bi, V. *et al.* Development of a human antibody tolerant mouse model to assess the immunogenicity risk due to aggregated biotherapeutics. *J. Pharm. Sci.* **102**, 3545–3555 (2013).
 26. Brinks, V., Jiskoot, W. & Schellekens, H. Immunogenicity of therapeutic proteins: The use of

- animal models. *Pharm. Res.* **28**, 2379–2385 (2011).
27. Giese, C. *et al.* A human lymph node in vitro-challenges and progress. *Artif. Organs* **30**, 803–808 (2006).
28. Giese, C. *et al.* Immunological substance testing on human lymphatic micro-organoids in vitro. *J. Biotechnol.* **148**, 38–45 (2010).
29. Hawe, A., Sutter, M. & Jiskoot, W. Extrinsic fluorescent dyes as tools for protein characterization. *Pharm. Res.* **25**, 1487–1499 (2008).
30. Mahler, H.-C., Friess, W., Grauschopf, U. & Kiese, S. Protein aggregation: Pathways, induction factors and analysis. *J. Pharm. Sci.* **98**, 2909–2934 (2009).
31. Zölls, S. *et al.* Particles in Therapeutic Protein Formulations, Part 1: Overview of Analytical Methods. *J. Pharm. Sci.* **101**, 914–935 (2012).
32. Ratanji, K. D. *et al.* Subvisible aggregates of immunogenic proteins promote a Th1-type response. *Toxicol. Sci.* **153**, 258–270 (2016).
33. Scheinfeld, N. Adalimumab: a review of side effects. *Expert Opin. Drug Saf.* **4**, 637–641 (2005).
34. Sardi, M., Lubitz, A. & Giese, C. Modeling Human Immunity In Vitro - Improving Artificial Lymph Node Physiology by Stromal Cells. *Appl. Vitro. Toxicol.* **2**, 143–150 (2016).
35. Joubert, M. K. *et al.* Use of in vitro assays to assess immunogenicity risk of antibody-based biotherapeutics. *PLoS One* **11**, 1–22 (2016).
36. Vazquez-Cobian, L. B. Adalimumab therapy for childhood uveitis. *J. Pediatr.* **149**, 572–575 (2006).
37. Willard-Mack, C. L. Normal Structure, Function, and Histology of Lymph Nodes. *Toxicol. Pathol.* **34**, 409–424 (2006).
38. Kaldjian, E. P., Elizabeth Gretz, J., Anderson, A. O., Shi, Y. & Shaw, S. Spatial and molecular organization of lymph node T cell cortex: A labyrinthine cavity bounded by an epithelium-like monolayer of fibroblastic reticular cells anchored to basement membrane-like extracellular matrix. *Int. Immunol.* **13**, 1243–1253 (2001).
39. Kraus, T. *et al.* Evaluation of a 3D human artificial lymph node model as test model for the assessemnt of immunogenicity of protein aggregates. *J. Pharm. Sci.* **108**, 2358–2366 (2019).

40. Kijanka, G. *et al.* Submicron Size Particles of a Murine Monoclonal Antibody Are More Immunogenic Than Soluble Oligomers or Micron Size Particles Upon Subcutaneous Administration in Mice. *J. Pharm. Sci.* **107**, 2847–2859 (2018).
41. Chirmule, N., Jawa, V. & Meibohm, B. Immunogenicity to Therapeutic Proteins: Impact on PK/PD and Efficacy. *AAPS J.* **14**, 296–302 (2012).
42. Bourdage, J. S., Cook, C. A., Farrington, D. L., Chain, J. S. & Konrad, R. J. An Affinity Capture Elution (ACE) assay for detection of anti-drug antibody to monoclonal antibody therapeutics in the presence of high levels of drug. *J. Immunol. Methods* **327**, 10–17 (2007).
43. Lofgren, J. A., Wala, I., Koren, E., Swanson, S. J. & Jing, S. Detection of neutralizing anti-therapeutic protein antibodies in serum or plasma samples containing high levels of the therapeutic protein. *J. Immunol. Methods* **308**, 101–108 (2006).
44. Krishna, M. & Nadler, S. G. Immunogenicity to biotherapeutics - The role of anti-drug immune complexes. *Front. Immunol.* **7**, 21 (2016).
45. Jani, M. *et al.* Detection of anti-drug antibodies using bridging ELISA compared with radioimmunoassay in adalimumab-treated rheumatoid arthritis patients with random drug levels. *Rheumatology* **55**, 2050–2055 (2016).
46. van Schouwenburg, P. A., Rispens, T. & Wolbink, G. J. Immunogenicity of anti-TNF biologic therapies for rheumatoid arthritis. *Nat. Rev. Rheumatol.* **9**, 164–172 (2013).
47. Bender, N. K. *et al.* Immunogenicity, efficacy and adverse events of adalimumab in RA patients. *Rheumatol. Int.* **27**, 269–274 (2007).
48. Coenen, M. J. *et al.* Pharmacogenetics of anti-TNF treatment in patients with rheumatoid arthritis. *Pharmacogenomics* **8**, 761–773 (2007).
49. Getts, D. R., Getts, M. T., McCarthy, D. P., Chastain, E. M. L. & Miller, S. D. Have we overestimated the benefit of human(ized) antibodies? *MAbs* **2**, 682–694 (2010).
50. Scherer, T. M., Leung, S., Owyang, L. & Shire, S. J. Issues and Challenges of Subvisible and Submicron Particulate Analysis in Protein Solutions. *Aaps J.* **14**, 236–243 (2012).
51. 2.9.19 Partikelkontamination- Nicht sichtbare Partikeln. *European Pharmacopoeia* 438–441 (2014).
52. Anderson, W., Kozak, D., Coleman, V. A., Jämting, Å. K. & Trau, M. A comparative study of

- submicron particle sizing platforms : Accuracy , precision and resolution analysis of polydisperse particle size distributions. *J. Colloid Interface Sci.* **405**, 322–330 (2013).
53. Weinbuch, D. *et al.* Micro – Flow Imaging and Resonant Mass Measurement (Archimedes) – Complementary Methods to Quantitatively. **102**, 2152–2165 (2013).
54. Panchal, J., Kotarek, J., Marszal, E. & Topp, E. M. Analyzing Subvisible Particles in Protein Drug Products : a Comparison of Dynamic Light Scattering (DLS) and Resonant Mass Measurement (RMM). *Aaps J.* **16**, 440–451 (2014).
55. Blundell, E. L. C. J., Mayne, L. J., Billinge, E. R. & Platt, M. Analytical Methods Emergence of tunable resistive pulse sensing as a biosensor. *Anal. Methods* **7**, 7055–7066 (2015).
56. Chau, D. Y. S., Johnson, C., Macneil, S., Haycock, J. W. & Ghaemmaghami, A. M. The development of a 3D immunocompetent model of human skin. *Biofabrication* **5**, 1–17 (2013).
57. Leonard, F., Collnot, E.-M. & Lehr, C.-M. A Three-Dimensional Coculture of Enterocytes, Monocytes and Dendritic Cells To Model Inflamed Intestinal Mucosa in Vitro. *Mol. Pharm.* **7**, 2103–2119 (2010).
58. Rothen-Rutishauser, B. M., Kiama, S. C. & Gehr, P. A three-dimensional cellular model of the human respiratory tract to study the interaction with particles. *Am. J. Respir. Cell Mol. Biol.* **32**, 281–289 (2005).
59. Di Maggio, N. *et al.* Toward modeling the bone marrow niche using scaffold-based 3D culture systems. *Biomaterials* **32**, 321–329 (2011).
60. Cupedo, T., Stroock, A. & Coles, M. Application of tissue engineering to the immune system: Development of artificial lymph nodes. *Front. Immunol.* **3**, 1–6 (2012).

Chapter 6

In-line filtration as a possibility to reduce the immunogenicity of protein aggregates

6.1 Introduction

Particulate matter in biopharmaceutical products is one of the complex challenges for pharmaceutical manufacturers. According to the European Pharmacopoeia injectable protein drugs must be “essentially free of visible particles”^{1,2} and the number of subvisible particles in a container having a volume of less than 100 mL is limited to 6000 particles $\geq 10\ \mu\text{m}$ and 600 particles $\geq 25\ \mu\text{m}$ ^{3,4} per container. In the past years, many research groups focused on investigating the potential of proteinaceous or non-proteinaceous particles to elicit immunogenicity^{5–9}. For several years now, subvisible particles in the size range of 1–10 μm are suspected to be most prone to trigger immunogenicity^{8,10}. The number of particles larger than 10 μm and 25 μm is limited by the European Pharmacopoeia and the USP^{3,4}, as described above, however, the number of particles smaller than 10 μm is not routinely monitored or limited¹¹. Recently, a research group published an article reporting that submicron, thus particles smaller than 1 μm , are more immunogenic than particles in the subvisible range⁶. Until it is not fully clarified, which type of particles elicit immunogenicity most, it is necessary to minimize particle burden in order to ensure a safe and efficient drug therapy. A possibility to reduce particle burden in infusions or injections is in-line filtration. In-line filtration, also known as bedside filtration, is defined as a filtration of the applied (protein) drug solution immediately prior to administration. It has been shown that in-line filtration is a highly effective tool to reduce particle numbers in biopharmaceutical products¹². In a study by Werner *et al.* the effectiveness of filters to reduce particles was investigated, but also critical aspects such as particle shedding from filters, protein adsorption, protein denaturation, leachables or the ejection force were assessed¹². Moreover, a comprehensive review by Werner *et al.* revealed that for nearly 16 % of all approved biopharmaceuticals in the German Rote Liste® a filter recommendation is provided by the pharmaceutical manufacturer already¹³. A recently published study by Villa *et al.* showed that in-line filtration reduced postoperative peripheral phlebitis associated with cannulation¹⁴. Moreover, studies of Perez *et al.* showed the effectiveness and need for in-line filtration for infusion therapy in pediatrics^{15,16}. Even though particles during infusion therapy do not necessarily originate from the drug itself but also from glass containers, plastic containers, infusion sets or incompatibilities arising from simultaneous administration of several drugs¹⁷, in-line filtration is an effective tool to reduce the particle burden and clinical complications associated with the administration of particulate matter. The listed examples show that in-line filtration is a relevant topic in practice, however, it is still not routinely used during administration of biopharmaceutical products. This is also due to the lack of studies evaluating in-line filtration as a common tool to reduce particle numbers and the link to reduced immunogenicity.

The aim of this study was to show the impact of in-line filtration on immunogenicity using a 3D human artificial lymph node model and a 2D dendritic cell (DC) assay. Bevacizumab, a monoclonal antibody, was exposed to stir and heat stress for the HuALN study and additionally to light stress and *tert*-butylhydroperoxide for the 2D DC assay to form protein aggregates. The samples were analyzed thoroughly prior to and after applying an in-line filtration step and finally, the human artificial lymph node model and dendritic cells were stimulated, accordingly, with unstressed and differently stressed Bevacizumab samples with or w/o in-line filtration step prior to stimulation. Finally, cell culture supernatants were tested for the presence of cytokines and IgM anti-drug antibodies (HuALN study only) and specific dendritic cell marker were analyzed.

6.2 Evaluation of the effect of in-line filtration using a 3D *in vitro* human artificial lymph node model

6.2.1 Results of protein analysis

6.2.1.1 Visual inspection

Figure 6-1 shows photographs of unstressed Bevacizumab and Bevacizumab after heat and stir stress prior to and after filtration. Due to a protein concentration of 26.1 mg/mL, unstressed Bevacizumab was slightly turbid compared to the unstressed formulation buffer. Bevacizumab after heat and stir stress showed an increased turbidity compared to the unstressed protein, whereby the stir stressed sample was the most turbid sample of all. After filtration, the solutions showed a comparable turbidity to the unstressed protein, indicating that filtration removed particles which resulted from heat or stir stress.

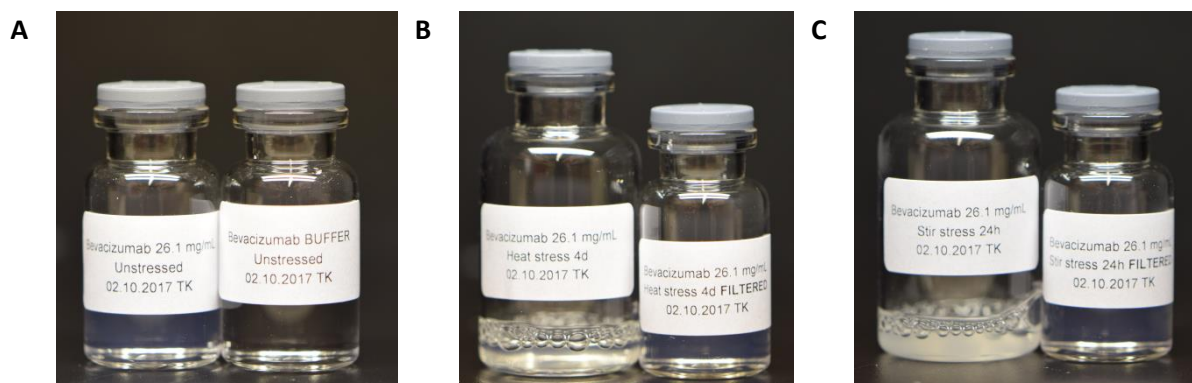


Figure 6-1: Photographs of unstressed and stressed Bevacizumab samples prior to and after filtration: A: Unstressed Bevacizumab at a concentration of 26.1 mg/mL (left) vs. unstressed formulation buffer (right). B: Bevacizumab at a concentration of 26.1 mg/mL after heat stress for 4 days prior to (left) and after filtration (right). C: Bevacizumab at a concentration of 26.1 mg/mL after stir stress for 24h prior to (left) and after filtration (right).

6.2.1.2 Turbidity

Results of turbidity measurements are depicted in Figure 6-2. A slight increase to a turbidity of 12.82 FNU was detected after heat stress compared to the unstressed protein (6.55 FNU). Filtration of the heat stressed sample resulted in a decrease of turbidity to 8.54 FNU which corresponded approximately to the level of turbidity of unstressed Bevacizumab (6.55 FNU). However, the difference in turbidity of 4.28 FNU prior to and after filtration of the heat stressed sample was rather small. In contrast, turbidity strongly increased to a value of 141.57 FNU after stir stress and decreased to 6.10 FNU after filtration. In both cases, filtration led to a decrease in turbidity, whereby the effect was more pronounced for Bevacizumab after stir stress than after heat stress.

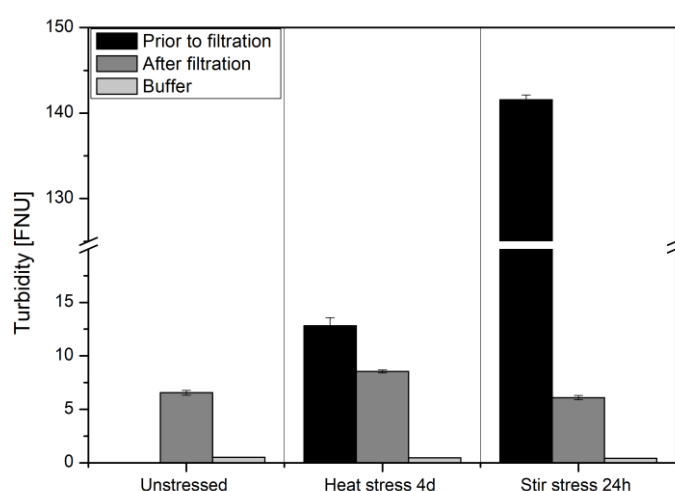


Figure 6-2: Results of turbidity measurements of unstressed Bevacizumab and after heat and stir stress prior to and after filtration. Turbidity is displayed in formazine nephelometric units (FNU).

6.2.1.3 Light obscuration

To detect particles larger than 1 μm , light obscuration measurements were performed. The results are displayed in Table 6-1. Heat stress as well as stir stress strongly triggered the formation of particles larger than 1 and 10 μm . The cumulative particle count after heat stress increased from 4350 particles/mL in the unstressed protein solution to 698583 particles/mL. Stir stress resulted in an even larger increase to a particle burden of 4623667 particles/mL. Filtration of the stressed Bevacizumab solutions resulted in a strong decrease in particle numbers. For the stir stressed samples, a particle burden of less than 2000 particles/mL could be found. The number of particles in the range of 1-10 μm after filtration of the heat stressed decreased in comparison to the particle burden prior to filtration. The number of particles in the range of 1-10 μm could be reduced to 28857 particles/mL, thus by factor 24, approximately. In contrast, the filtration factor (particle number prior to filtration/particle number after filtration) for the stir stressed sample was larger than 3000.

Table 6-1: Cumulative particle counts per mL of Bevacizumab after heat and stir stress prior to and after filtration determined by light obscuration.

Particle size	Unstressed	Formulation Buffer	Heat stress 4d	Heat stress 4d-Filtration
$\geq 1 \mu\text{m}$	4350 ± 229	17 ± 8	698583 ± 16557	28857 ± 1269
$\geq 10 \mu\text{m}$	192 ± 31	0 ± 0	3417 ± 1181	148 ± 18
$\geq 25 \mu\text{m}$	0 ± 0	0 ± 0	83 ± 144	0 ± 0
Particle size	Unstressed	Formulation Buffer	Stir stress 24h	Stir stress 24h-Filtration
$\geq 1 \mu\text{m}$	4350 ± 229	17 ± 8	4623667 ± 121715	1483 ± 1170
$\geq 10 \mu\text{m}$	192 ± 31	0 ± 0	39167 ± 2005	143 ± 24
$\geq 25 \mu\text{m}$	0 ± 0	0 ± 0	250 ± 250	12 ± 8

6.2.1.4 Flow Imaging

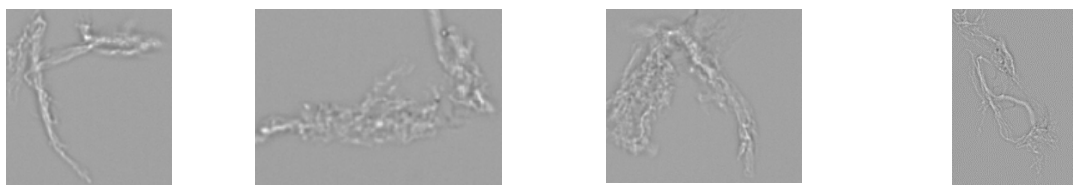
As an orthogonal method to light obscuration, particle numbers were also determined by Flow Imaging microscopy. Table 6-2 represents the particle numbers ≥ 1 , 10 and 25 μm of unstressed Bevacizumab and Bevacizumab after heat and stir stress prior to and after filtration. According to this data, heat as well as stir stress strongly triggered the formation of particles ≥ 1 , 10 and 25 μm . After filtration, particle numbers dropped to the level of particles of unstressed Bevacizumab implying a successful filtration regarding the particle burden.

In comparison to the results obtained from light obscuration measurements, the same trends were observed. Particle numbers increased upon exposure to stir and heat stress and filtration reduced particle numbers drastically. It is noticeable that, compared to the light obscuration data, a higher number of particles ≥ 10 and 25 μm after heat and stir stress could be detected using Flow Imaging microscopy. Moreover, using Flow Imaging microscopy, it was possible to analyze the morphology of the particles. Figure 6-3 displays photographs of some of the particles $\geq 25 \mu\text{m}$ after heat and stir stress, respectively. It is noticeable that particles $\geq 25 \mu\text{m}$ after heat stress had a filament-like structure and were transparent, while particles $\geq 25 \mu\text{m}$ after stir stress seemed to be more compact and had a denser structure. However, this was not evaluated statistically, but the differences in the morphology of the particles still represent a noteworthy difference between Bevacizumab after heat and stir stress.

Table 6-2: Cumulative particle counts per mL of Bevacizumab after heat and stir stress prior to and after filtration determined by Flow Imaging.

Particle size	Unstressed	Formulation Buffer	Heat stress 4d	Heat stress 4d Filtration
$\geq 1 \mu\text{m}$	7514 ± 1964	137 ± 59	1471800 ± 366921	2844 ± 2012
$\geq 10 \mu\text{m}$	954 ± 702	11 ± 11	187717 ± 20739	319 ± 247
$\geq 25 \mu\text{m}$	210 ± 128	0 ± 0	38567 ± 2691	33 ± 12
Particle size	Unstressed	Formulation Buffer	Stir stress 24h	Stir stress 24h Filtration
$\geq 1 \mu\text{m}$	7514 ± 1964	137 ± 59	28983400 ± 7151008	3116 ± 483
$\geq 10 \mu\text{m}$	954 ± 702	11 ± 11	748317 ± 233091	308 ± 113
$\geq 25 \mu\text{m}$	210 ± 128	0 ± 0	37500 ± 36680	50 ± 20

A



B



Figure 6-3: Representative photographs of particles $\geq 25 \mu\text{m}$ of Bevacizumab after heat stress for 4 days (A) and after stir stress for 24 hours (B) detected by Flow Imaging microscopy.

6.2.1.5 Dynamic light scattering (DLS)

To detect protein aggregates in the size range $1 \text{ nm} - 10 \mu\text{m}$ the samples were investigated by dynamic light scattering. Results are shown in Figure 6-4 and Table 6-3. After stir stress the Z_{ave} diameter increased to 492.87 nm and the intensity graph showed additional peaks at a larger particle size indicating the presence of larger aggregates. Moreover, the poly dispersity index (PDI) increased to 0.851 compared to a PDI value of 0.019 of the unstressed protein confirming an increased polydispersity of the samples after stirring. After filtration the additional peak in the intensity graph disappeared and only the monomer peak was present. The Z_{ave} diameter and PDI decreased again to the level of unstressed Bevacizumab (Table 6-3). In contrast, only small changes were seen for Bevacizumab after heat stress prior to and after filtration. After heat stress of Bevacizumab, the Z_{ave} diameter and the PDI value increased slightly to 13.28 nm and 0.177 , respectively. However, after

filtration there was no significant decrease in the Z_{ave} diameter and the PDI was even slightly increased (0.183).

Table 6-3: Z_{ave} and PDI values of unstressed Bevacizumab and after heat and stir stress prior to and after filtration.

	Unstressed	Heat stress 4d	Heat stress 4d-Filtration
Z_{ave} [nm]	11.47 ± 0.07	13.28 ± 0.04	13.13 ± 0.15
PDI	0.019 ± 0.015	0.177 ± 0.002	0.183 ± 0.016
	Unstressed	Stir stress 24h	Stir stress 24h-Filtration
Z_{ave} [nm]	11.47 ± 0.07	492.87 ± 42.75	11.48 ± 0.11
PDI	0.019 ± 0.015	0.851 ± 0.098	0.029 ± 0.022

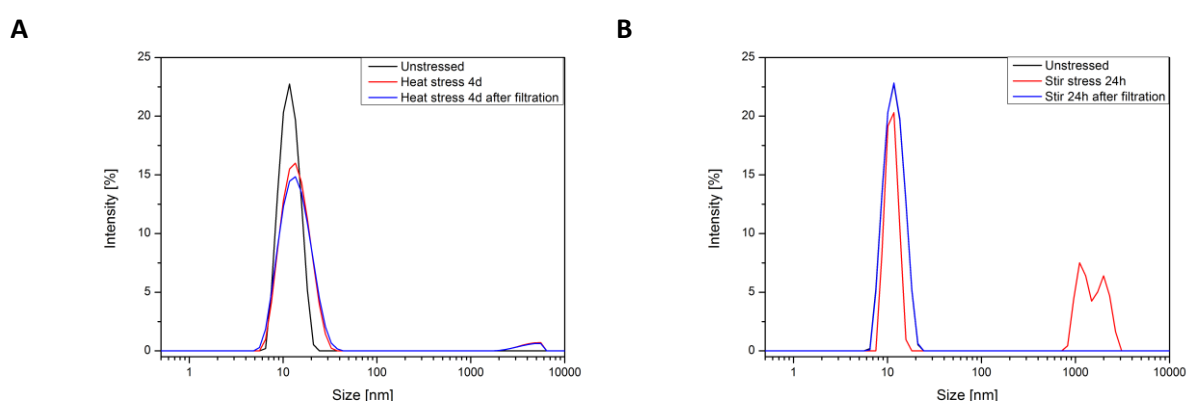


Figure 6-4: DLS graphs of unstressed Bevacizumab after heat stress (A) and after stir stress (B) prior to and after filtration.

6.2.1.6 Size exclusion chromatography (SEC)

For the analysis of soluble aggregates smaller than 100 nm, size exclusion chromatography was performed. The distribution of protein species and the total and monomer recovery of unstressed Bevacizumab, after heat and stir stress prior to and after filtration is displayed in Figure 6-5. It is apparent that heat stress triggered the formation of high molecular weight species (HMW). The heat stressed sample contained approximately 3.5% HMWs compared to 1% HMWs in the unstressed sample. Moreover, heat stress also triggered the formation of fragments (LMWs). In contrast, no soluble aggregates were formed during stir stress. The level of HMWs in the stir stressed sample did not change compared to unstressed Bevacizumab. The filtration process did not influence the level of soluble aggregates and no substantial differences between the percentages of HMWs and LMWs could be observed. Interestingly, the total recovery (Figure 6-5) increased slightly after filtration. However, the increase was only very small and within the standard deviations, so that no clear trend was visible.

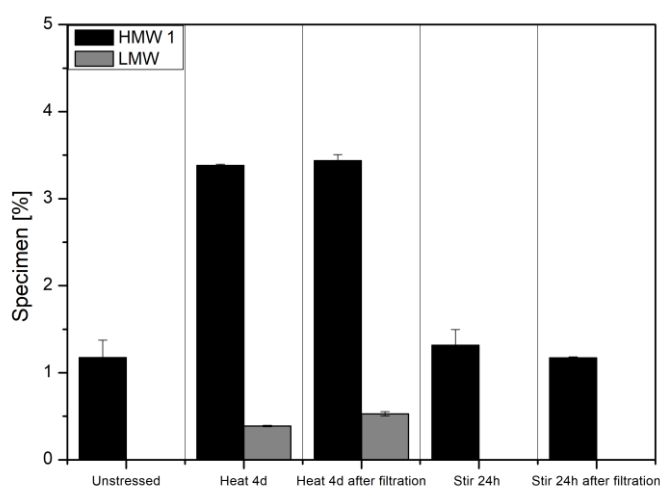
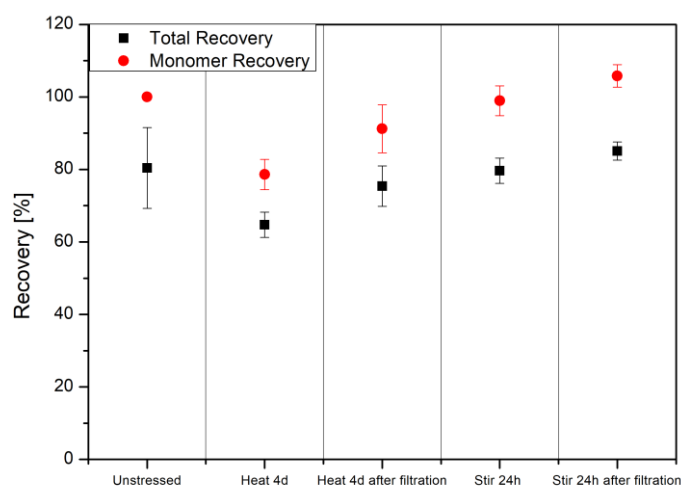
A**B**

Figure 6-5: Distribution of protein species (A) and total and monomer recovery in % (B) of unstressed Bevacizumab and after heat and stir stress prior to and after filtration.

6.2.1.7 Protein A chromatography

Protein A Chromatography is a well-known method to analyze methionine oxidation in the Fc-part of antibodies^{18,19}. Figure 6-6 displays the chromatograms of unstressed Bevacizumab after heat and stir stress prior to and after filtration. Bevacizumab after incubation with 2% *tert*-butyl hydroperoxide (tBHP) for 56 hours was used as positive control. The peak of the positive control was eluted faster compared to unstressed Bevacizumab indicating methionine oxidation. The chromatogram of Bevacizumab after stir stress prior to and after filtration did not show any differences compared to unstressed Bevacizumab. Thus, it can be assumed that stir stress did not lead to methionine oxidation in the Fc-part of the antibody. The chromatogram of the heat stressed Bevacizumab showed a second peak eluting later than the main peak (indicated by the red arrow in Figure 6-6A). If methionine

residues in the Fc-part of the antibody are oxidized, the species elute earlier than the main peak, since methionine oxidation weakens the Protein A affinity¹⁸. Thus, species eluting later than the main peak bind even more strongly to Protein A. However, the results of the heat stressed protein revealed no oxidation of the methionine residues in the Fc part of the antibody, but the appearance of an additional peak indicated chemical modifications. No changes in the chromatogram were detected after filtration of heat stressed Bevacizumab compared to the chromatogram prior to filtration. Moreover, it is noteworthy that there was a small overlap of the main peak of the Bevacizumab samples and the positive control indicating that all samples including unstressed Bevacizumab possibly contained small amounts of oxidized species.

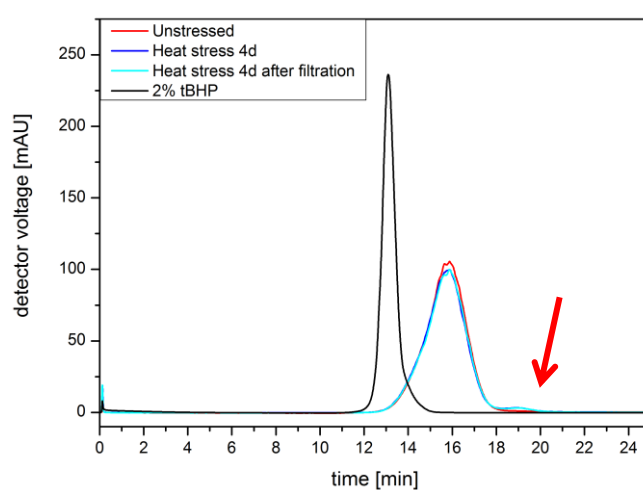
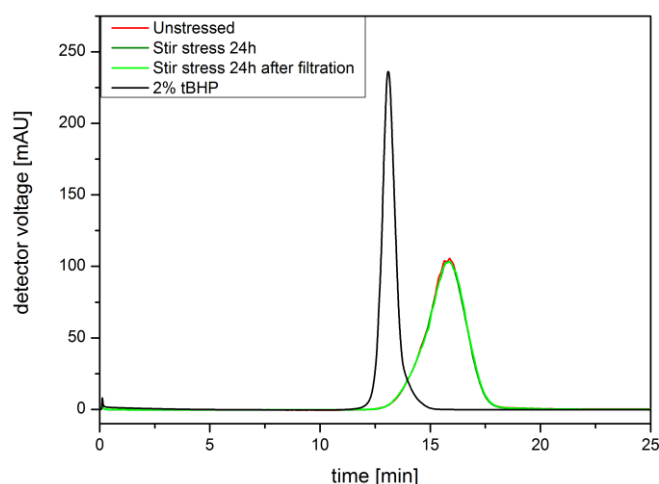
A**B**

Figure 6-6: Protein A chromatograms of unstressed Bevacizumab and after exposure to heat (A) and stir stress (B) prior to and after filtration.

6.2.1.8 Ion exchange chromatography (IEX)

In addition to Protein A chromatography, ion exchange chromatography (IEX) was performed to detect charge variants of Bevacizumab which were formed by exposure to stir or heat stress. The chromatograms of unstressed Bevacizumab and Bevacizumab after heat and stir stress prior to and after filtration and an exemplary chromatogram with the charge variants are shown in Figure 6-7 and Figure 6-8. It is clearly visible that Bevacizumab after exposure to heat for four days contained a larger amount of acidic and basic variants compared to unstressed Bevacizumab. Acidic variants can be formed due to deamidation, C-terminal lysine cleavage or glycation for instance. Conversely, basic variants can be formed due to the presence of C-terminal lysine or glycine amidation, succinimide formation or amino acid oxidation²⁰. Thus, heat stress triggered at least some of these chemical modifications since the content of acidic and basic variants increased during heat stress. No changes were detectable after filtration indicating that the filtration process itself did not have an influence on the level of charge variants in the sample. After stir stress no changes in the IEX chromatogram compared to unstressed Bevacizumab were visible. Accordingly, stir stress did not have any influence on the level of charge variants. Again, no alterations were observed after filtration of the stir stressed sample.

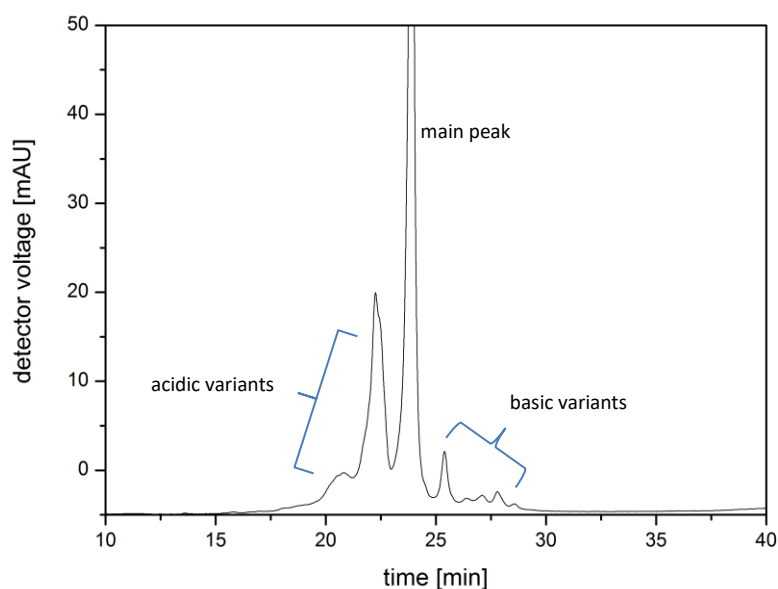


Figure 6-7: Representative IEX chromatogram of Bevacizumab after exposure to 50°C for four days.

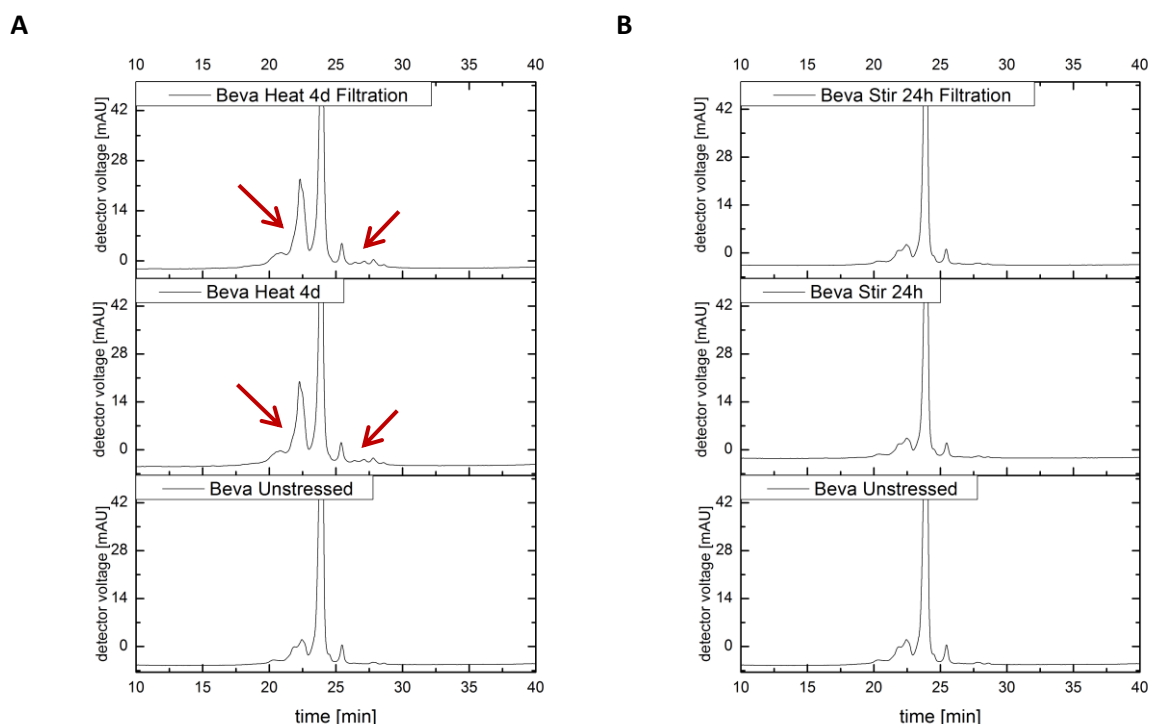


Figure 6-8 IEX chromatograms of unstressed Bevacizumab (bottom) and Bevacizumab after heat stress (A) and after stir stress (B) prior to (center) and after filtration (top).

6.2.1.9 Intrinsic fluorescence spectroscopy

Intrinsic fluorescence measurements were performed to investigate conformational changes after exposure to stir and heat stress and filtration of the stressed samples. The fluorescence of tryptophan is dependent on its environmental conditions. Thus, alterations in the environment of the protein can lead to an increase or decrease in fluorescence intensity²¹. For example, when tryptophan residues are embedded in the hydrophobic core of the protein, fluorescence intensity decreases²¹. In contrast, quenching amino acids surrounding tryptophan residues can also be removed due to unfolding of the protein, resulting in an increase in fluorescence intensity²². The emission spectra of Bevacizumab after exposure to heat and stir stress prior to and after filtration are displayed in Figure 6-9. After heat stress an increase in fluorescence intensity was detectable indicating alterations in the environment of tryptophan. Fluorescence intensity of the unstressed and filtered sample was almost on the same level and no shifts of the emission maxima were detectable. The fluorescence intensity of stir stressed Bevacizumab also increased slightly compared to unstressed Bevacizumab, displayed in Figure 6-9B. The fluorescence intensity of the filtered sample decreased slightly compared to unstressed Bevacizumab. However, also after stir stress no shifts of the emission maxima were detectable. The changes between the samples prior to and after filtration may depend on the presence or absence of particles. After filtration, fluorescence intensities of the samples were almost on the same level as of unstressed Bevacizumab.

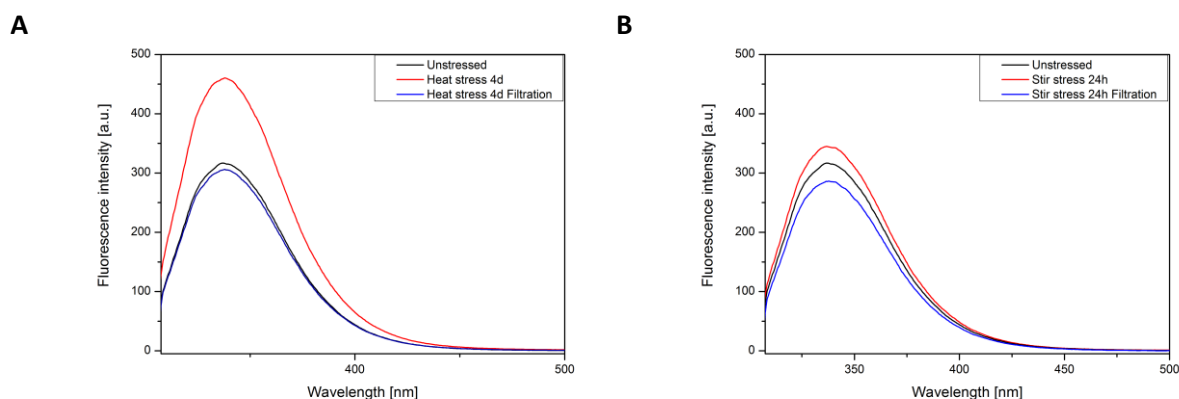


Figure 6-9: Intrinsic fluorescence of Bevacizumab after heat stress (A) and after stir stress prior to and after filtration at a concentration of 1 mg/mL and excitation at 295 nm.

6.2.1.10 Extrinsic fluorescence spectroscopy

In addition to intrinsic fluorescence, extrinsic fluorescence of unstressed Bevacizumab and the stressed samples using Bis-ANS as fluorescent dye was monitored. Figure 6-10 shows the extrinsic fluorescence emission spectra of Bevacizumab after heat and stir stress prior to and after filtration. The fluorescence intensity of Bevacizumab after heat and stir stress increased compared to unstressed protein. Despite a rather small increase from 2.5 a.u. to 10 a.u., the data still indicate changes in the local environment of the protein²³. After filtration of the heat and stir stressed sample, respectively, the fluorescence intensity increased even less, indicating only minor changes in the environment. In addition to an increase in fluorescence intensity the spectra are often blueshifted²¹. Comparing the emission maxima of Bevacizumab after heat and stir stress prior to and after filtration (Table 6-2) it can be observed that the spectra after filtration were approximately 2 nm blue-shifted, which represents only a minor shift. Compared to the maximum of unstressed Bevacizumab, the spectra of the heat and stir stressed sample were red-shifted, meaning that the spectra were shifted to larger wavelengths. However, the results indicate that stir and heat stress might have triggered some unfolding processes. The filtered samples resulted in a lower fluorescence intensity than the non-filtered samples indicating that the presence of particles might be the reason for this slight increase in fluorescence intensity.

Table 6-4: Peak positions of Bis-ANS fluorescence emission spectra of unstressed Bevacizumab and Bevacizumab after heat and stir stress prior to and after filtration.

	Unstressed	Heat stress 4d	Heat stress 4d Filtration	Stir stress 24h	Stir stress 24h Filtration
Peak position	486.56 nm	495.07 nm	492.98 nm	494.47 nm	492.98 nm

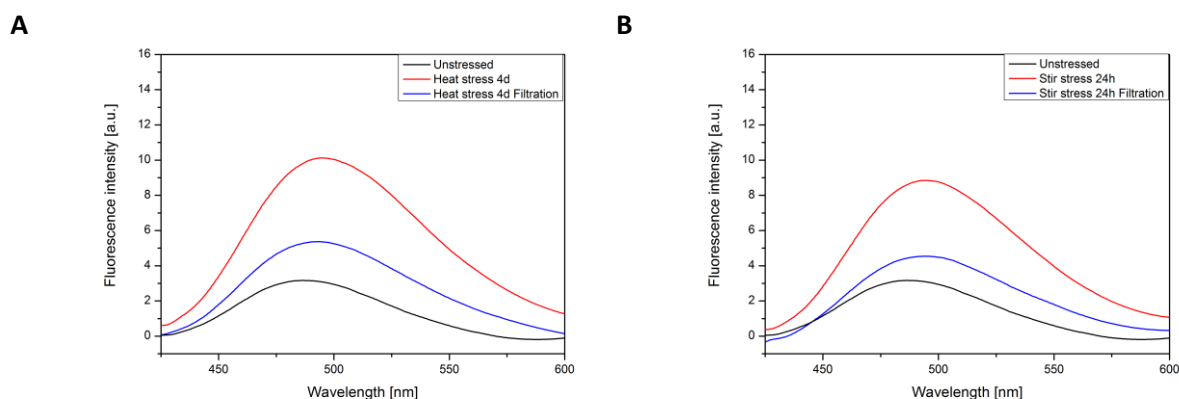


Figure 6-10: Extrinsic fluorescence emission spectra of 1 mg/mL Bevacizumab and 20 μ M Bis-ANS after heat stress and stir stress prior to and after filtration.

6.2.1.11 Fourier-transform infrared spectroscopy (FT-IR)

Alterations in the secondary structure of Bevacizumab after heat and stir stress were analyzed using FT-IR spectroscopy. The 2nd derivative FT-IR spectra of unstressed Bevacizumab and after heat and stir stress prior to and after filtration are shown in Figure 6-11. The amide band I, which appears between 1700-1600 cm^{-1} , is characteristic for an intact secondary structure²⁴. The 2nd derivative spectra of amide I band of Bevacizumab after heat and stir stress did not show any considerable alterations and the bands were not shifted significantly to different wavenumbers. Therefore, it can be assumed that the secondary structure of the protein was not or only little affected by heat or stir stress. Moreover, no alterations of the amide bands I of the heat and stir stressed Bevacizumab after filtration could be detected. Thus, the filtration process itself did not influence the secondary structure.

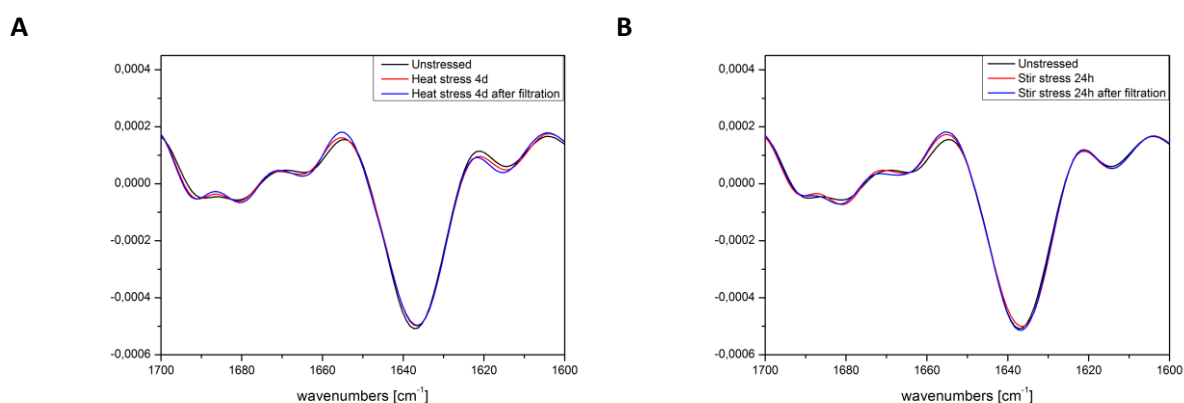


Figure 6-11: 2nd derivative FT-IR spectra of amide I band of unstressed Bevacizumab, after heat stress (A) and after stir stress (B) prior to and after filtration.

6.2.1.12 Hold-up volume PharmAssure® filter

Regarding material loss, the hold-up volume of filters is an important parameter. Therefore, the hold-up volume of the used PharmAssure® filters was determined with the formulation buffer of the Bevacizumab solution and results are shown in Figure 6-12. Without implementing an air purge, the hold-up volume was quite large with almost 700 µl. Purging the filter with approximately 3 mL air reduced the hold-up volume to 300 µl. Purging the filter with air until the bubble point was reached resulted in a hold-up volume of 150 µl. Based on these results a filtration instruction was prepared to optimize the filtrate yield.

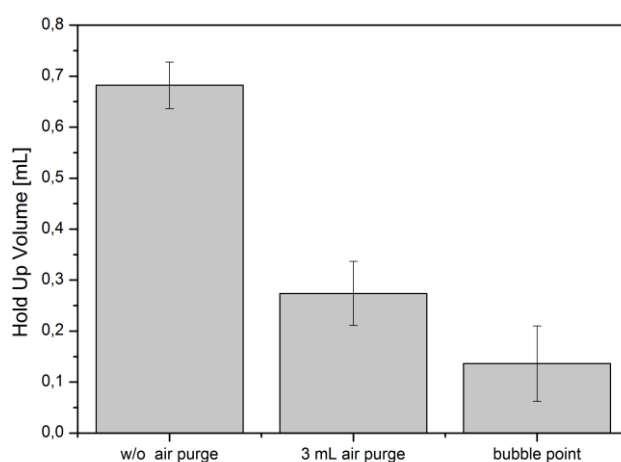


Figure 6-12: Hold up volume of PharmAssure® filter, ø25 mm, with a pore size of 0.2 µm w/o air purge, 3 mL air purge and air purge until the bubble point is reached.

6.2.1.13 Filter quality of PharmAssure® filter

To exclude filter defects, the quality of ten PharmAssure® filters was tested by filtering a model protein solution at a concentration of 25 mg/mL (approximately same concentration as Bevacizumab samples). The monoclonal antibody solution was exposed to stir stress for 24 hours and a volume of 3 mL was filtrated using PharmAssure® filters, respectively. The particle numbers of the filtered samples, the unstressed and stir stressed protein solution were determined by light obscuration and are displayed in Figure 6-13. Particles numbers $\geq 1, 2, 5$ and $10\text{ }\mu\text{m}$ clearly increased after stir stress, represented by the red bar in the graph. After filtration of the samples, particle numbers decreased strongly and were comparable to the unstressed protein. For the scope of our experiment it was positive to see that filtering a stressed protein solution using ten different filters resulted in particle numbers comparable to the unstressed protein solution and that no outlier could be detected. Thus, it can be assumed that the filter quality was given.

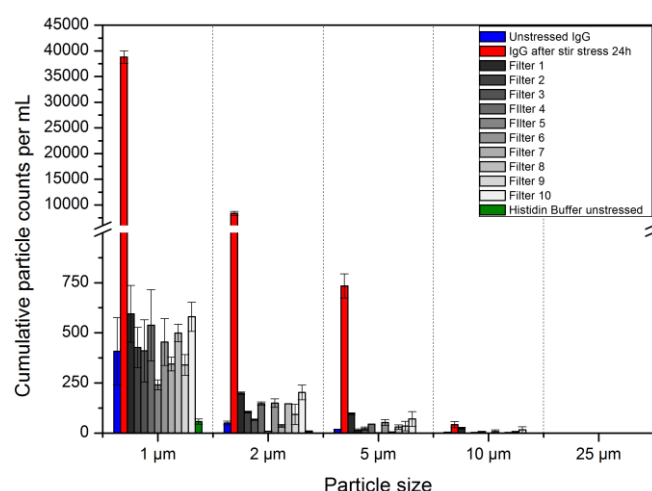


Figure 6-13: Cumulative particle counts per mL of a monoclonal antibody (IgG₁) at a concentration of 25 mg/mL prior to and after filtration using PharmAssure® filters, ø25 mm, with a pore size of 0.2 µm.

6.2.2 Results of 3D *in vitro* human artificial lymph node experiments

The experimental procedure of the 3D *in vitro* human artificial lymph node experiments is described in Chapter 3 and corresponded to the procedures of the HuALN study described in Chapter 5 (except for the filtration step).

6.2.2.1 Cytokine analysis

During the bioreactor run time of 28 days, sampling was performed daily, and the cell culture supernatants were analyzed for the presence of various cytokines (IL-2, IL-4, IL-1β, IL-8, IL-10, IL-12p70, IL-13, IFN-γ and TNF-α). The area under the curve of each cytokine secretion profile was calculated and normalized to the control run. Finally, the cytokines were assigned to different immune responses and results were illustrated in spider grid diagrams (see Materials and Methods, Chapter 3). Figure 6-14 displays the results of cytokine analysis after stimulation of the human artificial lymph node model with Bevacizumab after heat and stir stress prior to and after filtration. The spider grid diagrams showed, that the responses of the three donors varied significantly. It should be mentioned that a different cell culture medium had to be used for the experiment with donor 1 due to supply problems with the standard cell culture medium. Nevertheless, the bioreactor run with donor 1 revealed a slight tendency towards a pro-inflammatory and TH1 immune answer for the heat stressed samples compared to the other samples. This was also true for donor 3. The results indicated a slight tendency towards a pro-inflammatory and TH1 immune response. However, since the normalization to the unstressed control resulted in a value of 1, one cannot speak of a strong upregulation. In contrast to the results of donor 1 and donor 3, cytokine analysis of donor 2 resulted in a strong TH1 and pro-inflammatory immune response for Bevacizumab after stir stress and the formulation buffer. These

conflicting results indicate the importance of donor to donor variability. Regarding the difference in immune response of filtered and non-filtered samples, no clear trend or difference in cytokine response between the filtered and the non-filtered samples could be observed in the case of all three donors. In summary, the results revealed no clear trend towards a certain immune response and no effect of in-line filtration on the secretion of cytokines could be detected. However, difficulties such as a change in cell culture medium and contradictory results (donor 2) made the interpretation of the data difficult.

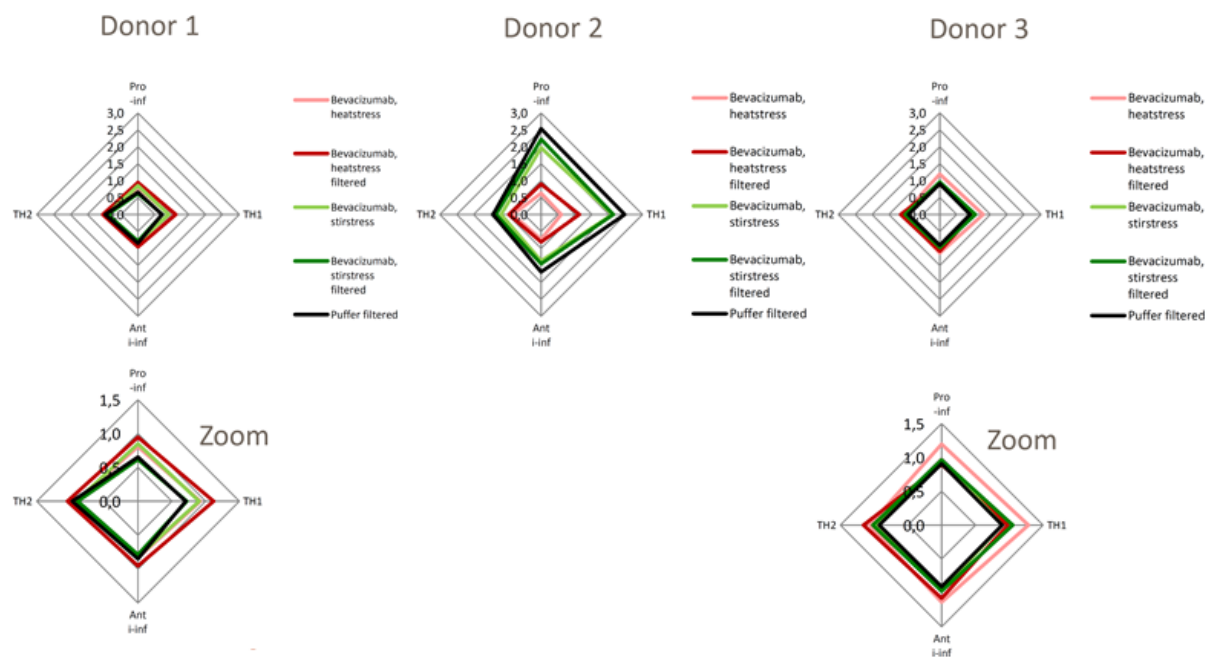


Figure 6-14: Cytokine secretion displayed in spider grid diagrams for tested Bevacizumab samples of Donor 1-3. AUC values of each cytokine secretion profile of the HuALN run time of 28 days are normalized to a control run (unstressed protein), allocated to cytokine groups (TH1, TH2, pro-inflammatory, anti-inflammatory) and displayed as spider grids. Values larger/smaller than 1 indicate up-/downregulation compared to the control run. A detailed description of the data evaluation is provided in Chapter 3. This data was provided by ProBioGen AG, Berlin.

6.2.2.2 Total IgM secretion

Besides the analysis of cytokine secretion, the cell culture supernatants were also tested for the presence of IgM antibodies. Figure 6-15 and Figure 6-16 display the results of IgM secretion over a HuALN run time of 28 days and after stimulation with Bevacizumab after heat and stir stress prior to and after filtration. It is true for all donors that there was an initial increase in the IgM concentration after the first stimulation which reached its maximum of about 40 ng/mL on day 3 or 4 and decreased again to 10 ng/mL and lower until day 7. Re-simulations of the HuALN on day 7, 14 and 21 did not lead to a renewed increase. The cumulative representation of the data (Figure 6-16) did not reveal any significant changes between the differently stressed samples, the buffer control or the samples prior to and after filtration.

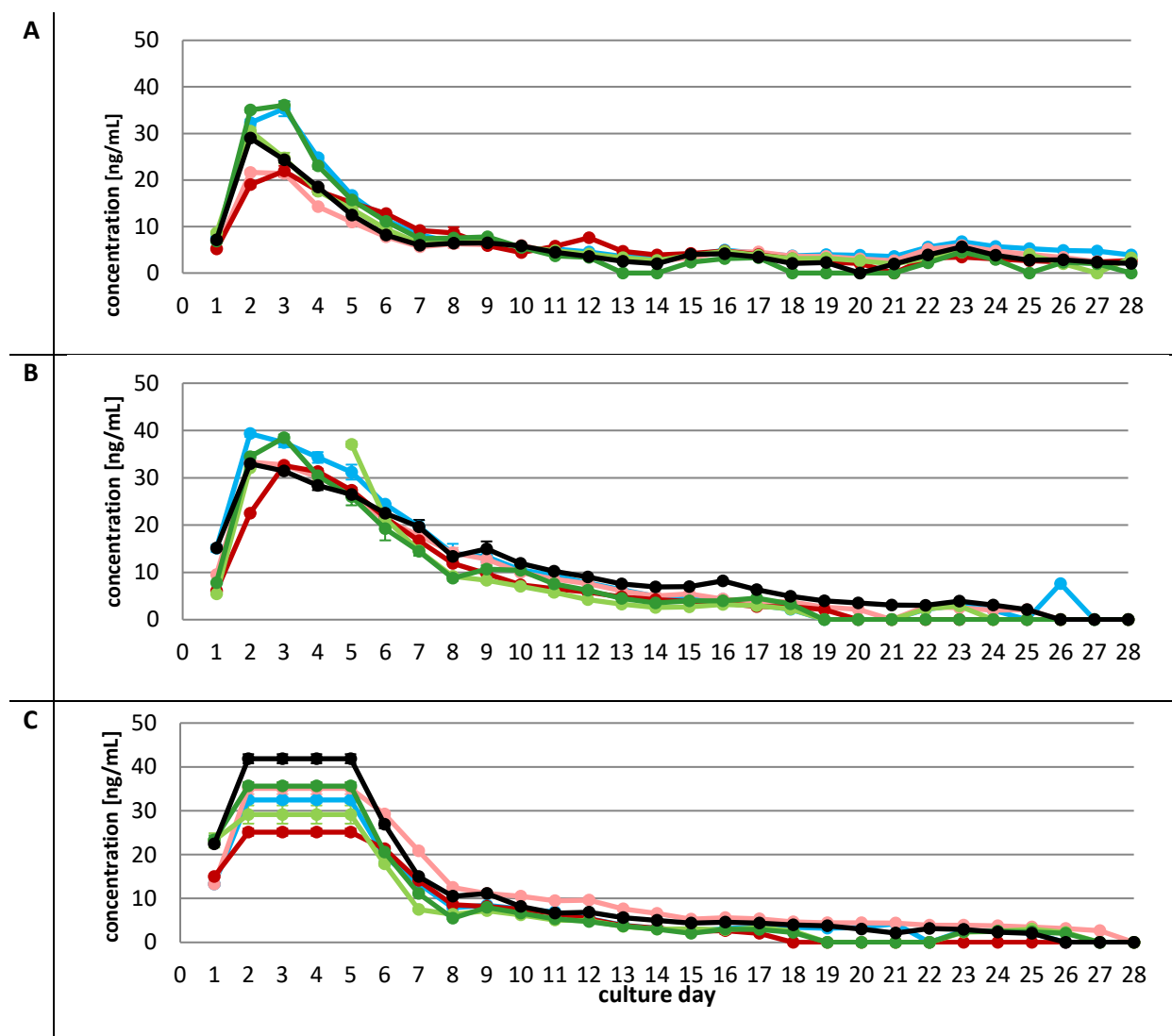


Figure 6-15: Secretion of IgM over a HuALN run period of 28 days of Donor 1 (A), Donor 2 (B) and Donor 3 (C). Blue line: Unstressed Bevacizumab, light pink line: Bevacizumab after 4d heat stress, red line: Bevacizumab after 4d heat stress and filtration, light green line: Bevacizumab after 24h stir stress, dark green line: Bevacizumab after 24h stir stress and filtration, black line: formulation buffer. This data was provided by ProBioGen AG, Berlin.

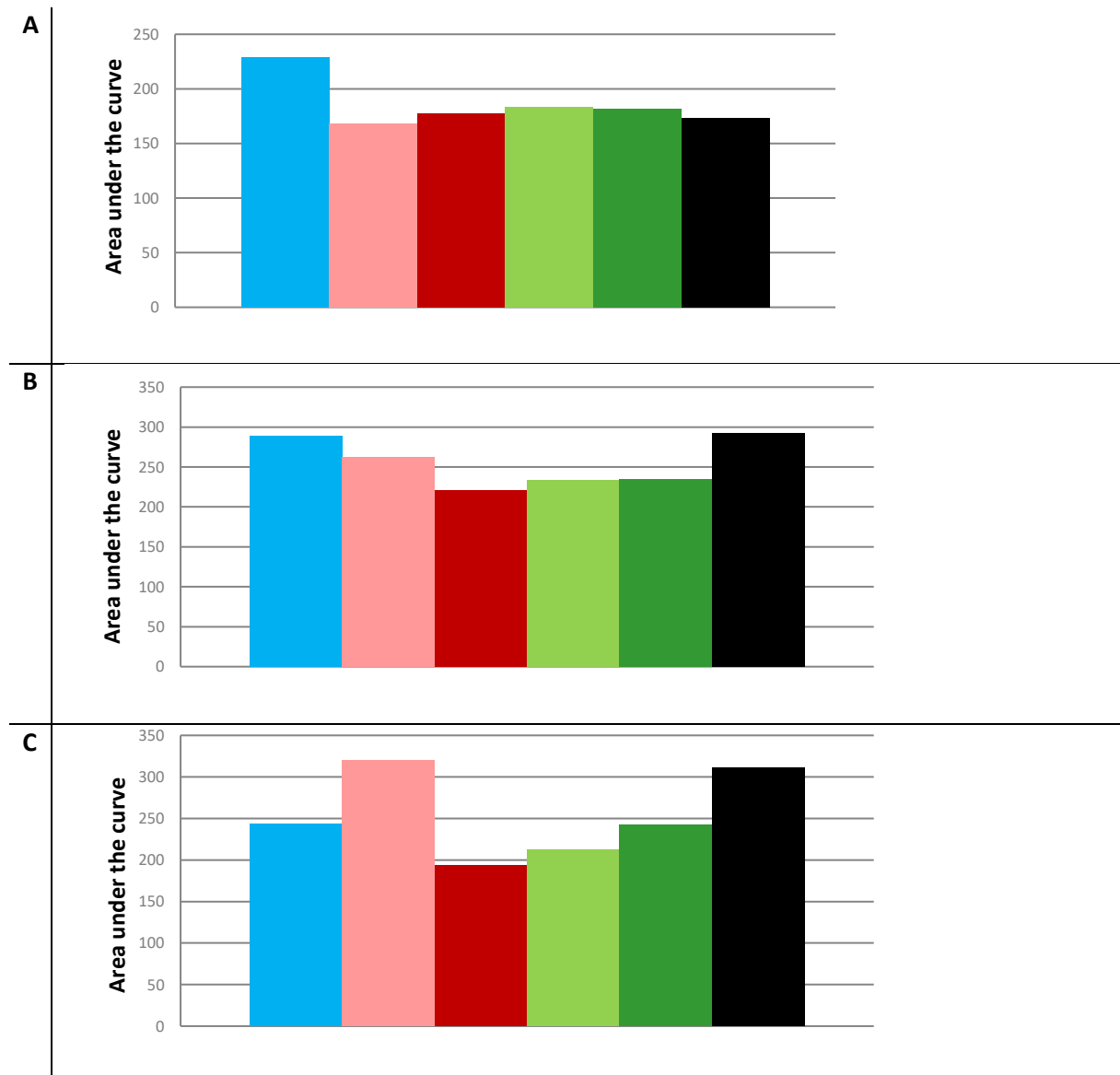


Figure 6-16: Overall IgM secretion (cumulative) of Donor 1 (A), Donor 2 (B) and Donor 3 (C). Blue bar: Unstressed Bevacizumab, light pink bar: Bevacizumab after 4d heat stress, red bar: Bevacizumab after 4d heat stress and filtration, light green bar: Bevacizumab after 24h stir stress, dark green bar: Bevacizumab after 24h stir stress and filtration, black bar: formulation buffer. This data was provided by ProBioGen AG, Berlin.

6.3 Evaluation of the effect of in-line filtration using a 2D *in vitro* dendritic cell assay

The biological effect of in-line filtration was also tested in a 2D *in vitro* dendritic cell assay. Besides heat and stir stressed Bevacizumab, Bevacizumab was also exposed to light and incubated with 1% *tert*-butyl hydroperoxide (tBHP) and the immunological effect was investigated prior to and after filtration. The analysis of Bevacizumab after light stress and chemically treated Bevacizumab is described in the following sections. The analysis of the heat and stir stressed samples was described in 6.2.

6.3.1 Results of protein analysis

6.3.1.1 Visual inspection

Unstressed and stressed Bevacizumab samples were visually inspected after the exposure to light and tBHP prior to and after filtration. The results are presented in Table 6-5. No particles were visible after the exposure of Bevacizumab to tBHP prior to and after filtration. In contrast, visible particles were detected after light stress prior to filtration. Moreover, the sample had a slight yellow color. After filtration, no particles were visible anymore, but the yellow color was still present.

Table 6-5: Results of visual inspection of Bevacizumab after exposure to light and incubation with 1% tBHP for 16 hours prior to and after filtration. A clear solution and no visible particles are marked by “-”; a visible increase in turbidity and the presence of visible particles are marked by “+”.

Sample	Prior to filtration	After filtration
Unstressed	-	-
1% tBHP 16h	-	-
Light stress 24h	+	-
	Slight yellow color	Slight yellow color

6.3.1.2 Turbidity

Results of turbidity measurements are shown in Figure 6-17. The turbidity of Bevacizumab after exposure to 1% tBHP was increased only slightly to 7.18 FNU compared to the unstressed protein (6.47 FNU). Consequently, the difference between the turbidity prior to and after filtration was negligible. In contrast, the turbidity of Bevacizumab after light stress for 24h increased strongly to 220.33 FNU compared to the unstressed protein and a significant decrease in turbidity of 204.8 FNU was detected after filtration.

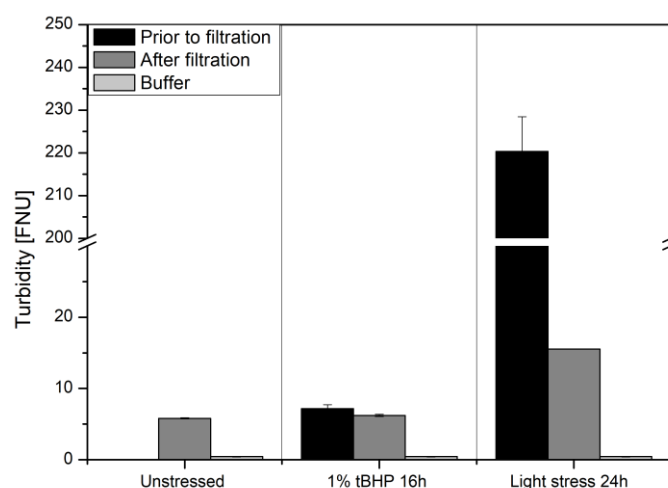


Figure 6-17: Results of turbidity measurements of unstressed Bevacizumab and Bevacizumab after 24h light stress and incubation with 1% tBHP for 16h. Results are shown in formazine nephelometric units (FNU).

6.3.1.3 Flow Imaging

In order to determine particle numbers $\geq 1 \mu\text{m}$, all samples were investigated using Flow Imaging. The results are represented in Table 6-6. In comparison to unstressed Bevacizumab, particle numbers after light and chemical oxidation stress increased in all size ranges. The total particle number increased to 161951 ± 8680 particles/mL after incubation with tBHP and to 75975 ± 25178 particles/mL after exposure to light. Filtration resulted in a strong decrease of particles ≥ 1 , 10 and $25 \mu\text{m}$ in the case of Bevacizumab after exposure to 1% tBHP. The reduction of particles $\geq 1 \mu\text{m}$ by filtration after light stress was not as effective as for the sample treated with tBHP, since the total particle count of particles $\geq 1 \mu\text{m}$ could only be reduced to 24697 ± 5804 particles. However, the number of particles ≥ 10 and $25 \mu\text{m}$ could be reduced strongly.

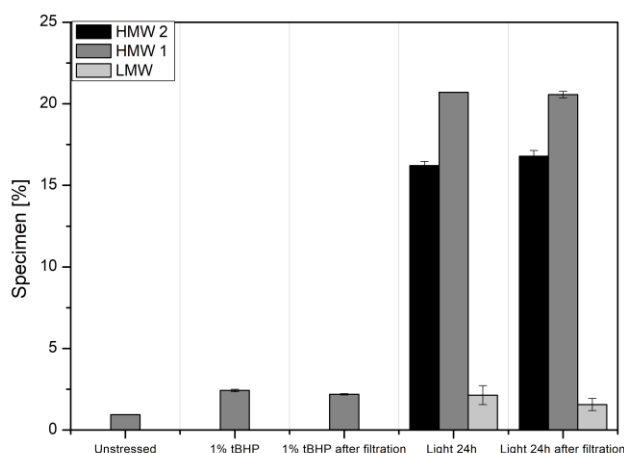
Table 6-6 Total particle counts ≥ 1 , 10 and $25 \mu\text{m}$ of unstressed Bevacizumab and Bevacizumab after 24h of light stress and incubation with 1%tBHP for 16h prior and after filtration determined by Flow Imaging.

Particle size	Unstressed	Formulation Buffer	1% tBHP	1% tBHP Filtration
$\geq 1 \mu\text{m}$	4449 ± 1527	223 ± 47	161951 ± 8680	5582 ± 2282
$\geq 10 \mu\text{m}$	573 ± 382	13 ± 8	12373 ± 240	213 ± 153
$\geq 25 \mu\text{m}$	115 ± 42	3 ± 5	944 ± 123	15 ± 7
Particle size	Unstressed	Formulation Buffer	Light stress 24h	Light stress 24h Filtration
$\geq 1 \mu\text{m}$	4449 ± 1527	223 ± 47	75975 ± 25178	24697 ± 5804
$\geq 10 \mu\text{m}$	573 ± 382	13 ± 8	8875 ± 1127	818 ± 162
$\geq 25 \mu\text{m}$	115 ± 42	3 ± 5	1268 ± 278	54 ± 21

6.3.1.4 Size exclusion chromatography (SEC)

In order to detect soluble aggregates, all samples were investigated by size exclusion chromatography. The distribution of protein species of unstressed Bevacizumab and Bevacizumab after 24h of light stress and incubation with 1% tBHP for 16 hours prior to and after filtration is displayed in Figure 6-18. The percentage of high molecular weight species after exposure of Bevacizumab to 1% tBHP increased to approximately 2.5%, while the monomer recovery decreased slightly (Figure 6-18B). The exposure of Bevacizumab to light for 24h resulted in a strong increase of high molecular weight species, so that the sample contained approx. 35% high molecular weight species (Figure 6-18A). Moreover, the formation of fragments was triggered (Figure 6-18A). The strong increase in aggregates is associated with a decrease in monomer recovery as shown in Figure 6-18B. The filtration process did not influence the level of soluble aggregates or fragments.

A



B

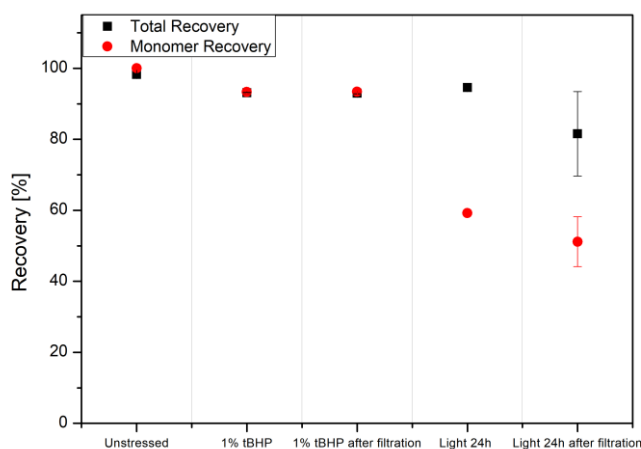


Figure 6-18: Distribution of protein species (A) and total and monomer recovery in % (B) of unstressed Bevacizumab and after light stress for 24h and incubation with 1% tBHP for 16h prior to and after filtration; HMW 2 > HMW 1 > LMW.

6.3.1.5 Protein A chromatography

Protein A Chromatography is a well-known method to analyze methionine oxidation in the Fc-part of antibodies^{18,25}. Figure 6-19 displays the chromatograms of unstressed Bevacizumab and Bevacizumab after light and chemical oxidation stress prior to and after filtration. Accordingly, both stress methods strongly triggered methionine oxidation of the Fc-part of Bevacizumab, since the peaks were clearly shifted to the left compared to the unstressed protein. Shifts to earlier elution times indicate less affinity to Protein A and therefore, it can be assumed that Bevacizumab after light stress for 24h and incubation with 1% tBHP for 16h contained substantial oxidative changes. However, the filtration process did not influence the peak position of the stressed samples. Thus, filtration did not trigger further oxidation according to this data.

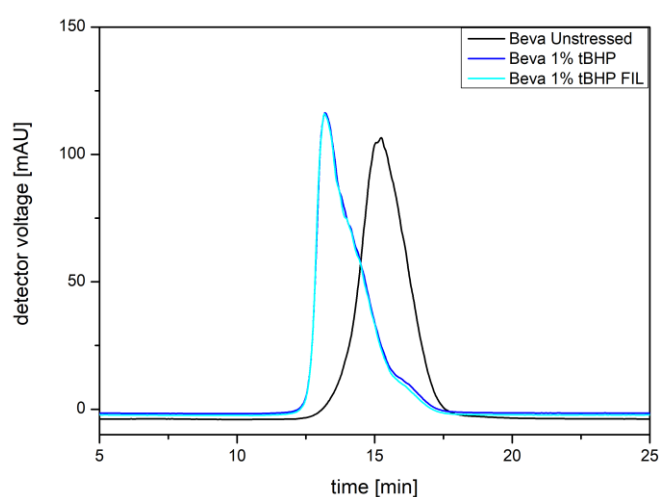
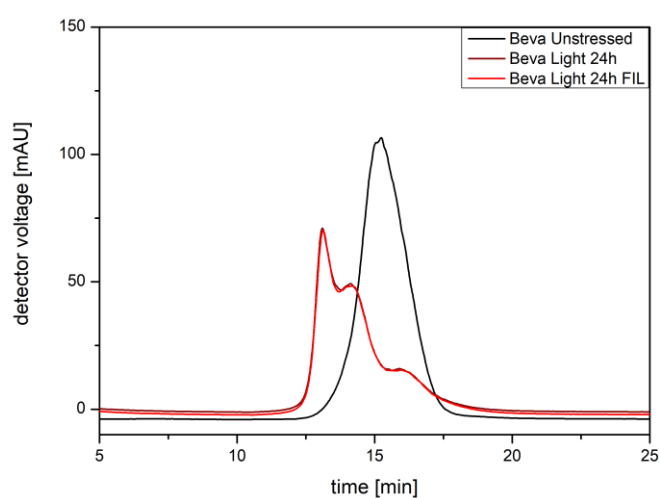
A**B**

Figure 6-19: Protein A chromatograms of unstressed Bevacizumab and after exposure to tBHP (A) and light (B) prior and after filtration.

6.3.1.6 Ion exchange chromatography (IEX)

Ion exchange chromatography was performed to detect alterations in charge variants of Bevacizumab formed during exposure to light or tBHP. The chromatograms of unstressed Bevacizumab and Bevacizumab after light and chemical oxidation stress prior to and after filtration are shown in Figure 6-20. Compared to unstressed Bevacizumab, the area under the curve of the monoclonal antibody after incubation with 1% tBHP decreased clearly and after light stress for 24h, no peaks were detectable by IEX chromatography. This indicates, that both stress methods modified the protein significantly regarding chemical modifications. To further investigate changes in charge variants after light stress of Bevacizumab, the antibody was exposed to light for different period of times and analyzed by ion exchange chromatography. The results are shown in Figure 6-21. Already after two hours of exposure to light stress at $55 \pm 5 \text{ W/m}^2$ the area under the curve decreased strongly compared to unstressed Bevacizumab. This trend continued until there was no peak detectable anymore after 24h of light stress. These results indicate that light stress had a significant influence on the level of charge variants and exposure times of a few hours only suffice to trigger chemical modifications of Bevacizumab.

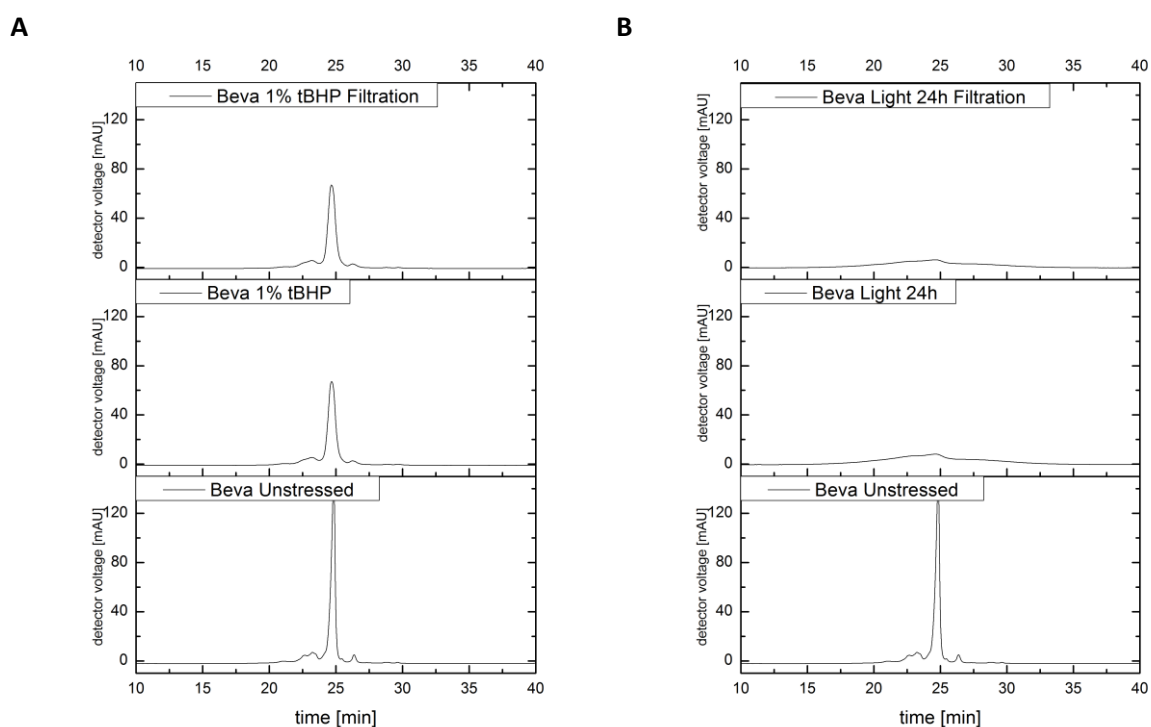


Figure 6-20: IEX chromatograms of unstressed Bevacizumab (bottom) and Bevacizumab after incubation with 1% tBHP for 16h (A) and after 24h of light stress (B) prior to (center) and after filtration (top).

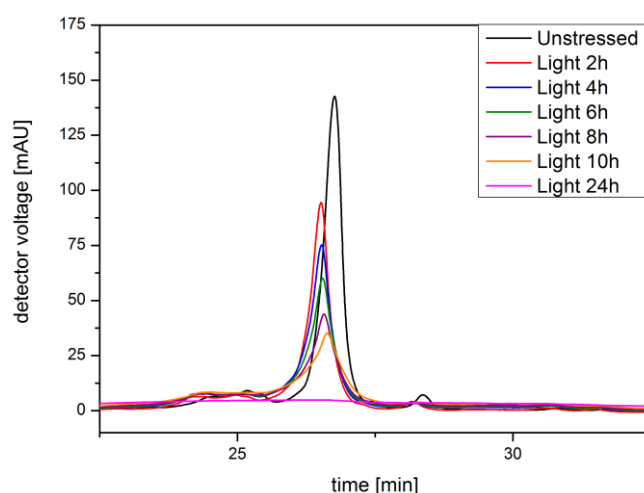


Figure 6-21: IEX chromatograms of unstressed Bevacizumab and Bevacizumab after different exposure times to light.

6.3.1.7 Hold-up volume Acrodisc® filter

Due to a relatively large hold-up volume for the PharmAssure® filter with a diameter of 25 mm, an Acrodisc® filter with a diameter of 13 mm was used for filtrating the samples for the 2D *in vitro* dendritic cell assay. As already described for the PharmAssure® filter above, the hold-up volume of the Acrodisc® filter was also determined and the results are displayed in Figure 6-22. The volume remaining in the filter after filtration was approximately 140 μL . After applying an air purge with a volume of 1 mL, the hold-up volume could be reduced to a volume of approximately 80 μL .

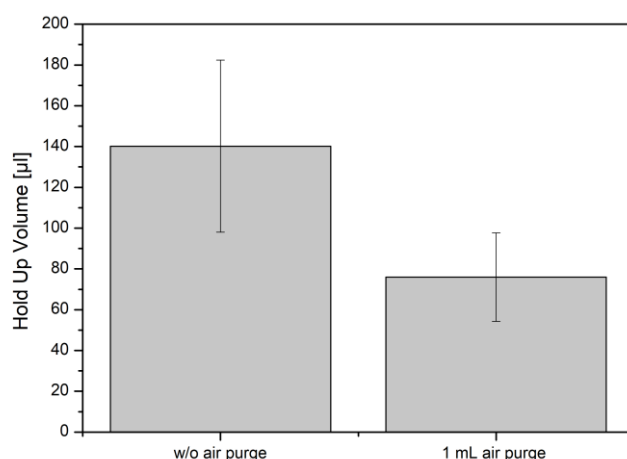


Figure 6-22: Hold up volume of Acrodisc® filter, $\varnothing 13$ mm, with a pore size of $0.2 \mu\text{m}$ w/o air purge and 1 mL air purge.

6.3.2 Results of 2D *in vitro* dendritic cell assay experiments

The experimental procedure of the 2D *in vitro* experiments is described in Chapter 3.

6.3.2.1 Analysis of dendritic cell surface marker

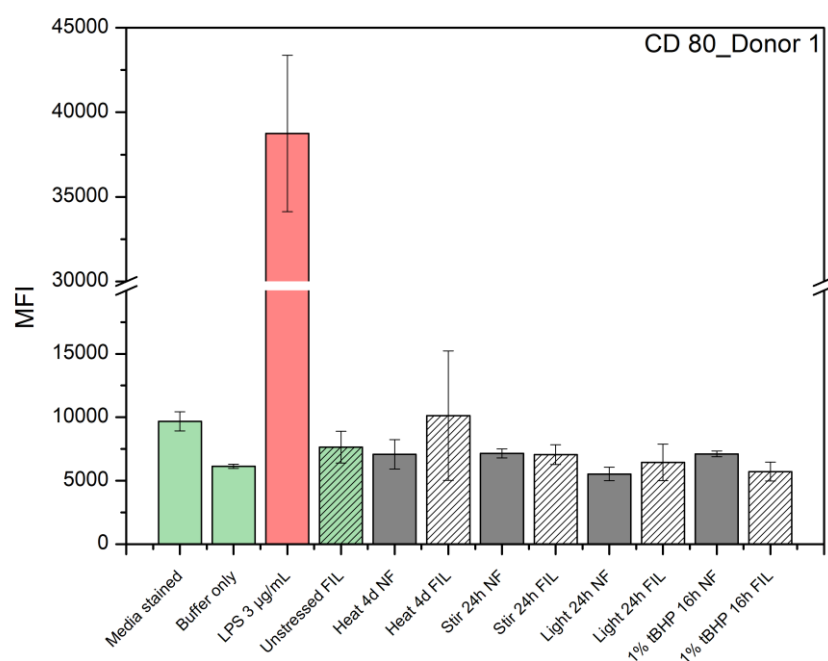
After incubation of immature dendritic cells with differently stressed samples of Bevacizumab prior to and after filtration, cells were harvested, and the expression of various DC markers was analyzed. The results are shown in Figure 6-23 - Figure 6-26. CD 80, 83 and 86 are important activation markers of dendritic cells^{26,27}. Therefore, their expression on immature DCs is low whereas on mature DCs, expression levels are high. Human leukocyte antigen-DR (HLA-DR) is highly expressed on mature dendritic cells but to a lower degree on immature dendritic cells. Thus, activated dendritic cells are supposed to show a higher expression of HLA-DR. The results showed that LPS could stimulate dendritic cells of both donors to express the examined activation markers. In contrast, none of the stressed Bevacizumab samples showed significant changes in the expression levels of CD 80, 83, 86 or HLA-DR. Moreover, there were no differences in expression levels between the unstressed and stressed samples prior to and after filtration. Donor 1 seemed to be more responsive, since some of the results indicated slight trends. For example, the expression of CD 80, 83, 86 and HLA-DR after stimulation with filtered, heat stressed Bevacizumab was higher than after stimulation with the non-filtered sample. However, taking the standard deviation into consideration, the expression level of all markers after filtration was still on a comparable level with the unstressed and the non-filtered sample. Donor 2 showed a small trend for samples treated with tBHP: The expressions of CD 83, 86 and HLA-DR were slightly elevated after stimulation with Bevacizumab treated with 1% tBHP. For the filtered tBHP sample, the expression levels were comparable to the unstressed protein. However, differences were rather small and within the standard deviation. In summary, no clear differences could be observed between the expression levels of CD 80, 83, 86 and HLA-DR among the differently stressed samples or prior to and after filtration.

6.3.2.2 Analysis of cytokines

A reduced panel of cytokines relevant for inflammatory (TNF- α , IFN- γ , IL-6) or anti-inflammatory (IL-6, IL-10) immune answers was investigated to assess a potential activation of dendritic cells upon stimulation with the stressed antibody samples. The results of cytokine analysis of cell culture supernatants for two donors are displayed in Figure 6-27 - Figure 6-30. LPS was used as a positive control and triggered the secretion of TNF- α , IL-6 and IL-10, but it could not trigger the secretion of IFN- γ . Overall, no significant changes in the secretion of any of the investigated cytokines could be observed between the negative controls and the stressed antibody samples prior to or after filtration. However, some samples indicated a positive effect of filtration: According to the results of donor 2, the concentration of IFN- γ and TNF- α was slightly lower for light stressed Bevacizumab after filtration compared to the non-filtered sample. However, it should be noted, that the concentration of the

cytokines for the light stressed samples prior to filtration was on the same level as the negative controls. Therefore, it is difficult to evaluate the effect of in-line filtration.

A



B

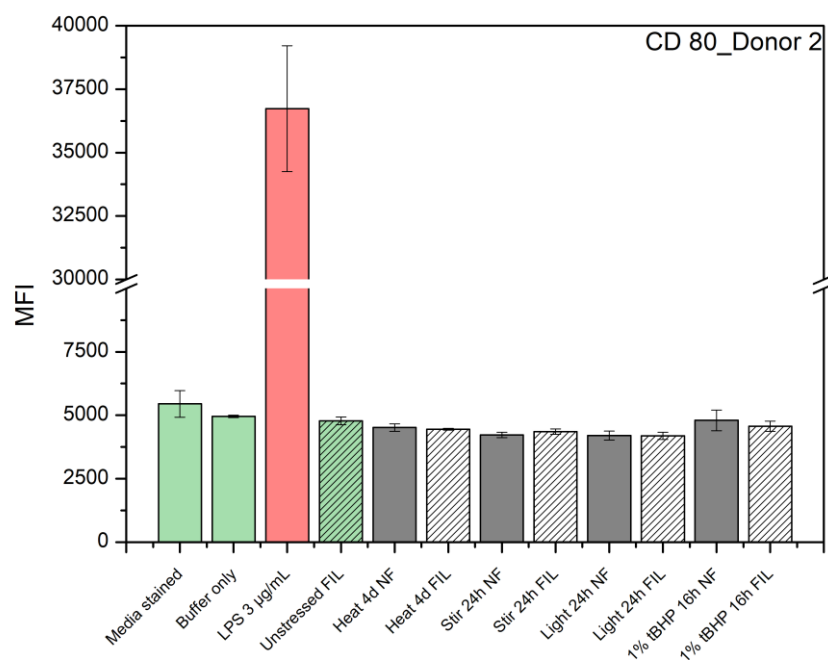
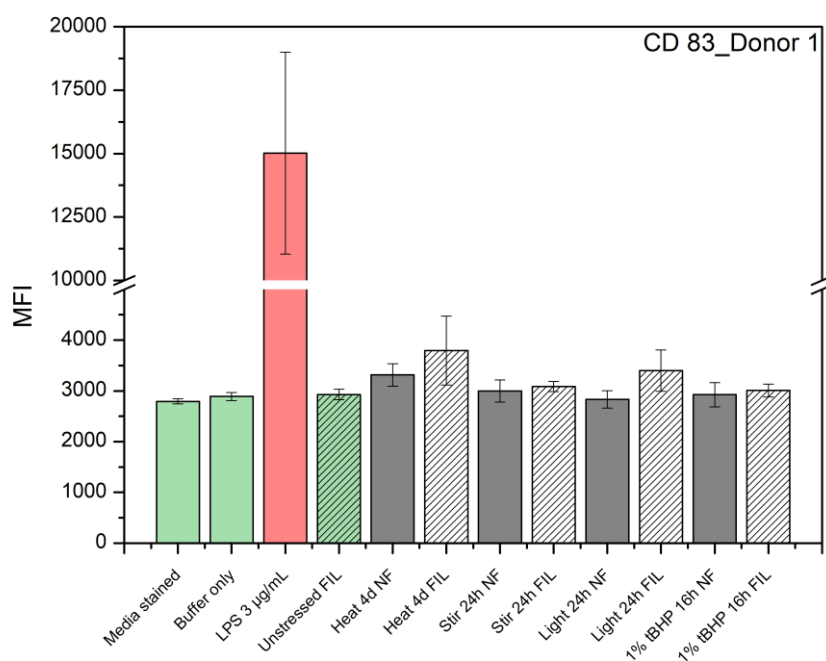


Figure 6-23: Expression of CD 80 on dendritic cells of donor 1 (A) and donor 2 (B). Dendritic cells were incubated with unstressed Bevacizumab and Bevacizumab after heat, stir, light stress and incubation with tBHP. The green bars display negative controls (media only, buffer only and unstressed Bevacizumab), the red bars represent the positive control (LPS). MFI = Mean Fluorescence Intensity. Non-filtered (NF) are marked by the grey bars, filtered (FIL) samples are marked by the striped pattern.

A



B

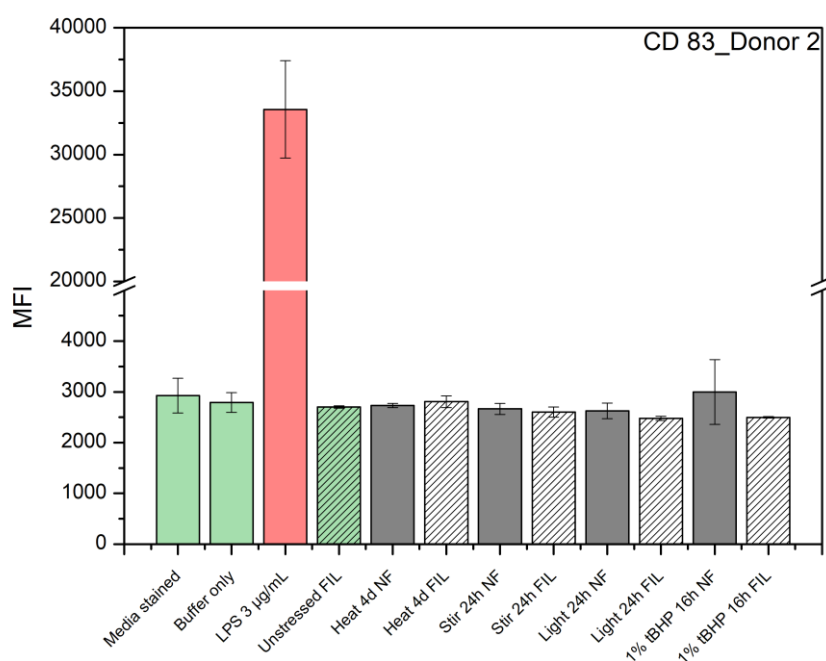


Figure 6-24: Expression of CD 83 on dendritic cells of donor 1 (A) and donor 2 (B). Dendritic cells were incubated with unstressed Bevacizumab and Bevacizumab after heat, stir, light stress and incubation with tBHP. The green bars display negative controls (media only, buffer only and unstressed Bevacizumab), the red bars represent the positive control (LPS). MFI = Mean Fluorescence Intensity. Non-filtered (NF) are marked by the grey bars, filtered (FIL) samples are marked by the striped pattern.

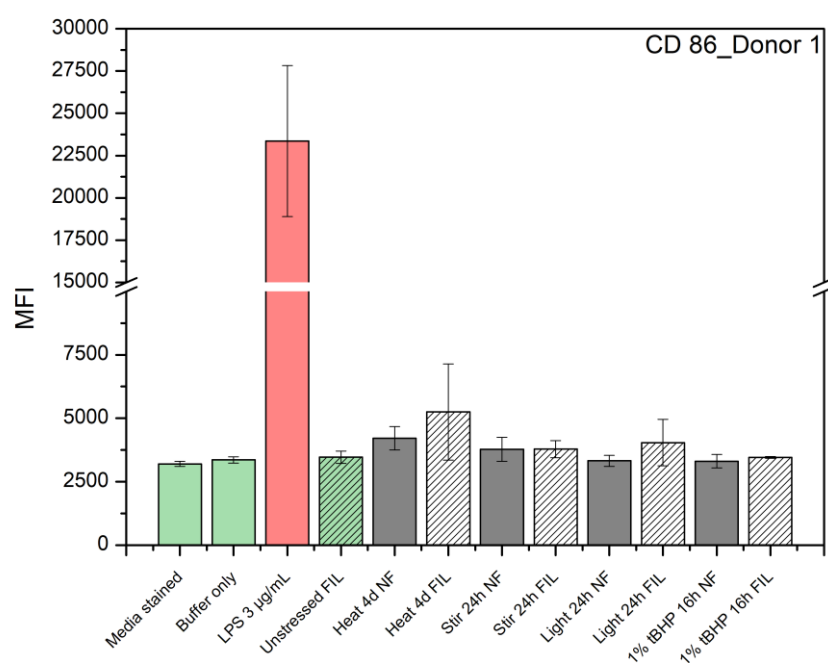
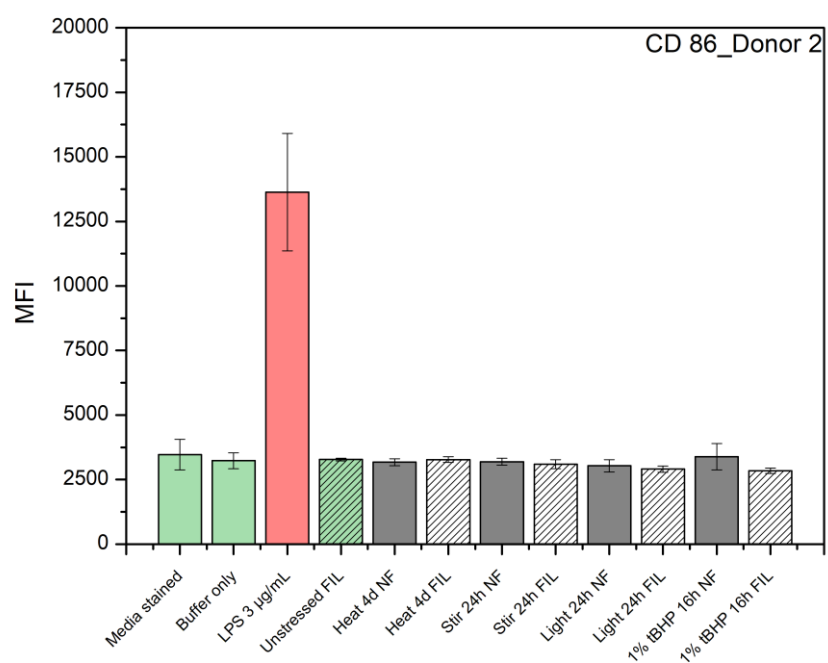
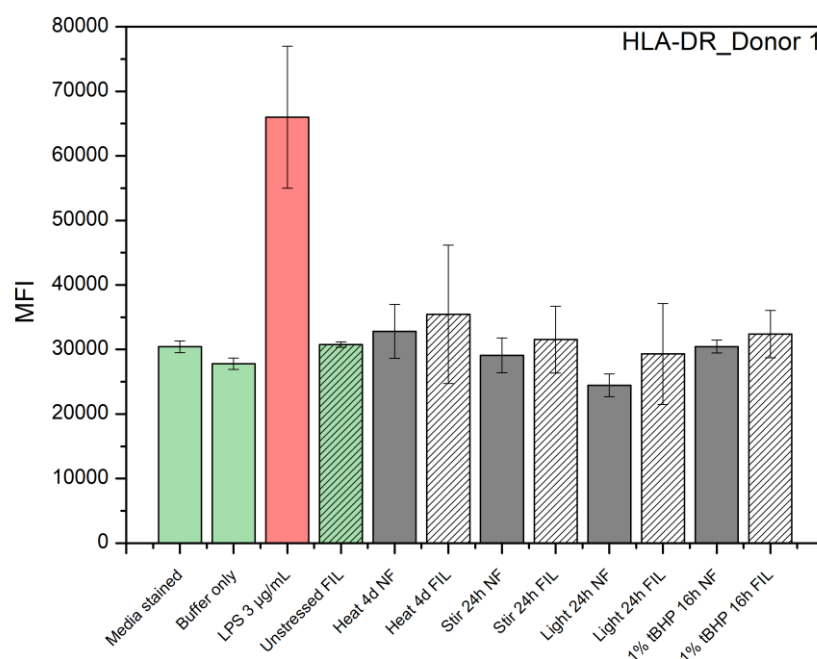
A**B**

Figure 6-25: Expression of CD 86 on dendritic cells of donor 1 (A) and donor 2 (B). Dendritic cells were incubated with unstressed Bevacizumab and Bevacizumab after heat, stir, light stress and incubation with tBHP. The green bars display negative controls (media only, buffer only and unstressed Bevacizumab), the red bars represent the positive control (LPS). MFI = Mean Fluorescence Intensity. Non-filtered (NF) are marked by the grey bars, filtered (FIL) samples are marked by the striped pattern.

A



B

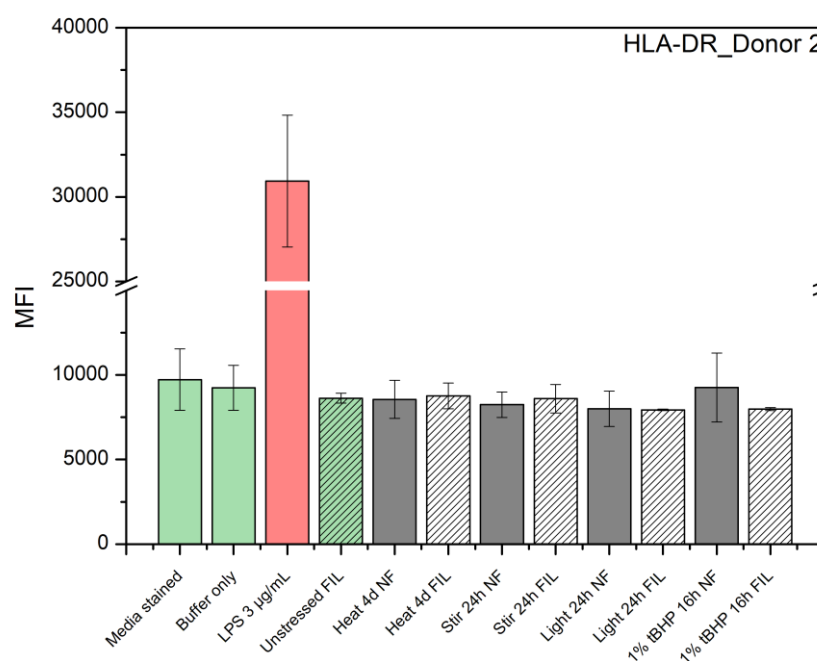


Figure 6-26: Expression of HLA-DR on dendritic cells of donor 1 (A) and donor 2 (B). Dendritic cells were incubated with unstressed Bevacizumab and Bevacizumab after heat, stir, light stress and incubation with tBHP. The green bars display negative controls (media only, buffer only and unstressed Bevacizumab), the red bars represent the positive control (LPS). MFI = Mean Fluorescence Intensity. Non-filtered (NF) are marked by the grey bars, filtered (FIL) samples are marked by the striped pattern.

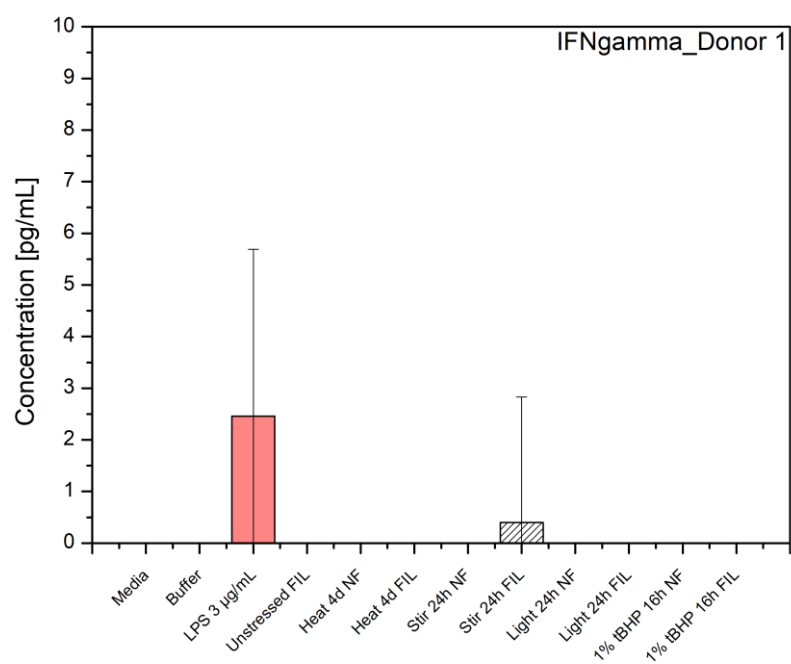
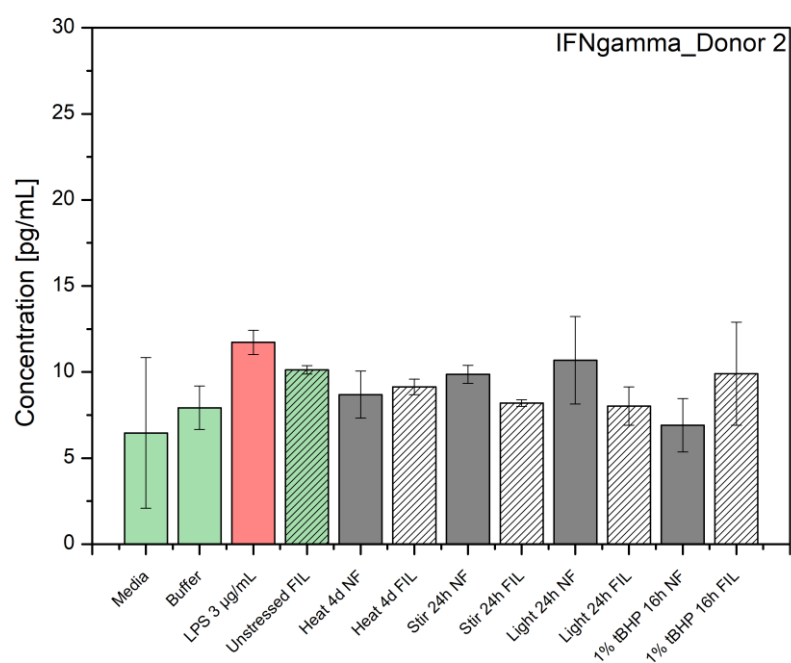
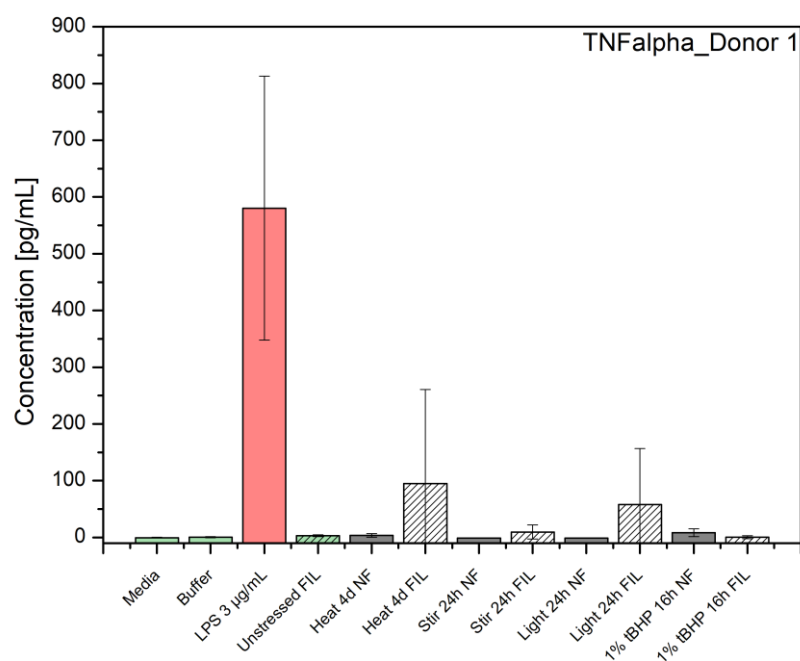
A**B**

Figure 6-27: Concentration of IFN- γ in the supernatant of a culture of dendritic cells of donor 1 (A) and donor 2 (B). Dendritic cells were incubated with unstressed Bevacizumab and Bevacizumab after heat, stir, light stress and incubation with tBHP for 22 hours. The green bars display negative controls (media only, buffer only and unstressed Bevacizumab), the red bars represent the positive control (LPS). Non-filtered (NF) are marked by the grey bars, filtered (FIL) samples are marked by the striped pattern.

A



B

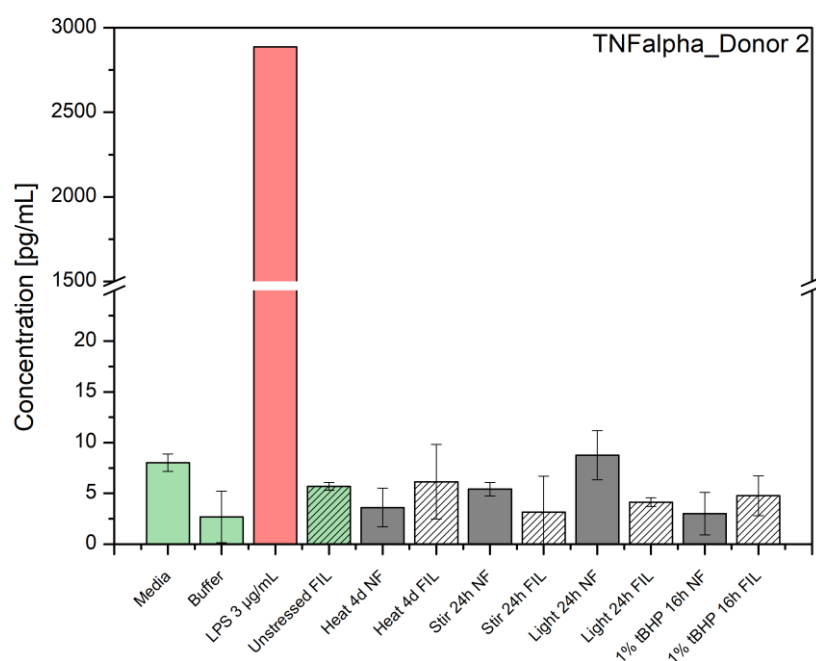


Figure 6-28: Concentration of TNF- α in the supernatant of a culture of dendritic cells of donor 1 (A) and donor 2 (B). Dendritic cells were incubated with unstressed Bevacizumab and Bevacizumab after heat, stir, light stress and incubation with tBHP for 22 hours. The green bars display negative controls (media only, buffer only and unstressed Bevacizumab), the red bars represent the positive control (LPS). Non-filtered (NF) are marked by the grey bars, filtered (FIL) samples are marked by the striped pattern.

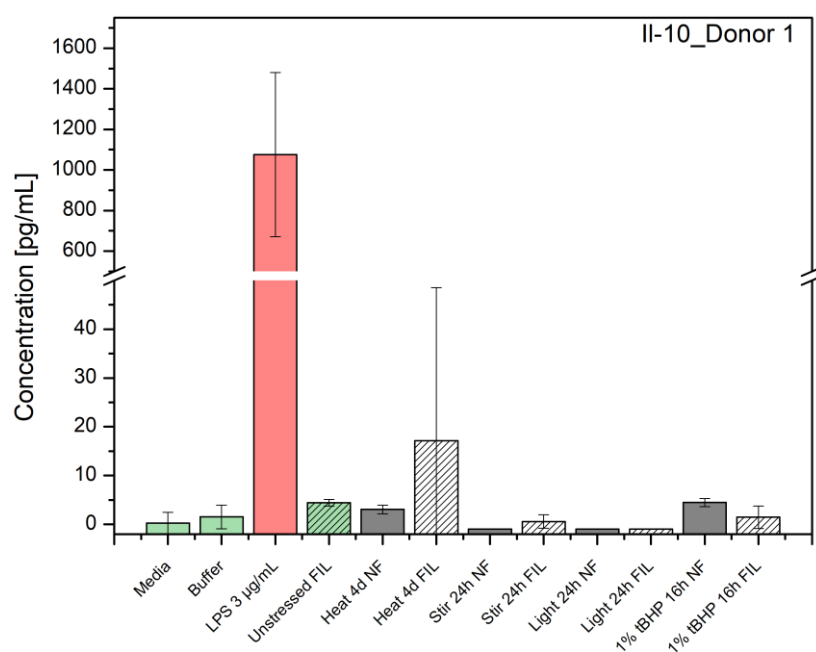
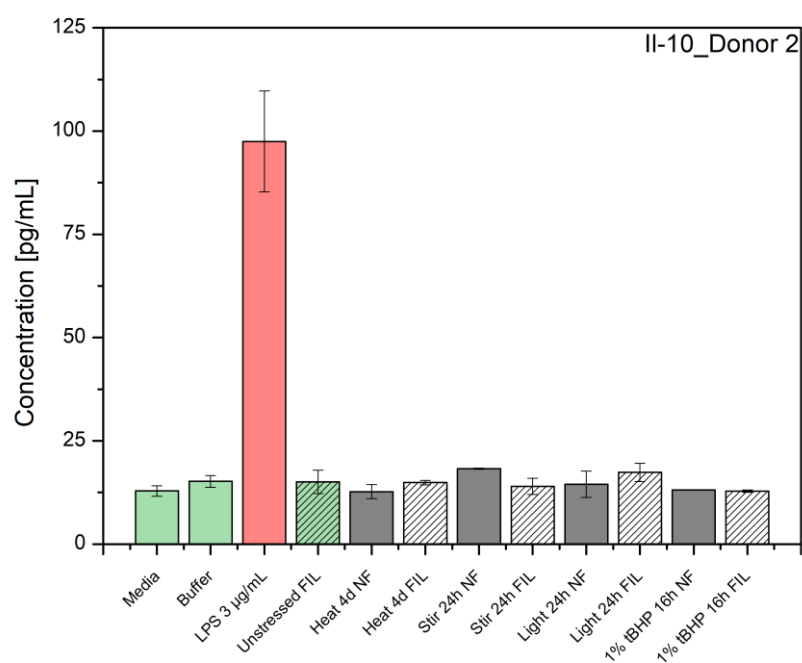
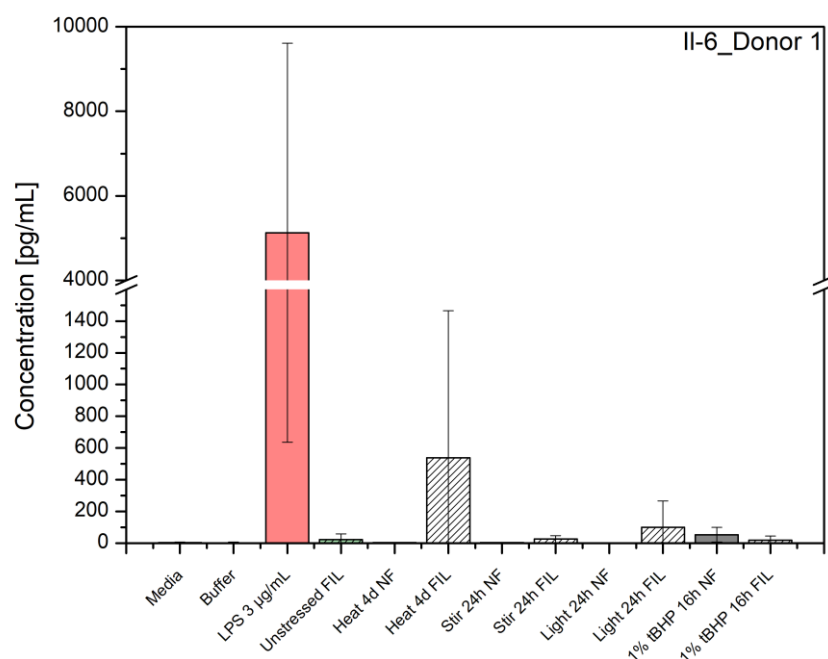
A**B**

Figure 6-29: Concentration of IL-10 in the supernatant of a culture of dendritic cells of donor 1 (A) and donor 2 (B). Dendritic cells were incubated with unstressed Bevacizumab and Bevacizumab after heat, stir, light stress and incubation with tBHP for 22 hours. The green bars display negative controls (media only, buffer only and unstressed Bevacizumab), the red bars represent the positive control (LPS). Non-filtered (NF) are marked by the grey bars, filtered (FIL) samples are marked by the striped pattern.

A



B

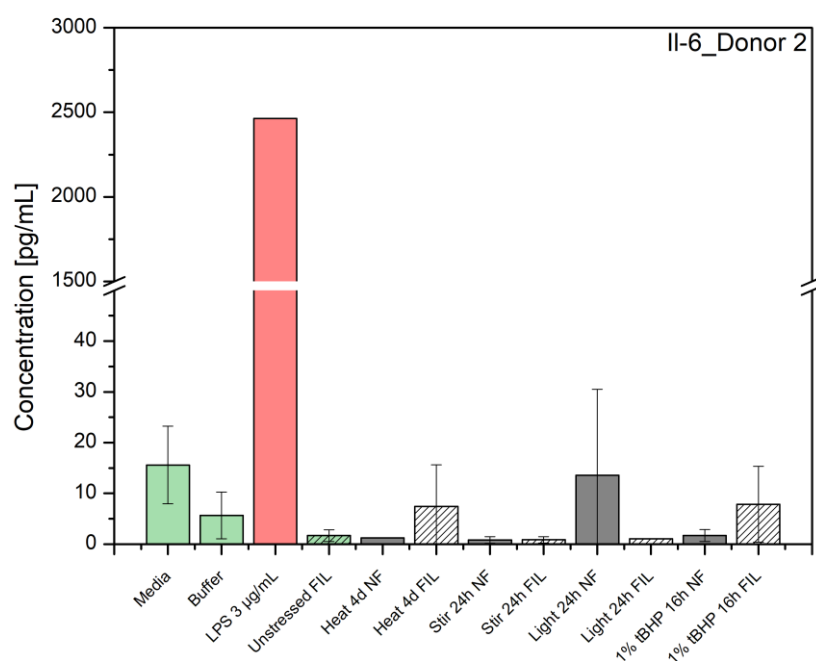


Figure 6-30: Concentration of IL-6 in the supernatant of a culture of dendritic cells of donor 1 (A) and donor 2 (B). Dendritic cells were incubated with unstressed Bevacizumab and Bevacizumab after heat, stir, light stress and incubation with tBHP for 22 hours. The green bars display negative controls (media only, buffer only and unstressed Bevacizumab), the red bars represent the positive control (LPS). Non-filtered (NF) are marked by the grey bars, filtered (FIL) samples are marked by the striped pattern.

6.4 Discussion

The aim of this study was to investigate the effect of in-line filtration on the immunogenicity of stressed samples of Bevacizumab. Besides a 3D human artificial lymph node model, a 2D *in vitro* dendritic cell assay was used to test the immunogenicity of stressed Bevacizumab samples prior to and after filtration. For testing the effect of in-line filtration on immunogenicity in a human artificial lymph node model, protein aggregates were generated by exposing the monoclonal antibody to elevated temperature and mechanical stress. Regarding filtration, the analysis of insoluble aggregates, thus particles, was of interest. Particle numbers in the stressed antibody samples were determined by light obscuration and flow imaging microscopy. The analysis of the stressed antibody samples revealed a strong increase in particle numbers upon heat and stir stress. It was noticeable, that the total particle count of heat stressed Bevacizumab was much higher when determined by flow imaging microscopy than by light obscuration. It is known from literature that particle numbers determined by flow imaging microscopy are higher than determined by light obscuration. Especially small, transparent particles cannot be detected easily by light obscuration^{28,29}. Thus, light obscuration might underestimate the number of subvisible particles present in a protein formulation²⁹. This could also be the reason for the higher particle count detected by flow imaging microscopy in heat stressed Bevacizumab samples. The section of pictures of some particles present in the sample show rather translucent, non-spherical particles which might not have been detected by light obscuration. However, the data confirm the general recommendation to use orthogonal methods to analyze and quantitate subvisible particles in protein formulations. After filtration of the stressed Bevacizumab samples, particle numbers decreased strongly and, according to the results of flow imaging microscopy, resulted in a particle burden comparable to the unstressed protein. This was expected, since it has already been shown that in-line filtration is a powerful tool to reduce particle numbers in biologics¹². Besides analyzing subvisible particles, the samples were also analyzed for the presence of soluble aggregates, chemical modifications or conformational changes. It could be shown that the filtration process itself did not have an influence on the level of soluble aggregates and the extent of chemical modifications. Slight differences between the filtered and non-filtered samples were observed in the tertiary structure of the protein. However, the slight changes in intrinsic and extrinsic fluorescence intensity for stir and heat stressed Bevacizumab samples prior to filtration might be due to the presence of particles in the sample. After filtration, fluorescence intensity was almost on the level of unstressed Bevacizumab again, indicating no dramatic changes in conformation by the filtration process. The same was true for the secondary structure which was analyzed by FT-IR spectroscopy. A critical issue, regarding protein loss, is the hold-up volume of filters which can vary among different filter products and is dependent of the filter diameter. For the PharmAssure® filter with a diameter of 25 mm used in this study, the

hold-up volume was very high with almost 700 µl. When using the Acrodisc® filter which holds a diameter of 13 mm, the hold-up volume was approximately 130 µl. In both cases, the hold-up volume could be minimized by an air purge. However, when only small amounts of protein solution are available, the hold-up volume is often too high and a critical point that should be addressed by manufacturers. This was also shown in Benjamin Werner's study¹². To exclude random filter defects, the quality of the PharmAssure® filter was assessed by filtering a solution of a model monoclonal antibody at a similar concentration as in the Bevacizumab samples. Among ten different filter of the same kind, no outlier could be detected. Therefore, it can be assumed that the filter quality of the used PharmAssure® filter was adequate for the HuALN study.

The effect of in-line filtration was also tested in a 2D *in vitro* dendritic cell assay. One advantage of 2D *in vitro* assays is the possibility to test many samples at the same time, since the assays are usually performed in a well-plate format. In addition to the exposure to heat and stir stress, Bevacizumab was also exposed to light and treated with 1% tert-butyl hydroperoxide (tBHP), for this study. Finally, the immunogenicity of all stressed samples prior to and after filtration was tested in the 2D dendritic cell assay. In contrast to Bevacizumab after stir and heat stress, whereby no or moderate chemical modifications could be observed by Protein A and ion exchange chromatography, exposure to light and incubation with 1% tBHP of Bevacizumab resulted in extensive chemical modifications. Light exposure as well as incubating the protein sample with tBHP are known methods to trigger oxidative reactions^{5,19,30,31}. Due to a reduced binding affinity of Bevacizumab after light stress and incubation with tBHP to Protein A, it can be assumed that methionine residues in the Fc part of the antibody were oxidized by exposure to light and tBHP. Additionally, the samples were also investigated using ion exchange (IEX) chromatography to detect further chemical modifications. IEX chromatography is based on the interaction of charge variants of the protein with the column material and often used to detect chemical changes of proteins such as C-terminal processing of lysin residues, deamidation, glycation or amino acid sequence variations^{32,33}. IEX chromatography of Bevacizumab after 24h light stress and incubation with 1% tBHP for 16h resulted in strong modifications of the charge variants of the monoclonal antibody, since the chromatogram clearly changed compared to unstressed Bevacizumab. In the case of Bevacizumab exposed to tBHP, protein still bound to the column, but no accurate peak separation could be achieved. For the light stressed samples, no peak was detectable anymore. To confirm that the correct method was used we analyzed Bevacizumab that was exposed to light for different time points and found that binding and separation affinity decreased with longer exposure times to light. This was already true for 2h light stress indicating that light had a significant influence on the charge level of Bevacizumab. Analysis of the samples by size exclusion chromatography revealed that light stress triggered the formation of soluble aggregates and fragments (as described in Chapter

4) whereas the level of soluble aggregates was only slightly elevated after incubation of Bevacizumab with 1% tBHP. As described for heat and stir stressed Bevacizumab, the filtration process did not have any influence on the level of soluble aggregates. Besides soluble aggregates and chemical alterations, light stress and tBHP also triggered the formation of particles. Particle numbers were decreased by the filtration process, even though the total particle count after filtration of the light stressed samples was only reduced by factor 3, approximately. However, particles larger 10 and 25 µm were removed efficiently by filtering the sample.

Summarizing the analysis of the unstressed and stressed Bevacizumab samples, it can be stated, that filtration of the samples primarily led to a decrease in particle numbers, as expected. Heat stressed Bevacizumab contained soluble aggregates and chemical modifications were detected. However, filtration did not influence the level of soluble aggregates or chemical modifications. This was also true for the light stressed Bevacizumab and Bevacizumab after incubation with tBHP. These samples were significantly altered by exposure to light and tBHP. It was true for all stressed samples that aggregate levels did not represent aggregate levels of marketed products. However, it has been shown recently that only particles with extensive chemical modifications triggered immunogenicity⁵.

The immunogenicity of Bevacizumab after heat and stir stress prior to and after filtration was tested in a 3D human artificial lymph node model. High donor to donor variability, a high response of donor 2 to the formulation buffer and problems with the cell culture medium during the bioreactor run with donor 1 made it difficult to interpret the data of the 3D HuALN study. Cytokine analysis of cultures of donor 1 and 2 revealed slight tendencies towards a TH1 and pro-inflammatory answer for the heat stressed sample, but normalized values were not much higher than 1 and therefore, it cannot be spoken of a significant upregulation. Moreover, due to supply difficulties, a different cell culture medium had to be used for bioreactor runs with donor 1. This might have changed the DC marker expression pattern and negatively influenced the ability of dendritic cells to be activated. Cytokine analysis of culture supernatants of the bioreactor run with donor 2 resulted in a strong TH1 and proinflammatory immune response for formulation buffer which served as negative control or “placebo”. High immune response to formulation buffer has also been observed in literature³⁴. The formulation buffer has been tested for the presence of endotoxins and the analysis revealed an endotoxin level of < 0.25 EU/mL fulfilling the limits of the European Pharmacopoeia for water for injection³⁵. Thus, there is no plausible explanation for the immune response to formulation buffer. Besides cytokine analysis, the cell culture supernatants were screened for the presence of IgM antibodies. All three donors showed an unspecific IgM profile, independent of the applied stress conditions or prior to or after filtration. The plateau in the IgM profile of donor 3 between day two and five is due to a pump failure of the automated sampling system during a weekend. Therefore, the

sample on day 5 represents a pool out of the samples of day two to five and the mean is displayed for all days. However, no differences between the stressed antibody samples could be observed. Based on this data and the results of the first HuALN experiment (Chapter 5), it becomes obvious, that the number of donors plays a significant role. Using three donors for one experiment is not sufficient, especially when there is one outlier as it was the case for this study (donor 2). Increasing the number of donors implies a higher number of bioreactors which comes along with longer run times, costs and space issues. Therefore, it must be evaluated carefully if the HIRIS III model is the right model to test the immunogenicity of protein aggregates or if a miniature HuALN, which is currently under development³⁶, is more appropriate for this purpose.

In the 2D DC assay, the immunogenicity of Bevacizumab after heat, stir, light and chemical oxidation stress using tBHP was tested prior to and after filtration. Analysis of several DC marker and cytokines revealed no significant difference between filtered and non-filtered samples. The basic issue was that levels of the different DC marker or cytokines after stimulation with any of the stressed samples were barely increased compared to the negative controls including, media and buffer only and the unstressed protein solution. Therefore, it is also difficult to make a statement about the effect of in-line filtration. The reason for the low responses might be a short incubation time of 22 hours of the stressed samples with dendritic cells. It is common for 2D assays to keep incubation times rather short with the aim to observe early events of an immune response^{7,37–39}. Few studies prolonged incubation times to 72 hours⁴⁰ or added a time point after 7 days^{7,39}. However, compared to a run time of up to four weeks for the HuALN model, incubation times for 2D *in vitro* assays are short and the focus is on early immune responses. As for the experiments using the HuALN model, high donor to donor variability was observed. The levels regarding the cytokine concentrations differed substantially. This is a known problem and often faced in studies using *in vitro* assays with cells from human donors. Joubert *et al.* used PBMCs from 50 donors to include a high number and frequency of HLA-types³⁹. Due to difficulties with the supply of blood samples, only two donors could be included in the 2D *in vitro* assay in this study. The possibility to include several donors in a 2D DC assay represents an advantage of the 2D assay, since it is easier to include more donors in a well plate format than to run several bioreactors at the same time.

6.5 Conclusion

In this study, the effect of in-line filtration on the immunogenicity of protein aggregates of Bevacizumab was investigated using a 3D human artificial lymph node model and a 2D dendritic cell assay. Whereas small trends towards a TH1 and pro-inflammatory immune answer could be observed in the HuALN model, only negligible differences in the cytokine secretion profile or the activation of

DC marker could be detected in the 2D dendritic cell assay. Thus, no remarkable differences in the immune responses of the formulation buffer, unstressed and stressed Bevacizumab samples could be detected. Besides, the study underlines the issue of donor to donor variability indicating that more than two to six donors are needed for *in vitro* assays to draw reasonable assumptions. Unfortunately, the effect of in-line filtration could not be evaluated. The results of this study lead to the assumption that stressed Bevacizumab samples either lead to no or only low immunogenicity or that the HuALN model in its current edition (HIRIS III) is not able to evaluate the effect of in-line filtration. However, further investigations are necessary to show a positive effect of in-line filtration on the immunogenicity of biologics.

6.6 References

1. 2.9.20 Partikelkontamination – Sichtbare Partikeln. *European Pharmacopoeia* **9.0**, 458 (2017).
2. 9.0/0520 Parenteralia. *European Pharmacopoeia* 1323–1327 (2017).
3. 2.9.19 Partikelkontamination- Nicht sichtbare Partikeln. *European Pharmacopoeia* 438–441 (2014).
4. United States Pharmacopeia. <788> Particulate Matter in Injections. *USP* **34**, 326–328 (2011).
5. Boll, B. *et al.* Extensive chemical modifications in the primary protein structure of IgG1 subvisible particles are necessary for breaking immune tolerance. *Mol. Pharm.* **14**, 1292–1299 (2017).
6. Kijanka, G. *et al.* Submicron Size Particles of a Murine Monoclonal Antibody Are More Immunogenic Than Soluble Oligomers or Micron Size Particles Upon Subcutaneous Administration in Mice. *J. Pharm. Sci.* **107**, 2847–2859 (2018).
7. Telikepalli, S. *et al.* Physical characterization and in vitro biological impact of highly aggregated antibodies separated into size-enriched populations by fluorescence-activated cell sorting. *J. Pharm. Sci.* **104**, 1575–1591 (2015).
8. Ratanji, K. D. *et al.* Subvisible aggregates of immunogenic proteins promote a Th1-type response. *Toxicol. Sci.* **153**, 258–270 (2016).
9. Chisholm, C. F. *et al.* Silicone Oil Microdroplets Can Induce Antibody Responses Against Recombinant Murine Growth Hormone in Mice. *J. Pharm. Sci.* **105**, 1623–1632 (2016).
10. Joubert, M. K. *et al.* Highly aggregated antibody therapeutics can enhance the in vitro innate and late-stage T-cell immune responses. *J. Biol. Chem.* **287**, 25266–25279 (2012).
11. Carpenter, J. F. *et al.* Overlooking Subvisible Particles in Therapeutic Protein Products: Gaps That May Compromise Product Quality. *J. Pharm. Sci.* **98**, 1201–1205 (2009).
12. Werner, B. P. & Winter, G. Expanding bedside filtration – a powerful tool to protect patients from protein aggregates. *J. Pharm. Sci.* **107**, 2775–2788 (2018).
13. Werner, B. P. & Winter, G. Particle contamination of parenteralia and in-line filtration of proteinaceous drugs. *Int. J. Pharm.* **496**, 250–267 (2015).
14. Villa, G. *et al.* In-Line Filtration Reduces Postoperative Venous Peripheral Phlebitis Associated

- With Cannulation: A Randomized Clinical Trial. *Anesth. Analg.* **127**, 1367–1374 (2018).
15. Perez, M. *et al.* Dynamic Image Analysis to Evaluate Subvisible Particles during Continuous Drug Infusion in a Neonatal Intensive Care Unit. *Sci. Rep.* **7**, 1–8 (2017).
 16. Perez, M. *et al.* Effectiveness of in-Line Filters to Completely Remove Particulate Contamination during a Pediatric Multidrug Infusion Protocol. *Sci. Rep.* **8**, 4–11 (2018).
 17. Perez, M., Maiguy-Foinard, A., Barthélémy, C., Décaudin, B. & Odou, P. Particulate Matter in Injectable Drugs: Evaluation of Risks to Patients. *Pharm. Technol. Hosp. Pharm.* **1**, 91–103 (2016).
 18. Pan, H. *et al.* Methionine oxidation in human IgG2 Fc decreases binding affinities to protein A and FcRn. *Protein Sci.* **18**, 424–433 (2009).
 19. Loew, C. *et al.* Analytical protein a chromatography as a quantitative tool for the screening of methionine oxidation in monoclonal antibodies. *J. Pharm. Sci.* **101**, 4248–4257 (2012).
 20. Khawli, L. A. *et al.* Charge variants in IgG1: Isolation, characterization, in vitro binding properties and pharmacokinetics in rats. *MAbs* **2**, 613–624 (2010).
 21. Poole, R. A., Hawe, A. & Jiskoot, W. in *Analysis of Aggregates and Particles* (eds. Mahler, H.-C. & Jiskoot, W.) 201–226 (2012).
 22. Ladokhin, A. S. in *Encyclopedia of Analytical Chemistry* (ed. Meyers, R. A.) 5762–5779 (John Wiley&Sons Ltd, 2000).
 23. Hawe, A., Sutter, M. & Jiskoot, W. Extrinsic fluorescent dyes as tools for protein characterization. *Pharm. Res.* **25**, 1487–1499 (2008).
 24. Kong, J. & Yu, S. Fourier transform infrared spectroscopic analysis of protein secondary structures. *Acta Biochim. Biophys. Sin. (Shanghai)*. **39**, 549–559 (2007).
 25. Loew, C. *et al.* Analytical protein a chromatography as a quantitative tool for the screening of methionine oxidation in monoclonal antibodies. *J. Pharm. Sci.* **101**, 4248–4257 (2012).
 26. Banchereau, J. & Steinmann, R. M. Dendritic cells and the control of immunity. *Nature* **392**, 245–252 (1998).
 27. Nascimento, C. R. *et al.* The influence of Ouabain on human dendritic cells maturation. *Mediators Inflamm.* **2014**, 1–15 (2014).

28. Zöls, S. *et al.* Flow Imaging Microscopy for Protein Particle Analysis-A Comparative Evaluation of Four Different Analytical Instruments. *AAPS J.* **15**, 1200–1211 (2013).
29. Huang, C. T., Sharma, D., Oma, P. & Krishnamurthy, R. Quantitation of protein particles in parenteral solutions using micro-flow imaging. *J. Pharm. Sci.* **98**, 3058–3071 (2009).
30. Li, S., Schöneich, C. & Borchardt, R. T. Chemical Instability of Protein Pharmaceuticals : Mechanisms of Oxidation and Strategies for Stabilization. *Biotechnol. Bioeng.* **48**, 490–500 (1995).
31. Gaza-Bulseco, G., Faldu, S., Hurkmans, K., Chumsae, C. & Liu, H. Effect of methionine oxidation of a recombinant monoclonal antibody on the binding affinity to protein A and protein G. *J. Chromatogr. B Anal. Technol. Biomed. Life Sci.* **870**, 55–62 (2008).
32. Farnan, D. & Moreno, G. T. Multiproduct high-resolution monoclonal antibody charge variant separations by pH gradient ion-exchange chromatography. *Anal. Chem.* **81**, 8846–8857 (2009).
33. Williams, A. & Frasca, V. Ion-Exchange Chromatography. *Curr. Protoc. Protein Sci.* **15**, 8.2.1.-8.2.30 (1999).
34. Freitag, A. J. *et al.* Investigation of the immunogenicity of different types of aggregates of a murine monoclonal antibody in mice. *Pharm. Res.* **32**, 430–444 (2015).
35. 9.1/0169 Wasser für Injektionszwecke. *European Pharmacopoeia* 6111–6115
36. Giese, C. *et al.* Immunological substance testing on human lymphatic micro-organoids in vitro. *J. Biotechnol.* **148**, 38–45 (2010).
37. Moussa, E. M., Kotarek, J., Blum, J. S., Marszal, E. & Topp, E. M. Physical Characterization and Innate Immunogenicity of Aggregated Intravenous Immunoglobulin (IGIV) in an In Vitro Cell-Based Model. *Pharm. Res.* **33**, 1736–1751 (2016).
38. Ahmadi, M. *et al.* Small amounts of sub-visible aggregates enhance the immunogenic potential of monoclonal antibody therapeutics. *Pharm. Res.* **32**, 1383–1394 (2015).
39. Joubert, M. K. *et al.* Use of in vitro assays to assess immunogenicity risk of antibody-based biotherapeutics. *PLoS One* **11**, 1–22 (2016).
40. Rombach-Riegraf, V. *et al.* Aggregation of human recombinant monoclonal antibodies influences the capacity of dendritic cells to stimulate adaptive T-cell responses in vitro. *PLoS One* **9**, e86322 (2014).

Chapter 7

Particle numbers in biologics: Can in-line filtration reduce the particle burden?

7.1 Introduction

Particulate matter in biopharmaceutical products has always been a challenge for pharmaceutical manufacturers and poses risks to patients¹⁻⁴. Even though pharmaceutical manufacturers strive to develop and produce high quality products meeting the specifications of the Pharmacopoeias regarding particle numbers⁵, complications in clinical routine such as infusion or injection of particulate matter still occur⁶. A critical parameter is post-production handling of biopharmaceutical products by end-users such as nurses, doctors or patients.^{7,8} Transportation or incorrect handling of the product by clinic staff such as exposure to mechanical stresses, contact with interfaces, temperature fluctuations, freeze-thaw cycles, or exposure to light might trigger protein aggregation and particle formation^{7,8}. Jiskoot *et al.* recently described post-production handling as “a weak link” in the supply chain of biological products⁸. In this study, the authors surveyed procedures in a hospital and observed several incidents such as agitation of a vial filled with a biological, turbid protein solutions or careless handling of infusion bags with protein pharmaceuticals⁸. The infusion or injection of particulate matter to patients might trigger complications and side reactions such as phlebitis⁹. Therefore, it is recommended to remove any particulate material prior to infusion or injection to the patient. A very effective tool to reduce the particle burden in biologics is in-line filtration. Werner *et al.* analyzed particle counts of liquid protein products prior to and after in-line filtration and showed that in-line filtration is a powerful tool to reduce particle numbers above 0.2 μm ^{10,11}. Besides the effect of in-line filtration, also critical parameters such as particle shedding, protein adsorption, protein denaturation or the hold-up volume of filters were assessed. The focus in the current study was especially on lyophilized biologics. Particle numbers after reconstitution might be elevated due to incorrect reconstitution procedures of the product. Telikepalli *et al.* investigated a lyophilized monoclonal antibody IgG₁ after performing a shaking stress study and found that the number of subvisible particles and the turbidity were increased after reconstitution¹². Usually, biologics are lyophilized to increase stability and shelf life time of a liquid protein formulation¹³. However, with regards to particle formation and mistreatment of biologics, lyophilized products are critical products since a reconstitution step is necessary before use.

The aim of this study was to analyze the particle burden in marketed products and to evaluate if in-line filtration is a possibility to reduce the particle burden. The focus hereby was on lyophilized products. Three biologics varying in molecular size, indication and protein concentration were included in this study. While Gammagard® had a protein concentration of 50 mg/mL after reconstitution, Actilyse® had a concentration of 1 mg/mL after reconstitution. Flixabi® was at a moderate protein concentration of 10 mg/mL after reconstitution. Liquid products were also investigated to compare the particle burden between liquid and lyophilized products. A lyophilized model monoclonal antibody

IgG₁, three lyophilized and three liquid marketed protein drugs were selected and purchased. The turbidity was measured and the number of subvisible and submicron particles was determined by light obscuration, flow imaging and tunable resistive pulse sensing (TRPS) prior to and after in-line filtration. This study was carried out in collaboration with Andreas Stelzl who performed all TRPS measurements.

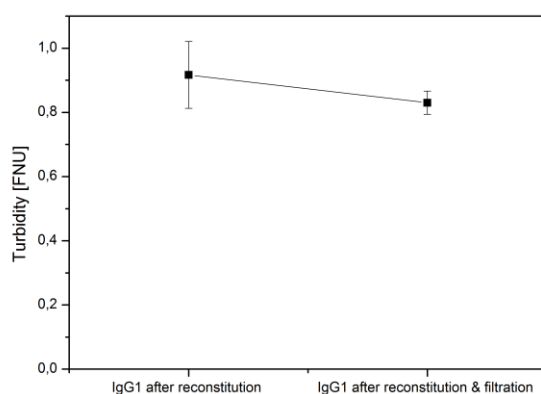
7.2 Results

7.2.1 Turbidity

7.2.1.1 Monoclonal antibody IgG₁

After lyophilization of the monoclonal antibody IgG₁ and subsequent reconstitution, the turbidity of the protein solution was analyzed prior to and after applying an in-line filtration step using an Acrodisc® syringe filter with a pore size of 0.2 µm. The results are displayed in Figure 7-1A. The turbidity of the reconstituted protein solution was at 0.92 FNU and could be decreased to 0.83 FNU after filtration. The lyophilized product was stored for six months at 2-8°C, reconstituted, and analyzed again. Results (Figure 7-1B) showed that the turbidity of the reconstituted protein solution was at 0.82 FNU prior to and at 0.86 FNU after filtration. Thus, a storage period over six months did not influence the turbidity of the reconstituted monoclonal antibody substantially.

A



B

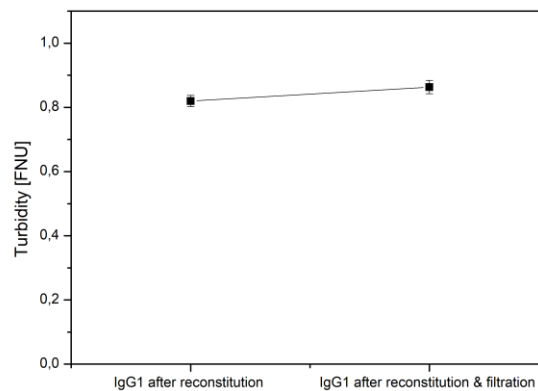


Figure 7-1: Turbidity measurements of IgG₁ directly after lyophilization and reconstitution (A) and after storage of the lyophilized protein for six months at 2-8°C and reconstitution (B). Turbidity was measured prior to and after in-line filtration using an Acrodisc® filter with a pore size of 0.2 µm.

7.2.1.2 Marketed lyophilized products

The lyophilized products Actilyse® (Alteplase), Gammagard® (human immune globulin) and Flixabi® (Infliximab) were reconstituted according to the technical information (see also Chapter 3), and the turbidity of the reconstituted protein solutions was measured prior to and after filtration using an Acrodisc® syringe filter with a pore size of 0.2 µm. The results are displayed in Figure 7-2A-C. It was true for all products that filtration led to a decrease in turbidity. However, turbidity values prior to filtration differed. The turbidity of Actilyse® after reconstitution was at 0.81 FNU and could be decreased to 0.58 FNU after filtration (Figure 7-2A). In contrast, Gammagard® showed a relatively high turbidity of 9.02 FNU prior to filtration which could be reduced to 7.70 FNU by filtration of the reconstituted protein solution (Figure 7-2B). The turbidity of reconstituted Flixabi® prior to filtration was at 2.94 FNU and could slightly be reduced by filtration to a value of 2.73 FNU (Figure 7-2C). Even though the levels of turbidity prior to filtration were different for each of the products, a decrease in turbidity after filtration was achieved for all products.

7.2.1.3 Marketed liquid products

Besides lyophilized products, the turbidity of liquid biological products was analyzed. Three products were chosen: Pulmozyme® (Dornase alfa) at a concentration of 1 mg/mL, Beriglobin® (human immune globulin) at a concentration of 160 mg/mL and Truxima® (Rituximab) at a concentration of 10 mg/mL. The results of turbidity measurements prior to and after filtration are displayed in Figure 7-3A-C. The turbidity of Pulmozyme® was at 0.49 FNU prior to filtration and did not change upon filtration (Figure 7-3A). Turbidity measurements of Truxima® (Figure 7-3B) revealed similar results: Turbidity was at 2.67 FNU prior to filtration and could only be reduced by only 0.06 FNU to 2.61 FNU after filtration. In contrast, the turbidity of Beriglobin® (Figure 7-3C), containing human immune globulin, was at 24.3 FNU prior to filtration. After filtration, turbidity of Beriglobin® was at 18.24 FNU. Thus, a decrease

of approximately 6 FNU could be achieved by filtration of the protein solution. In contrast to the lyophilized products, which showed a trend of decreasing turbidity after applying a filtration step, a notable decrease in turbidity after filtration could only be detected for Beriglobin® for the group of liquid products.

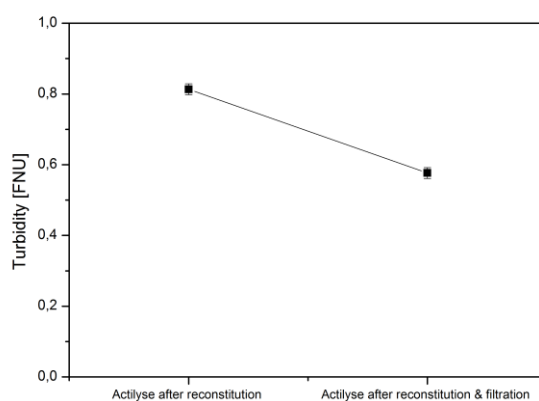
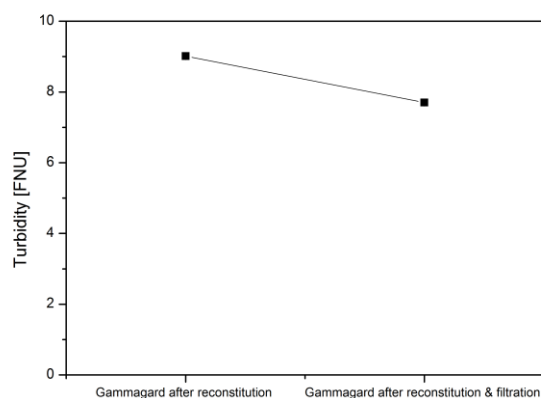
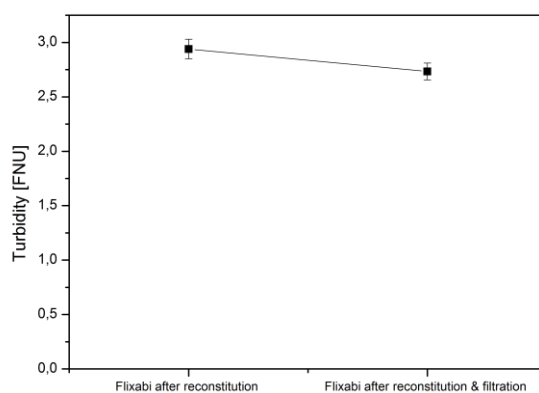
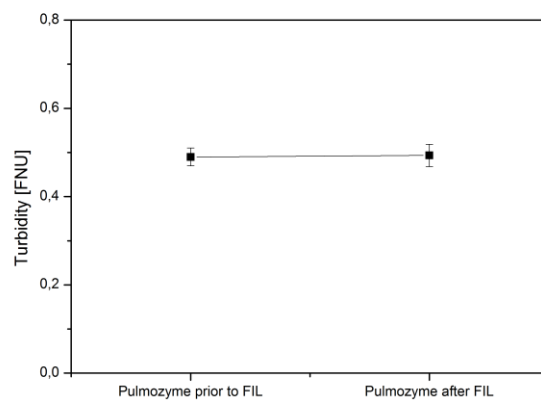
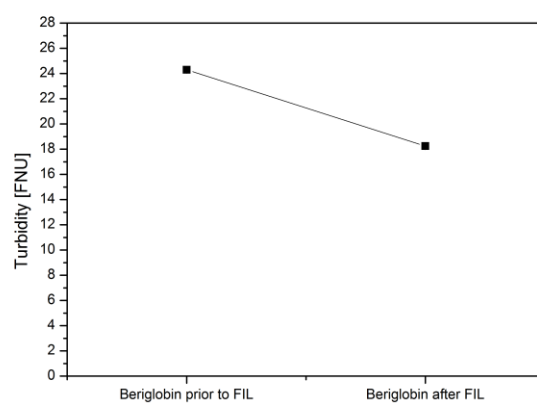
A**B****C**

Figure 7-2: Turbidity measurements of the lyophilized products Actilyse® (A), Gammagard® (B) and Flixabi® (C). Turbidity was measured prior to and after in-line filtration using an Acrodisc® filter with a pore size of 0.2 µm.

A



B



C

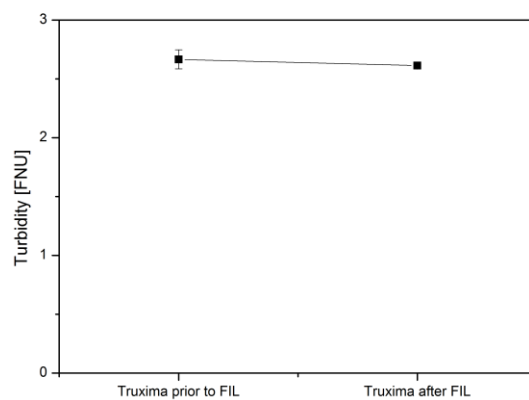


Figure 7-3: Turbidity measurements of Pulmozyme® (A), Beriglobin® (B) and Truxima® (C). Turbidity was measured prior to and after in-line filtration using an Acrodisc® filter with a pore size of 0.2 µm.

7.2.2 Analysis of subvisible particles by light obscuration and flow imaging

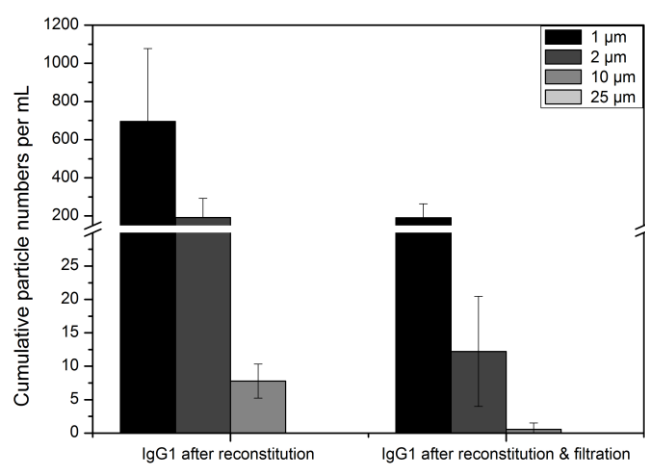
7.2.2.1 Monoclonal antibody IgG₁

The number of subvisible particles $\geq 1 \mu\text{m}$ of the lyophilized monoclonal antibody IgG₁ was determined by light obscuration and flow imaging. The measurements were performed directly after lyophilization and reconstitution of the monoclonal antibody and after six months storage at 2-8°C and reconstitution prior to and after filtration of the reconstituted protein solution. The results of light obscuration and flow imaging measurements are displayed in Figure 7-4 and Figure 7-5, respectively. The total particle count for particles $\geq 1 \mu\text{m}$ directly after lyophilization and reconstitution was 695 ± 383 particles/ mL determined by light obscuration (Figure 7-4A) and 1599 ± 209 particles/mL determined by flow imaging (Figure 7-5A). After filtration of the reconstituted solution, the total particle count could be reduced to less than 200 particles/mL (Figure 7-4A and Figure 7-5A). After six months of storage at 2-8°C, particle numbers increased to 2418 ± 1292 particles/mL and 3132 ± 234 particles/mL determined by light obscuration (Figure 7-4B) and flow imaging (Figure 7-5B), respectively. Filtration of the stored and reconstituted protein solution resulted again in a decrease of particle burden to approximately 200 particles/mL or less (Figure 7-4B and Figure 7-5B). In summary, particle counts of the lyophilized monoclonal antibody were rather low. However, an increase in particle numbers during storage for six months at 2-8°C could be detected. Particle numbers after filtration could be reduced to approximately 200 particles/mL.

7.2.2.2 Marketed lyophilized products

The results of particle measurements for particles $\geq 1 \mu\text{m}$ of the marketed lyophilized products Actilyse®, Gammagard® and Flixabi® after reconstitution prior to and after filtration are displayed in Figure 7-6 and Figure 7-7. Common for all proteins was that filtration resulted in a decrease of particles, as expected. The total particle count of all filtered reconstituted protein solutions could be reduced to less than 1000 particles/mL. However, the total particle counts directly after reconstitution and prior to filtration differed between the proteins. The highest particle number was detected for Gammagard®. The reconstituted, non-filtered protein solution had a particle burden of 13120 ± 2196 particles/mL measured by light obscuration (Figure 7-6B) and 49530 ± 1222 particles/mL determined by flow imaging (Figure 7-7B). Light obscuration measurements of reconstituted Actilyse® (Figure 7-6A) and Flixabi® (Figure 7-6C) resulted in 5707 ± 223 and 4772 ± 366 particles/mL, respectively. Flow imaging measurements revealed higher particle numbers of 16498 ± 1607 particles /mL for Actilyse® (Figure 7-7A) and 13092 ± 269 particles/mL for Flixabi® (Figure 7-7C).

A



B

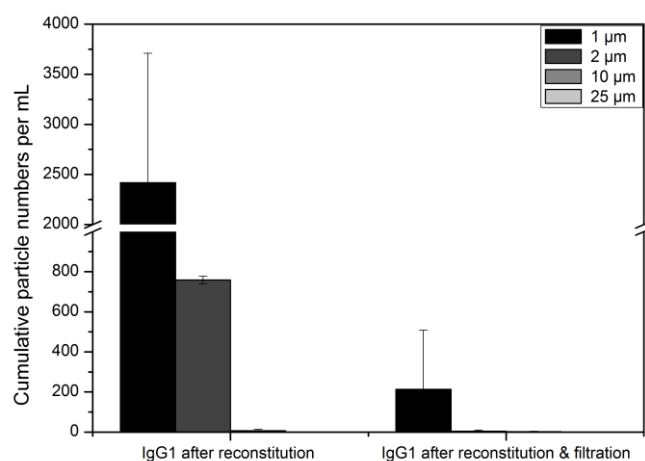


Figure 7-4: Total particle counts per mL determined by light obscuration of the monoclonal antibody IgG₁ directly after lyophilization (A) and after six months of storage at 2-8°C of the lyophilized protein (B). Particle numbers were measured directly after reconstitution and after an additional filtration step using an Acrodisc® syringe filter with a pore size of 0.2 µm.

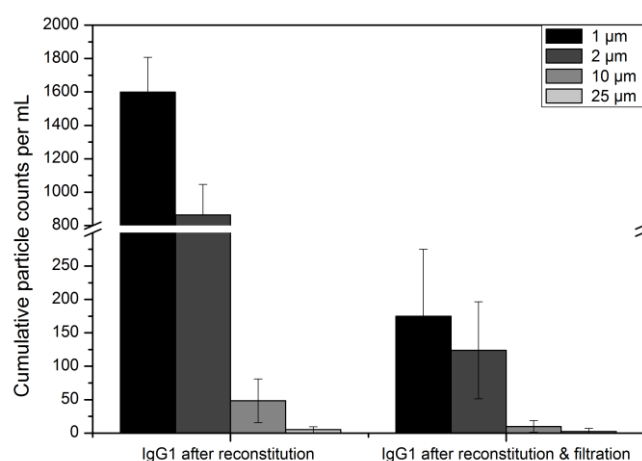
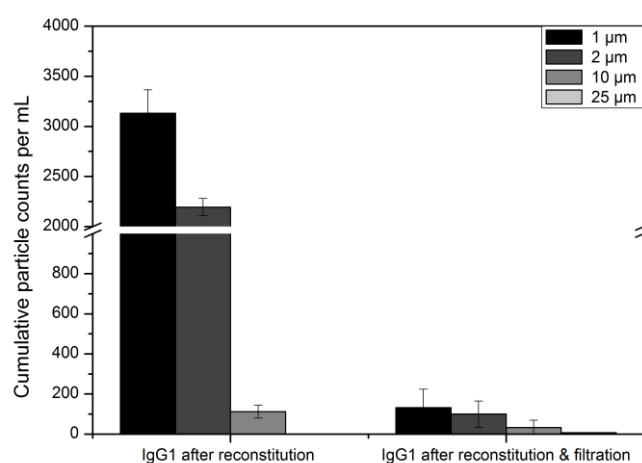
A**B**

Figure 7-5: Total particle counts per mL determined by flow imaging of the monoclonal antibody IgG₁ directly after lyophilization (A) and after six months of storage at 2-8°C of the lyophilized protein (B). Particle numbers were measured directly after reconstitution and after an additional filtration step using an Acrodisc® syringe filter with a pore size of 0.2 µm.

7.2.2.3 Marketed liquid products

As for the lyophilized products, the particle burden of particles $\geq 1 \mu\text{m}$ was also determined prior to and after filtration of three selected liquid products. Pulmozyme® (Dornase alfa), Beriglobin® (human immune globulin) and Truxima® (Rituximab) were chosen as liquid formulations to compare particle counts in liquid and lyophilized protein formulations. The number of subvisible particles was analyzed by light obscuration and flow imaging and results are displayed in Figure 7-8A-C and Figure 7-9A-C. Again, common for all products was that filtration resulted in a decrease of particles $\geq 1 \mu\text{m}$. However, particle numbers prior to filtration were at different levels. Pulmozyme® had a rather low particle burden of 832 ± 85 particles/mL and 2319 ± 170 particles/mL prior to filtration measured by light obscuration (Figure 7-8A) and flow imaging (Figure 7-9A), respectively. After filtration, particle

numbers were even lower resulting in a total particle count of 283 ± 25 and 516 ± 40 particles/mL determined by light obscuration and flow imaging, respectively. In contrast, the particle burden of Beriglobin®, containing human immune globulin, was at 77905 ± 2625 particles/mL (determined by light obscuration, Figure 7-8B) and 354593 ± 33201 particles/mL (determined by flow imaging, Figure 7-9B). Filtration of the human immune globulin solution resulted in a decrease of particles to 13530 ± 8935 (determined by light obscuration) and 28487 ± 1509 particles/mL $\geq 1 \mu\text{m}$ (determined by flow imaging). However, the particle burden after filtration remained higher than for Pulmozyme®, Truxima® or the lyophilized products. The particle burden of Truxima®, containing the monoclonal antibody Rituximab, was at approximately 6000 particles/ml prior to filtration and 300 particles/mL after filtration (Figure 7-8C and Figure 7-9C). The difference in particle numbers measured by light obscuration or flow imaging was negligible for this protein. In summary, it was also true for liquid products that filtration resulted in a decrease of the total particle count for particles $\geq 1 \mu\text{m}$.

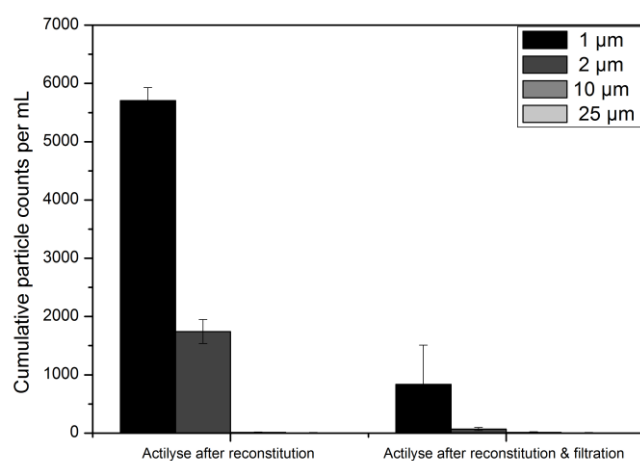
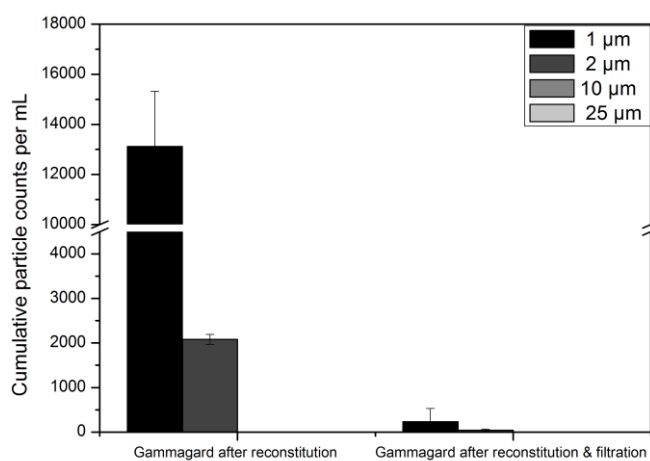
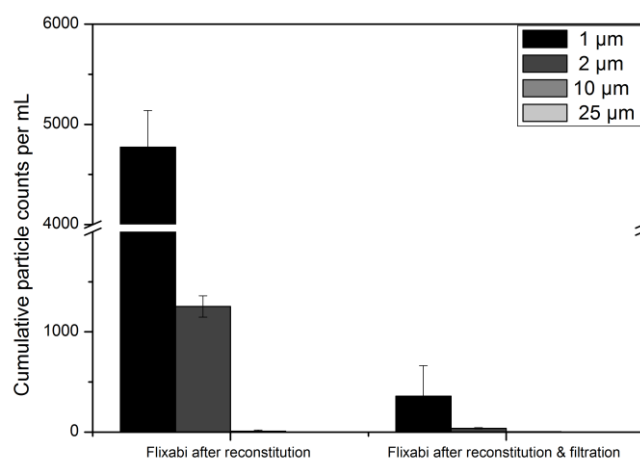
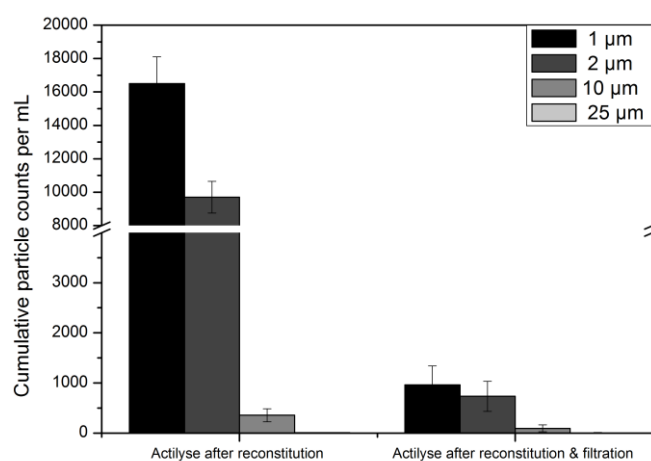
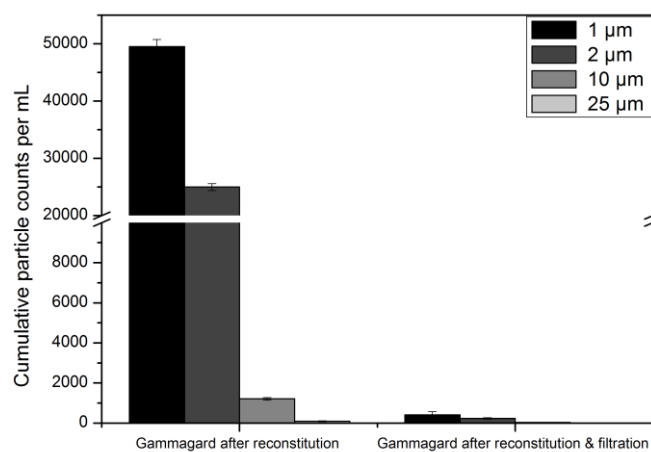
A**B****C**

Figure 7-6: Total particle counts per mL determined by light obscuration of Actilyse® (A), Gammagard®(B) and Flixabi®(C). Particle numbers were measured directly after reconstitution and after an additional filtration step using an Acrodisc® syringe filter with a pore size of 0.2 µm.

A



B



C

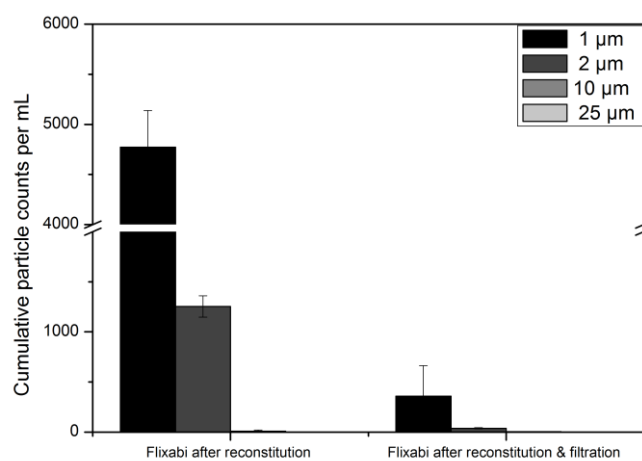


Figure 7-7: Total particle counts per mL determined by flow imaging of Actilyse® (A), Gammagard®(B) and Flixabi®(C). Particle numbers were measured directly after reconstitution and after an additional filtration step using an Acrodisc® syringe filter with a pore size of 0.2 µm.

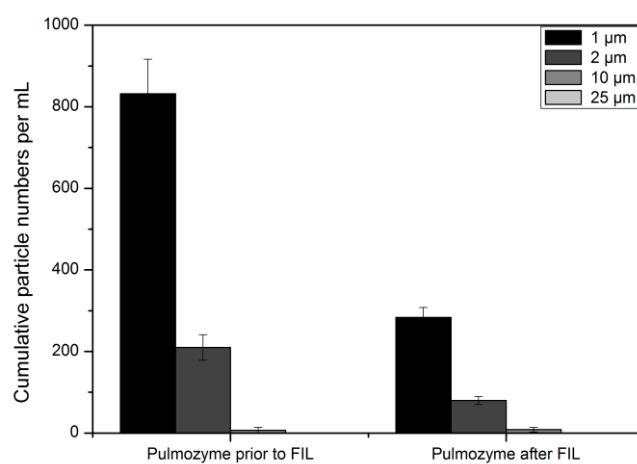
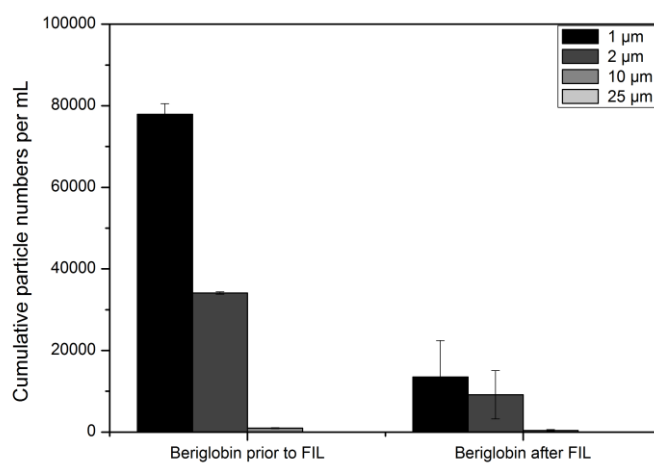
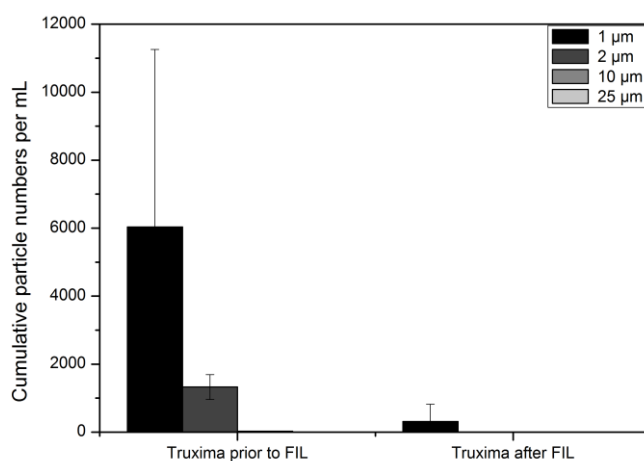
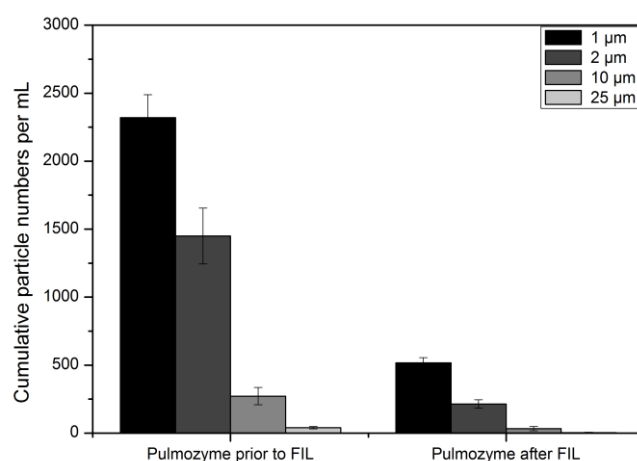
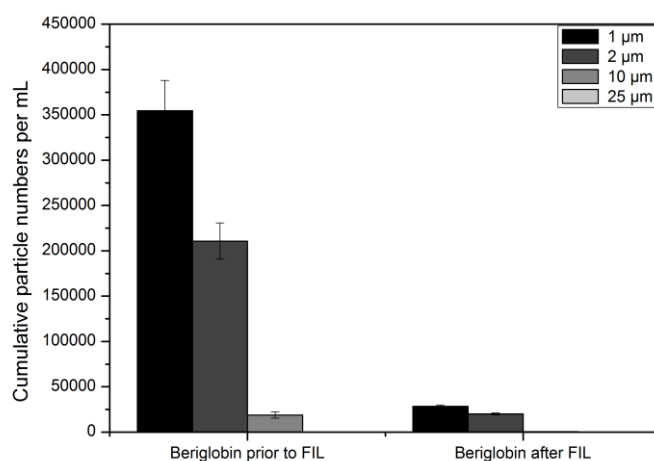
A**B****C**

Figure 7-8: Total particle counts per mL determined by light obscuration of Pulmozyme®(A), Beriglobin®(B) and Truxima®(C) prior to and after (in-line-) filtration using an Acrodisc® syringe filter with a pore size of 0.2 µm.

A



B



C

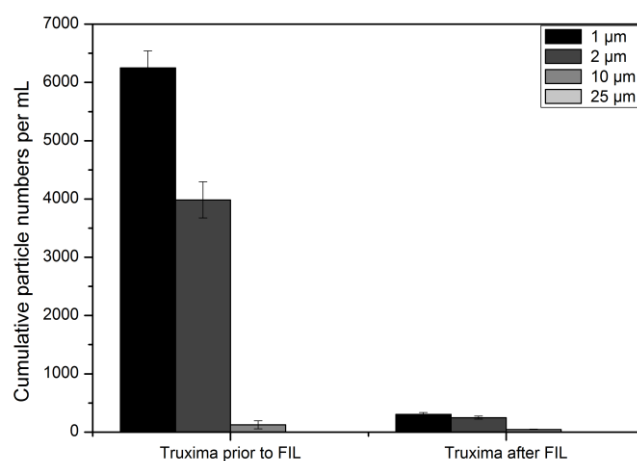


Figure 7-9: Total particle counts per mL determined by flow imaging of Pulmozyme®(A), Beriglobin®(B) and Truxima®(C) prior to and after (in-line-) filtration using an Acrodisc® syringe filter with a pore size of 0.2 µm.

7.2.3 Analysis of submicron particles by tunable resistive pulse sensing (TRPS)

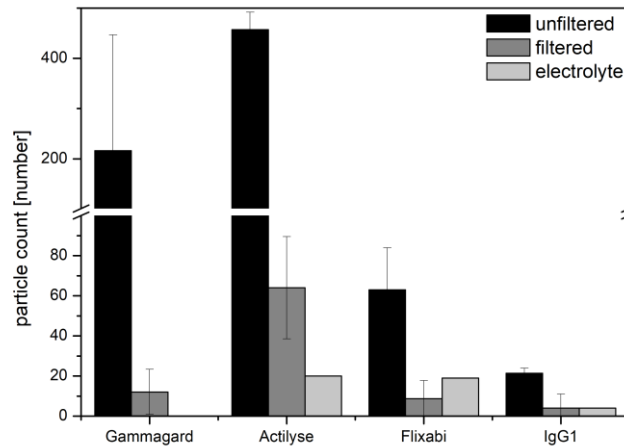
Tunable resistive pulse sensing (TRPS) is a relatively new technique to measure the number of submicron particles in protein solutions. TRPS has been successfully used to analyze submicron particle levels in blood plasma¹⁴, to analyze bacterial cell concentration and cell volume¹⁵ or for quantifying virus particles^{16,17}. Until now, no literature is available on using TRPS to monitor the levels of submicron particles in biologicals. The technique is based on the coulter counter principle with the difference that TRPS uses a tunable pore¹⁸. The operating principle of TRPS and details of sample preparation have been described in Chapter 5 (Section 5.3.2) and Chapter 3 (Section 3.7.2.1), respectively. All TRPS measurements in this study were performed by Andreas Stelzl.

7.2.3.1 Monoclonal antibody IgG₁ and marketed lyophilized products

Figure 7-10 displays the results of TRPS measurements of the marketed lyophilized products Gammagard®, Actilyse®, Flixabi® and a monoclonal antibody IgG₁ after reconstitution prior to or after filtration using an Acrodisc® syringe filter with a pore size of 0.2 µm. The graphs show the number of particle counts which were acquired within 10 minutes (Figure 7-10A) and the particle concentration (particles /mL) (Figure 7-10B), which was calculated based on calibration beads measurements. For TRPS measurements, only the stored (6 months, 2-8°C) monoclonal antibody IgG₁ was used. The calculation of particle concentration revealed that Gammagard®, human immune globulin at a concentration of 50 mg/mL, showed the highest particle concentration of particles of approximately $4 \cdot 10^7$ particles/mL, followed by Actilyse® with a particle concentration of approximately $1.5 \cdot 10^7$ particles/mL in the size range of 200 - 2000 nm. Flixabi®, containing the monoclonal antibody Infliximab, had a particle concentration of approximately $2.5 \cdot 10^6$ particles /mL and the monoclonal antibody IgG₁ showed the lowest particle concentration of particles sized between 200 and 2000 nm of less than 10^6 particles/mL. After filtration of the reconstituted protein solutions, the particle concentrations in the range of 200 - 2000 nm were reduced. In the case of the model monoclonal antibody IgG₁ and Flixabi®, the particle concentration could even be reduced to the particle concentration of the electrolyte which was used as blank. The evaluation of particle counts during a measurement time of 10 minutes (Figure 7-10A) showed the same trends with the exception that less particle counts for Gammagard® than for Actilyse® were detected, even though the particle concentration for Gammagard® was higher (Figure 7-10B). This can be explained by different sample preparation procedures. Due to the protein concentration of 50 mg/mL and therefore increased viscosity of the solution, Gammagard® had to be diluted 1/10 prior to TRPS measurements. Due to the dilution, less particles were counted in the Gammagard® sample than in the Actilyse® sample. However, the final calculated particle concentration was higher for Gammagard® than for Actilyse®. In

summary, TRPS revealed that a conventional sterile syringe filter with a pore size of 0.2 µm can be used to reduce the particle burden of submicron particles in the tested lyophilized biologics.

A



B

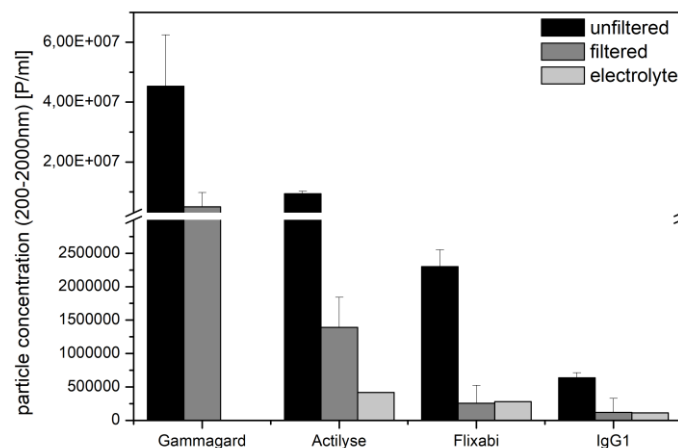


Figure 7-10: Number of particles counts/ 10 minutes as intermediate result (A) and the final particle concentration (particles/mL) (B) of the lyophilized products detected by TRPS using a NP 300 nanopore.

Figure 7-11 displays the concentrations of submicron (determined by TRPS) and micron particles (determined by light obscuration) of Gammagard®, Actilyse®, Flixabi® and the monoclonal antibody IgG₁. The graph illustrates that products with high levels of micron particles also contained a substantial amount of submicron particles as shown for Gammagard®, for example. Products containing less particles in the micron range such as Flixabi® or the monoclonal antibody IgG₁ also contained less submicron particles.

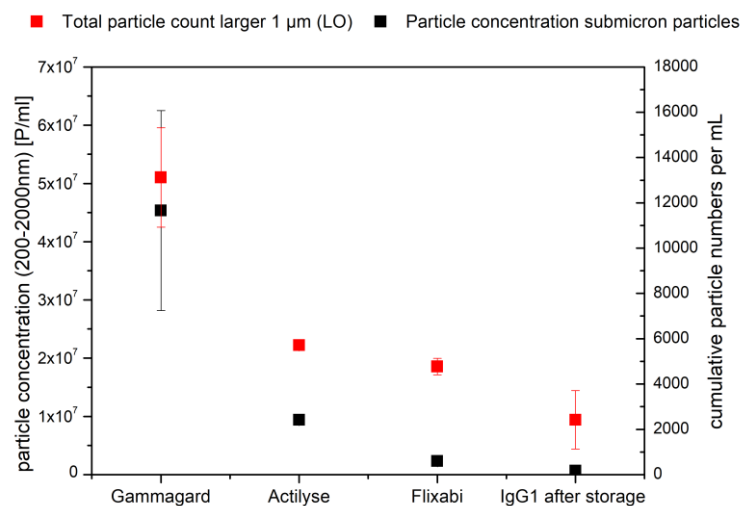
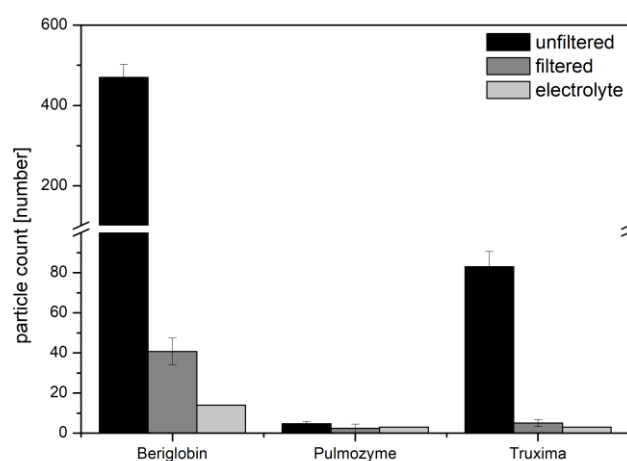


Figure 7-11: Graphical illustration of the particle concentration of submicron particles (black dots) determined by TRPS and of micron particles (red dots) determined by light obscuration of Gammagard®, Actilyse®, Flixabi® and the lyophilized monoclonal antibody IgG₁.

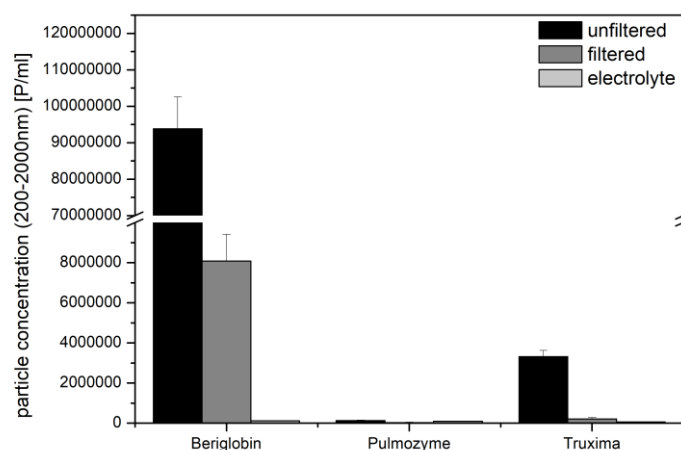
7.2.3.2 Marketed liquid products

The results of TRPS measurements of the marketed liquid products Beriglobin®, Pulmozyme® and Truxima® are displayed in Figure 7-12. As displayed for the lyophilized products, Figure 7-12 displays the number of particle counts which were acquired within 10 minutes (Figure 7-12A) and the particle concentration (particles /mL) (Figure 7-12B) which was calculated based on calibration beads measurements. The measurements were performed with the liquid protein formulation prior to and after a filtration step using an Acrodisc® syringe filter with a pore size of 0.2 µm. Again, the product containing human immune globulin, Beriglobin®, contained the highest number of particles in the range of 200 – 2000 nm. TRPS measurements revealed the highest particle count of approximately 450 particles within 10 minutes measurement time and approximately 10⁸ particles/mL in the range of 200 – 2000 nm for Beriglobin®. In contrast, Pulmozyme® had a very low submicron particle burden of less than 20 particle counts within 10 minutes and a particle concentration of approximately 10⁵ particles/mL. The particle concentration of the monoclonal antibody Rituximab (Truxima®) was at approximately 3*10⁶ particles/mL. It was true for all liquid protein products that filtration by a syringe filter with a pore size of 0.2 µm resulted in a decrease of particle counts and particle concentration as indicated by the dark grey bars in Figure 7-12A and B.

A



B



C

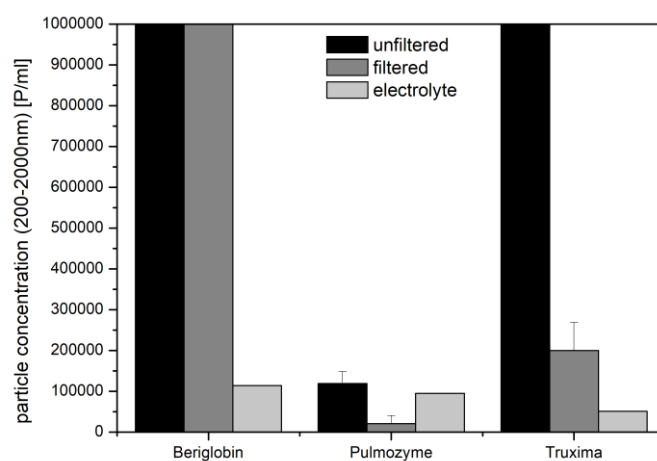


Figure 7-12: Number of particles counts/ 10 minutes as intermediate result (A) and the final particle concentration (particles/mL) (B) of the liquid products detected by TRPS using a NP 300 nanopore. Graph C displays an enlargement of graph B.

As already described for the lyophilized products, a relation between the level of micron and submicron particles could also be shown for the liquid products. Figure 7-13 displays the concentrations of submicron and micron particles of Beriglobin®, Pulmozyme® and Truxima®. It was also true for the liquid biologicals that high numbers of micron particles correlated to high numbers of submicron particles as shown for Beriglobin®. Accordingly, lower numbers of micron particles were related to lower numbers of submicron particles as shown for Pulmozyme® and Truxima®.

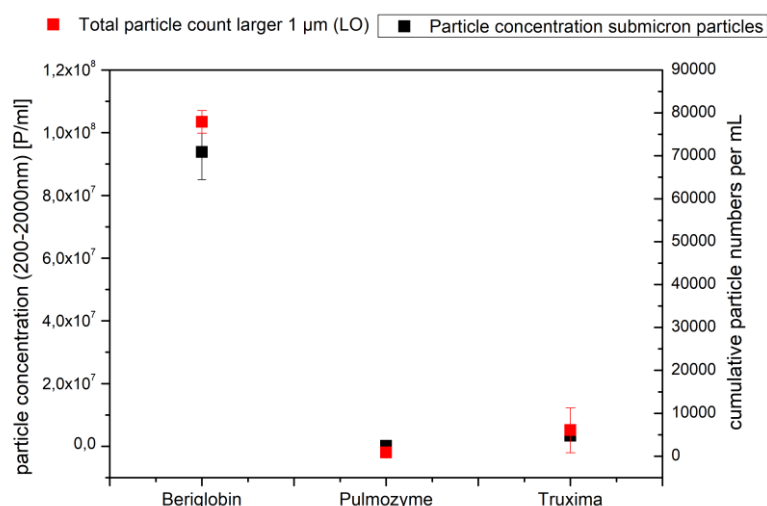


Figure 7-13: Graphical illustration of the particle concentration of submicron particles (black dots) determined by TRPS and of micron particles (red dots) determined by light obscuration of Beriglobin®, Pulmozyme®, Truxima®.

7.3 Discussion

The aim of this study was to investigate the particle burden in marketed lyophilized products and evaluate if in-line filtration might be a possibility to reduce not only the number of subvisible but also of submicron particles and thus, possibly reduce side effects associated with the infusion or injection of biologics. Four different lyophilized proteins were selected as test products: A lyophilized monoclonal antibody IgG₁, highly concentrated human immune globulin (Gammagard®), recombinant tissue plasminogen activator (rt-PA, Actilyse®) and a monoclonal antibody (Infliximab, Flixabi®). For comparison, particle numbers were also tested in three marketed liquid products.

Even though it is challenging to quantify protein aggregation by measuring turbidity, an increased or decreased turbidity might indicate the initiation or reduction of protein aggregation¹⁹. In this study, the turbidity of most of the tested products was decreased after filtration. Differences in turbidity prior to and after filtration were dependent on the protein concentrations of the tested products. The turbidity of Pulmozyme® containing Dornase alfa at a concentration of 1 mg/mL was at 0.49 FNU prior to filtration and could not be decreased remarkably by filtration. Contrarily, the turbidity of products

with a high protein concentration such as Gammagard® and Beriglobin® was higher prior to filtration and a clear decrease in turbidity was detectable after filtration. In summary, the overall trend, especially for the lyophilized products, was a decrease in turbidity after filtration indicating a reduced particle burden after filtration.

Particles $\geq 1 \mu\text{m}$ were analyzed by light obscuration and flow imaging. In-line filtration of the products resulted in a reduction of particles in all cases. However, particle numbers prior to filtration differed between the different products. While particle numbers of Gammagard® and Beriglobin®, both containing human immune globulin at relatively high concentrations of 50 mg/mL and 160 mg/mL, respectively, were higher, the particle burden of the monoclonal antibody products Flixabi® and Truxima®, both at a concentration of 10 mg/mL, was lower. Pulmozyme®, containing Dornase alfa at a concentration of 1 mg/mL, showed low particle counts. Differences in particle numbers determined by light obscuration and flow imaging can be explained by the different underlying techniques. Flow imaging microscopy is superior in detecting small transparent particles and therefore particle numbers are often higher than detected by light obscuration²⁰. One should keep in my mind, that all marketed products fulfilled the limitations of the European Pharmacopoeia limiting the number of particles $\geq 10 \mu\text{m}$ and $\geq 25 \mu\text{m}$. Accordingly, for containers with a volume of less than 100 mL, particles $\geq 10 \mu\text{m}$ are limited to 6000 particles/container and particles $\geq 25 \mu\text{m}$ to 600 particles/container⁵. However, the number of particles smaller than $10 \mu\text{m}$ is not limited by the European Pharmacopoeia or the USP. The gap in monitoring subvisible particles between $0.1 - 10 \mu\text{m}$ may lead to a compromised product quality as discussed in a commentary article by Carpenter and co-authors²¹. The particle measurements in the current study showed that the products contained a considerable number of particles between 1 and $10 \mu\text{m}$ of partially more than 5000 particles/mL with some exceptions to higher particle numbers such as Gammagard® or Beriglobin® and others to lower particles numbers such as Pulmozyme®. The comparison of the particle burden of a lyophilized monoclonal antibody IgG₁ after reconstitution directly after production and after storage for six months resulted in elevated particle numbers for the stored product. This indicates that storage of a lyophilized product may influence the particle burden.

For evaluating the effect of in-line filtration, depletion factors for particles ≥ 1 , 2 and $10 \mu\text{m}$ were calculated by dividing the particle counts prior to filtration by the particle counts after filtration. Depending on the particle numbers prior to filtration, the effect of in-line filtration was larger or smaller. Depletion factors for particles $\geq 1 \mu\text{m}$ (Figure 7-14) varied strongly between factors of 10 to 120 . However, the depletion factors for most of the products was between $10 - 20$. This was also true for the depletion factors for particles $\geq 2 \mu\text{m}$ (Figure 7-15). The number of particles $\geq 10 \mu\text{m}$ could be reduced $5-10$ -fold, on average (Figure 7-16). In some cases, depletion factors which were calculated based on the results of flow imaging microscopy were much higher than those calculated based on

light obscuration results. This can be explained by the higher particle counts detected by flow imaging prior to filtration as described above. Recently, the analysis of submicron particles attracted great interest. Not only because submicron particles are not limited by the Pharmacopoeia, but also because of the suspicion to trigger immunogenicity. Kijanka and co-authors recently published a study showing that submicron particles of a murine monoclonal antibody were more immunogenic than micron size or soluble aggregates after subcutaneous administration to mice²². Even though several analysis methods such as particle tracking analysis (PTA), differential centrifugal sedimentation (DCS), dynamic light scattering (DLS), transmission electron microscopy (TEM), resonant mass measurements (RMM) or flow cytometry are available to measure submicron particles^{1,18,23–25}, the analysis of submicron particles remains complex and challenging. In this study, tunable resistive pulse sensing (TRPS) was used to analyze submicron particles prior to and after filtration of the purchased biopharmaceutical products. The measurements showed that the tested products also contained particles in the submicron range. Depletion factors for submicron particles (Figure 7-17) revealed that the submicron particle burden after filtration could be reduced 10-fold, on average. Thus, it could be shown that also the number of particles in the range of 200 - 2000 nm could be reduced by using a standard sterile syringe filter with a pore size of 0.2 μm .

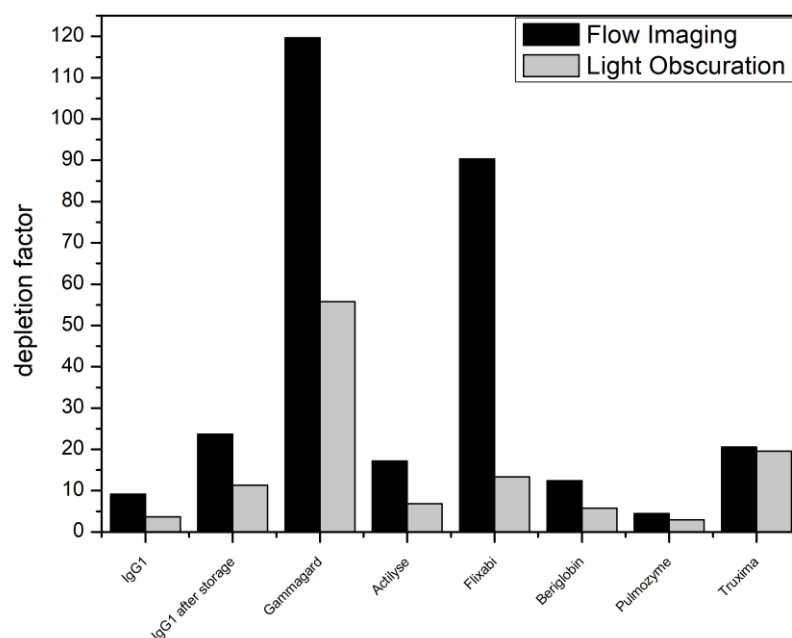


Figure 7-14: Depletion factor for particles $\geq 1 \mu\text{m}$ of IgG₁ prior to and after storage, Gammagard®, Actilyse®, Flixabi®, Beriglobin®, Pulmozyme® and Truxima®. The depletion factors were calculated by dividing the particle burden prior to filtration by the particle burden after filtration.

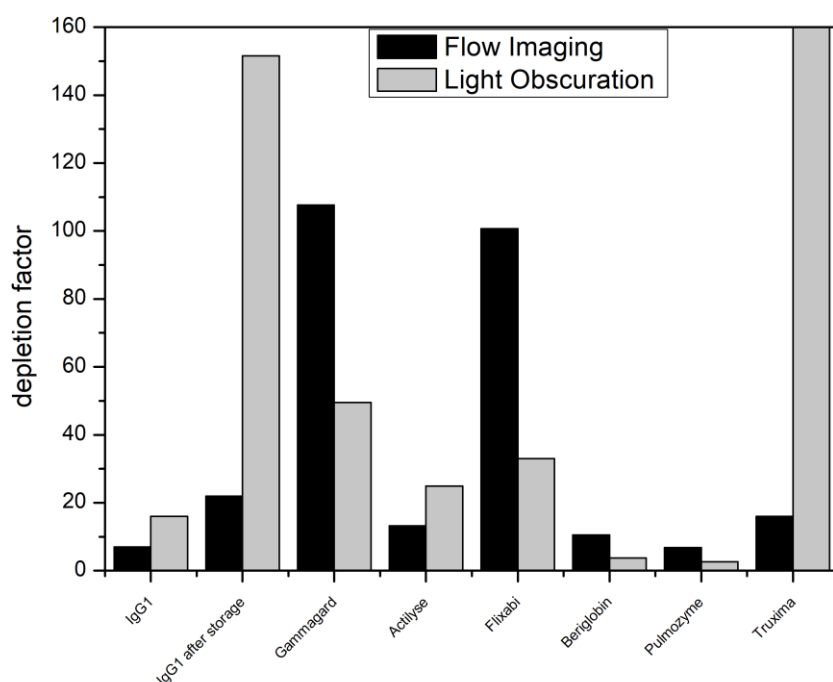


Figure 7-15: Depletion factor for particles $\geq 2 \mu\text{m}$ of IgG₁ prior to and after storage, Gammagard®, Actilyse®, Flixabi®, Beriglobin®, Pulmozyme® and Truxima®. The depletion factors were calculated by dividing the particle burden prior to filtration by the particle burden after filtration. The value for the depletion factor of Truxima® (light obscuration) is 441.

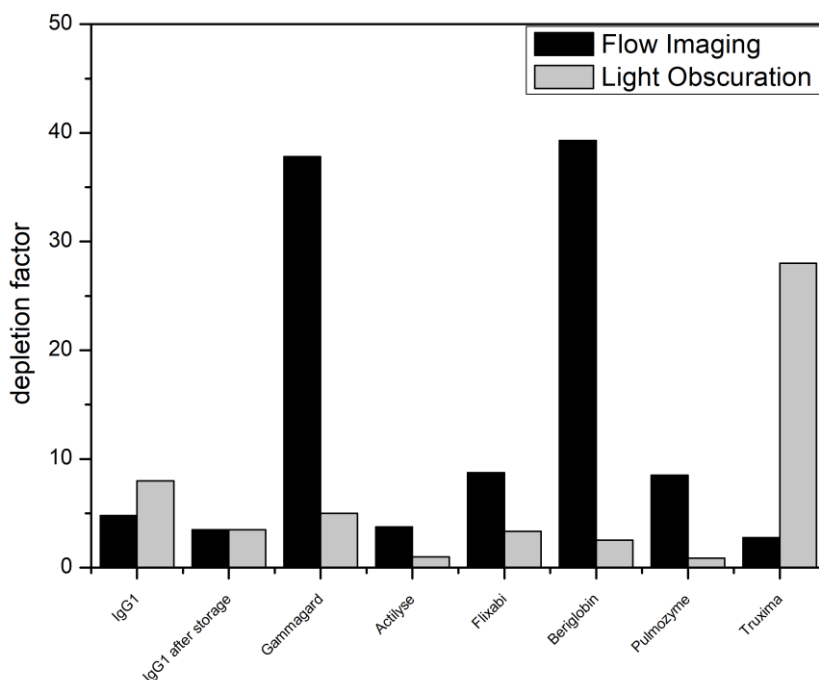


Figure 7-16: Depletion factor for particles $\geq 10 \mu\text{m}$ of IgG₁ prior to and after storage, Gammagard®, Actilyse®, Flixabi®, Beriglobin®, Pulmozyme® and Truxima®. The depletion factors were calculated by dividing the particle burden prior to filtration by the particle burden after filtration.

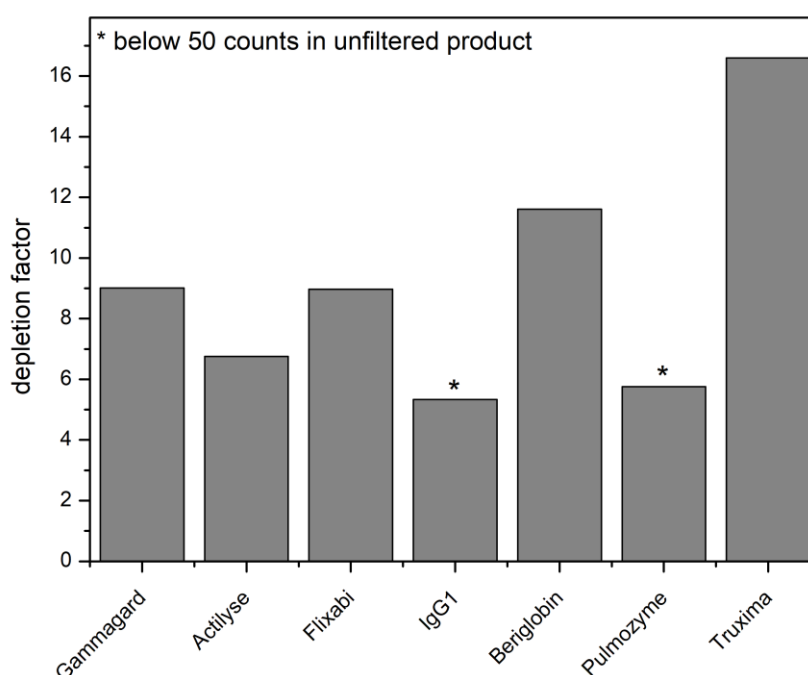


Figure 7-17: Depletion factor for submicron particles of IgG₁ after storage, Gammagard®, Actilyse®, Flixabi®, Beriglobin®, Pulmozyme® and Truxima®. The depletion factors were calculated by dividing the particle burden prior to filtration by the particle burden after filtration.

In summary, it could be shown that some of the tested products contained a considerable number of particles smaller than 10 µm. Moreover, the results of this study showed a relation between the level of submicron and micron particles in biologics. Products with a high number of particles in the micron range also showed high levels of submicron particles. However, further studies are needed to show a mathematical correlation between the levels of submicron and micron particles. In addition, this study revealed that in-line filtration using a standard sterile syringe filter with a pore size of 0.2 µm represents an effective tool to reduce not only the number of micron size but also the number of submicron particles in biopharmaceutical lyophilized or liquid products. Based on the results of this study, total particle counts were slightly higher in lyophilized products than in liquid products. To investigate if the particle burden in lyophilized products is constantly higher than in liquid formulations, a larger scale study would be necessary. Moreover, it should be mentioned that the particle burden in protein solutions is not only dependent on the formulation (lyophilized or liquid) but also on further parameters such as protein concentration or formulation excipients such as the addition of sugars or detergents^{26–29}. However, regarding the post production handling by end-users such as doctors and clinic staff, lyophilized products pose a greater risk to be treated incorrectly, since a reconstitution step is necessary prior to application. It has been shown before that the reconstitution step including reconstitution time and medium may be critical parameters regarding the formation of protein aggregates^{30,31}.

7.4 References

1. Scherer, T. M., Leung, S., Owyang, L. & Shire, S. J. Issues and Challenges of Subvisible and Submicron Particulate Analysis in Protein Solutions. *Aaps J.* **14**, 236–243 (2012).
2. Langille, S. E. Particulate Matter in Injectable Drug Products Particulate Matter in Injectable Drug Products. *PDA J. Pharm. Science Technol.* **67**, 186–200 (2013).
3. Perez, M., Maiguy-Foinard, A., Barthélémy, C., Décaudin, B. & Odou, P. Particulate Matter in Injectable Drugs: Evaluation of Risks to Patients. *Pharm. Technol. Hosp. Pharm.* **1**, 91–103 (2016).
4. Narhi, L. O. *et al.* Subvisible (2 – 100 μm) Particle Analysis During Biotherapeutic Drug Product Development : Part 1 , Considerations and Strategy. *J. Pharm. Sci.* **104**, 1899–1908 (2015).
5. 2.9.19 Partikelkontamination- Nicht sichtbare Partikeln. *European Pharmacopoeia* 438–441 (2014).
6. Pardeshi, N. N., Qi, W., Dahl, K., Caplan, L. & Carpenter, J. F. Microparticles and Nanoparticles Delivered in Intravenous Saline and in an Intravenous Solution of a Therapeutic Antibody Product. *J. Pharm. Sci.* **106**, 511–520 (2017).
7. Nejadnik, M. R. *et al.* Postproduction Handling and Administration of Protein Pharmaceuticals and Potential Instability Issues. *J. Pharm. Sci.* **107**, 2013–2019 (2018).
8. Jiskoot, W., Nejadnik, M. R. & Sediq, A. S. Potential Issues With the Handling of Biologicals in a Hospital. *J. Pharm. Sci.* **106**, 1688–1689 (2017).
9. Villa, G. *et al.* In-Line Filtration Reduces Postoperative Venous Peripheral Phlebitis Associated With Cannulation: A Randomized Clinical Trial. *Anesth. Analg.* **127**, 1367–1374 (2018).
10. Werner, B. P. & Winter, G. Expanding bedside filtration – a powerful tool to protect patients from protein aggregates. *J. Pharm. Sci.* **107**, 2775–2788 (2018).
11. Werner, B. P. Filtration and novel polymeric containers for the improved quality of biotech drug products. (Ludwig-Maximilians-Universität München, 2017).
12. Telikepalli, S. *et al.* Characterization of the physical stability of a lyophilized IgG1 mAb after accelerated shipping-like stress. *J. Pharm. Sci.* **104**, 495–507 (2016).
13. Kasper, J. C. & Friess, W. The freezing step in lyophilization : Physico-chemical fundamentals ,

- freezing methods and consequences on process performance and quality attributes of biopharmaceuticals. *Eur. J. Pharm. Biopharm.* **78**, 248–263 (2011).
14. Mørk, M., Pedersen, S., Botha, J., Lund, S. M. & Risom, S. Preanalytical, analytical and biological variation of blood plasma submicron particle levels measured with nanoparticle tracking analysis and tunable resistive pulse sensing. *Scand. J. clinical Lab. Investig.* **76**, 349–360 (2016).
 15. Yu, A. C. S., Loo, J. F. C., Yu, S., Kong, S. K. & Chan, T. Monitoring bacterial growth using tunable resistive pulse sensing with a pore-based technique. *Appl Microbiol Biotechnol* **98**, 855–862 (2014).
 16. Yang, L. & Yamamoto, T. Quantification of Virus Particles Using Nanopore-Based Resistive-Pulse Sensing Techniques. *Front. Microbiol.* **7**, 1500 (2016).
 17. Vogel, R. *et al.* Quantitative Sizing of Nano/Microparticles with a Tunable Elastomeric Pore Sensor. *Anal. Chem.* **83**, 3499–3506 (2011).
 18. Anderson, W., Kozak, D., Coleman, V. A., Jämting, Å. K. & Trau, M. A comparative study of submicron particle sizing platforms: Accuracy, precision and resolution analysis of polydisperse particle size distributions. *J. Colloid Interface Sci.* **405**, 322–330 (2013).
 19. Chaudhuri, R., Cheng, Y., Middaugh, C. R. & Volkin, D. B. High-Throughput Biophysical Analysis of Protein Therapeutics to Examine Interrelationships Between Aggregate Formation and Conformational Stability. *AAPS J.* **16**, 48–64 (2014).
 20. Zölls, S. *et al.* Flow Imaging Microscopy for Protein Particle Analysis-A Comparative Evaluation of Four Different Analytical Instruments. *AAPS J.* **15**, 1200–1211 (2013).
 21. Carpenter, J. F. *et al.* Overlooking subvisible particles in therapeutic protein products: Gaps that may compromise product quality. *J. Pharm. Sci.* **98**, 1202–1205 (2009).
 22. Kijanka, G. *et al.* Submicron Size Particles of a Murine Monoclonal Antibody Are More Immunogenic Than Soluble Oligomers or Micron Size Particles Upon Subcutaneous Administration in Mice. *J. Pharm. Sci.* **107**, 2847–2859 (2018).
 23. Zhang, L., Shi, S. & Antochshuk, V. Closing the Gap: Counting and Sizing of Particles Across Submicron Range by Flow Cytometry in Therapeutic Protein Products. *J. Pharm. Sci.* **106**, 3215–3221 (2017).
 24. Panchal, J., Kotarek, J., Marszal, E. & Topp, E. M. Analyzing Subvisible Particles in Protein Drug

- Products : a Comparison of Dynamic Light Scattering (DLS) and Resonant Mass Measurement (RMM). *Aaps J.* **16**, 440–451 (2014).
25. Zhou, C., Krueger, A. B., Barnard, J. G., Qi, W. E. I. & Carpenter, J. F. Characterization of Nanoparticle Tracking Analysis for Quantification and Sizing of Submicron Particles of Therapeutic Proteins. *J. Pharm. Sci.* **104**, 2441–2450 (2015).
 26. Harn, N., Allan, C., Oliver, C. & Middaugh, C. R. Highly Concentrated Monoclonal Antibody Solutions : Direct Analysis of Physical Structure and Thermal Stability. **96**, 532–546 (2007).
 27. Wang, B., Tchessalov, S., Cicerone, M. T., Warne, N. W. & Pikal, M. J. Impact of Sucrose Level on Storage Stability of Proteins in Freeze-Dried Solids : II . Correlation of Aggregation Rate with Protein Structure and Molecular Mobility. *J. Am. Pharm. Assoc.* **98**, 3145–3166 (2009).
 28. Mahler, H. C., Müller, R., Frieß, W., Delille, A. & Matheus, S. Induction and analysis of aggregates in a liquid IgG1-antibody formulation. *Eur. J. Pharm. Biopharm.* **59**, 407–417 (2005).
 29. Cao, W., Krishnan, S., Speed, M., Shih, L. & Liu, D. European Journal of Pharmaceutics and Biopharmaceutics Rational design of lyophilized high concentration protein formulations- mitigating the challenge of slow reconstitution with multidisciplinary strategies. *Eur. J. Pharm. Biopharm.* **85**, 287–293 (2013).
 30. Webb, S. D., Cleland, J. L., Carpenter, J. F. & Randolph, T. W. A New Mechanism for Decreasing Aggregation of Recombinant Human Interferon- γ by a Surfactant : Slowed Dissolution of Lyophilized Formulations in a Solution Containing 0 . 03 % Polysorbate 20. *J. Pharm. Sci.* **91**, 543–558 (2002).
 31. Sarciaux, J.-M., Mansour, S., Hagemann, M. J. & Nail, S. L. Effects of Buffer Composition and Processing Conditions on Aggregation of Bovine IgG during Freeze-Drying. *J. Pharmaceutical Sci.* **88**, 1354–1361 (1999).

Chapter 8

Final summary

8.1 Summary

The overall aim of this thesis was to evaluate the immunogenicity of protein aggregates in a 3D matrix assisted human artificial lymph node model which was developed by Giese and co-workers¹. The HuALN has been used successfully to test the immunogenicity of vaccines before² but has not been utilized for testing unwanted immunogenicity.

Within the scope of this thesis, the HuALN was used for the first time to test and evaluate the immunogenicity of protein aggregates of two monoclonal antibodies. The focus of this thesis laid especially on investigating the capability of the 3D HuALN model to represent a new test model for evaluating the immunogenicity of protein aggregates. Besides, differently produced protein aggregates were investigated to gain insight which types of protein aggregates are most immunogenic. In order to test the immunogenicity of protein aggregates in the HuALN model, several studies were necessary to determine suitable concentrations of the monoclonal antibodies and stress conditions, and to generate protein aggregates in a reproducible way. Moreover, the stability of the generated protein aggregates had to be ensured over the reactor run time of the HuALN model.

Further, the 3D human artificial lymph node model was used to investigate the biological effect of in-line filtration. In addition, the effect of in-line filtration was investigated using a 2D *in vitro* dendritic cell assay which was established within the scope of this thesis. Finally, it was investigated if in-line filtration would be a possibility to reduce particle numbers in marketed lyophilized and liquid products.

Chapter 1 provides a general introduction of the topic immunogenicity of protein aggregates. In **Chapter 2**, the scope of this thesis is described, and **Chapter 3** includes all materials and methods used for this thesis.

In **Chapter 4**, aggregation studies on the monoclonal antibodies Adalimumab and Bevacizumab were described. Adalimumab and Bevacizumab were exposed to stir, light and heat (only Bevacizumab) stress for different periods of time and analyzed by various protein analysis methods such as light obscuration, size exclusion chromatography, dynamic light scattering, FT-IR and fluorescence spectroscopy. Exposing the monoclonal antibodies to different stress conditions for distinct periods of time resulted in different aggregation levels. While stir stress primarily led to insoluble aggregates, light stress strongly triggered the formation of soluble aggregates. Heat stress of Bevacizumab resulted in the formation of soluble and insoluble aggregates at the same time. Based on the results of this study, time points for all stress conditions for Adalimumab and Bevacizumab were selected: 24 hours stir stress with a rotation speed of 240 rpm for Adalimumab and Bevacizumab, 24 hours (Bevacizumab)

or 48 hours (Adalimumab) exposure to light at $55 \pm 5 \text{ W/m}^2$ and four days exposure to 50°C of Bevacizumab. The selected conditions were used for further studies.

To ensure a consistent composition of the stressed samples during the 3D HuALN reactor run time of four weeks, the stability of the stressed Adalimumab and Bevacizumab samples was investigated after storage at $2-8^\circ\text{C}$ for a period of six weeks directly after production and after being stored at -80°C . The study revealed that the composition of stressed samples of Adalimumab and Bevacizumab did not change dramatically when stored at $2-8^\circ\text{C}$ for six weeks. When the stressed samples were stored at -80°C for six months, thawed and subsequently stored at $2-8^\circ\text{C}$ for further six weeks, light stressed Adalimumab trended towards the formation of larger aggregates, whereas no changes in the composition of Bevacizumab samples were detected. Thus, it was possible to store all stressed samples at $2-8^\circ\text{C}$ for a period of six weeks and therefore, the quality of the stressed samples was ensured during the 3D HuALN reactor time of four weeks.

The evaluation of immunogenicity of the differently produced protein aggregates of Adalimumab and Bevacizumab in a 3D human artificial lymph node model is described in **Chapter 5**. Prior to the stimulation of the 3D HuALN model, a 2D DC-/T-cell assay was performed to determine an appropriate concentration of the stressed samples for the HuALN study. Results revealed that stressed samples of Adalimumab were used at concentrations of 1 mg/mL and stressed Bevacizumab samples at concentrations of 0.5 mg/mL for further cell or HuALN studies.

3D HuALN bioreactors were stimulated with the differently stressed samples of Adalimumab and Bevacizumab, and with dendritic cells that have already been stimulated with the stressed samples prior to the reactor start. The reactor run time was 28 days including repeated stimulations on day 0, 7, 14 and 21. The analysis of cytokines revealed that Bevacizumab after heat stress resulted in a pro-inflammatory and TH1 immune response. No trends in immune response could be shown for any of the stressed samples of Adalimumab. Besides the analysis of cytokines, cell culture supernatants were also analyzed for the presence of IgM antibodies and anti- drug antibodies (ADAs). The analysis revealed unspecific IgM profiles for all stressed samples and no ADAs could be found in any of the samples.

Irrespective of the pro-inflammatory and TH1 immune response upon stimulation with heat stressed Bevacizumab, no trends of immune response could be detected. The rather low immune response and the fact that no anti-drug antibodies could be found led to the investigation of the diffusion behavior of polystyrene particles as a surrogate for particles formed by aggregated antibodies through a dextran gel which was used as matrix in the 3D HuALN bioreactors for stromal and immune cells. In this study, a Franz cell model was used to mimic the HuALN model and polystyrene particles at sizes of 26 nm and

2 μm served as model particles to investigate the diffusion behavior of particles through the dextran matrix. Whereas 26 nm sized particles were equally distributed throughout the gel, 2 μm sized particles accumulated primarily at the top of the gel, indicating a potential self-selecting effect for larger aggregates.

The focus of **Chapter 6 and 7** was on in-line filtration of biologicals. In **Chapter 6**, the effect of in-line filtration on immunogenicity was investigated using the 3D HuALN model. Stir and heat stressed samples of Bevacizumab were prepared and the HuALN system was stimulated with the stressed samples prior to and after filtration. Sampling was performed daily, and cell culture supernatants were analyzed for the presence of cytokines and IgM antibodies. A high donor to donor variability between the three tested donors impeded a proper evaluation of the results, thus it was almost impossible to evaluate the difference in immune response between the filtered and non-filtered samples.

Besides, the effect of in-line filtration was also investigated using a 2D dendritic cell assay. In addition to stir and heat stress, Bevacizumab was also exposed to light and incubated with tert-butyl hydroperoxide (tBHP). All stressed samples were analyzed thoroughly, and dendritic cells were stimulated with the stressed samples prior to and after filtration. Results of cytokine and DC marker analysis revealed no difference between filtered and non-filtered samples. However, the low immune response of dendritic cells and the variability between the immune response of the used donors impeded again a sound evaluation of the biological effect of in-line filtration.

In **Chapter 7**, a study investigating particle numbers in marketed lyophilized products and the effect of in-line filtration of reconstituted lyophilized biopharmaceuticals was described. Three marketed lyophilized biologicals were reconstituted according to the manufacturer's description and numbers of particles $\geq 1 \mu\text{m}$ and $\leq 1 \mu\text{m}$ were analyzed prior to and after applying an in-line filtration step using a standard syringe filter with a pore size of 0.2 μm . For comparison, the particle numbers were also determined in liquid biopharmaceutical products prior to and after filtration. The results showed that some of the tested products contained a considerable number of particles $\leq 10 \mu\text{m}$ which are not limited by the European Pharmacopoeia or the USP. Lyophilized products slightly tended to higher particle numbers than liquid products. However, filtration of the protein solutions resulted in a strong decrease of particle numbers in all products. It was remarkable that even the number of particles in the submicron range could be reduced by filtration with a standard sterile syringe filter with a pore size of 0.2 μm .

8.2 Conclusion and Outlook

Within the scope of this thesis a 3D human artificial lymph node model could be evaluated as a new test model for the evaluation of immunogenicity of protein aggregates. The HuALN study revealed a pro-inflammatory and TH1 response for heat stressed Bevacizumab compared to unstressed Bevacizumab or stressed samples of Adalimumab. Thus, the system could differentiate between the immunogenicity of different proteins (Adalimumab and Bevacizumab) and differently produced protein aggregates of the same protein. This thesis also revealed that the capability of the HuALN system to investigate the long-term immune answer is useful, especially regarding a long-term therapy with biologicals. In addition, the cellular structure of a human lymph node with germinal centers and follicles is simulated by implementing stromal cells³ and also the set-up of the experiment is close to the processes of the human immune response. Therefore, the human artificial lymph node model represents a promising model to improve the predictability of immunogenicity of protein aggregates in humans.

Despite of all advantages of the human artificial lymph node model (see Chapter 1 and 5), there are also limitations which became apparent during the experiments performed as part of this thesis. First, a high donor to donor variability made assessment of the results not straight forward and it was almost impossible to draw profound assumptions. To determine the number of donors for immunological cell assays is one of the major challenges. On the one hand, a large number of donors is valuable to represent a broad HLA diversity⁴. On the other hand, costs, time and practicability of the experiment must be taken into consideration. Additionally, the number of donors is also dependent on the assay. Cell assays in a well-plate format allow to include a higher number of donors than *in vivo* animal studies or *in vitro* bioreactor studies. For the HuALN experiments described in this thesis, three donors were used, respectively. However, due to high donor to donor variability, it is recommended to use at least 6-10 donors for future studies using the 3D HuALN as test model for immunogenicity. Since each bioreactor is connected to a fluidic system and tempered in a cabinet dryer, only a limited number of bioreactors can be run at the same time. To implement a higher number of bioreactors running at the same time, it is necessary to further develop the 3D HuALN, e.g. by increasing its throughput volume. ProBioGen is currently developing a miniaturized human artificial lymph node model. The so-called IG-device™ combines 12 culture units on a base plate² and may represent a meaningful step to include a higher number of donors and samples into immunogenicity studies.

The study in this thesis indicated that particles in the micron range might not be able to diffuse through the dextran matrix and thus, cannot get in contact with embedded immune cells. If this hypothesis will be confirmed by studies using the human artificial lymph node instead of a Franz Cell model, the 3D

human artificial lymph node model could not be used for testing the immunogenicity of protein aggregates in the micron size range.

The low immune responses of most of the stressed samples of Adalimumab and Bevacizumab might also counter the on-going debate about protein aggregates as a trigger for immunogenicity and lead to the question how critical protein aggregates regarding immunogenicity really are. To date, the immunogenicity of protein aggregates has been primarily tested in 2D dendritic cell assays and mice as described in Chapter 1 and published as review article⁵. The studies were often contradictory and 2D *in vitro* assays and *in vivo* mouse models have limitations, primarily the questionable predictiveness of immunogenicity in humans. Testing the immunogenicity of protein aggregates in a 3D human artificial lymph node system mimicking the human immune system best compared to a 2D cell assay or a mouse model, even high levels of protein aggregates of Adalimumab and Bevacizumab did not lead to strong immunogenic responses.

Concerning the types of protein aggregates posing the greatest risk to be immunogenic, at present, protein aggregates with chemical modifications and submicron particles are strongly discussed^{6,7}. This could partly also be shown in this thesis, since oxidative changes and submicron particles could be detected in the heat stressed sample of Bevacizumab. On the other hand, strongly oxidized Bevacizumab (by light or tBHP) did not lead to the secretion of cytokines or activation of dendritic cells in a 2D cell assay. This might indicate that protein aggregates, even with strong chemical modifications, might not be as critical as suspected in regard to immunogenicity. However, the focus of this thesis was on the evaluation of the HuALN as a new test model. By carefully selecting stress conditions samples containing primarily insoluble or soluble aggregates could be generated. However, protein aggregates were not further fractionated, thus the stressed samples contained a variety of protein aggregates. The relatively high amount of protein aggregates in the samples was intended and we were aware that aggregate levels in the samples did not correspond to those present in marketed biologics. To investigate the immunological risk of certain types of protein aggregates a fractionation by asymmetrical flow field flow fractionation as shown by Angelika Freitag⁸, for example, would be necessary.

In-line filtration showed to be an effective tool to reduce particles in the submicron and micron range and might be helpful to reduce increased particle levels in biologics, especially particles generated by incorrect post-production handling, transportation or storage. However, it remains unclear if in-line filtration is also an effective tool to reduce immunogenicity. Further studies are needed to show the biological effect of in-line filtration.

In summary, a 3D human artificial lymph model has been evaluated as new model for testing the immunogenicity of protein aggregates. Even if further studies are needed to investigate the diffusion behavior of particles through the dextran gel matrix or to improve the economic efficiency, the 3D human artificial lymph node is a promising step into the future regarding test models for immunogenicity of biologicals and might bridge the gap between animal studies and clinical studies.

8.3 References

1. Giese, C. *et al.* A human lymph node in vitro-challenges and progress. *Artif. Organs* **30**, 803–808 (2006).
2. Giese, C. *et al.* Immunological substance testing on human lymphatic micro-organoids in vitro. *J. Biotechnol.* **148**, 38–45 (2010).
3. Sardi, M., Lubitz, A. & Giese, C. Modeling Human Immunity In Vitro - Improving Artificial Lymph Node Physiology by Stromal Cells. *Appl. Vitro. Toxicol.* **2**, 143–150 (2016).
4. Joubert, M. K. *et al.* Use of in vitro assays to assess immunogenicity risk of antibody-based biotherapeutics. *PLoS One* **11**, 1–22 (2016).
5. Kraus, T., Winter, G. & Engert, J. Test models for the evaluation of immunogenicity of protein aggregates. *Int. J. Pharm.* **559**, 192–200 (2019).
6. Boll, B. *et al.* Extensive chemical modifications in the primary protein structure of IgG1 subvisible particles are necessary for breaking immune tolerance. *Mol. Pharm.* **14**, 1292–1299 (2017).
7. Kijanka, G. *et al.* Submicron Size Particles of a Murine Monoclonal Antibody Are More Immunogenic Than Soluble Oligomers or Micron Size Particles Upon Subcutaneous Administration in Mice. *J. Pharm. Sci.* **107**, 2847–2859 (2018).
8. Freitag, A. J. *et al.* Investigation of the immunogenicity of different types of aggregates of a murine monoclonal antibody in mice. *Pharm. Res.* **32**, 430–444 (2015).

Chapter 9

Appendix

9.1 List of abbreviations

ADA	Anti-drug antibody
AF4	Asymmetrical flow field flow fractionation
ANS	8-Anilino-1-naphthalenesulfonic acid
APC	Antigen presenting cell
ATSVF	Adipose tissue stromal vascular fraction
AUC	Area under the curve
BCR	B-cell receptor
Bis-ANS	4,4'-Dianilino-1,1'-binaphthyl-5,5'-disulfonic acid
BSA	Bovine serum albumine
CD	Cluster of differentiation
ConA	Concanavalin A
CSFE	Carboxyfluorescein succinimidyl ester
DC	Dendritic cell
DLS	Dynamic light scattering
DPBS	Dulbecco's phosphate buffered saline
EDTA	Ethylenediaminetetraacetic acid
ELISA	Enzyme-linked immunosorbent assay
FACS	Fluorescence activated cell sorting
FNU	Formazine nephelometric unit
FRC	Fibroblastic reticular cells
FT-IR	Fourier transform infra-red spectroscopy
GM-CSF	Granulocyte macrophage colony stimulating factor
hGH	Human growth hormone
HLA	Human leukocyte antigen
HMW	High molecular weight
HuALN	Human artificial lymph node model
IEX	Ion exchange chromatography
INF- γ	Interferon gamma
LMW	Low molecular weight
LPS	Lipopolysaccharide
mAb	Monoclonal antibody

MHC	Major histocompatibility complex
MoDC	Monocyte-derived dendritic cells
NTA	Nanoparticle tracking analysis
OVA	Ovalbumin
PBMC	Peripheral blood mononuclear cells
PBS	Phosphate buffered saline
PDI	Poly dispersity index
PGE2	Prostaglandin E2
PK	Pharmacokinetics
PTFE	Polytetrafluorethylene
RMM	Resonant mass measurement
tBHP	tert-butyl hydroperoxide
TCR	T-cell receptor
TD	T-cell dependent
TH1/Th1	T-helper cells 1
TH2/Th2	T-helper cells 2
TI	T-cell independent
TNF- α	Tumor necrosis factor alpha
TRPS	Tunable resistive pulse sensing
scFV	Humanized single chain variable antibody fragments
SEC	Size exclusion chromatography
USP	United States Pharmacopoeia
WCX	Weak cation exchange
Z _{ave}	Z-average

9.2 List of publications and presentations associated with this thesis

Publications:

Teresa Kraus, Gerhard Winter, Julia Engert

Test models for the Evaluation of Immunogenicity of Protein Aggregates

International Journal of Pharmaceutics 559 (2019) 192–200

Teresa Kraus, Ulrike Schließer, Annika Lubitz, Christoph Giese, Jana Reuschel, Rene Brecht, Julia Engert, Gerhard Winter

Evaluation of a 3D Human Artificial Lymph Node as Test Model for the Assessment of Immunogenicity of Protein Aggregates

Journal of Pharmaceutical Sciences 108 (2019) 2358-2366

Poster Presentations:

Teresa Kraus, Ulrike Schließer, Annika Lubitz, Christoph Giese, Gerhard Winter, Julia Engert

The Evaluation of Immunogenicity of Protein Aggregates in a Human Artificial Lymph Node Model

2018 Workshop on Protein Aggregation and Immunogenicity, Breckenridge, Colorado, USA, July 30 - August 2, 2018

Short Talks:

Teresa Kraus

The Evaluation of Immunogenicity of Protein Aggregates in a Human Artificial Lymph Node Model

11th Worlds Meeting on Pharmaceutics, Biopharmaceutics and Pharmaceutical Technology, 19 to 22 March 2018, Granada, Spain

Grants:

DAAD (Deutscher Akademischer Austauschdienst) Travel Grant 2018 to visit the Workshop on Protein Aggregation and Immunogenicity in Breckenridge, Colorado, USA from July 30 – August 2, 2018

9.3 Curriculum Vitae

Teresa Franziska Kraus

Wohnhaft in München

Geboren am 28.07.1989 in Weingarten

Seit 02/2019	SaniPEP Apotheke, München <i>Laborleitung und angestellte Apothekerin</i>
05/2015 – 06/2019	Weiterbildung zur Fachapothekerin für Pharmazeutische Technologie , Bayrische Landesapothekerkammer
Seit 03/2015 – 12/2018	Lehrstuhl für Pharmazeutische Technologie, LMU München , München <i>Promotion unter Prof. Dr. Gerhard Winter und PD Dr. Julia Engert</i> <i>Thema: Immunogenicity of Protein Aggregates</i>
01/2015 - 03/2015	Apotheke 14 Nothelfer, Weingarten <i>Angestellte Apothekerin</i>
05/2014 - 11/2014	Klösterl-Apotheke München <i>Zweiter Teil des Praktischen Jahres</i>
11/2013 - 05/2014	Department of Pharmaceutical Sciences, Wayne State University , Detroit, MI, USA <i>unter Prof. Dr. Olivia Merkel</i> <i>Erster Teil des Praktischen Jahres</i>
02/2013	Lehrstuhl für Pharmazeutische Technologie, LMU München , München <i>unter Prof. Dr. Gerhard Winter und Prof. Dr. Wolfgang Frieß</i> <i>Wahlpflichtpraktikum</i>
08/2012 – 09/2012 und 03/2011 – 04/2011	Dragenopharm Apotheker Püschl GmbH , Tittmoning <i>Zweiter Teil der Famulatur und Studentische Hilfskraft</i>
12/2014	Approbation als Apothekerin
10/2009 – 10/2013	Ludwig-Maximilians-Universität , München <i>Studium der Pharmazie</i>
09/2000 – 06/2009	Gymnasium Weingarten , Weingarten <i>Abitur</i>
07/2006 – 07/2007	Logan Park High School , Dunedin, Neuseeland <i>Auslandsschuljahr</i>
